# MAGNETOM Flash

The Magazine of MR

Issue Number 3/2009
RSNA Edition

SIEMENS

## Clinical

**_syngo_ NATIVE in Transplanted Kidney Assessment**
Page 15

**Tumor Detection by DWI and ADC Mapping**
Page 47

**3D Knee Imaging using _syngo_ SPACE**
Page 84

## How I do it

**Visualizing the Distal Biceps Tendon**
Page 92

*The information about this product is being provided for planning purposes. The product is pending 510(k) review and is not commercially available in the U.S.

42

# Faster scan times

"Faster scan times amount to a significant increase of at least 4 procedures per day on an average of at least 20 MR studies per working week."

John Murray, Mater Misericordiae University Hospital, Dublin, Irland on the Symphony Tim Upgrade

# increased scanning speed

"The increased scanning speed has raised throughput by 50%, now allowing 6 patients to be scanned in a 4 hour session rather than only 4 before."

Russell Bull, Royal Bournemouth Hospital, UK on a WIP version of the Cardio Dot Engine*

# higher clinical throughput

"The overall acquisition time can be reduced from 20–30% in abdominal studies to up to 50% for whole-body examinations [...] this led to a higher clinical throughput, as up to 4 additional patients could be examined each day."

Henrik Michaely, University Medical Center Mannheim, Germany on _syngo_ TimCT Oncology

Results may vary. Data on file.

Matthias Lichy, M.D.

# Dear MAGNETOM user,

Dynamic contrast-enhanced (DCE) liver MRI plays a major role in the detection and differentiation of liver disease. However, those who scan liver patients in their daily routine understand the level of experience and interaction required. In his article, Prof. Martin deals with timing and sequence adjustments of the arterial phase DCE scan, which are significant elements of liver MRI. He shows how this technique helps to improve the standard of DCE liver MRI.

Together with our collaboration partners we are focused on improving the quality and therefore the accuracy of MRI. Very often, complex tasks which require a high level of experience prevent a method from becoming daily routine. In their first clinical experience with a work-in-progress implementation of the Cardiac Dot Engine*, Dr. Russell Bull and Matthew Benbow demonstrate how intelligent automation and user guidance can not only increase reproducibility but also help to optimize daily routine and increase the throughput of even complex cardiac stress examinations.

These improvements in workflow and image quality are also based on hardware technology. The advantages of Tim (Total imaging matrix) compared to conventional MR systems are well known and in their article Dr. John Murray et al. demonstrate that simply by adding Tim technology to their 1.5T MAGNETOM Symphony system they could significantly improve their productivity. They now offer the latest MR applications such as highly temporal resolved MR angiography for planning of thoracic surgery or multi-stage examinations of spine injuries. With Tim 4G* the next generation of coil and RF technology is now available and will again contribute to the ease and flexible usage of MRI.

We also feature in this edition of Flash 3D large FOV imaging of the cervical spine and 3D knee imaging (*syngo* SPACE). We show how non-ce MRA (*syngo* NATIVE TrueFISP) can be used for evaluation of renal transplants and explain the latest developments of the arterial spin labelling sequence and diffusion-weighted imaging techniques.

You can read about the comparison of the results of whole-body MRI with PET/CT in a case of metastatic breast cancer. All these applications show a clear potential to change our daily clinical routine. And together they make MRI an invaluable diagnostic tool, thanks to its ease-of-use, flexibility and productivity.

We hope you will enjoy reading this latest edition of Flash!

**Matthias Lichy, M.D.**

*The information about this product is being provided for planning purposes. The product is pending 510(k) review and is not commercially available in the U.S.

# The Editorial Team

We appreciate your comments.
Please contact us at magnetomworld.med@siemens.com

Antje Hellwich
Associate Editor

Dagmar Thomsik-Schröpfer,
Ph.D., MR Marketing-Products,
Erlangen, Germany

Okan Ekinci, M.D.
Segment Manager
Cardiovascular MRI
Erlangen, Germany

Peter Kreisler, Ph.D.
Collaborations & Applications,
Erlangen, Germany

Heike Weh,
Clinical Data Manager,
Erlangen, Germany

Bernhard Baden,
Clinical Data Manager,
Erlangen, Germany

Ignacio Vallines, Ph.D.,
Applications Manager,
Erlangen, Germany

Wellesley Were
MR Business Development
Manager
Australia and New Zealand

Milind Dhamankar, M.D.
Sr. Director, MR Product
Marketing, Malvern, USA

Michelle Kessler, US
Installed Base Manager,
Malvern, PA, USA

Gary R. McNeal, MS (BME)
Advanced Application Specialist,
Cardiovascular MR Imaging
Hoffman Estates, USA

Dr. Sunil Kumar S.L.
Senior Manager Applications,
Canada

# Content

15
*syngo* NATIVE TrueFISP

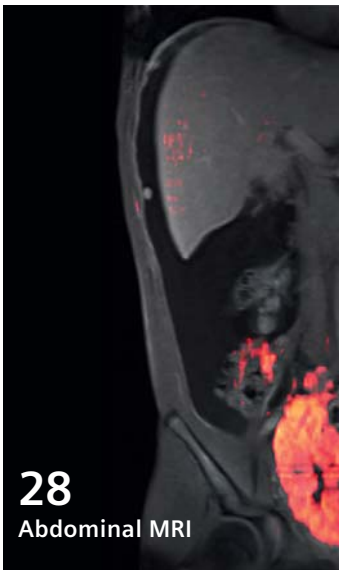

28
Abdominal MRI

## Further clinical information

Visit the MAGNETOM World Internet pages at **www.siemens.com/magnetom-world** for further clinical information and talks by international experts.

## Clinical Cardiovascular


**6** First Clinical Experiences with a Prototype of a Novel Cardiac Workflow Engine
*Russell Bull, Matthew Benbow*

**12** Case Report: Cardiac MR Imaging of a Rare Primary Cardiac Angiosarcoma
*MR Moynagh, et al.*

**15** *syngo* NATIVE TrueFISP in the Assessment of the Transplanted Kidney
*Peter Weale, et al.*


## Clinical → How I do it


**18** Non Contrast-Enhanced MR Angiography (*syngo* NATIVE)
*Manuela Rick, et al.*


## Clinical Abdomen / Pelvis


**24** *syngo* TimCT – Increasing Clinical Throughput and Efficacy
*K. Lederle, et al.*

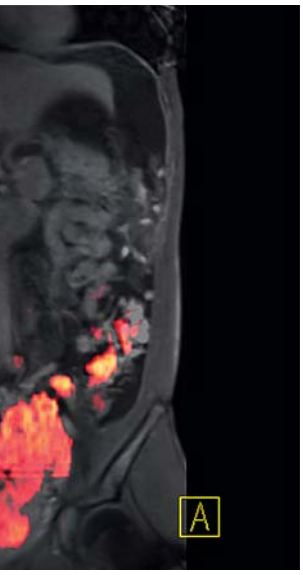

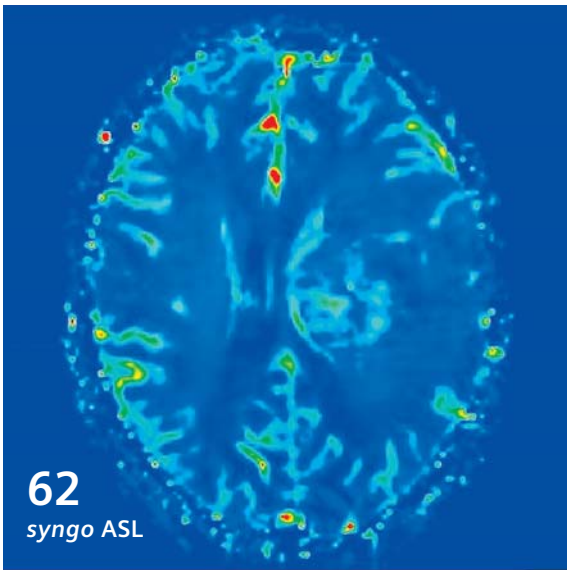

**28** Case Report: Comprehensive Staging of the Abdomen and Pelvis with *syngo* TimCT Oncology in a Patient with Metastatic Hepatoid Carcinoma of the Prostate
*Henrik J. Michaely*

**32** Case Report: MRI-guided Prostate Biopsy in a Patient with Prior Negative TRUS-Guided Biopsies and Persistently Elevated PSA-Levels
*Matthias Philipp Lichy, et al.*

**36** Intravoxel Incoherent Motion (IVIM): A Potential Application in Cirrhosis Assessment
*Alexandre Vignaud, et al.*

**40** Challenges and Clinical Value of Automated and Patient-Specific Dynamically Timed Contrast-Enhanced Liver MRI Examination
*Diego R. Martin, et al.*

**47** Case Reports: Tumor Detection by Diffusion-Weighted MRI and ADC-Mapping with Correlation to PET/CT Results
*Matthias Philipp Lichy, et al.*

## Clinical Women's Health

**52** Whole-Body MRI for Accurate Assessment of Tumor Load of Bone Metastases Originate from Mamma Carcinoma
*Philip Aschoff, et al.*

**58** Case Report: Klippel-Trénaunay-Weber Syndrome
*Chawla Tanya, et al.*

## Clinical Neurology

**62** Cerebral Blood Flow Imaging with 3D GRASE ASL Sequence Increases SNR and Shortens Acquisition Time
*David A. Feinberg, Matthias Günther*

**70** Cervical Spine MRI. *syngo* SPACE in a Claustrophobic Patient with Congenital Scoliosis
*Marietta Garmer, et al.*

**74** IMRISneuro 70 cm Bore 3T in Intra-Operative Neurosurgery
*Jeanne Elliott*

## Clinical Whole Body

**80** Whole-body dynamic MR Imaging for Evaluation of Bone Marrow in Multiple Myeloma
*Alexandre Vignaud, et al.*

## Clinical Orthopedic imaging

**84** 3D High Resolution MRI of the Knee at 3T Using a Moderately T2-weighted 3D-TSE-fs (*syngo* SPACE) sequence – Useful or Not?
*A. Horng, et al.*

## Clinical → How I do it

**92** FABS View of the Elbow for Visualization of Distal Biceps Tendon
*Peter Cazares, et al.*

## Business

**94** MAGNETOM Symphony Tim Upgrade: The Mater Misericordiae University -Hospital Experience
*F. Bolster, et al.*

# First Clinical Experiences with a Prototype* of a Novel Cardiac Workflow Engine

Russell Bull, MRCP, FRCR.; Matthew Benbow

*Royal Bournemouth Hospital, Bournemouth, UK*

## Introduction

In November 2007 a novel cardiac work in progress (WIP) software package was introduced on our 1.5T Siemens MAGNETOM Avanto MRI system (high-order shim, 32-channels, SQ gradients). This WIP system automates or augments most user interactions during cardiac scanning. For localization of standard cardiac planes users select anatomical reference points on the heart, supported by guidance images and text (Fig. 1). The software then calculates all cardiac planes automatically and applies them to all subsequent measurements. Sequences are automatically adapted to the patients heart rate and breath-hold capability according to the exam settings entered by the user (Fig. 2). The field-of-view is automatically adjusted for each combination of planes to fit the individual patient. Reliable, robust protocols can be constructed ensuring a comprehensive cardiac exam but still allowing enough flexibility to add additional sequences such as flow, tagged grid, constriction tests, etc.

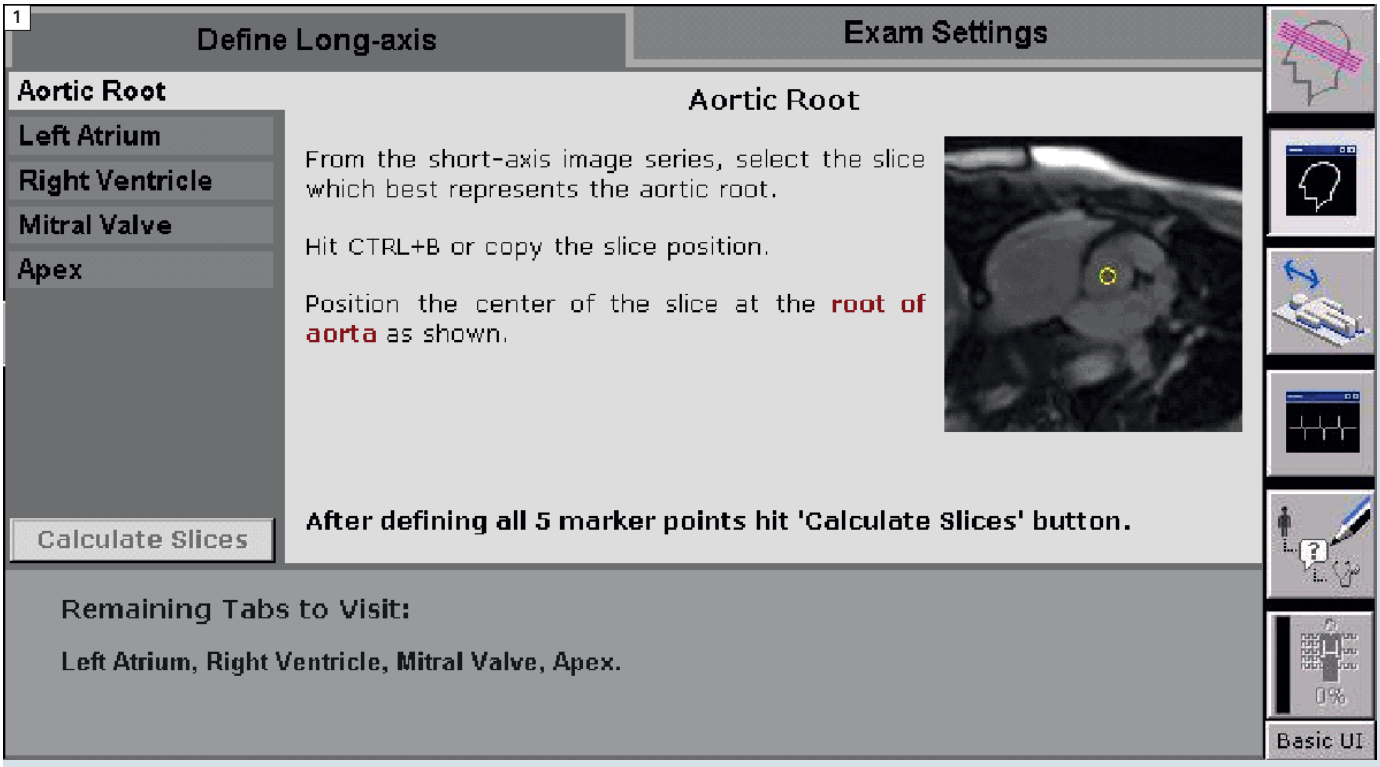


**1** Novel way of localization of the heart: The user marks five anatomical landmarks. To find the landmarks, guiding text and example images are displayed. These landmarks are consecutively used to calculate all cardiac planes.

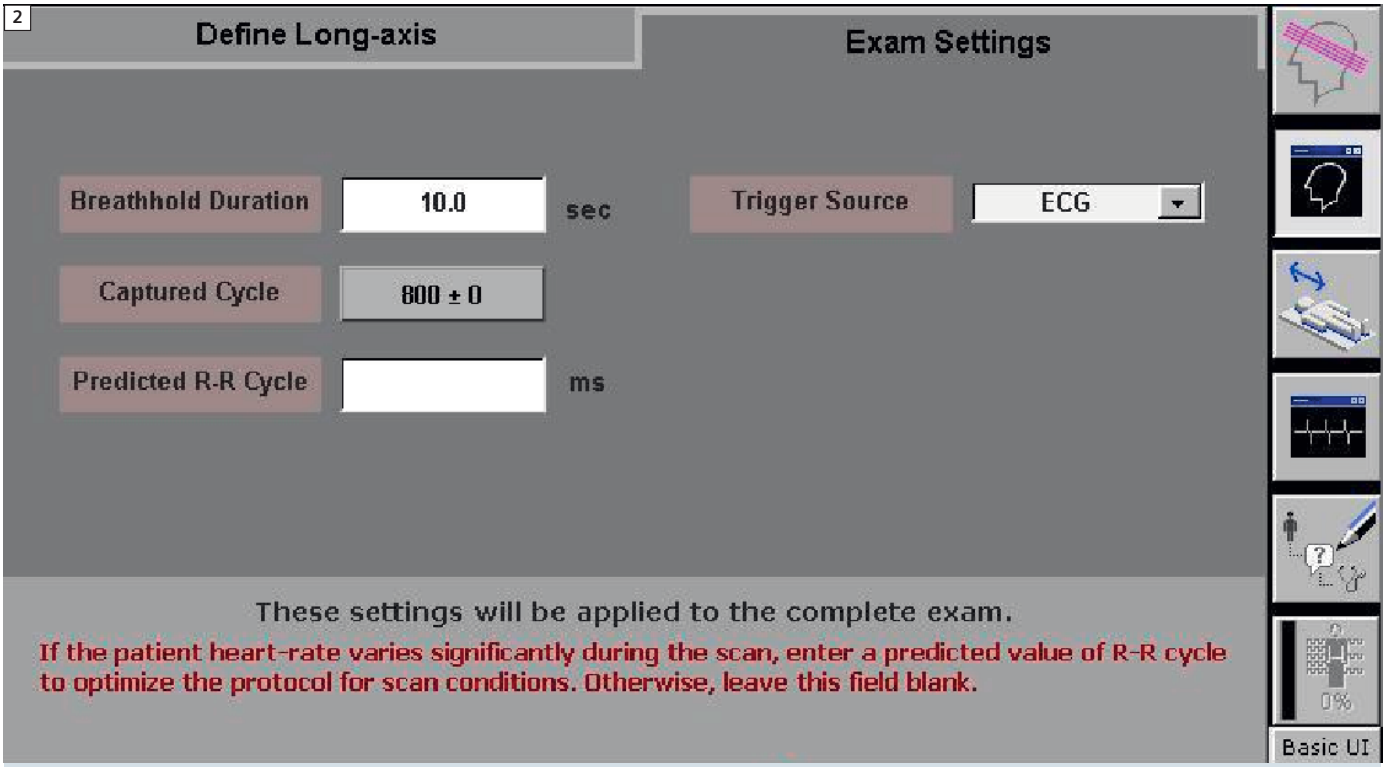


**2** Exam Settings – Patient-centric parameters which globally influence the whole exam and are used to initialize the scan protocols.

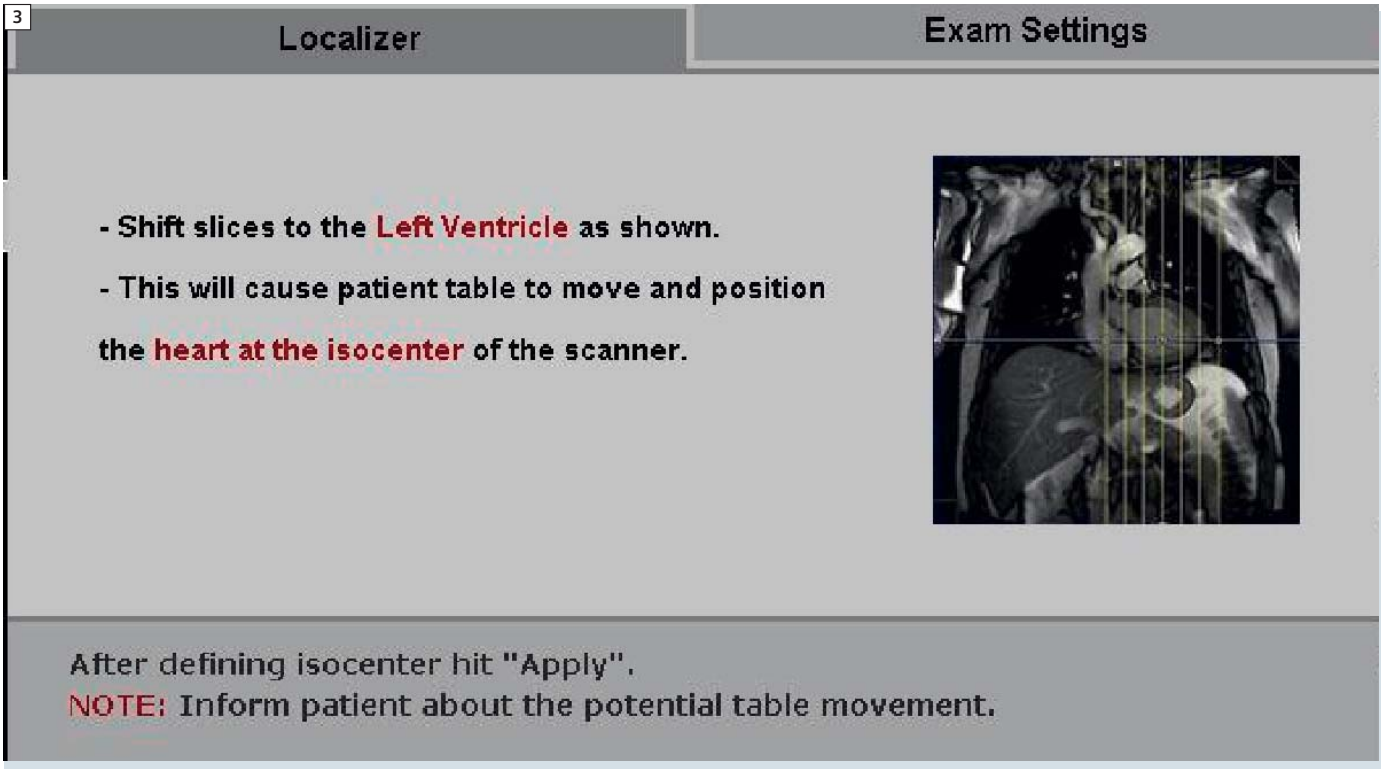


**3** Iso-center scanning. Support by guidance images and text the user can move the left ventricle to the iso-center to ensure high scan quality

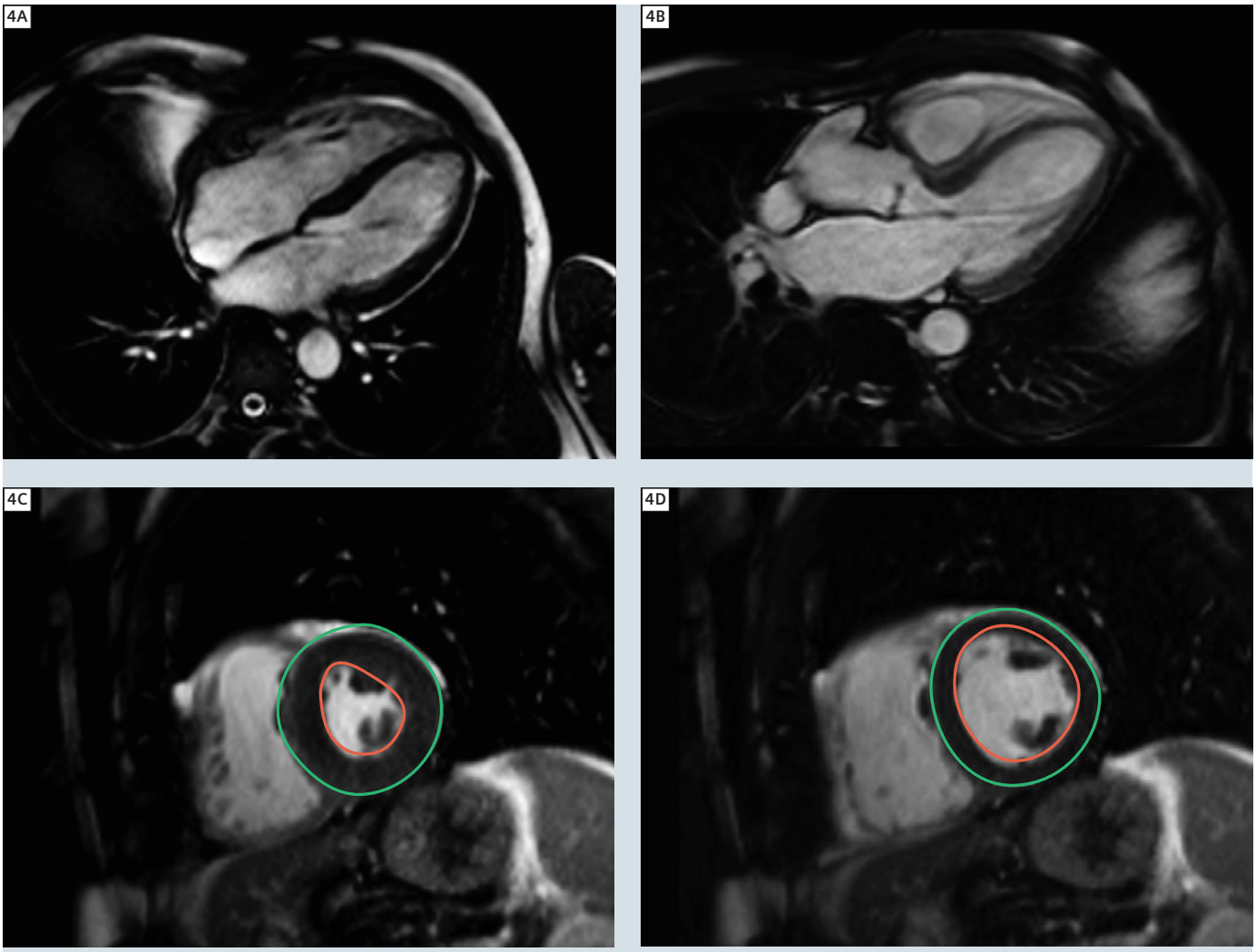


**4** Examplatory cine-images from a typical CMR exam, performed after the introduction of the WIP software package, scanned by a less experienced technologist. A standard 4-chamber view is shown in **4A**. No manual adjustments were required, not even for dedicated planes like the LVOT (left ventricular outflow tract). Segmentation of the left ventricular wall on the short axis **(4C, D)** was calculated by the integrated Inline segmentation tool and required no interaction neither by the technologist nor the radiologist.

## Clinical setting

The Royal Bournemouth is an acute-care general hospital (900 beds) with a large regional cardiac unit performing over 2500 procedures per year. The cardiac MRI (CMR) service started in 2004, initially providing basic structural information only. CMR stress exams started in 2007. Our patient population is almost exclusively adult. CMR is used to provide structural and functional information and is used particularly for planning revascularisation strategies in patients with known coronary artery disease.

Extensive process-mapping was undertaken in order to identify areas in which the scanning process could be accelerated. Even with these changes, stress heart exams required a time-slot of 1 hour using conventional software. There were also major issues regarding

5A

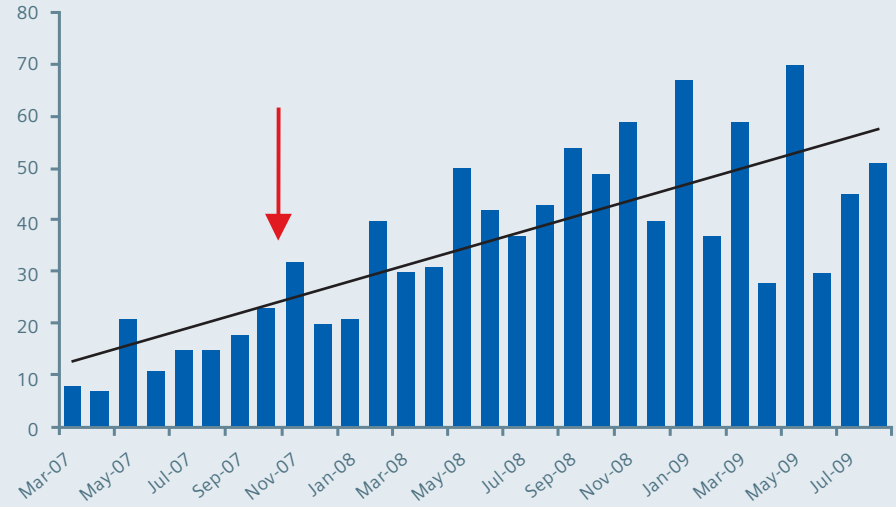


**5A** Development of the number of stress CMR studies per month performed at our institution (red arrow: cardiac prototype installed). Note that at our institution during this timeframe all cardiac MR exams were reported by only two cardiac radiologists; variations in patient throughput from month to month have now been addressed by appointment of a cardiac radiology fellow.

5B

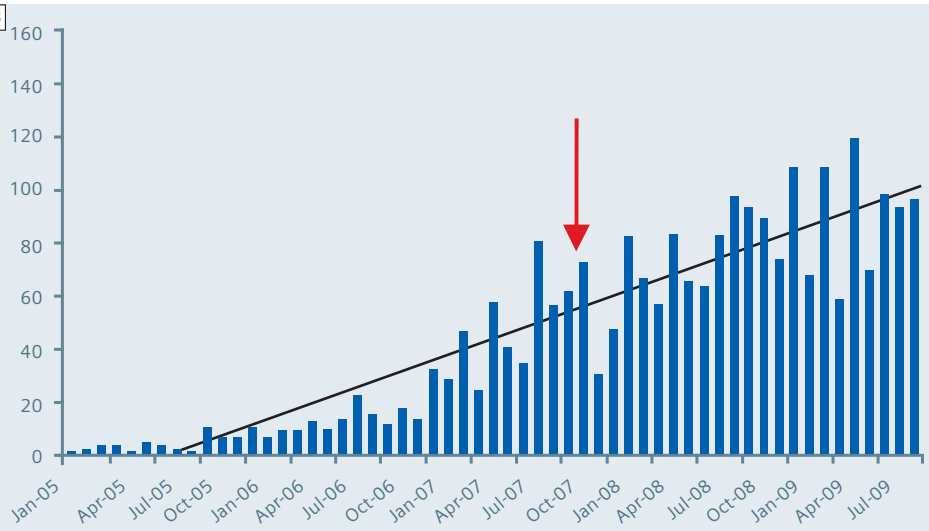


**5B** Total number of all CMR studies per month (red arrow – cardiac prototype installed).

staff training due to the complexity of the procedures and the lack of familiarity with cardiac anatomy and cardiac planes.

## Clinical experiences

The cardiac WIP software has transformed the scanning process for cardiac MRI patients. The most difficult MR examination has become much more straightforward and now, even relatively inexperienced staff members are able to scan cardiac patients quickly and efficiently. The increased scanning speed has raised throughput by 50%**, now allowing 6 patients to be scanned in a 4 hour session rather than only 4 before. This software enables us to scan over 1000 cardiac patients per year in a general department, scanning up to 120 cases per month using only 10% of total scanning capacity. The prototype

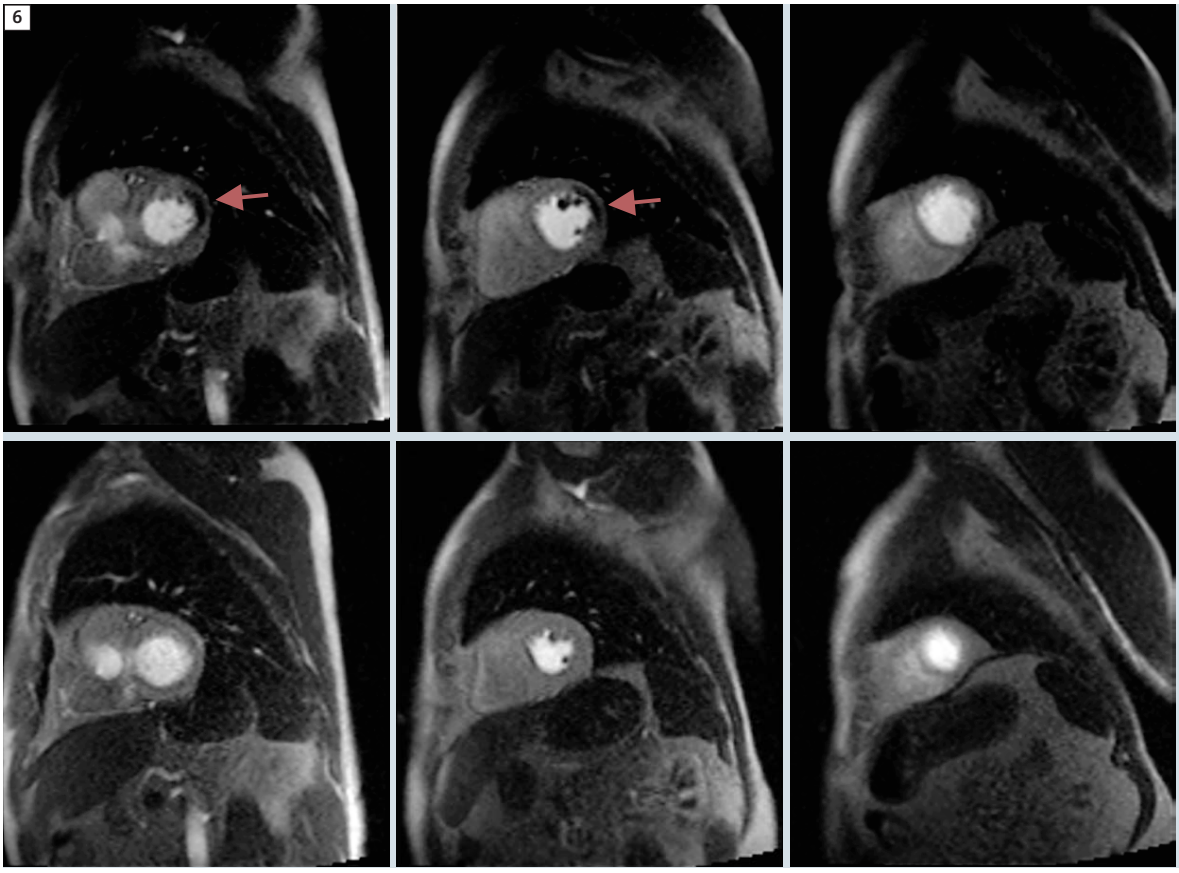

**6** Short axis stress CMR images using cardiac prototype showing lateral wall subendocardial defect (arrow) secondary to circumflex lesion (upper row). This resolved following successful stenting (lower row).

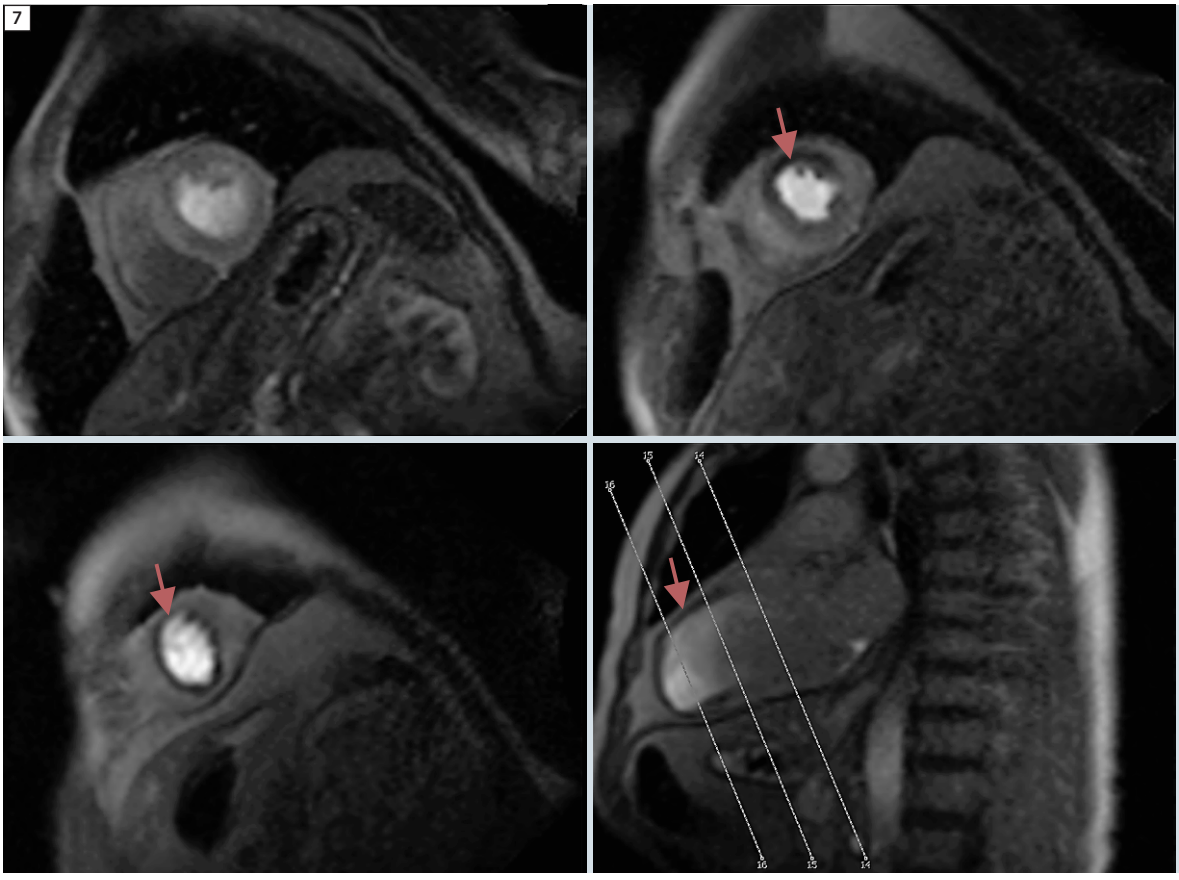

**7** Stress CMR using cardiac prototype showing anterior wall/apical subendocardial defect (arrow) secondary to critical mid-LAD lesion. The prototype always acquires 3 short axis stress images and adaptively includes additional selected views if R-R interval allows (additional 2-chamber view shown in Fig. 8).

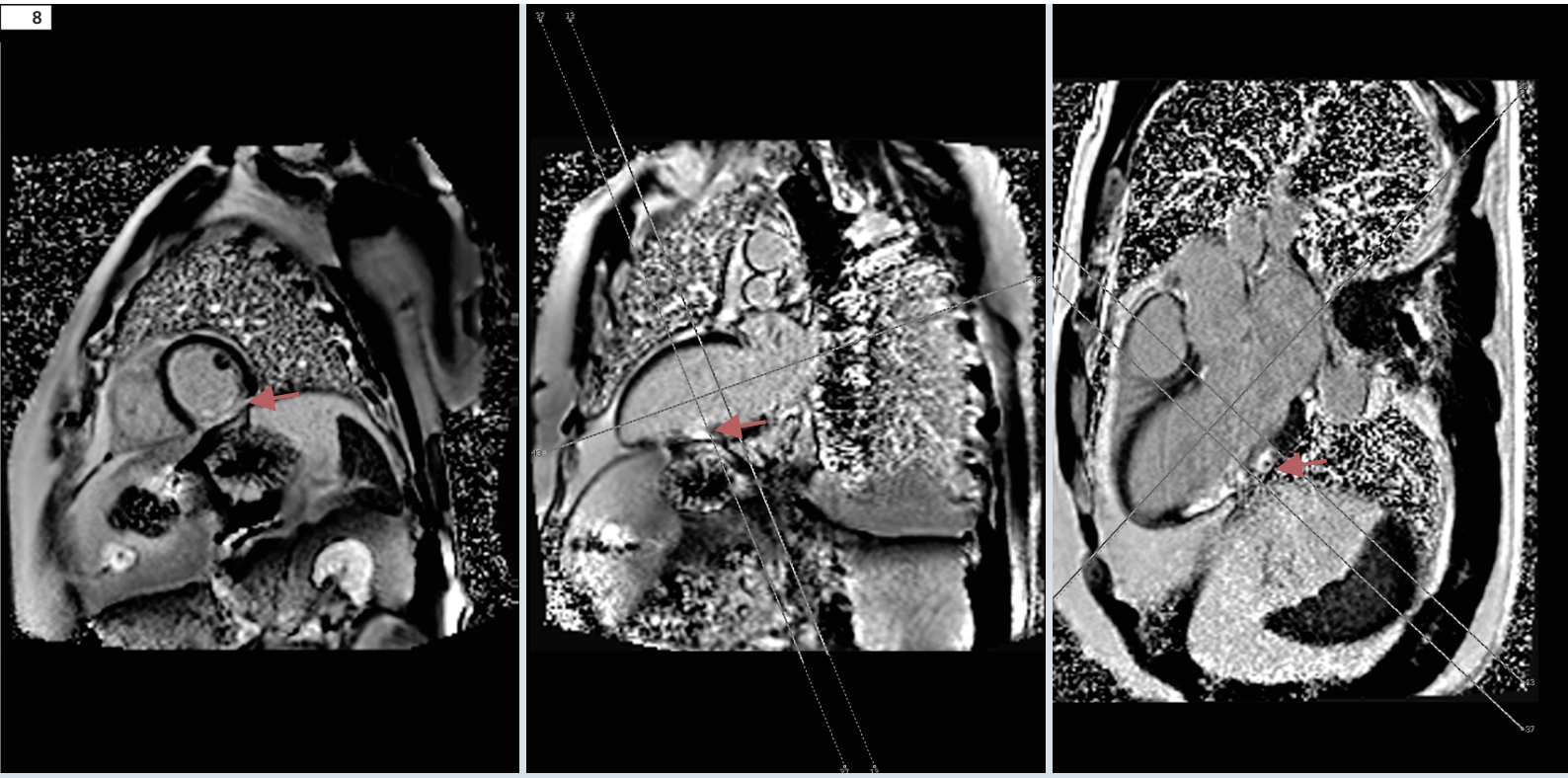

**8** Short axis, 2-chamber and LVOT PSIR images showing old inferior infarct (arrow).

Dr. Russel Bull and Matthew Benbow (left).

has made training easier and scanning much simpler and faster thus enabling incorporation of cardiac examinations into the workload of a busy general hospital. All 16 scanning staff now perform cardiac examinations compared with just 3 before. The imaging results are now much more robust and quality is consistently high due to standardization. The increased speed has also made the scanning process more pleasant for patients, particularly for those suffering from claustrophobia.

*WIP – Work in progress. The information about this product is preliminary. The product is under development and not commercially available in the U.S., and its future availability cannot be ensured.
**Results may vary. Data on file.

**Contact**
Dr. Russell Bull , MRCP, FRCR
Consultant Radiologist
Royal Bournemouth Hospital
Castle Lane East
Bournemouth
UK
Russell.Bull@rbch.nhs.uk

# Case Report: Cardiac MR Imaging of a Rare Primary Cardiac Angiosarcoma

MR Moynagh[1], A Mc Gee[1], A Cradock[1], M Da Costa[3], J Bruzzi[2], JG Murray[1]

*[1]Dept. of Radiology, Mater Misericordiae University Hospital, Dublin, Ireland*
*[2]Dept. of Radiology and [3]Dept. Surgery, University College Hospital Galway, Galway, Ireland*

## Clinical details

A 24-year-old male was admitted under the cardiology service of a university hospital with dyspnoea and a new onset systolic murmur. Echocardiography and CT demonstrated a mass overlying the right heart, with possible pulmonary metastases. Histology from closed chest biopsy was suggestive of a cardiac angiosarcoma, however resectability status and exact diagnosis was unclear. The patient was then referred to the Radiology Department of the National

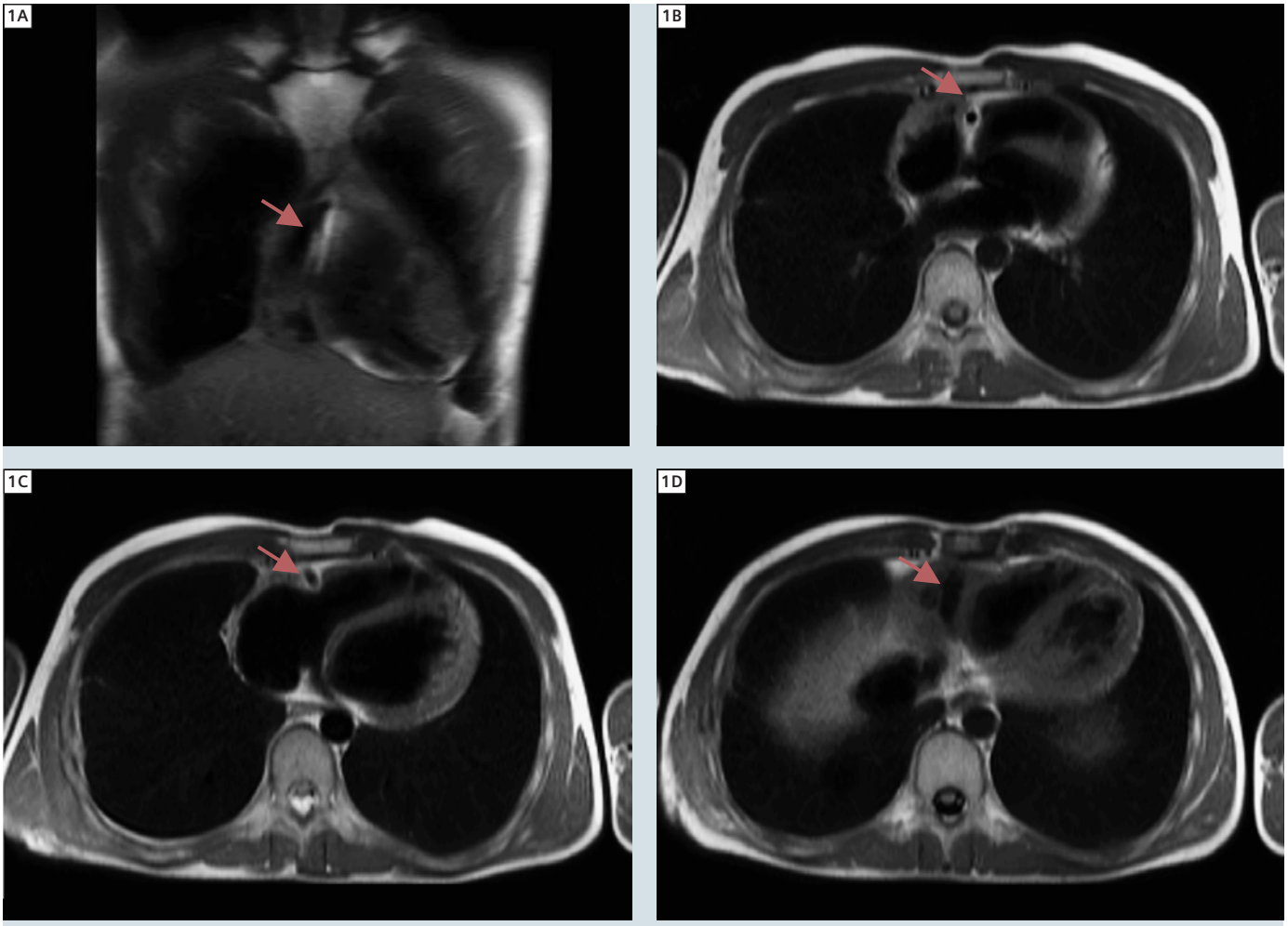


**1** Coronal **(1A)** and transversal **(1B–D)** showing a mass at the ventral border of the right ventricle. A large feeding right coronary artery can be seen; because of the clear flow-void phenomena (arrows), higher flow within the right coronary artery has to be assumed.

Centre for Cardiothoracic Surgery for further assessment. Cardiac MRI was performed to further characterize the right atrial mass and identify the relationship to coronary vasculature.

## Sequence details

All images shown were acquired at a 1.5T MAGNETOM Symphony, A Tim System with a combination of the Body Matrix coil and spine coil elements. The imaging protocol included transversal and coronal HASTE, 4-chamber view and oblique oriented transversal cine-True-FISP and pre- and postcontrast 2D FLASH in transversal and oblique sagittal planes. For assessment of the vascular architecture of the lesion, a highly temporal resolved MR angiography was applied, using the *syngo* TWIST technique (TR / TE = 3.29 / 1.39 ms; FOV 400 mm, matrix 294 x 448, temporal resolution 6 s).

## Imaging findings

6 x 4.3 cm intensely enhancing mass overlying the anterior margin of the right atrium and right ventricle, which extended across the atrioventricular groove to about the free wall of the right ventricle. The right coronary artery and adjacent cardiac vein were partially encased, with intimate relationship to the tricuspid valve ring. Direct blood

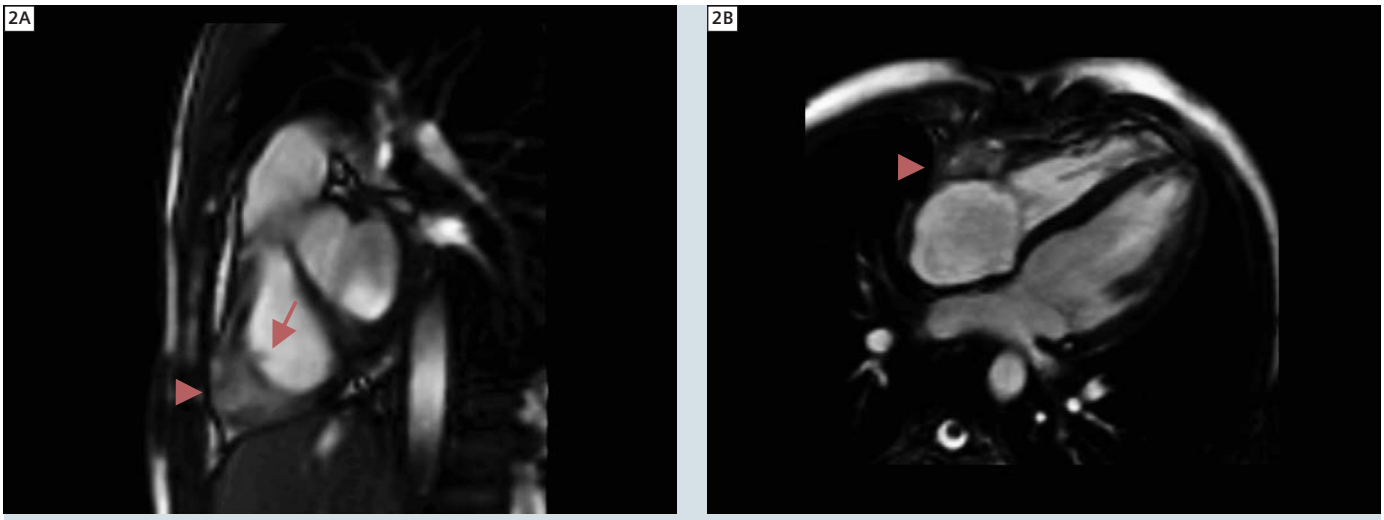


**2** Cine TrueFISP sequences are shown. In Fig. **2A** a small irregular signal-loss can be seen on the sagittal oblique view (arrow), indicating a draining vein to the right ventricle.

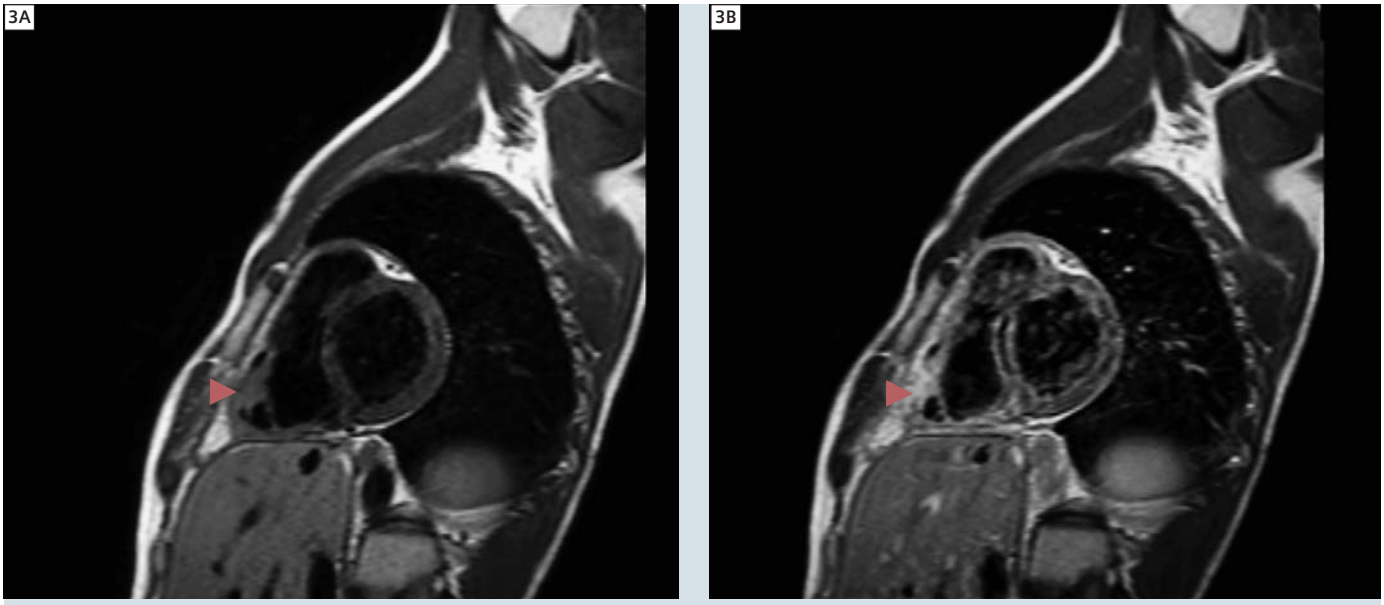


**3** Avid enhancement of the mass was observed, suggesting angiosarcoma.

**4** Thinslice MIP of the *syngo* TWIST MR Angiography are shown. Temporal resolution was 6 seconds. A large arterial feeder (right coronary artery) and vascular mass can be seen in Fig. **4B** (VRT of the vessel shown in **4L**). An atypical enhancement of the blood within the right ventricle can be seen in Figs. **4G** and **4I**, indicating a potential shunt between the mass and the right ventricle.

supply arising from the right coronary artery and probable partial venous return directly to the right atrium. Image findings were consistent with a cardiac angiosarcoma.

References

1 Best AK, Dobson RL, Ahmad AR. Best cases from the AFIP, Cardiac Angiosarcoma. Radiographics 2003 ; 23:S141-S145. Erratum in: N Engl J Med 1991; 325(18):1324.
2 Kalra MK, Abbara S. Imaging cardiac tumors. Cancer Treat Res. 2008; 143:177-196.
3 Neragi-Miandoab S, Kim J, Vlahakes GJ Malignant tumours of the heart: a review of tumour type, diagnosis and therapy. Clin Oncol (R Coll Radiol). 2007 Dec;19(10):748-56.
4 Kurian KC, Weisshaar D, Parekh H, Berry GJ, Reitz B. Primary cardiac angiosarcoma: case report and review of the literature. Cardiovasc Pathol 2006 Mar-Apr;15(2):110-2.

**Contact**
Dr. John Murray, M.D.
Dept. of Radiology
The Mater Misericordiae University Hospital
Eccles Street
Dublin 7
Ireland
jmurray@mater.ie

# *syngo* NATIVE TrueFISP in the Assessment of the Transplanted Kidney

**Peter Weale[1]; Jeremy Collins, M.D.[2]; James C. Carr, M.D.[3]**

*[1]Staff Scientist ,Siemens Healthcare, Cardiovascular MR Research and Development, Chicago, IL, USA*
*[2]Fellow, Department of Radiology, Northwestern University Medical School, Chicago, IL, USA*
*[3]Associate Professor, Director, Cardiovascular Imaging, Department of Radiology, Northwestern University Medical School, Chicago, IL, USA*

## Introduction

Assessment of the vascular integrity of a transplanted kidney is a request we receive occasionally, most commonly when transplant recipients present with compromised renal function.
The fact that the patient presents with impaired renal function and has recently undergone transplant surgery makes the nephrologist understandably nervous about referring them for contrast-enhanced MR Angiography of the transplanted kidney. While the risk may be small, it makes sense to use a completely non-invasive method without the potential risk of Nephrogenic Systemic Fibrosis, if the diagnostic yield can be sufficient to answer the clinical question.
In our institution we recently published a study [1] where the effectiveness of TrueFISP with selective inversion recovery preparation, now known as *syngo* NATIVE TrueFISP, was evaluated for its utility in the assessment of the transplanted renal artery. Our results showed that the technique was essentially the same in diagnostic performance as low dose contrast-enhanced angiography and the method provides a low-risk method for the initial evaluation of the transplanted kidney.

## Principles

*syngo* NATIVE TrueFISP is a method which generates angiographic contrast by preparing the region which contains

**1** Volume rendered depiction of the anastomosis and proximal branches in this transplanted kidney. A slight "waisting" is seen at the site of the anastomosis.

**2** Thin MIP (50 mm) demonstrates the anastomosis and the upper pole accessory / early branching artery which originates very close to the site of the anastomosis. Depiction of 2nd and 3rd order branches of the renal artery provides qualitative evidence of good perfusion as the mechanism behind this technique relies upon in-flow during the prescribed inversion time. In this case blood depicted at the distal ends of the demonstrated arteries has travelled from the top if the inversion band (essentially top of this image) within 900 ms.

the vascular territory of interest by use of a selective inversion recovery pulse. The inversion pulse reduces the signal from the static tissue and blood which remains in the area but blood which flows into the slice during a defined inversion time is not inverted and, when the image data (3D TrueFISP) is collected there is a large difference in signal between blood which has moved into the area and other tissues which remain attenuated as a consequence of the inversion preparation.
This preparation region is not simply slice selective but has a graphically positioned inversion preparation which allows targeting of the desired vessel, independent of the orientation of the imaging volume.

## Case study

A 64-year-old male patient with hypertension and type-2 diabetes who had been the recipient of a transplanted kidney was referred for evaluation of the transplanted renal artery to rule out an anastomotic stenosis as a cause for diminishing renal function. Recent Doppler ultrasound had demonstrated elevated velocities in the transplant renal artery, raising the suspicion of transplant arterial stenosis.
The patient and referring physician had concerns relating to the administration of Gadolinium containing contrast agents as his eGFR was reduced (35 ml/min/1.73 $m^2$). 30 ml/min/1.73 $m^2$ is the cut off point for administration of contrast in our institution.
After localization with 2D HASTE images the imaging volume of the *syngo* NATIVE TrueFISP protocol was positioned to depict the iliac arteries and the renal transplant anastomosis. The selective inversion band was positioned transversely with its upper border a few cm proximal to the assumed position of the anastomosis. The inversion preparation was larger than the imaging volume in the superior-inferior direction and covered around 4 cm distal to the imaging volume to invert any inflowing blood in the iliac veins (Fig. 3).
In this case, we used ECG triggering but in practice this is largely optional for renal transplants. We have found that the degree of respiratory motion in the pelvic region is small enough so as not to be a significant source of artifact in most patients, where the transplanted kidney is positioned against the pelvic sidewall and largely free of any significant respiratory motion.
The spatial resolution of this protocol was 1.25 x 1.25 x 1.25 mm (interpolated to 1 mm in the slice direction). 112 slices per 3D slab were acquired giving just over 11 cm of head-to-foot coverage. An inversion time of 900 ms was

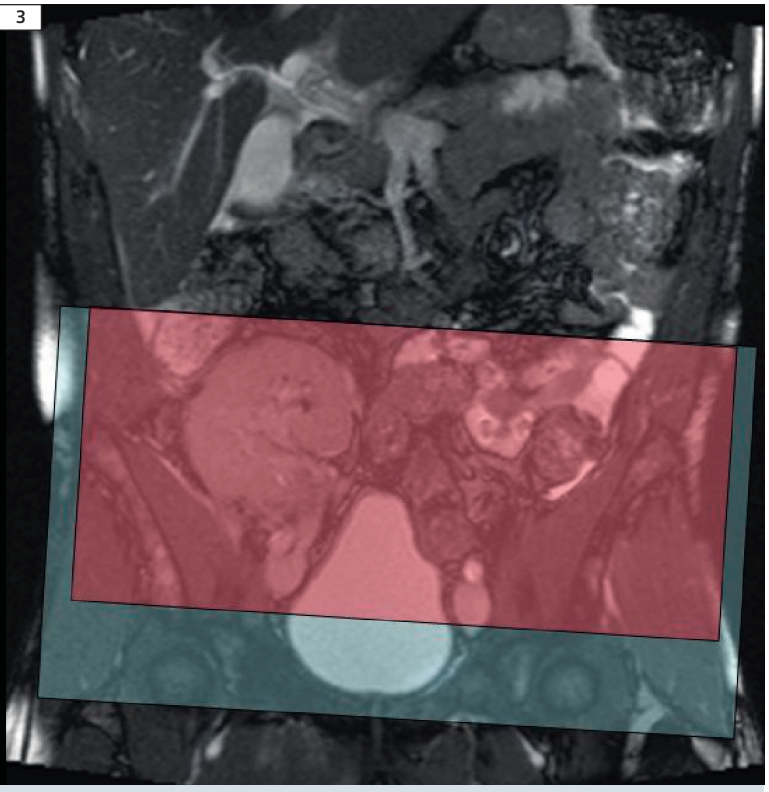

**3** In this example the inversion preparation (gray) was positioned asymmetrically in the head-foot direction in relation to the imaging volume (red) to reduce the signal from any inflow via the iliac veins.

**4** A cross sectional thin MIP of the iliac artery at the level of the anastamosis showing the main renal artery demonstrates a minor degree of narrowing which is probably of limited hemodynamic significance as the artery is well seen with 2nd and 3rd order branches well seen.

used which allowed the TI and acquisition to be completed within one heart beat resulting in completion of the scan in 3 minutes.
The TrueFISP readout scheme used a flip angle of 90 degrees.

## Findings

The renal artery to external iliac artery anastomosis was well demonstrated and depicts a mild stenosis which is probably not a factor in this patient's diminishing renal function (Fig. 2).
The upper pole accessory artery (or what was probably an early branching upper pole artery in the native kidney) is also well seen distally, though the spatial resolution of this protocol inhibits the confident depiction of this very small vessel to the degree where an assessment of its diameter or severity of stenosis can be given.
The physiological nature of the contrast mechanism in NATIVE TrueFISP, however, gives some indication that this branch does not have a hemodynamically significant stenosis as the upper pole branch is filled with fresh blood within one cardiac cycle.

## Conclusion

*syngo* NATIVE TrueFISP is a technique which allows depiction of the anastomotic site of a transplanted renal artery and the major branches of the implanted organ.
The mechanism whereby the angiographic contrast is generated in this sequence has a physiological component which can be seen as both a positive and a negative feature.
In the absence of sufficient flow, or in significantly impaired flow, the lumen of the vessel of interest may not be filled with sufficient "non-inverted" blood. This can be addressed to a degree by careful planning of the position of the inversion region so that large volumes of blood proximal to the vessel of interest are not inverted, which will reduce the available contrast.
In the example of renal transplants, if blood flow is compromised, the inversion preparation can be targeted so that the proximal external iliac artery is outside the preparation region, so that the non-inverted blood which gives the required signal has less far to travel – so less "fresh blood" is wasted filling a vessel of no clinical significance. Increasing the inversion time may also help in depiction of arteries where inflow into the kidney is reduced.
The physiological nature of the contrast mechanism is a benefit in that it gives a qualitative feel to the significance of any demonstrated stenosis.
In this example the mild stenosis seen at the anastomosis seems to have no significant effect on the filling of the distal branches of the intra-renal arteries suggesting that the kidney is well perfused.
*syngo* NATIVE TrueFISP is a useful addition to the available methods for performing MR angiography. As with all techniques a full understanding of the mechanisms behind the technique will give more consistent results and provide additional diagnostic information.

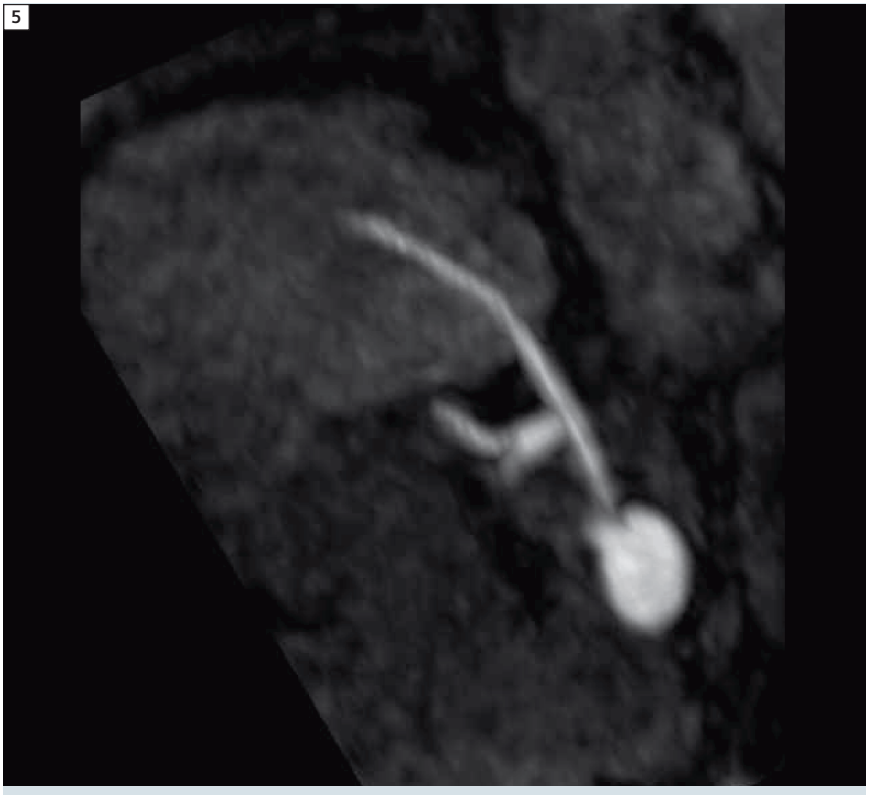

**5** The upper pole accessory artery is well demonstrated, though the assessment of the lumen of this very small artery at the site of the anastomosis is somewhat compromised due to spatial resolution limitations.

**References**

1 Liu X, Berg N, Sheehan J, Bi X, Weale P, Jerecic R, Carr J. Renal transplant: nonenhanced renal MR angiography with magnetization-prepared steady-state free precession. Radiology. 2009 May;251(2):535-42.

**Contact**
Peter Weale
Siemens Healthcare
Cardiovascular Research and Development
737 N Michigan Ave
STE 1600
Chicago, IL 60611
USA
peter.weale@siemens.com

# How I do it: Non Contrast-Enhanced MR Angiography (*syngo* NATIVE)

Manuela Rick, Nina Kaarmann, Peter Weale, Peter Schmitt

*Siemens Healthcare, Erlangen, Germany*

## Introduction

The realization that the administration of gadolinium-based contrast agents may be a factor in the development of Nephrogenic Systemic Fibrosis (NSF) in patients with renal failure has created a renewed interest in the in angiographic methods using intrinsic rather than extrinsic contrast mechanisms. The current economic climate in the Healtcare industry means that there is an increasing need to develop more cost-effective methods and reduction of contrast agent utilization is one element which might contribute to this. The existing non contrast-enhanced sequences, such as the Time-of-Flight (TOF) sequence, have their advantages in regions like the intracranial vasculature, but may have limitations for abdominal or peripheral imaging.

*syngo* NATIVE was introduced with software version *syngo* MR B17. It comprises two different non-contrast MRA techniques:

- *syngo* NATIVE TrueFISP (optimized for the renal arteries)
- *syngo* NATIVE SPACE (optimized for peripheral regions)

Both applications use mechanisms for contrast generation which depend on physiological processes. In NATIVE TrueFISP the inflow of non-inverted blood is exploited to depict the vessels. In NATIVE SPACE the image contrast is based on the pulsatility of the blood flow. Hence, the methods might be limited (reduced or no contrast-to-noise-ratio (CNR)) for patients with severe pathologies that have a direct influence on these physiological processes. This article not only demonstrates how to plan and perform a *syngo* NATIVE examination, but also gives some hints and tricks in cases where it may be difficult to get good image quality.

A clear understanding of the technical background of these measurements gives the user the opportunity to adapt the scan parameters individually, with respect to the patient's physiology. The ability to tailor the measurement can maximize the success rate.

## The theory behind *syngo* NATIVE TrueFISP

*syngo* NATIVE TrueFISP is based on the TrueFISP sequence which typically yields a bright blood signal.

To enhance the contrast between flowing and static magnetization, an inversion pulse is applied to the region of interest. When imaging takes place after an inversion time TI, when the magnetization of surrounding tissue is close to zero, the background will have low signal. During the TI, however, fresh blood, with no history of inversion, enters the inverted slab, and the filled vasculature appears bright. The higher the more blood volume entering the inverted region, the better the contrast and the assessment of the small branches of the vessels. Figure 1 shows the basic principle of *syngo* NATIVE TrueFISP. With *syngo* NATIVE TrueFISP, respiratory synchronization can be realized with the 1D PACE Navigator. In this case the images are usually acquired in end-expiration to prevent breathing artefacts.

To increase the effectiveness and to reduce further artefacts from pulsatile vessels, you can combine 1D PACE with ECG-triggering. When a new inversion is played out with each ECG trigger signal,

1

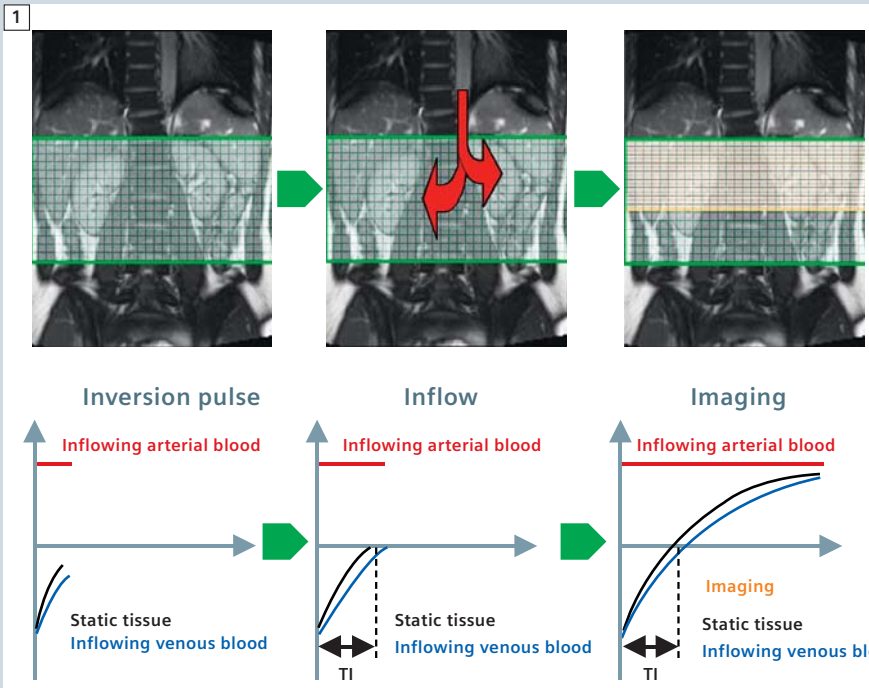


**1** Basic principles of *syngo* NATIVE TrueFISP

the total blood volume available for imaging is proportional to the stroke volume within one heartbeat.

## Patient preparation

The patient is positioned supine, head or feet first.
It is highly recommended to use ECG-triggering. To reduce patient set-up time, *syngo* NATIVE TrueFISP data can be acquired without ECG triggering. If doing so it is necessary to ensure that the inversion time is long enough so that that there is sufficient inflow into the area of interest – with pulsatile flow if the TI chosen is too short (shorter than the RR interval of the patient) there is the likliehood that a significant proportion of the acquired data is acquired without capturing an inflow event. To reduce this likelihood set the TI to be long enough to always include an inflow episode (eg 1200 to 1400 ms). Remember that the volume of non-inverted blood has to be large enough to fill all the small vessel branches.
Position the Body Matrix coil on the patient, so that both regions the kidneys and the diaphragm are covered. The respiratory gating is usually performed with the 1D PACE Navigator, alternatively the respiratory cushion can be used. All the protocols are set up in the reference mode. This is essential on the Siemens open bore systems MAGNETOM Espree and MAGNETOM Verio, to achieve a good signal-to-noise-ratio for the renal arteries and the navigator.
Position the laser marker in the middle of the renal hilum and the dome of the diaphragm. On the MAGNETOM Avanto, the examination can also be performed in the isocenter since the FOV in z-Axis is 50 cm. With software version *syngo* MR B17, a new functionality regarding the ECG display has been introduced. The learning cycle is demonstrated with a count-up mechanism, to show when the necessary 10 heartbeats are covered. The learning phase reduces the likelihood of inappropriate trigger detection, for example from artefacts due to the magneto-hydrodynamic effect.

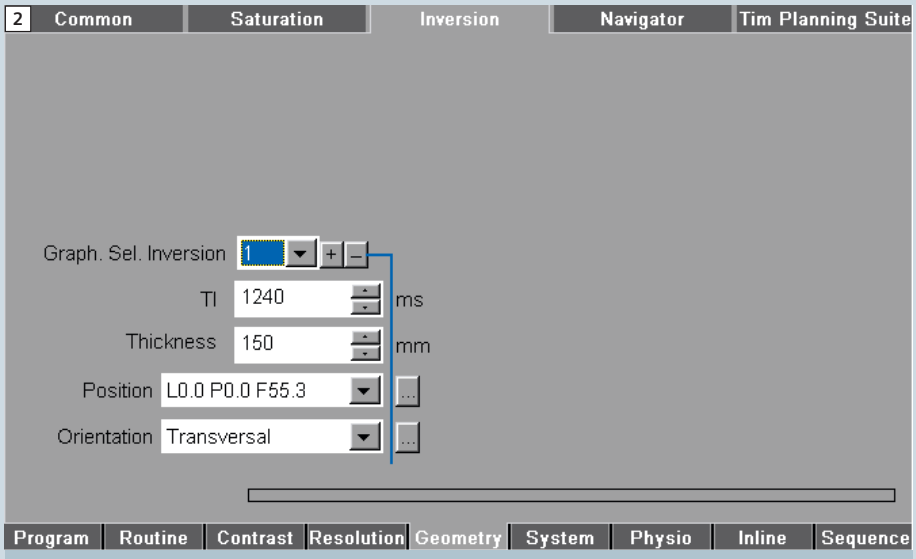


**2** "Inversion" Subcard

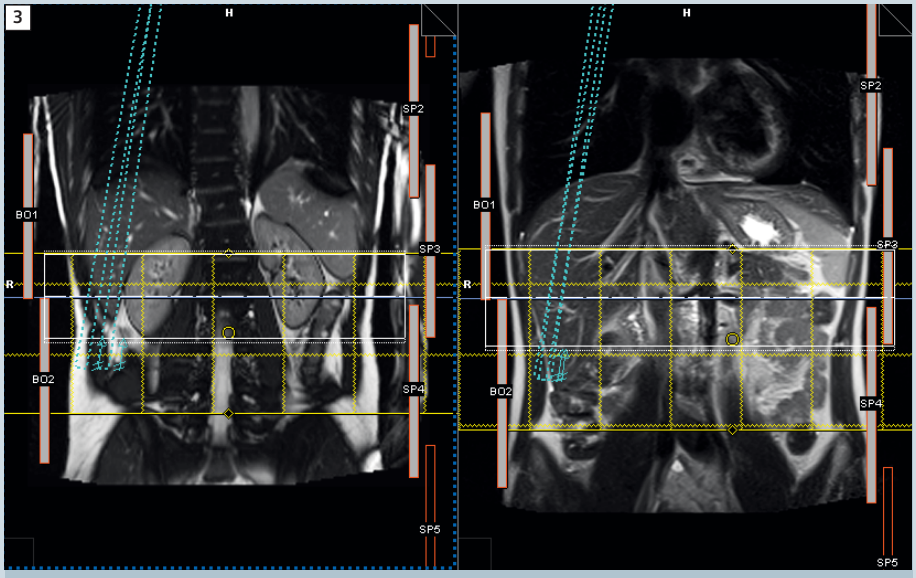


**3** Coronal localizers. The TrueFISP localizer (left image) is standard in the protocol set-up, the HASTE sequence (right image) can be used alternatively.

## Protocol set-up

The axial and coronal TrueFISP localizers are acquired as non-breath-hold examinations.
When opening the *syngo* NATIVE TrueFISP protocol, three graphical elements are shown, which have to be positioned correctly. We recommend to start with the navigator positioning, so that the center of the navigator is located at the dome of the diaphragm. Tilt the navigator beams, so that the signal intensity of the kidneys is not affected (compare Fig. 2).
The navigator has a new off-center readout support. If you shift the center of the navigator to the dome of the diaphragm, the respiratory trace, generated by the interface between the lung and liver, will be shown in the middle of the Inline Display. A scout mode is therefore no longer necessary. Due to the automatic tracing, the system will

detect the end expiration phase automatically. This new capability to off-center the navigator in the Z direction is essential for applications where the anatomy of interest is significantly offset from the diaphragm in the Z direction. Make sure that the coils for the kidneys, as well as for the navigator in z-axis direction, are selected.
The next step is to position the imaging FOV. Set the upper border of the FOV very close to the origin of the vessel of interest. Do not include too much proximal aorta in the FOV. To maximize the inflow effect, the upper limit of the inversion band should exactly match the upper limit of the FOV. This way, there will be no loss of signal of the inflowing, arterial blood. For the inversion pulse, a new graphical element has been designed and a new parameter subcard implemented into the UI (Fig. 3). The graphical element of the inversion pulse covers
a larger area inferiorly, to also saturate the inflowing blood from the veins and therefore, prevent the veins from causing unwanted signal in the images.
Finally, set the captured cycle. The maximization of the inversion time is automated within the sequence and there is usually no need to change this parameter. To verify this value, it can be checked on the Geometry-Inversion subcard.
The acquisition time is usually between 2–5 minutes, strongly depending on the heart rate and the breathing cycle of the patient. Monitor the navigator signal and the ECG- triggering during the measurement, to ensure a successful completion.

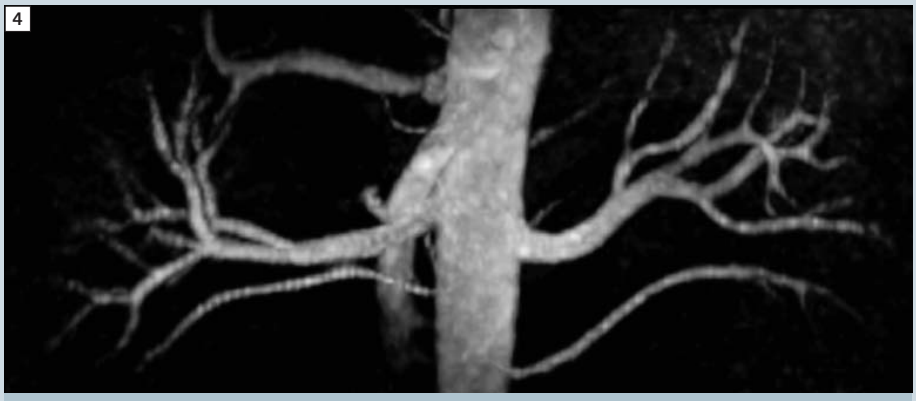

**4** Example of a *syngo* NATIVE TrueFISP MIP reconstruction (healthy volunteer).

## Postprocessing

Coronal and axial Maximum Intensity Projections (MIPs) are reconstructed Inline. For reconstruction of radial ranges, load the 3D dataset to the 3D-card and use the MIP and radial ranges button.
For further evaluation, the ThinMIP button can also be used and the volume adapted to the maximum possible. Figure 4 shows a radial ThinMIP reconstruction of a healthy volunteer.

## Challenges and possibilities

- Imaging of renal transplants: In the pelvis region motion artifacts due to breathing are not usually of great significance. Thus, the respiratory gating is not needed in this region. There is a dedicated protocol for this specific application in the Siemens Exam Explorer.
- In elderly patients or patients with a known heart failure, the stroke volume may not be sufficient to fill the complete arterial tree of the kidneys with fresh blood within one heart cycle. In this case longer TI values such as 1400 ms may be useful. The UI allows 1400 ms when both acquisition window and TR are long enough. Keep in mind, that this leads to a situation where every second trigger signal is used, while the value of the trigger pulse parameter remains 1 (Fig. 5).
- Patient is dehydrated: Elderly patients in particular tend to drink less, which can have a negative influence on the blood volume and flow. Ensure that the patient is well-prepared for the examination. Perhaps communicate that topic with the responsible medical doctor.
- ECG-signal is disturbed during the measurement. Try to position the ECG amplifier in the direction of the head rather than the feet.
- In some cases, the detection of the renal arteries may be difficult on the

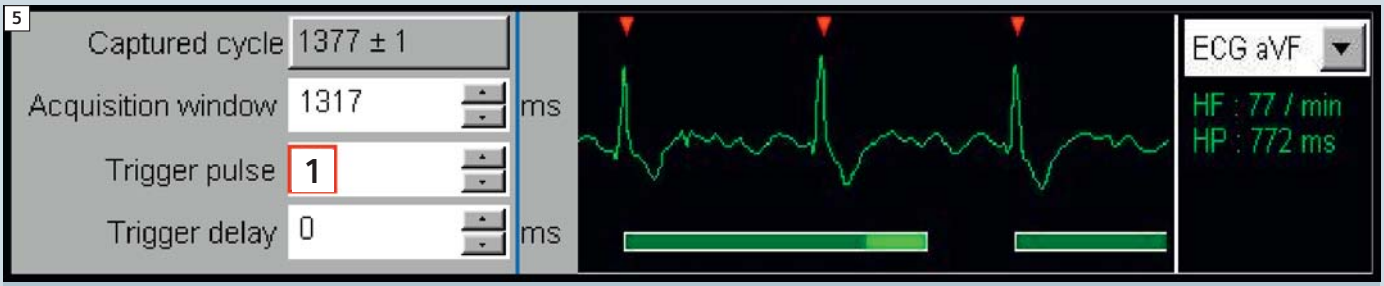


**5** Trigger settings for long TI values (every second trigger used).

TrueFISP Localizer. Alternatively, an axial and coronal multi-breath-hold HASTE sequence can be run.

## The theory behind *syngo* NATIVE SPACE

The *syngo* NATIVE SPACE sequence is a flow-sensitive 3D Turbo Spin Echo (TSE) sequence which allows fast scanning with high spatial resolution.
The sequence offers non-selective refocusing pulses and thus ultra-short echo-spacing.
The contrast of the *syngo* NATIVE SPACE sequence is based on the difference in the signal-intensity between static or slow-flowing blood (diastole) and fast-flowing blood (systole).
In diastole, the arteries appear bright (bright blood image). In systole, the arteries are dark (black blood image).
*syngo* NATIVE SPACE includes two measurements in one protocol, each with a different trigger delay. One measurement is acquired when the blood within the vessel is at its peak velocity, the other at its lowest velocity. The two images are subtracted voxel-wise, which removes background and venous signals, and the user is presented with immediate results (Inline subtraction and Inline coronal MIP). The Inline functionalities are chosen on the subcard Inline-Common. To manipulate the sensitivity to moving spins, different flow spoiling gradients can be selected.
The key to obtaining best image quality is to clearly identify the flow patterns in the R-R cycle. For this purpose, a cine FLASH sequence with a fairly high flip angle is used. The high flip angle enhances the in-flow effect.
Another important point is a stable ECG-signal, since the data must be collected consistently at the right time in the cardiac cycle. Therefore, ensure the correct positioning and preparation of the ECG device.

## Patient preparation

The patient is positioned feet-first supine. The protocol in the Siemens Exam Explorer is set up with the peripheral angiography coil and the upper spine coil elements. Position the laser marker on the centre of the lower leg.

## Protocol set-up

The standard exam consists of three protocols:

- a TrueFISP localizer including imaging of coronal and transversal slices
- a Cine_TDscout, and
- the NATIVE_SPACE_3D sequence.

The localizer starts automatically.
Position the FOV of the Cine_TDscout sequence transversely in the middle of the scan range. Use the captured cycle button to set the number of phases.
Load the images of the Cine_TDscout to the Mean Curve Application and draw a circle over an artery in each leg and begin the evaluation.
The scale on the curve image can be changed to Trigger Time, using the right mouse-button and selecting Scaling/Sorting.
Figure 6 shows a typical result of a healthy volunteer. In this case, you can easily identify the peak flow and the slow flow period.
The Cine_TDscout may also be used as a predictor for the chance of success. If the selected vessel does not show pulsatility in the flow pattern, it is very likely that the NATIVE SPACE technique will not provide enough contrast.
When running a multi-step protocol, it is beneficial to perform as many cine scouts as imaging steps. The trigger delay for each step may vary significantly (normally around 20–30 ms for each step). If a peripheral angiography with multiple steps is preferred, use the Tim Planning Suite and add as many steps as necessary. Figure 7 shows the

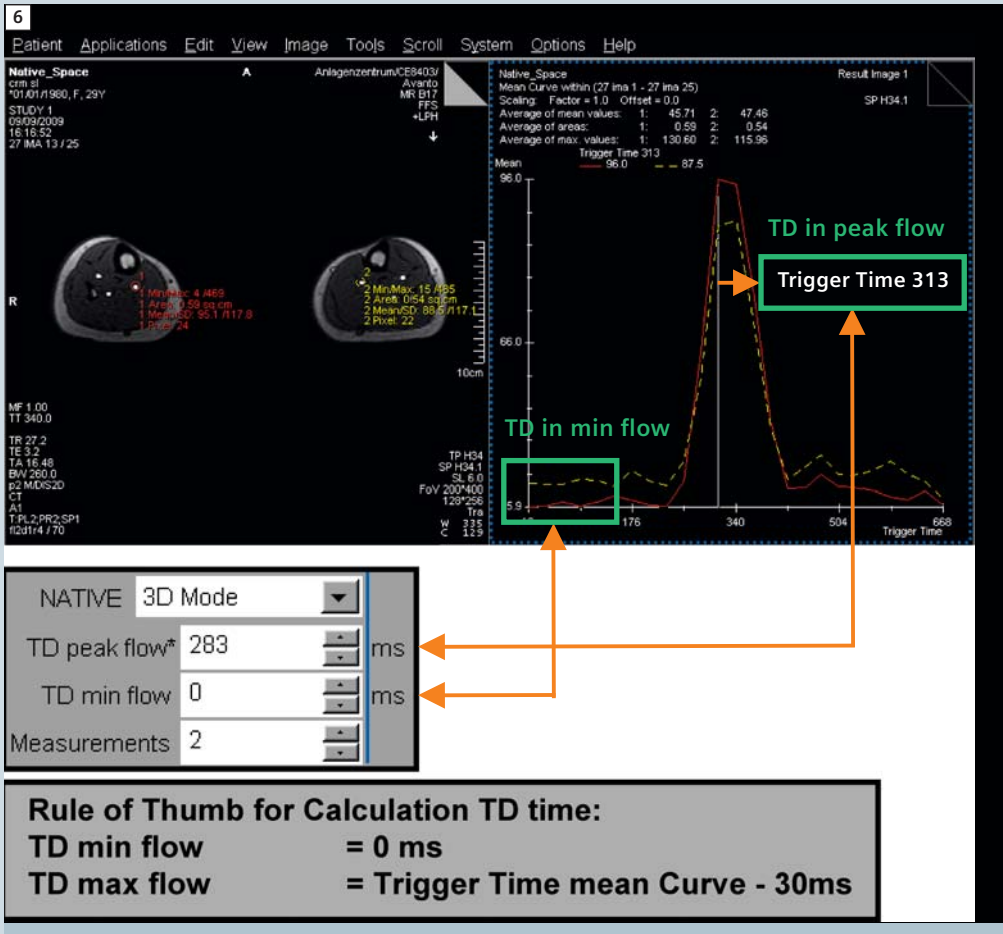


**6** Mean Curve Application within the *syngo* NATIVE SPACE protocol and calculation of the delay times.

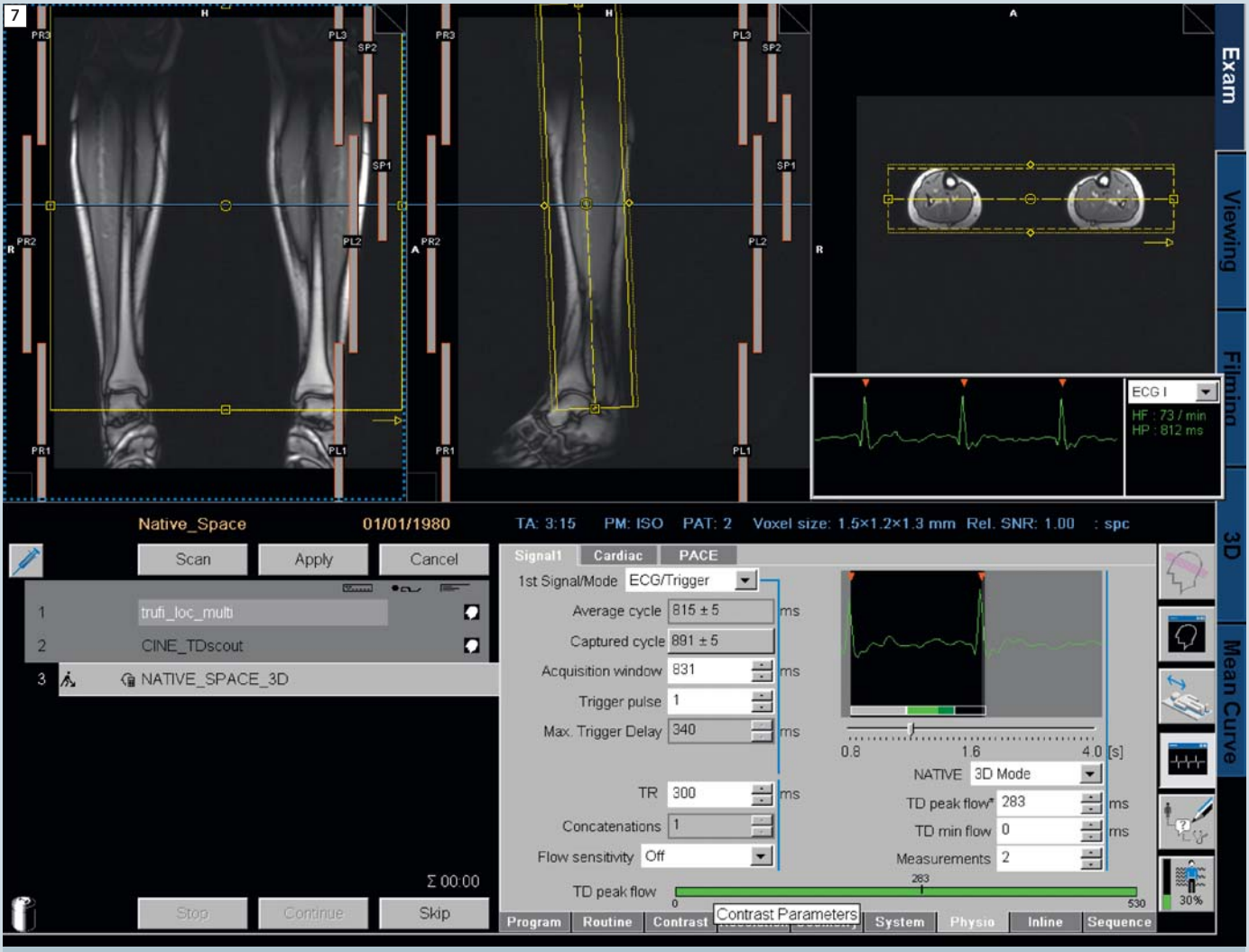


7 Planning of a single-step standard protocol in the lower leg region.

planning of a single-step standard protocol in the lower leg region.
Do not forget to adapt the time delay for the peak flow to the corresponding area. To set the Trigger Delay times for the peak and the minimum flow, open the 3D SPACE sequence on the Physio – Signal 1 subcard. We have good results by subtracting 30 ms from the peak trigger time in the Mean Curve Application, as shown in Fig. 6. In most cases, a trigger delay of 0 ms should be well-suited for the minimum flow acquisition.
During the scan remember to monitor the stability of the ECG.
As a result of the *syngo* NATIVE SPACE sequence, four different image series are displayed in the Viewing Card:

- Peak Flow image with dark arteries
- Min Flow image with bright arteries
- Inline subtraction showing arteries only, and
- Inline coronal MIP (Fig. 8).

## Postprocessing

Similar to the *syngo* NATIVE TrueFISP sequence, an Inline coronal MIP is reconstructed to give a first impression. For further manipulation, load the subtracted data to the 3D card. Comparable to the *syngo* NATIVE TrueFISP postprocessing, also try the ThinMip button for refinements. Figure 9 shows a multi-step MIP approach on a healthy volunteer.

## Challenges and Possibilities

- The method can be considered as robust even if contrast agent has already been applied. Therefore, the technique may be used as a backup, if a contrast-enhanced examination did not work out perfectly.
- If there are different blood transit times on each leg due to a severe stenosis in one extremity (seen on the Cine_TDscout images in the Mean Curve application card), consider running two measurements, each of them optimized for one leg.
- Reduced contrast behind stenosis due to lack of pulsatility of flow and high-grade change of direction: To enhance the flow sensitivity, work with the

8

8 Results derived from a *syngo* NATIVE SPACE non-ce MR angiography exam.

9

9 Coronal MIP of a multistep protocol.

extra flow sensitizing spoiler gradients. They support the collection of dark blood images since they additionally destroy the signal in moving blood. There are four different possibilities available (found on Physio-Signal1 subcard):

- **off –** means the normal way of using the flow-spoiling gradients as implemented in the *syngo* SPACE sequence. (Value between weak and medium.)
- **weak** – no flow-spoiling gradient used (Value = 0%)
- **medium** – higher flow sensitivity than "off", due to sophisticated spoiler gradients (Value = 25%)
- **strong** – highest flow sensitivity (Value = 50%)

## Conclusion

*syngo* NATIVE SPACE and *syngo* NATIVE TrueFISP do not claim to replace contrast-enhanced angiography, but are complementary methods in cases where contrast agent is not applied for different reasons or where the contrast technique did not turn out well.
With these techniques, the user can overcome known weaknesses of the non-contrast enhanced MR angiographies used to date and may improve the overall diagnostic value of the MRI examination.

**Contact**
Manuela Rick
Siemens Healthcare
MR CRM-SL
Postbox 32 60
91052 Erlangen
Germany
Phone: +49 (9131) 84-4126
manuela.rick@siemens.com

# *syngo* TimCT – Increasing Clinical Throughput and Efficacy

**K. Lederle, G. Weisser, S. O. Schoenberg, H. Michaely**

*Institute of Clinical Radiology and Nuclear Medicine, University Medical Center Mannheim, Mannheim, Germany*

The University Medical Center Mannheim is a large 1300-bed hospital with currently four clinical MR-units installed (MAGNETOM Trio, A Tim System, 2 x MAGNETOM Avanto, MAGNETOM Sonata). The MAGNETOM Trio, A Tim System and the MAGNETOM Avanto are fully equipped with 32 independent receiver channels and the *syngo* TimCT-Oncology and *syngo* TimCT-MRA suites. The TimCT-Oncology suite has been clinically evaluated as a standard imaging technique in abdominal and whole-body exams at the University Medical Center for approximately one year.

There are several disadvantages of traditional large z-axis field-of-view (FOV) imaging: Firstly, technologists have to plan every sequence separately stack-by-stack to cover a large z-axis FOV. This planning procedure is error-prone and time-consuming. This stack-wise procedure applies not only to the initial localizers but to every single weighting (T1 and T2) before and after contrast media application. Secondly, imaging with separate stacks increases the time needed for adjustment and shimming as this has to be done before every single sequence. Thus, the time efficiency of planning and scan time needs to be improved to enable the technologists to take care of administrative work such as billing or patient preparation.

*syngo* TimCT is a new approach of MRI imaging with continuous table movement with a continuous z-axis FOV of up to 1200 mm. Conventional imaging is limited to a single FOV of 400 to 500

1

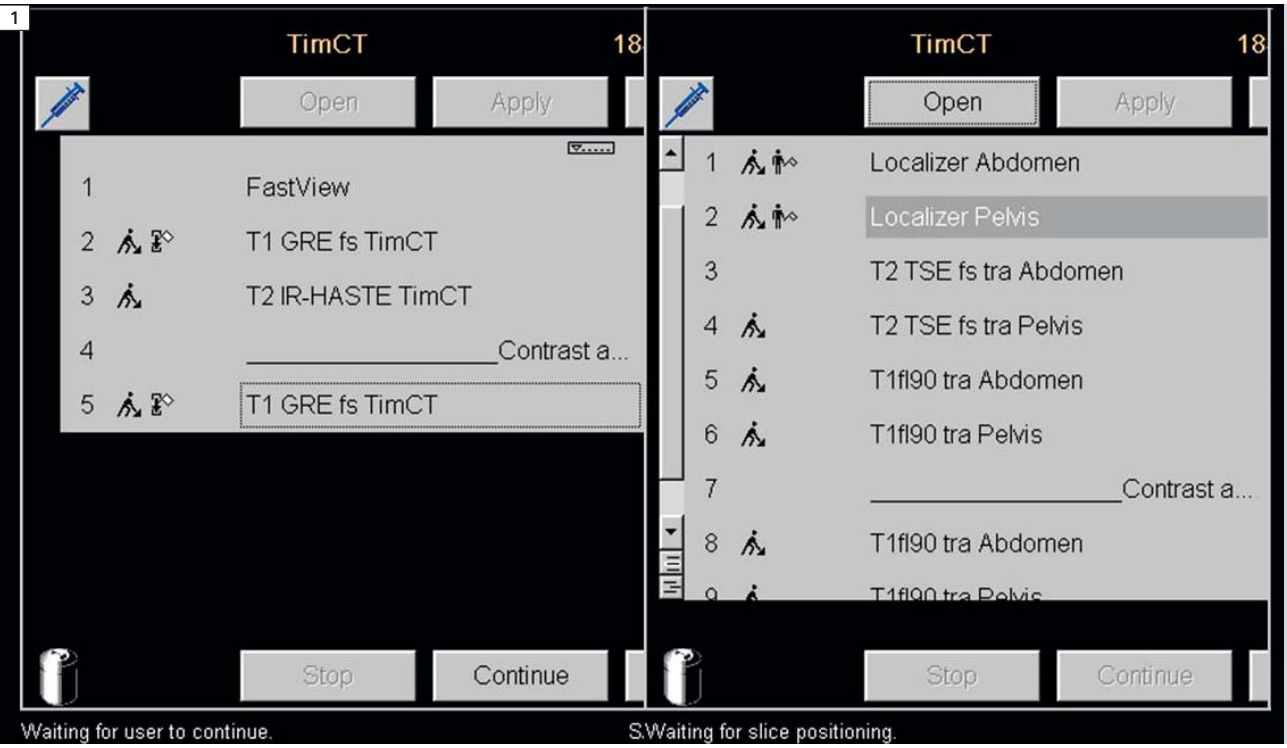


**1** Comparison between the planning of *syngo* TimCT-sequences (left) vs. traditional planning (right).

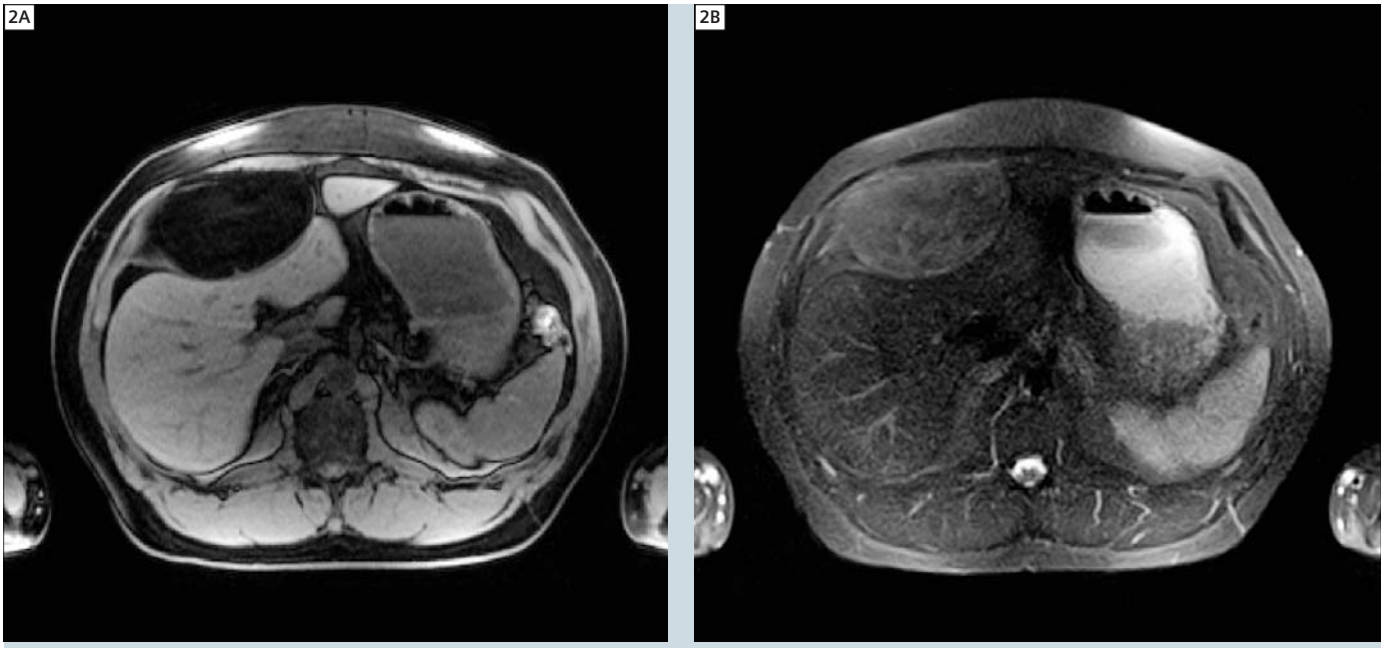


**2** Transversal T1 and T2-weighted images of a patient with liposarcoma within the transverse abdominal muscles.

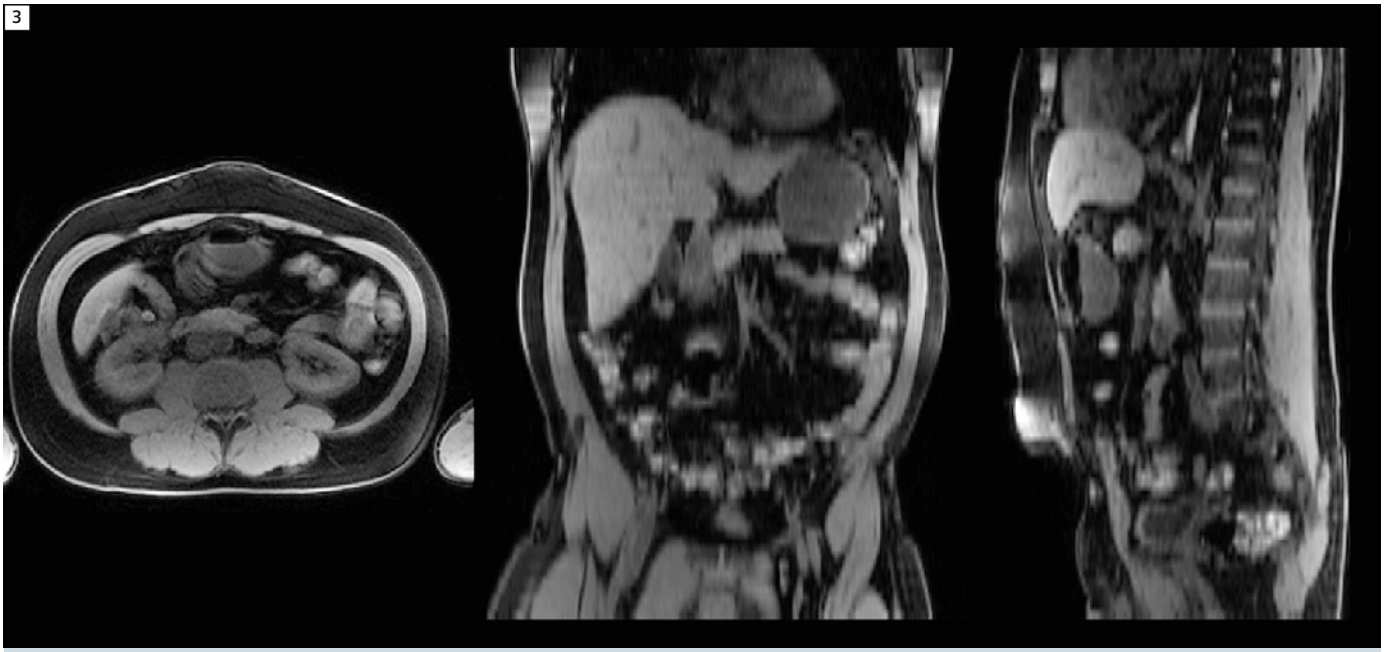


**3** Reformatted *syngo* TimCT T1-weighted series in orthogonal 3D-viewer, the coronary and sagittal reformation show only minor stairstep artifacts.

mm depending on the equipment used. Moreover, with *syngo* TimCT enables, for example, imaging of the abdomen and pelvis with only three sequences, compared to up to 6 sequences in traditional imaging (Fig. 1). Thus the time needed for planning of sequences or shimming is much shorter, resulting in a substantial improvement in workflow.

In our institution, the main indications for *syngo* TimCT are abdominal exams requiring a large field-of-view – for example, tumor staging or screening for malignant lymph nodes. While these exams seem to be typical Computed Tomography (CT)-indications, the increasing awareness of the potential harm of ionizing radiation particularly in young adults has led to a shift towards Magnetic Resonance Imaging (MRI). Typical clinical requests include follow-up of patients with lymphoma, Hodgkin's disease, testicular cancer or with abdominal discomfort of unknown origin. Many of these patients require follow-up exams on a regular basis, which makes the application of MRI even more favorable. Scanning these patients with the *syngo* TimCT technique yielded consistently good image quality (Fig. 2).

The protocol is very simple and includes a transversal fat-saturated T1w-GRE sequence before and after contrast administration (TR/TE 131 ms / 4.76 ms, spatial resolution 1.6 x 1.6 x 6 mm²) and a transversal inversion-recovery T2w *syngo* BLADE sequence (TR/TE 6790 ms / 127 ms, spatial resolution 1.3 x 1.3 x 6 mm²).

Dedicated exams of the liver or of the adrenal glands which require dedicated sequences including in- and opposed phase imaging as well as multiphasic dynamic imaging after contrast media application do not include *syngo* TimCT sequences at this time.

With the new *syngo* TimCT technique it is possible to acquire one set of data for the entire scan region which then can be reformatted within a 3D-viewer (Figs. 3 and 4). Depending on the sequence parameters chosen, the overall acquisition time can be reduced by 20–30% in abdominal studies and by up to 50% for whole-body examinations in patients with multiple myelomas, according to initial results. While the spatial resolution of *syngo* TimCT is currently slightly inferior to that of dedicated step-by-step whole-body programs our initial results suggest that the number of reported lesions is equal for both approaches. This reduction of overall acquisition time has led to a higher clinical throughput, as up to four additional patients* can now be examined each day.

Overall, *syngo* TimCT-Oncology is a further substantial improvement in body MRI. It enables us, to cover a large z-axis FOV with a single slab and is hence very easily planned as well as very time-efficient. Good clinical indications for *syngo* TimCT-Oncology in the abdomen are staging of lymphomas and oncologic follow-up exams in young patients.

In the future, further improvements of the technique are expected to allow for true three-dimensional imaging and further automization of the acquisition.

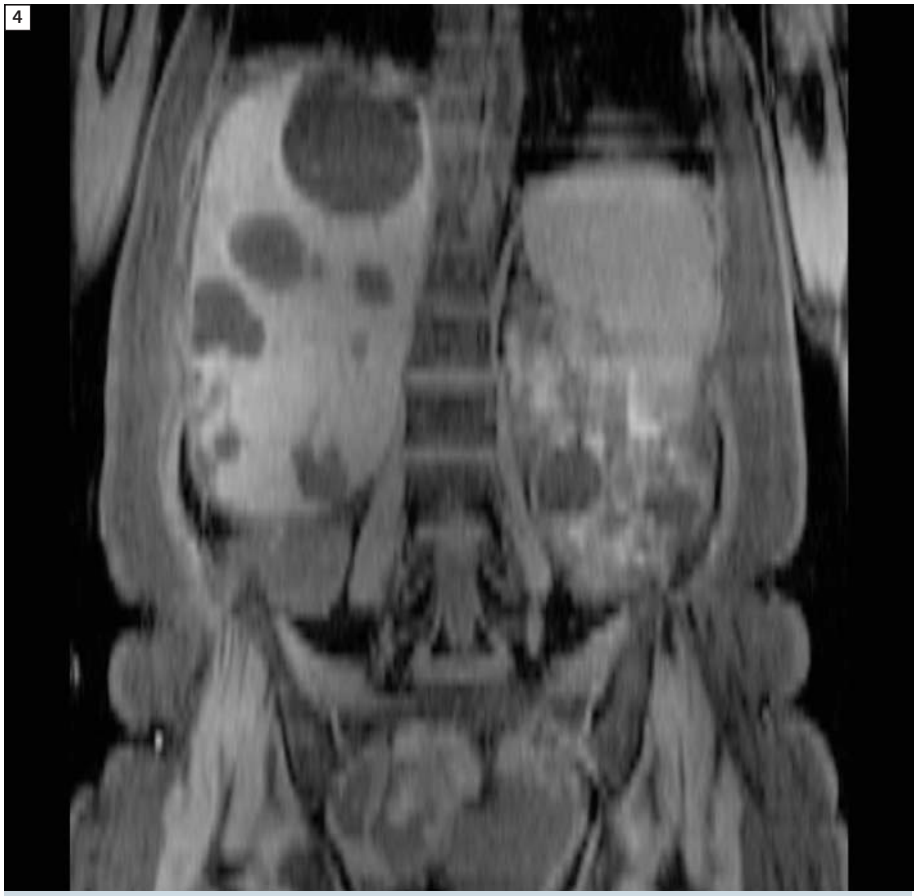

**4** Reformatted coronary view (T1w, slice thickness 6 mm) with multiple renal and hepatic cysts.

*Results may vary. Data on file.

**Contact**
Henrik J. Michaely, M.D.
Associate Professor of Radiology
Section Chief Abdominal
and Vascular MRI
Institute of Clinical Radiology and
Nuclear Medicine
University Medical Center Mannheim
Theodor-Kutzer-Ufer 1–3
68167 Mannheim
Germany
henrik.michaely@umm.de

# Try them on your system

Trial licenses for most of the applications featured in this issue of MAGNETOM Flash are available free of charge for a period of 90 days: Please contact your local Siemens representative for system requirements and ordering details or visit us online* at **www.siemens.com/discoverMR** for further details, product overviews, image galleries, step-by-step demos, case studies and general requirement information.

*Direct link for US customers:
**www.siemens.com/WebShop**
Direct link for UK customers:
**www.siemens.co.uk/mrwebshop**

1 High resolution time-resolved 3D MRA with *syngo* TWIST (page 14).

2 Non-contrast MRA with *syngo* NATIVE TrueFISP (page 15).

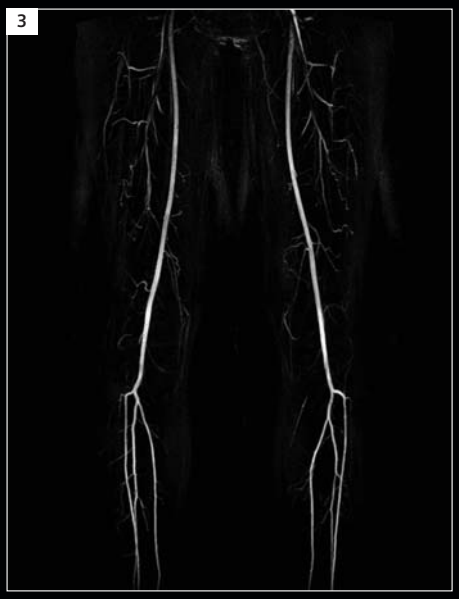

3 Non-contrast MRA and automatic composing from different table positions with *syngo* NATIVE SPACE and *syngo* Inline Composing (page 23).

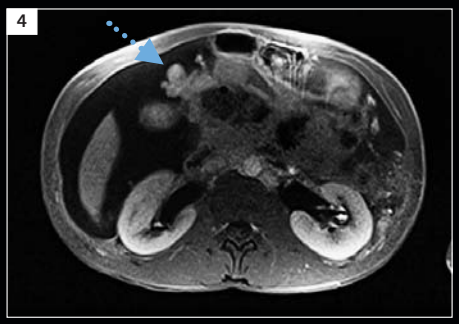

4 Continuous table movement for motion insensitive whole-body imaging *syngo* TimCT Oncology and *syngo* BLADE (page 29).

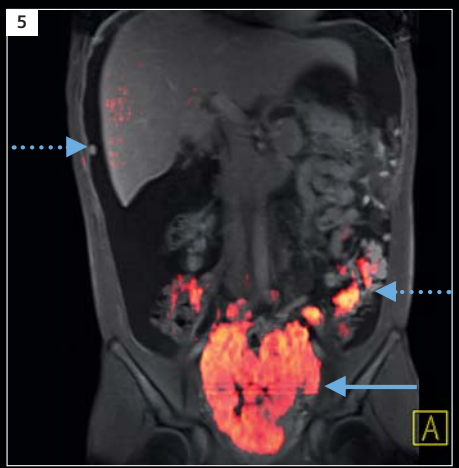


5 Spatial alignment and visualization for images from different modalities or multimple examinations with *syngo* Image Fusion (page 31).

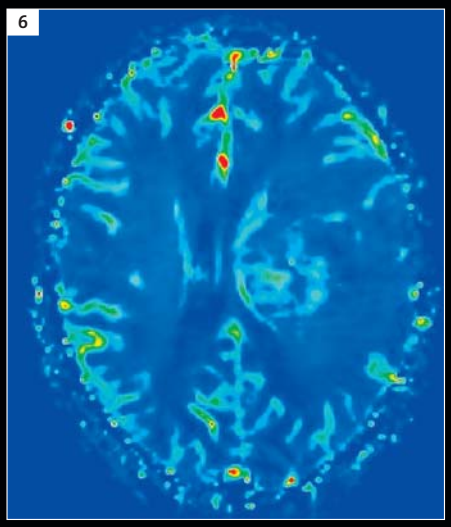

6 Non-contrast perfusion evaluation with *syngo* ASL (page 68).

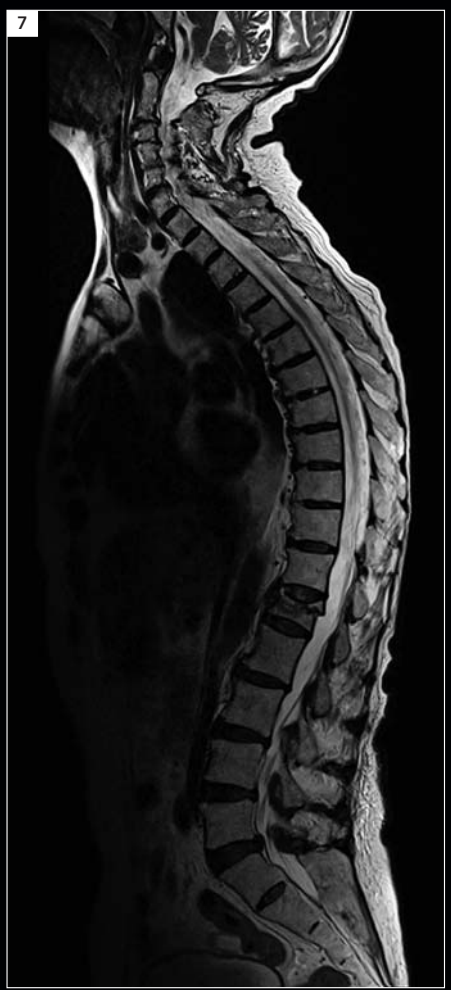

7 Composing of images from different table positions to show the complete anatomy with *syngo* Composing (page 96).

# Case Report: Comprehensive Staging of the Abdomen and Pelvis with *syngo* TimCT Oncology in a Patient with Metastatic Hepatoid Carcinoma of the Prostate

**Henrik J. Michaely, M.D.**

*Institute of Clinical Radiology and Nuclear Medicine, University Medical Center Mannheim, Mannheim, Germany*

The evaluation of the tumor load in a case of peritoneal metastatic spread is still a domain of computed tomography (CT), mainly because of its availability in daily clinical routine and also because of the short examination times. However, within recent years evolving MR techniques and especially developments in coil design (Tim technology), parallel imaging (iPAT) and continuous table movement MR imaging (*syngo* TimCT) have enabled the evaluation of large parts of the body within a reasonable examination time. Additionally, relatively motion-insensitive MR techniques like the HASTE sequence and *syngo* BLADE help to acquire high-quality images not only of motion artefact prone tissue like the bowel but also in cases of patients with impaired condition who are hardly able to follow breathhold commands. Despite the intrinsic superior soft-tissue contrast of MRI compared to CT, diffusion-weighted imaging (DWI) adds functional information about the cellular packing density of tissues yielding an improved diagnostic accuracy, not only for tumor detection but also characterization. As a consequence, MRI of the abdomen can now also be considered an alternative to CT in daily clinical practice.

## MR protocol

The MR protocol used in our department (1.5T MAGNETOM Avanto) for a fast and yet accurate assessment of potential metastatic spread in the abdomen comprises the following steps:

1. Continuous table movement T2w TSE with *syngo* BLADE (*syngo* TimCT) ranging from the diaphragm to groin (TR/TE 5460/111 ms, scan speed 3 mm/sec, PAT 2, TA 3:11min)
2. Multi-step EPI Spin Echo DWI (TR/TE 3780/76 ms, b-values 50 and 800 s/mm², spectral fat suppression, ADC maps generated by the scanner's Inline function, PAT 2, TA 7:11min)
3. Continuous table movement pre- and post-contrast 2D T1w FLASH with spectral fat suppression (*syngo* TimCT) from the diaphragm to the groin (TR/TE 130/2.38 ms, scan speed 8 mm/sec, PAT 2, TA 1:11min)
4. Dynamic contrast-enhanced coronal 3D T1w VIBE covering the whole abdomen with spectral fat suppression (TR/TE 4.79/1.72 ms, PAT 2, TA 0:18 min)

Depending on body size, the average imaging time for the abdomen with this protocol is 15–18 minutes.

## Case

A 32-year-old male was referred to our institution because of hydronephrosis (asterisk on the MR images) caused by a large tumor in the pelvis which was thought to be a rhabdomyosarkoma of the prostate. In the MR-images, a multilobular confluent large mass within the pelvis is seen (arrows). No differentiation between the tumor and the prostate is possible anymore. This mass displaces not only the bladder but also the rectum. In addition, a large amount ascites is present in all quadrants of the abdomen. Large tumor nodules (dotted arrows) can also be found within the omentum without signs of small or large bowel obstruction. A mild spleenomegaly can be appreciated. Small metastases

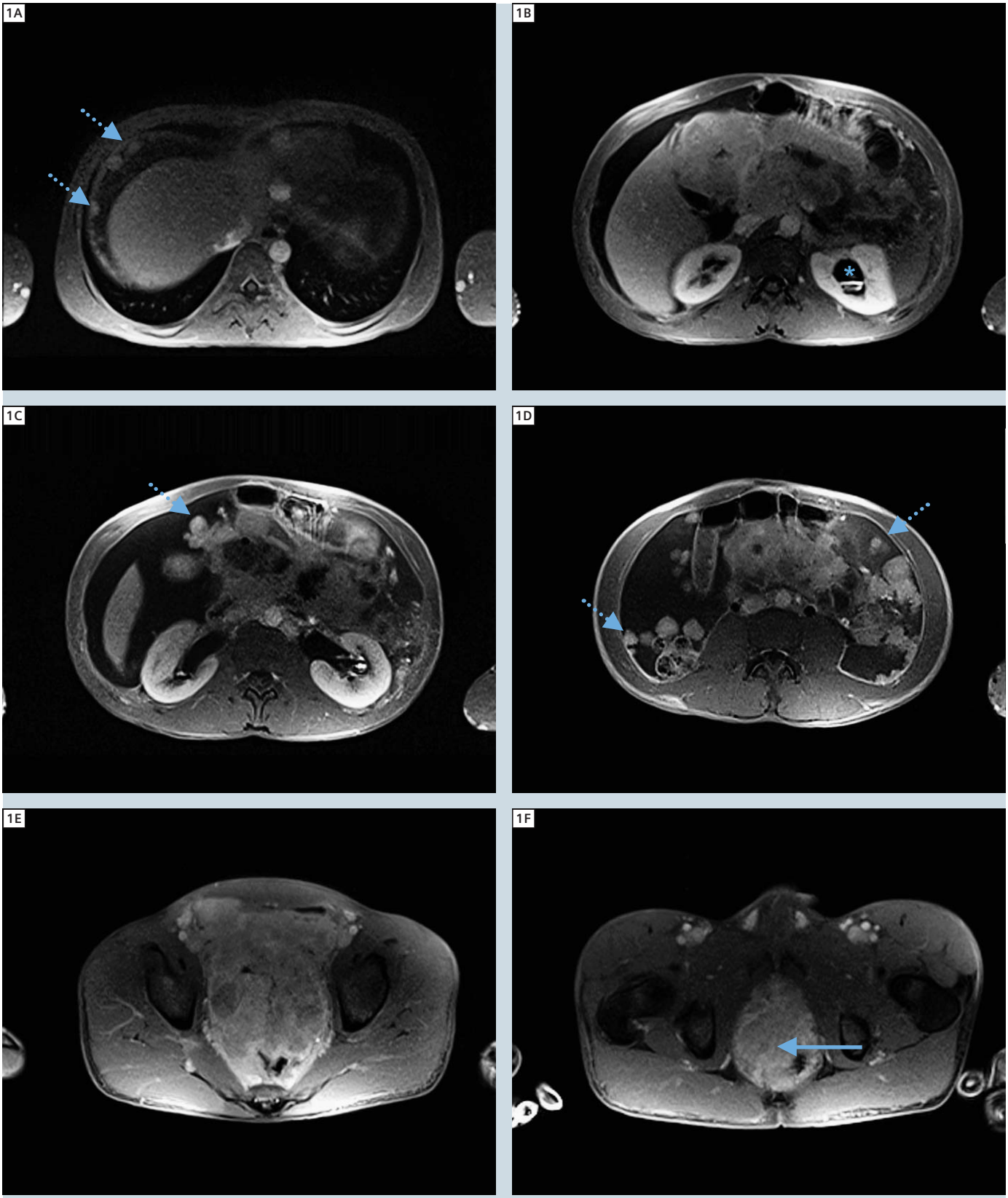


**1A–1F** Contrast-enhanced T1-weighed *syngo* TimCT examination.

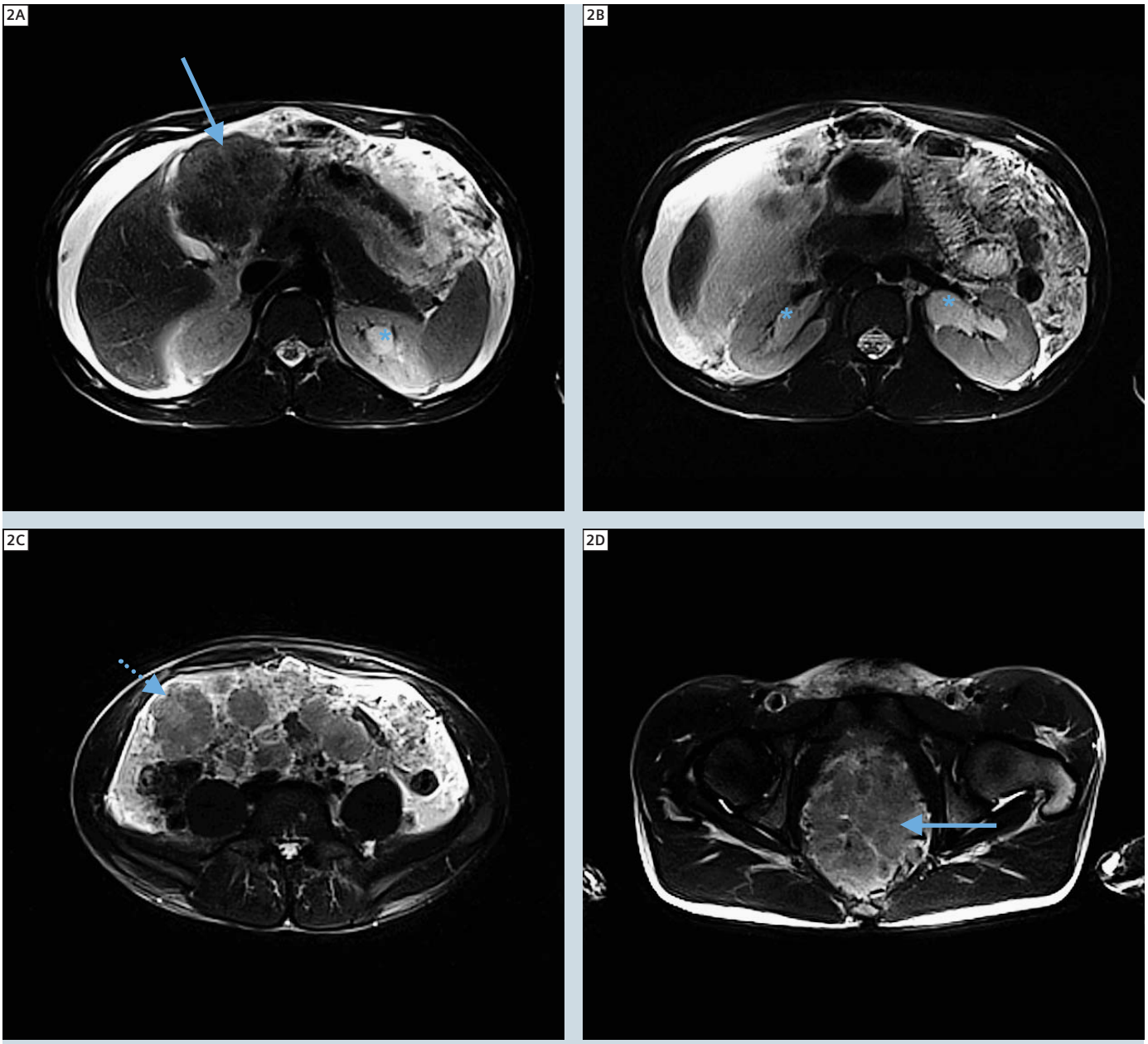


**2A–2F** T2-weighted TSE *syngo* TimCT examination with *syngo* BLADE motion correction.

can also be found subdiaphragmally. There is also contrast-enhancement of the peritoneum as another sign of diffuse peritoneal tumor spread. A large nodular mass at the caudomedial border of the left liver lobe with direct contact to the falciform ligament is seen (arrow in Fig. 2A). This nodule has slightly different signal intensity compared to the other tumor metastases. No further lesions can be seen in the liver, bones and basal lung. After this examination, a CT-guided biopsy of the large pelvic mass was performed which revealed a rare case of a hepatoid carcinoma of the prostate.

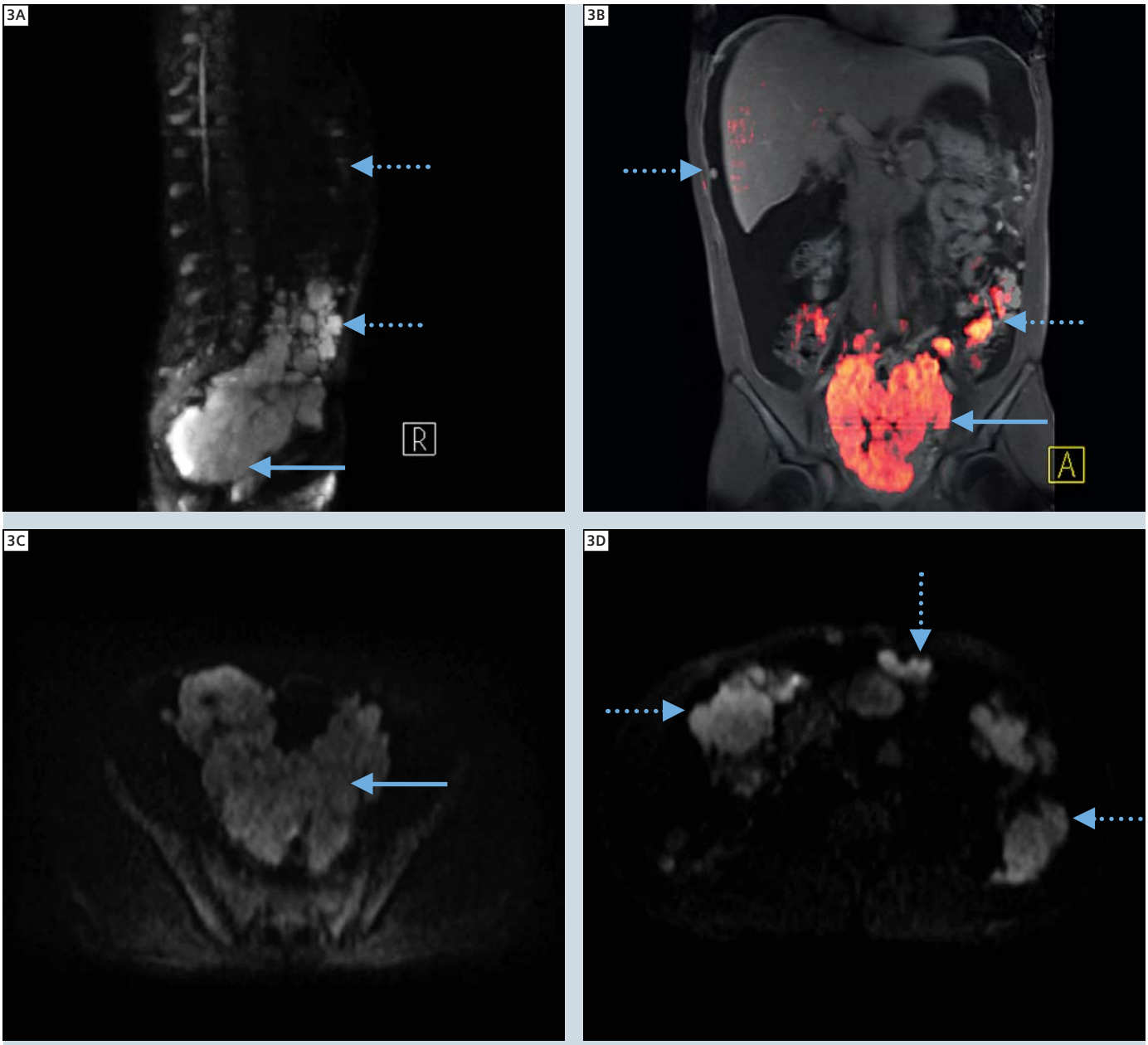


**3A–3D** Multi-step diffusion-weighted imaging (DWI): **A:** Sagittal reformation of the b = 800 s/mm² images. **B:** Superimpose high b-value image on contrast-enhanced single-step 3D T1w FLASH image (with spectral fat suppression). **C, D:** Original transversal high b-value images.

**Contact**
Henrik J. Michaely, M.D.
Associate Professor of Radiology
Section Chief Abdominal and Vascular MRI
Institute of Clinical Radiology and
Nuclear Medicine
University Medical Center Mannheim
Theodor-Kutzer-Ufer 1–3
68167 Mannheim
Germany
henrik.michaely@umm.de

# Case Report:
# MRI-guided Prostate Biopsy in a Patient with Prior Negative TRUS-Guided Biopsies and Persistently Elevated PSA-Levels

**Matthias Philipp Lichy, M.D., MSc[1]; David Schilling, M.D.[2]; Matthias Röthke, M.D. MSc[1]; Phillip Aschoff, M.D.[1]; Karl Sotlar, M.D.[3]; Christina Pfannenberg, M.D.[1]; Heinz-Peter Schlemmer, M.D., Ph.D.[1]**

*Departments of Diagnostic and Interventional Radiology[1], Urology[2], Pathology[3], Eberhard-Karls-University Tuebingen, Germany*

**1** Coronal reformation of the initially performed 11C-Choline PET-CT.

With the widespread introduction of prostate-specific antigen (PSA) testing, the characteristics of prostate cancer (PCa) patients have changed dramatically in the last fifteen years in favor of individuals with organ-confined disease. Histological confirmation of PCa remains essential for initiating therapy but, unfortunately, repeated negative prostate biopsies are not uncommon. Only 25–40% of all men with a PSA-level between 4 and 10 ng/ml are reported to have PCa, and therefore cancer detection rates by conventional prostate biopsy are low in this patient cohort [1]. Additional rounds of TRUS-biopsies in case of former negative prostate biopsies do not seem to improve cancer detection rates in patients with persistently elevated PSA-levels significantly. In fact, on first, second, third and fourth round, detection rates of a PCa have been reported to be only 14–22%, 10–15%, 5–10%, and 4%, respectively [2, 3]. Endorectal magnetic resonance imaging (endoMRI) is the most sensitive imaging method for detection and localization of PCa. In contrast to guided transrectal ultrasound (TRUS) prostate biopsy, MRI-guided biopsy offers the possibility to integrate metabolic and functional information and to perform prostate biopsy with direct control of the probe placement [4]. MRI-guided biopsy can be used to increase cancer detection rate after a negative TRUS-biopsy [5–7].

## Case report

A 65-year-old man was referred to our institution for combined whole-body (wb) [$^{11}$C]-Choline positron-emission-tomography for tumor screening after two negative sessions of TRUS prostate biopsies and persistently elevated PSA-levels over a period of 27 months (PSA at the time of presentation was 6.37 ng/ml, the estimated prostate volume was 45 cm$^3$). PET-CT revealed focal pathologic tracer uptake in the right dorsal peripheral gland. An endoMRI for planning an eventual MRI-guided biopsy of the prostate was recommended and performed 20 days after the PET-CT. EndoMRI at 1.5 Tesla (MAGNETOM Sonata, Siemens Healthcare, Erlangen, Germany) showed a corresponding suspicious area in the right very lateral peripheral gland with a maximal diameter of 1.1 cm. MR spectroscopic imaging (3D MRSI) was additionally performed, but no suspicious elevation of the (Cho+Cr)/Ci ratio was found in the suspicious area. The time-interval between endoMRI and MRI-guided prostate biopsy was 13 days. MRI-guided biopsy was performed at 1.5 Tesla MR scanner without use of an endorectal coil (MAGNETOM Avanto, Siemens Healthcare, Erlangen, Germany).

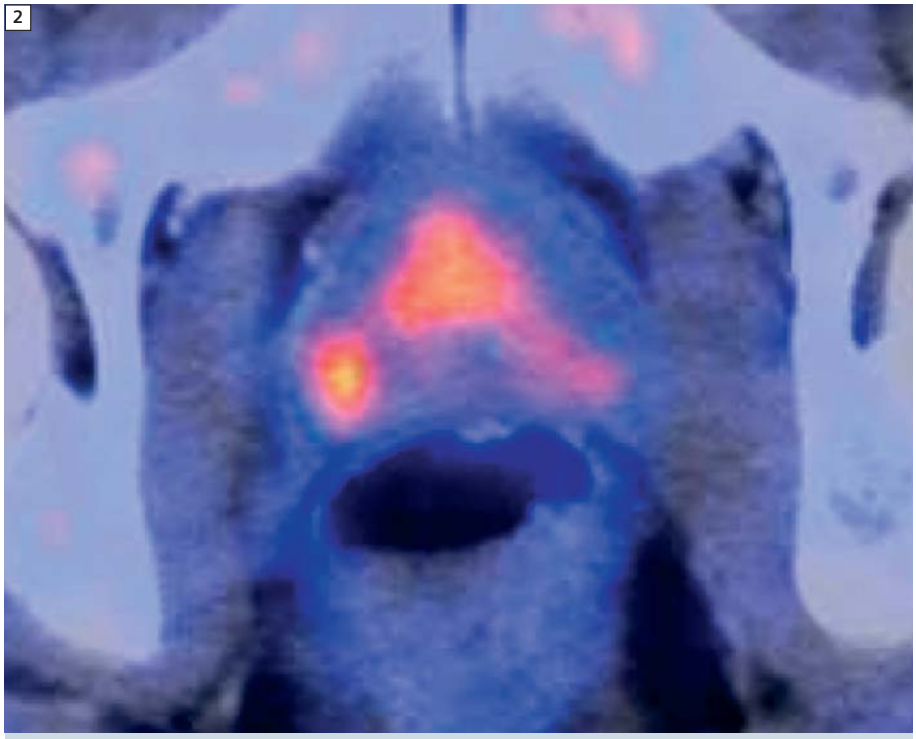

**2** Fused PET/CT, revealing a focal and therefore suspicious area within the right, very lateral peripheral gland.

T2w imaging was used for guidance of the 18-gauge fully automatic biopsy gun (TSK Laboratory, Japan/MRI Devices Daum GmbH, Schwerin, Germany). For fixation and adjustment of the needle, a biopsy devise described by Beyersdorff, et al. [1] was used (Invivo Daum GmbH, Schwerin, Germany). Diffusion-weighted imaging (*syngo* REVEAL) with high b-values at the time point of the biopsy showed a restriction of water mobility in the suspicious area. MRI-guided biopsies of the medial parts of the suspicious lesion could be performed. A total of 3 specimens from this area and additionally one specimen for coverage of the contralateral peripheral gland were taken during the MR intervention. Histological examination of routinely processed formalin-fixed and paraffin-embedded biopsy specimen revealed the infiltrates of a moderately differentiated tubular adenocarcinoma (Gleason score 2 + 3 = 5) in all 3 guided biopsy specimens Figure 6 shows one of the three biopsy specimens with infiltration of moderately differentiated tubular adenocarcinoma; anti-cytokeratin 5/6 immunostaining highlighting some non-neoplastic glands with ck 5/6-positive basal cells; non-neoplastic and neoplastic glands are shown, the latter with enlarged nuclei and prominent nucleoli; low proliferative activity with Ki-67 (clone Mib1).

**3** High-resolution T2w TSE, acquired at 1.5T with an endorectal coil, demonstrates a small circumscribed lesion with correlation to the PET finding.

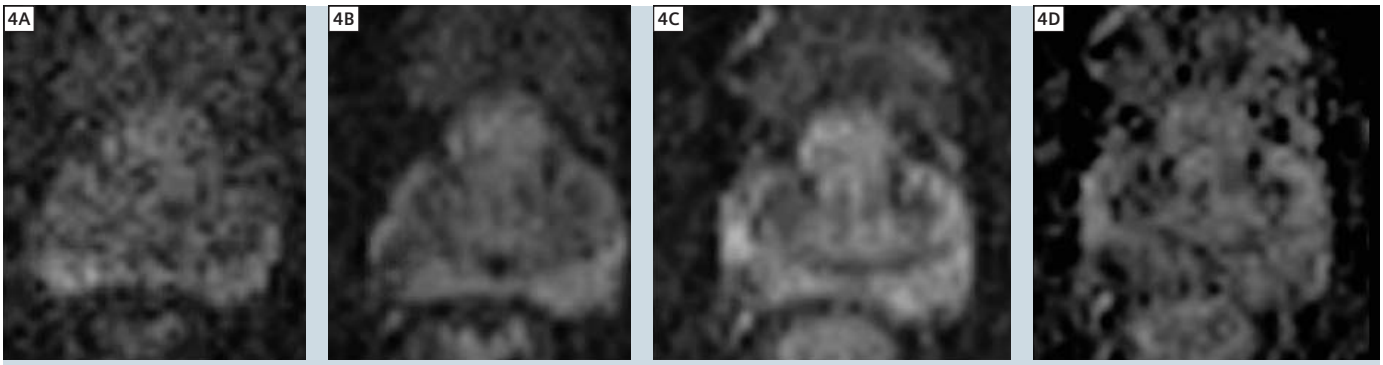


**4** DWI measured with a 3-scan trace technique showing a clear restriction of water diffusion of the lesion (from right to left: b = 1000/400/0 s/mm², ADC map).

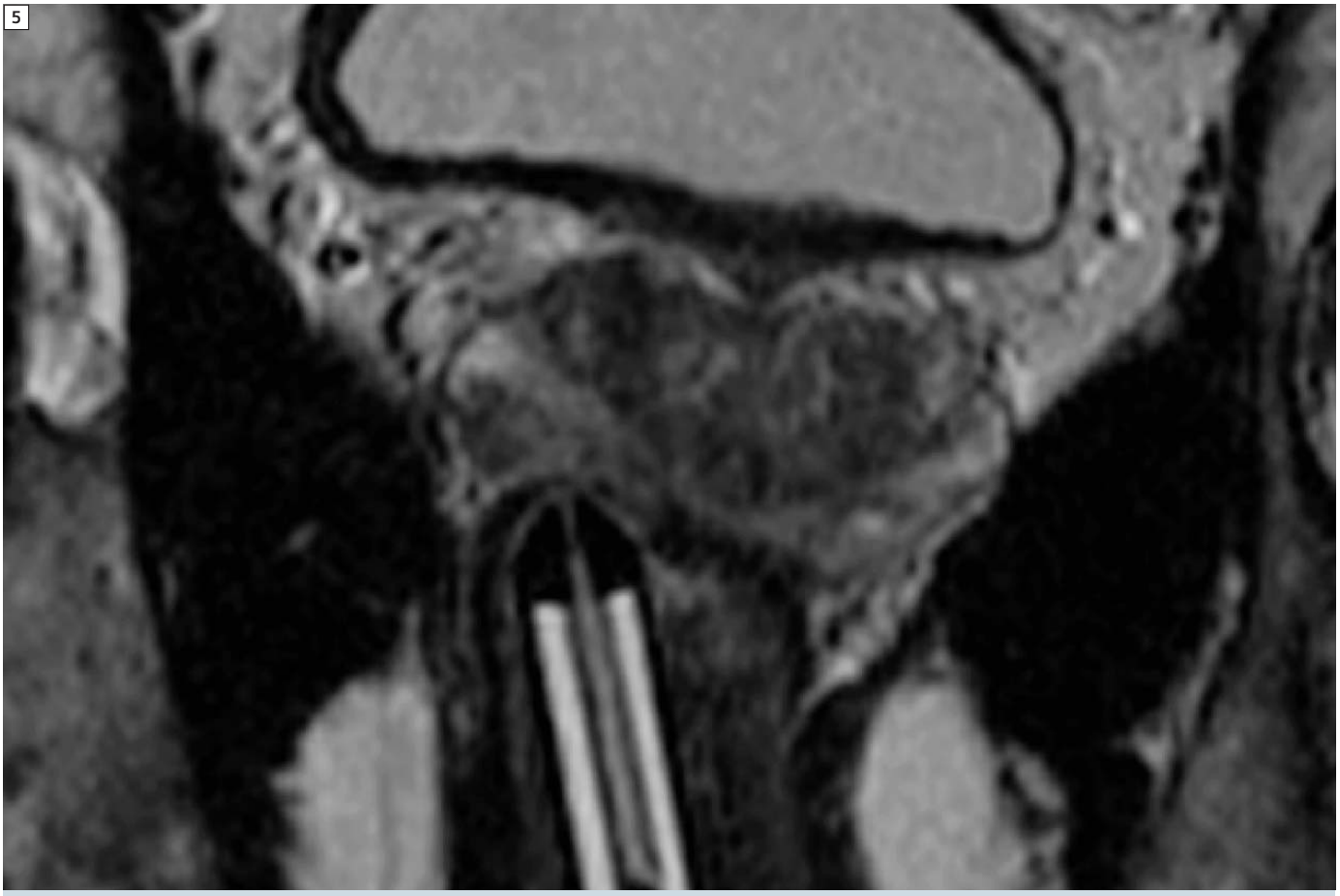


**5** T2w TSE for intervention planning; the transrectal inserted needle guide points directly to the medial portion of the suspicious lesion (image acquired at 1.5 Tesla with a combination of the Tim Spine and Body Matrix coil and without use of an endorectal coil).

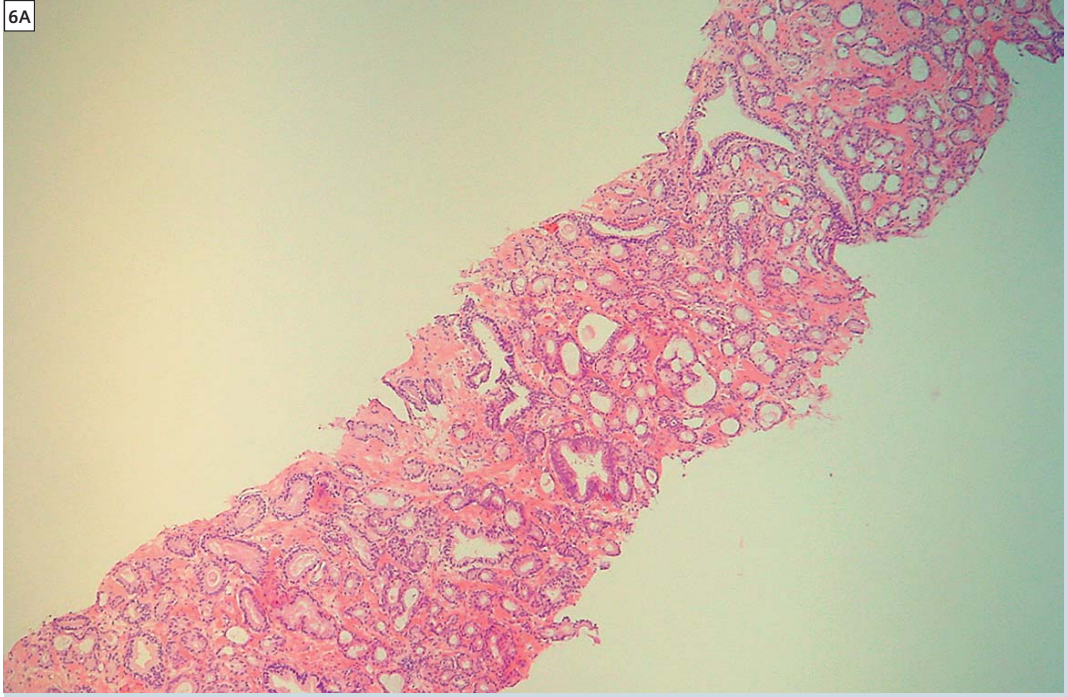

**6A** Histology specimen demonstrating infiltrates of a moderately differentiated tubular adenocarcinoma (Gleason score 2 + 3 = 5).

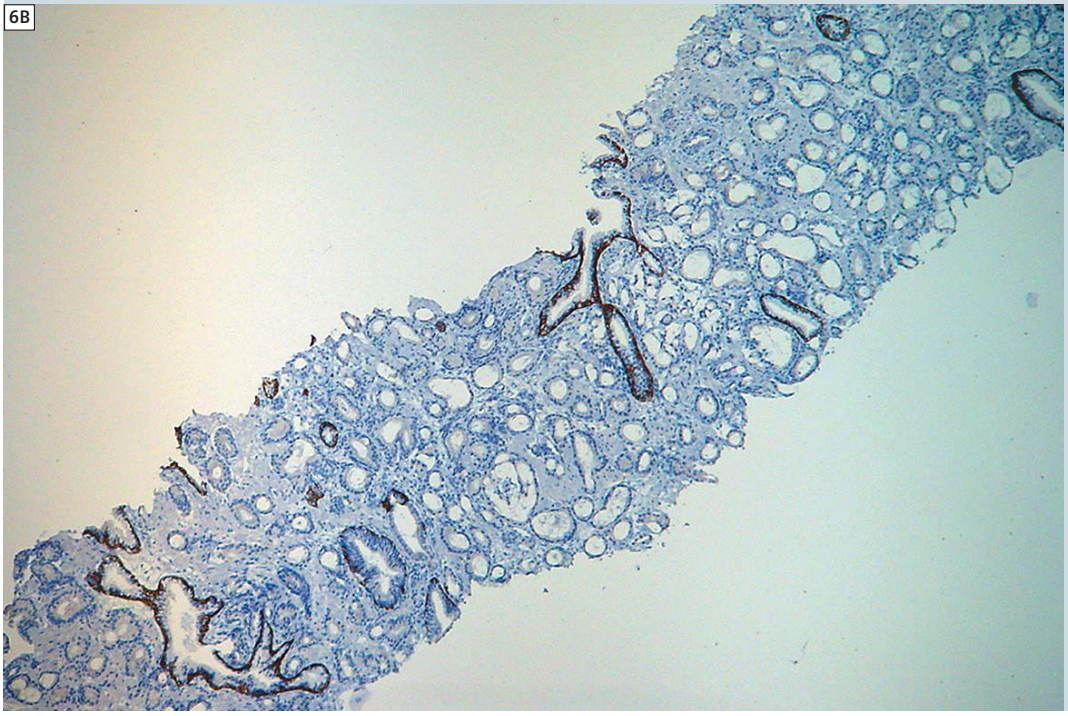

**6B** Anti-cytokeratin 5/6 immunostaining highlighting some non-neoplastic glands with ck 5/6-positive basal cells.


References

1 Catalona WJ, Smith DS, Ratliff TL, Dodds KM, Coplen DE, Yuan JJ, Petros JA, Andriole GL. Measurement of prostate-specific antigen in serum as a screening test for prostate cancer. N Engl J Med. 1991; 324(17):1156-61. Erratum in: N Engl J Med 1991; 325(18):1324.

2 Djavan B, Milani S, Remzi M. Prostate biopsy: who, how, and when. An update. Can J Urol 2005; 12 Suppl1: 44-8.

3 Lujan M, Paez A, SAntonja C, Pascual T, Fernandez I, Berenguer A. Prostate cancer detection and tumor characteristics in men with multiple biopsy sessions. Prostate Cancer Prostatic Dis 2004; 7: 238-42.

4 Beyersdorff D, Winkel A, Hamm B, Lenk S, Loening SA, Taupitz M. MR imaging-guided prostate biopsy with a closed MR unit at 1.5 T: initial results. Radiology. 2005; 234(2):576-81.

5 Anastasiadis AG, Lichy MP, Nagele U, Kuczyk MA, Merseburger AS, Hennenlotter J, Corvin S, Sievert KD, Claussen CD, Stenzl A, Schlemmer HP. MRI-guided biopsy of the prostate increases diagnostic performance in men with elevated or increasing PSA levels after previous negative TRUS biopsies. Eur Urol. 2006 Oct;50(4):738-48; discussion 748-9. Epub 2006 Mar 24.

6 Engelhard K, Hollenbach HP, Kiefer B, Winkel A, Goeb K, Engehausen D. Prostate biopsy in the supine position in a standard 1.5-T scanner under real time MR-imaging control using a MR-compatible endorectal biopsy device. Eur Radiol. 2006 Jun;16(6):1237-43. Epub 2006 Feb 1.

7 Pondman KM, Fütterer JJ, ten Haken B, Schultze Kool LJ, Witjes JA, Hambrock T, Macura KJ, Barentsz JO. MR-guided biopsy of the prostate: an overview of techniques and a systematic review. Eur Urol. 2008 Sep;54(3):517-27. Epub 2008 Jun 12. Review.



**Contact**
Matthias Lichy, M.D.
Siemens Healthcare
MR CRM MK CCA
Phone: +49 (9131)84-3266
Matthias.lichy@siemens.com

# Intravoxel Incoherent Motion (IVIM)*: A Potential Application in Cirrhosis Assessment

**Alexandre Vignaud, Ph.D.[1]; Alain Luciani, M.D., Ph.D.[2]; Alain Rahmouni, M.D.[2]**

[1] *Siemens Healthcare, Saint Denis, France*
[2] *Service de Radiologie, Centre hospitalo-universitaire Henri Mondor, Assistance Publique-Hopitaux de Paris, Université Paris XII Créteil, France*

## Introduction

In 1988 Le Bihan et al. [1] defined intravoxel incoherent motion (IVIM) as the microscopic translational motions that occur in each image voxel in Magnetic Resonance (MR) imaging. In biological tissues these motions include molecular diffusion of water and microcirculation of blood in the capillary network. Microcirculation of the blood in capillary network, also called "perfusion", can also be considered as an incoherent motion since the capillary organization can be seen at the voxel size as random.
These two phenomena account for the bi-exponential decay of the signal observed on diffusion-weighted imaging (DWI) when different diffusion b-values are applied. The IVIM sequence allows the extraction of two diffusion coefficients, one related to molecular diffusion restriction, D, another related to the tissue perfusion called D* and finally the vascular volume fraction f.
In their seminal paper Le Bihan et al. wrote: "Thoracoabdominal studies were not possible at the time of this work, due to motion artifacts and signal-to-noise ratio (SNR) considerations". The sequence used could only allow cardiac gating. Long TE was necessary to achieve the highest b-value needed for the study, while T2 relaxation in abdominal tissue is shorter than in the brain [2] leaving very low signal left. Strong gradient amplitudes could not be used because Eddy current was not sufficiently compensated on their scanner at this time.
Nowadays, diffusion-weighted (DW) Echo Planar Imaging (EPI) sequence, available on MAGNETOM MR scanners, allows both respiratory gating using a pneumatic belt, or more recently, a navigator. Eddy currents are now well compensated

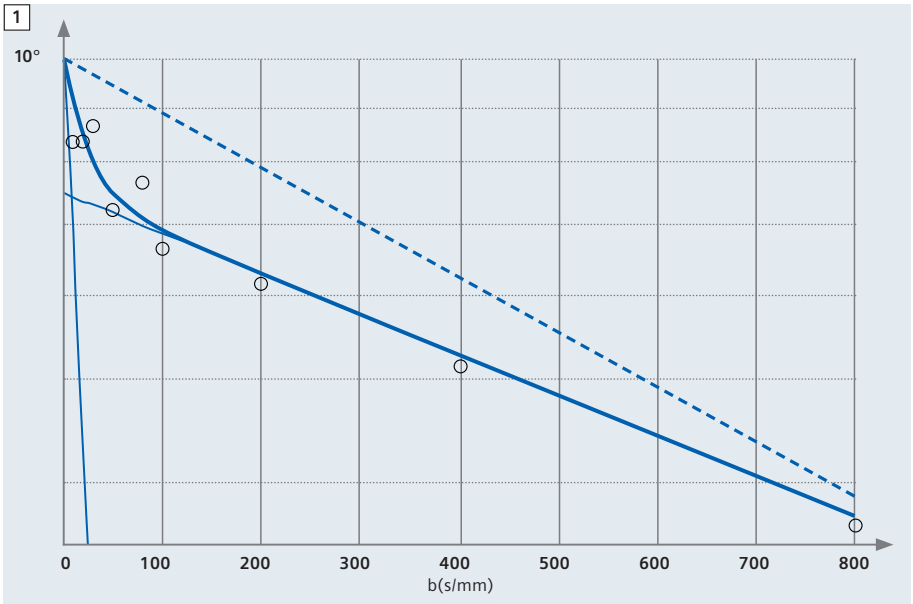


**1** Example of signal decay as a function of the diffusion b-values in a given voxel of a right lobe of the liver of a cirrhotic liver. Circles represent Normalized Signal, the bold solid line is the IVIM non-linear regression fit providing D, D* and f. Light solid lines represent D and D* decay curves separately. Finally the dashed line is the mono-exponential fit applied on b 0, 400, 800 s/mm², as described in [6], which provides ADC.

*WIP – Work in progress. The information about this product is preliminary. The product is under development and not commercially available in the U.S., and its future availability cannot be ensured.

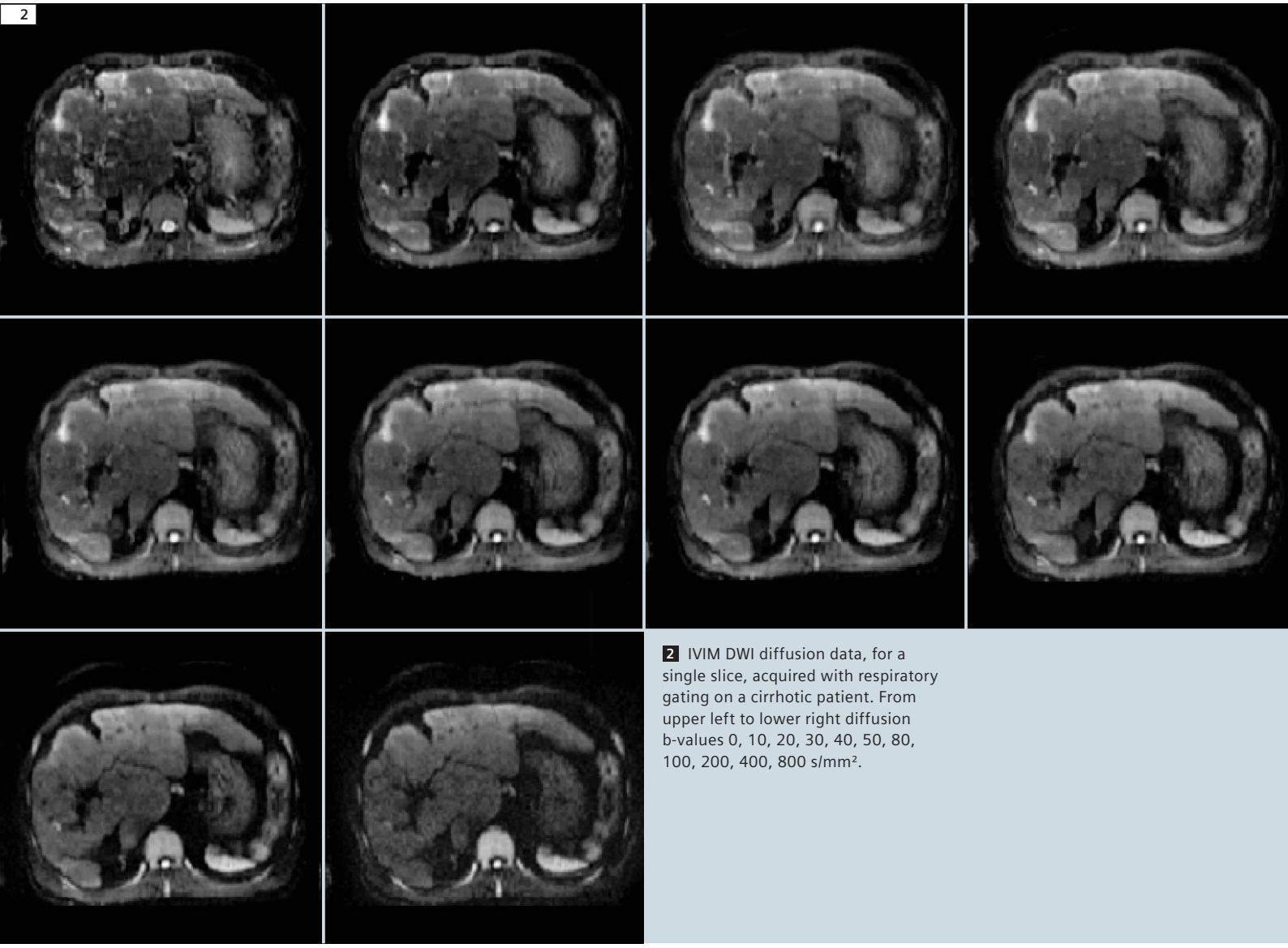

**2** IVIM DWI diffusion data, for a single slice, acquired with respiratory gating on a cirrhotic patient. From upper left to lower right diffusion b-values 0, 10, 20, 30, 40, 50, 80, 100, 200, 400, 800 s/mm².

[3]. Strong gradient amplitudes can be achieved while decreasing the minimum TE reachable for DW imaging. All these evolutions now allow the application of IVIM technique to the moving organs and more particularly to the liver.

In highly perfused tissue, such as the liver, the D* component is expected to strongly affect the signal decay especially at low diffusion b-values [4]. Lemke et al. have recently shown [5] that, in the liver, the suppression of the vascular component of the signal, using Dark Blood preparation, could strongly reduce the D* contribution. These findings confirm that the vascular component has an effect on the signal decay when it is weighted by diffusion gradients.

Classic liver disease can progressively lead to diffuse fibrosis with cirrhosis as an end stage. The diagnostic of cirrhosis is based on pathological examination of a tissue sample. Functional imaging techniques using either ultrasound, or computed tomography and MR imaging have been proposed to assess and follow-up cirrhosis [6]. Recently, Luciani et al. [7] proposed the application of the IVIM-DWI technique to the assessment of cirrhotic liver with liver pathology on explanted livers taken as the reference. The preliminary results of this study are reported below.

## Clinical protocol

The measurements were performed on a 1.5T Siemens MAGNETOM Avanto. Six elements of the Spine Matrix coil array embedded in the patient table and 6 ele-

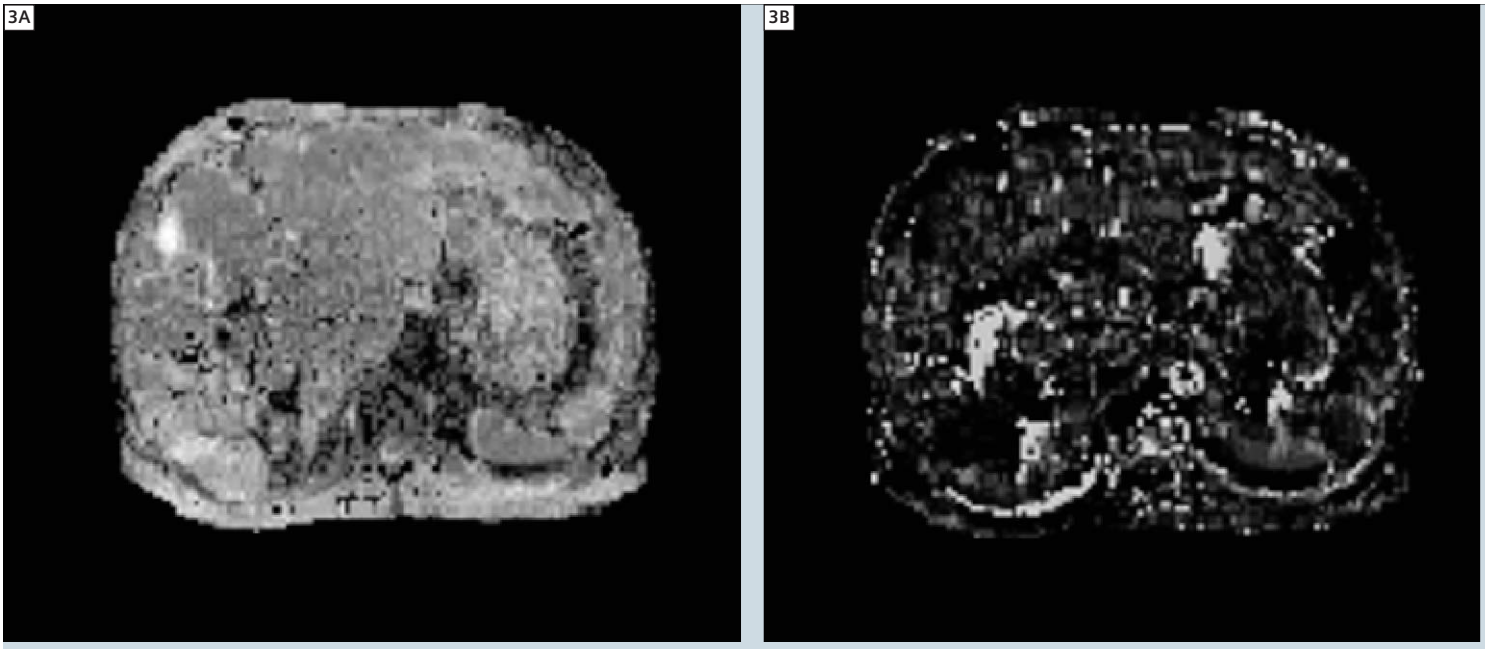


**3** IVIM maps for a cirrhotic patient, obtained using data presented in Fig. 2. From upper left to lower right D, D*, f, and ADC maps are respectively presented.

ments of the Body Matrix coil array were selected for optimum signal reception. The IVIM DW sequence was designed to study liver routinely. The sequence parameters were the following: FOV 300 x 250 mm², matrix 138 x 90, twelve 5 mm thick slices were acquired with 3 averages, BW 1342 Hz/px, acceleration factor 2 with *syngo* GRAPPA reconstruction. The sequence was triggered with a pneumatic respiratory belt but could also be done with a PACE (Prospective Acquisition CorrEction) navigator [9] leading to a TR ~3 sec. Ten b-values (b = 0, 10, 20, 30, 40, 50, 80, 100, 200, 400, 800 s/mm²) were applied in the 3 perpendicular directions once by scan for a TE 70 msec. TA, depending on the respiration rate, was equal to 2–3 min. The analysis was done pixel by pixel at Matlab (Mathworks, Natick, MA, USA) in two steps as described extensively in [7]. Firstly, since D* contribution can be neglected at high b-values, D was extracted using high b-values (b ≥ 200 s/mm²) and a mono-exponential fit. Secondly, a non-linear regression was applied to solve remaining parameters: f the vascular volume faction and D*. In addition an ADC measurement was calculated using b = 0, 200, 400, 800 s/mm² and a simple mono-exponential fit to compare our findings with the literature [6].

The study was approved by the Institutional Review Board of the University Hospital. The IVIM sequence was applied in addition to the routine liver MR imaging protocol. Two populations were included in the study: livers with METAVIR F4 score at the liver biopsy [8] performed within the past two months and healthy livers with no history of hepatic diseases and no evidence found during the MR exam.

## Discussion

All curves of signal decrease demonstrated a bi-exponential decay whether the measurements were obtained in the healthy liver group or in the cirrhotic liver group (Fig. 1). Figure 1 also shows that the mono exponential fit usually applied does not fit well with the decay observed in liver tissue. Figures 2 and 3 show examples of diffusion maps both for healthy and cirrhotic patients. Findings show that the liver diffusion component linked to perfusion (D*) significantly decreased in the cirrhotic liver group compared the healthy liver group and could account for the reduced ADC in cirrhotic livers reported in previous studies [6] and also seen in this study (Figures 2 and 3).

It is generally accepted that liver cirrhosis is associated with reduced liver perfusion: The increased arterial flow triggered by intra-hepatic portal hypertension in liver fibrosis is insufficient to compensate for the reduced portal flow [10]. For Moreno et al. [10, 11], the mean portal flow in healthy subjects was 20.9 ± 4.1 ml/min/kg as opposed to 6.5 ± 5.6 ml/min/kg in patients with cirrhosis. This could explain the observed decay of D* in cirrhotic livers.

ADC was found comparable to the literature for healthy and cirrhotic groups. ADC was significantly higher than D both in the healthy liver group and in the cirrhotic liver group.

Results of IVIM DW imaging suggest that the diffusion component related to the molecular displacement (D) does not differ significantly between cirrhotic and healthy livers. Similar findings have already been reported by Yamada et al. [4], who found that D was significantly lower than ADC, thus suggesting that

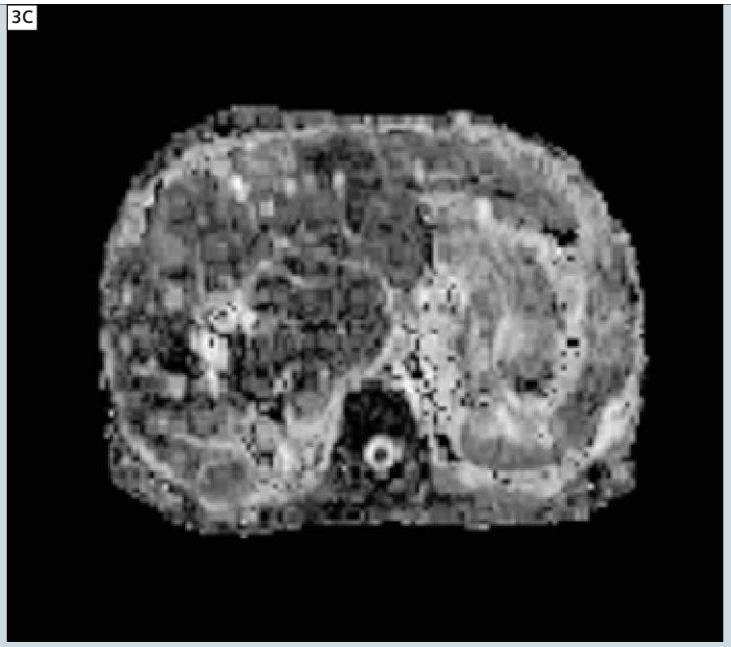


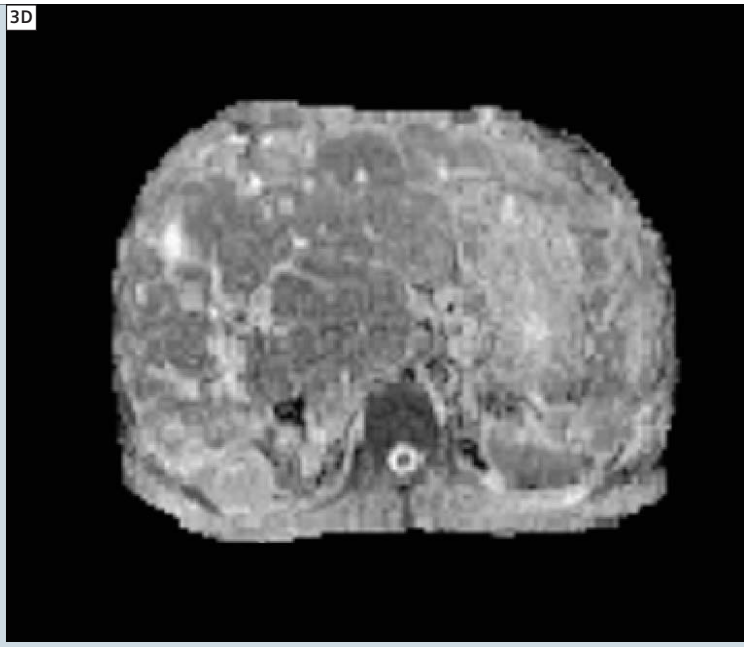


differences reported in ADC between patients with cirrhosis and healthy patients were mainly related to the perfusion component of liver diffusion. Therefore, even if the study is preliminary and limited, it is clear that the IVIM model seems to be more properly designed to accurately fit the diffusion behavior of liver tissue (Fig. 1). It shows also that the assessment of D* may potentially be considered as a surrogate marker of capillary liver perfusion especially and could be a good indicator of the fibrosis disease. Further investigations are expected to confirm its potential to discriminate liver fibrosis.

*WIP – Work in progress. The information about this product is preliminary. The product is under development and not commercially available in the U.S., and its future availability cannot be ensured.

**Contact**
Alexandre Vignaud
Siemens Healthcare
9, boulevard Finot
93527 Saint-Denis
France
Phone: 00-33-6-07-33-40-87
alexandre.vignaud@siemens.com

**References**

1 D. Le Bihan, E. Breton, D. Lallemand, M. L. Aubin, J. Vignaud, M. Laval-Jeantet. Separation of diffusion and perfusion in intravoxel incoherent motion MR imaging. Radiology 1988; 168:497–505.
2 G. J. Stanisz, E. E. Odrobina, J. Pun, M. Escaravage, S. J. Graham, M. J. Bronskill, R. M. Henkelman. T1, T2 Relaxation and Magnetization Transfer in Tissue at 3T. Magn Reson Med2005; 54:507–512.
3 T.G. Reese, O. Heid, R.M. Weisskoff and V.J. Wedeen. Reduction of Eddy-Current-Induced Distortion in Diffusion MRI Using a Twice-Refocused Spin Echo. Magnetic Resonance in Medicine 2003;49:177-182.
4 I. Yamada, W. Aung, Y. Himeno, T. Nakagawa, H. Shibuya, Diffusion Coefficients in Abdominal Organs and Hepatic Lesions: Evaluation with Intravoxel Incoherent Motion Echo-planar MR Imaging. Radiology 1999; 210:617–623.
5 A. Lemke, L. R. Schad, B. Stieltjes, F. Laun. Evidence for a vascular contribution to the biexponential signal decay as a function of the b-value in DWI: A verification of the IVIM-model. Proc. Intl. Soc. Mag. Reson. Med. 17 (2009) 1365.
6 M. Lewin, A. Poujol-Robert, P.Y. Boelle et al. Diffusion-weighted magnetic resonance imaging for the assessment of fibrosis in chronic hepatitis C. Hepatology 2007; 46: 658–665.
7 A. Luciani, A. Vignaud, M. Cavet, J. Tran Van Nhieu, A. Mallat, L. Ruel, A.Laurent, J.-F. Deux, P. Brugieres,, A. Rahmouni. Liver Cirrhosis: Intravoxel Incoherent Motion MR Imaging-Pilot Study. Radiology 2008;249: 891-899.
8 P. Bedossa, T. Poynard. An algorithm for the grading of activity in chronic hepatitis C. The METAVIR Cooperative Study Group. Hepatology 1996;24:289–293.
9 R.L. Ehman, J.P. Felmlee. Adaptive technique for high-definition MR imaging of moving structures. Radiology 1989;173:255-63.
10 A.H. Moreno,A.R. Burchell,L.M. Rousselot,W.F. Panke,F. Slafsky, J.H. Burke. Portal blood flow in cirrhosis of the liver. J Clin Invest 1967; 46: 436-445.
11 A.H. Moreno, L.M. Rousselot,W.F. Panke, M.L. Burke. The rate of hepatic blood flow in normal subjects and in patients with portal hypertension. Surg Gynecol Obstet 1960; 111: 443-450.

# Challenges and Clinical Value of Automated and Patient-Specific Dynamically Timed Contrast-Enhanced Liver MRI Examination

**Diego R. Martin, M.D., Ph.D.; Puneet Sharma, Ph.D.; Hiroumi Kitajima, Ph.D.**

*Emory University, Atlanta, GA, USA*

It has been widely accepted that optimal capture of multi-phase (dynamic) contrast media enhanced (DCE) liver images are an important and often critical component to diagnostically optimized MRI examination [1-8]. Especially the arterial-phase images are frequently a unique additional marker for differentiating characteristics of benign, malignant, primary and metastatic liver tumors [3, 4, 8, 9]; also it is known that arterial-phase images do help to analyze active hepatitis in the setting of acute and chronic liver diseases [5, 10]. In this article we describe the technical and clinical requirements for optimized DCE liver imaging and how our developments for patient-adopted scanning help to overcome some of the limitations in clinical routine. And finally, a short outlook on the further implementations of these developments for DCE liver MRI is provided.

The technical requirement for capturing the critical arterial-phase is defined by the dynamic imaging point where there is a maximal image contrast between arterial-enhancing liver lesions and the surrounding liver parenchyma. The commencement and duration of this arterial window however depends greatly on subject-specific vascular transit times. Therefore it is essential to understand the relationship between the contrast enhancement behavior of the liver vessels, parenchyma and liver pathologies and to adopt these requirements to DCE liver MRI. In figure 1A detailed analysis of the signal intensity (SI) time curves, optimal timing of the DCE phases and exemplary SI time curve of an arterialized tumor (HCC nodule) is displayed. Figures 2–4 show the relevance of optimal timing of the DCE liver MR exam in selected cases. In each patient scan presented there is transient important diagnostic information that can only be captured during a narrow time window related to the arterial phase. Based on our observations derived from a large patient cohort, approximately 30% of our patients show a large variation of vascular transit times from the mean population. While imaging the diagnostically important arterial-phase depends upon capture of a transient period that spans approximately 10 seconds in most cases, the time-window for capture of the venous and late phases are relatively broader and therefore less error-prone. Therefore, adoption of a patient specific dynamically timed arterial phase DCE liver MRI technique is essential for reproducible optimal diagnostic images. However, in a clinical setting, DCE liver MRI is very often performed with rigid and therefore sub-optimal timing delays between initiating the contrast infusion and initiating the image acquisitions.

Individually-tailored timing for the phases of DCE liver MRI has been suggested for optimized arterial phase imaging. This can be achieved by applying a test bolus for calculation of circulation time [3], or tracking bolus arrival in the descending aorta using real-time image acquisition [11]. To further simplify the arterial-phase timing calculations, this imaging step can be incorporated into the arterial phase acquisition by applying a real-time bolus tracking methodology similar to the strategy employed for contrast enhanced MR angiography [11–14]. A real-time contrast bolus-triggering methodology for liver offers technical simplification and speed as compared to pre-scan test bolus techniques. In addition to accounting for differences in the vascular transit times between patients, adjustments of the optimal time-point for read-out of the central k-space data must be taken into consideration when using gradient echo technique, such as VIBE. Sequence parameters that affect the peak central k-space acquisition timing include use of centric versus non-centric k-space sampling schemes, but also include field-of-view, resolution, breath-hold duration, and number of slices.

Until now, the usage of bolus-tracking sequences has not been in widespread use for dynamic liver imaging because of the complexity of patient-specific DCE

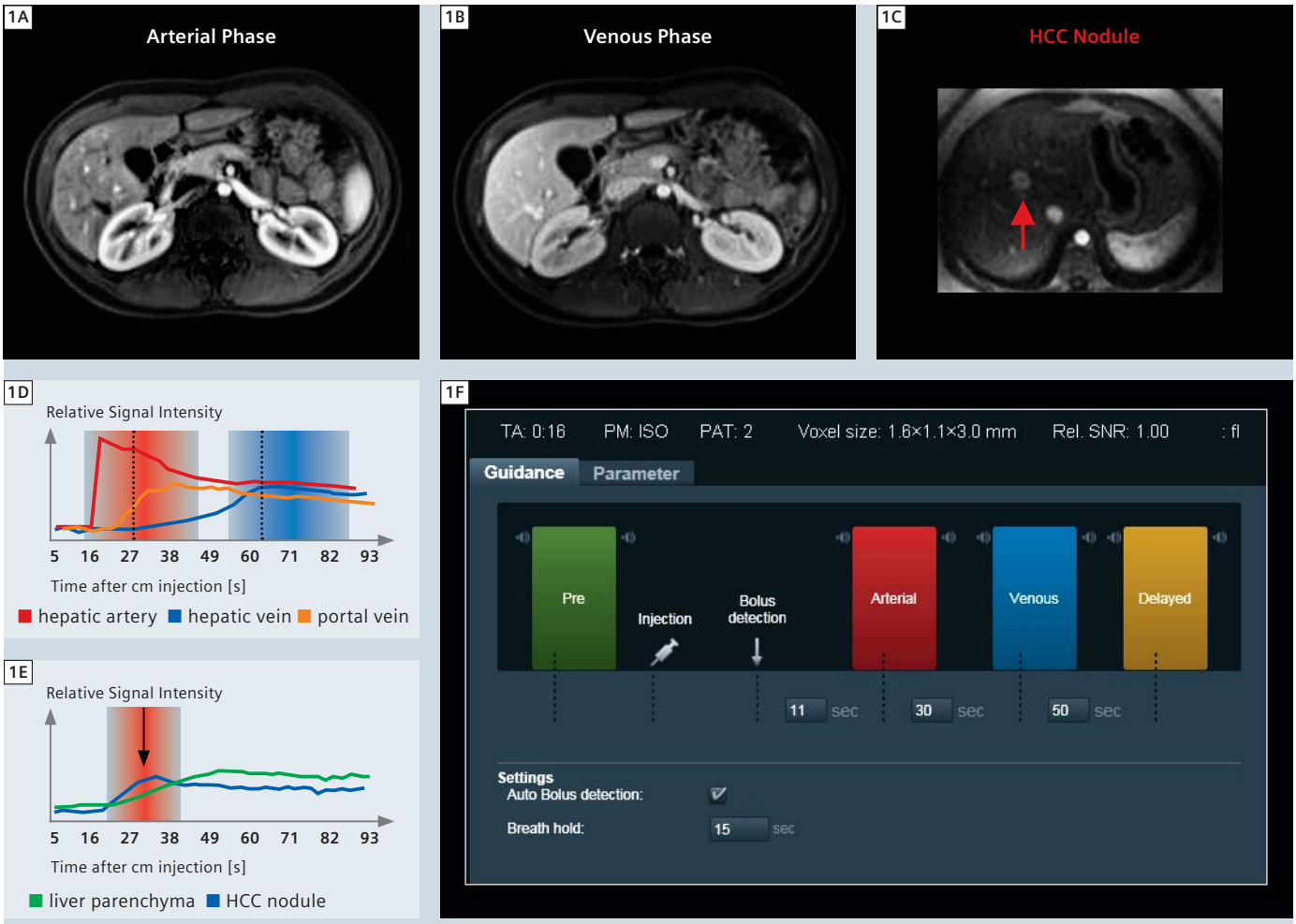


**1 Patient-specific DCE liver MRI**

For optimized diagnostic imaging, an individualized patient-specific liver DCE technique is essential for reproducible capture of the arterial phase. An ideal arterial **(A)** and venous phase **(B)** image is shown. To understand the relationship between the different phases and the clinical relevance for optimal timing, especially for the arterial phase images, an example of an arterialized hepatocellular carcinoma (HCC) nodule is provided captured during the arterial phase **(C)**. In this image the enhancing nodule is conspicuous during the transient period when the lesion-to-liver background contrast ratio is elevated. The relative changes in signal-intensities (SI) within the hepatic artery, portal and hepatic veins are provided as a function of time for this patient **(D)**. Additionally the time-windows for capturing an arterial (red zone) and venous (blue zone) image are displayed. The time during which the HCC nodule enhances above the adjacent liver parenchyma is used to define the arterial phase and the basis for this calculation is shown for this patient **(E)**. Note that the time window for capture of the transient arterial tumor enhancement is short (~10 s) and that imaging the arterial enhancement is critical for detection, diagnosis, and for assessing treatment response. A screenshot from the Abdomen Dot Engine is provided **(F)**. This Dot Engine* optimizes timing delay between the arrival of contrast bolus, provides the breath-hold commands, initiates sequence acquisition and also adopts the imaging sequence programming to bolus-timing specifications. Also, the user can adjust the time delays between the detection of the contrast media bolus and the optimal time-point for read-out of the VIBE central k-space acquisition data. All phases of the DCE study may be subsequently acquired without the need of any further manual interactions with the sequence parameters.

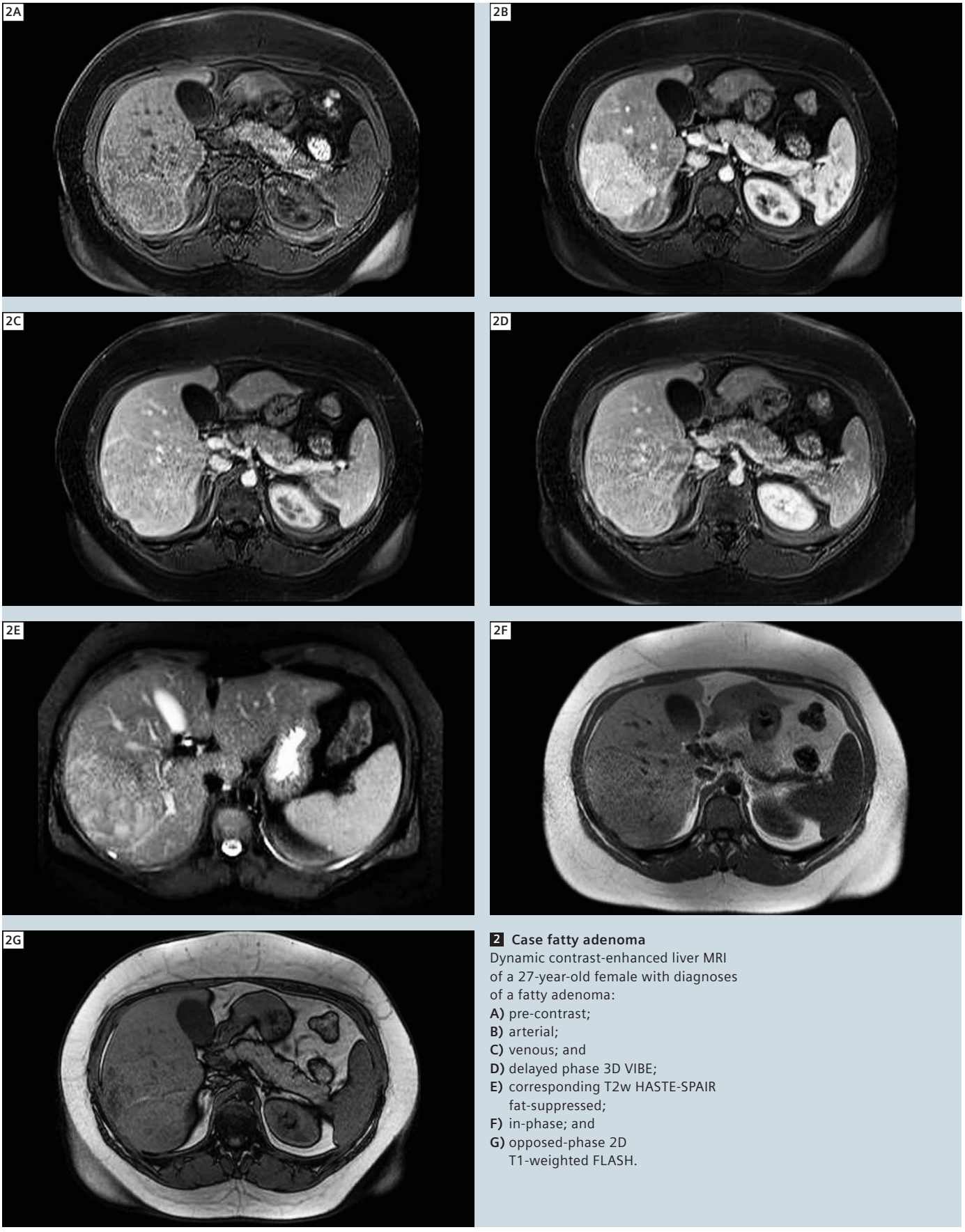


**2 Case fatty adenoma**
Dynamic contrast-enhanced liver MRI of a 27-year-old female with diagnoses of a fatty adenoma:
**A)** pre-contrast;
**B)** arterial;
**C)** venous; and
**D)** delayed phase 3D VIBE;
**E)** corresponding T2w HASTE-SPAIR fat-suppressed;
**F)** in-phase; and
**G)** opposed-phase 2D T1-weighted FLASH.

**3 Case hepatocellular carcinoma (HCC)**
Patient with liver cirrhoses: a small HCC nodule (red arrow) with a maximum diameter of 1 cm can be seen only because of an optimally timed arterial phase liver scan **(3A)**.
On venous (70 s after contrast media injection) and delayed phase (180 seconds delay) a corresponding focal washout lesion with subtle capsule enhancement can be seen progressively on the more delayed image (white arrows).
In addition, the delayed enhanced images show a fine reticular pattern of contrast uptake characteristic of hepatic fibrosis.
The patient had two HCC nodules of similar size, both identified on MRI and confirmed on explanted liver pathology acquired after liver transplantation.
This patient had hepatitis C viral infection, associated with increased risk for HCC at even relatively early stage chronic liver disease, as in this patient.
On a background of chronic liver disease, a transiently arterial enhancing lesion (on arterial phase images) with progressive washout and capsule enhancement (on venous and delayed phase images) represents HCC.
MRI diagnosis is accepted over biopsy for purpose of liver transplant evaluation. While all phases of the DCE MRI are necessary for comprehensive evaluation, sub-optimal arterial phase timing would seriously impair diagnostic sensitivity and specificity of HCC diagnosis.

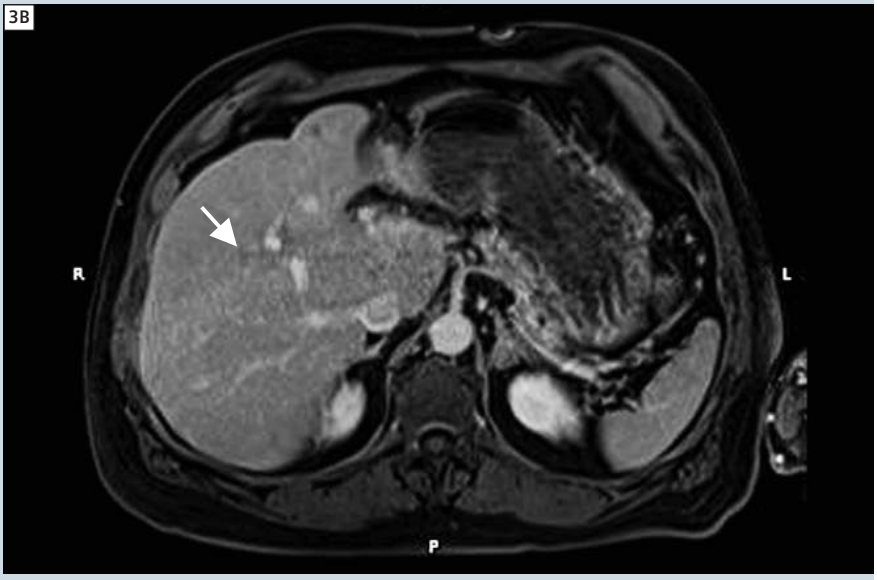


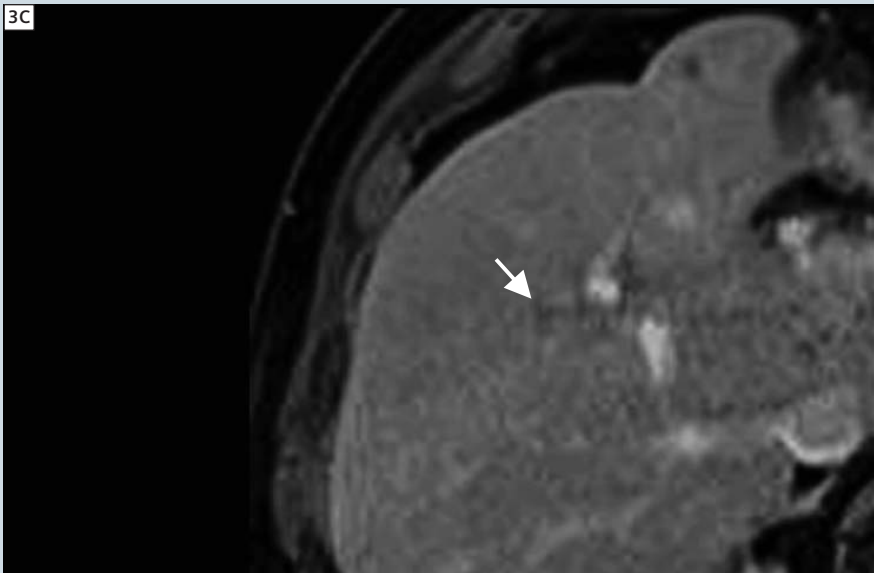

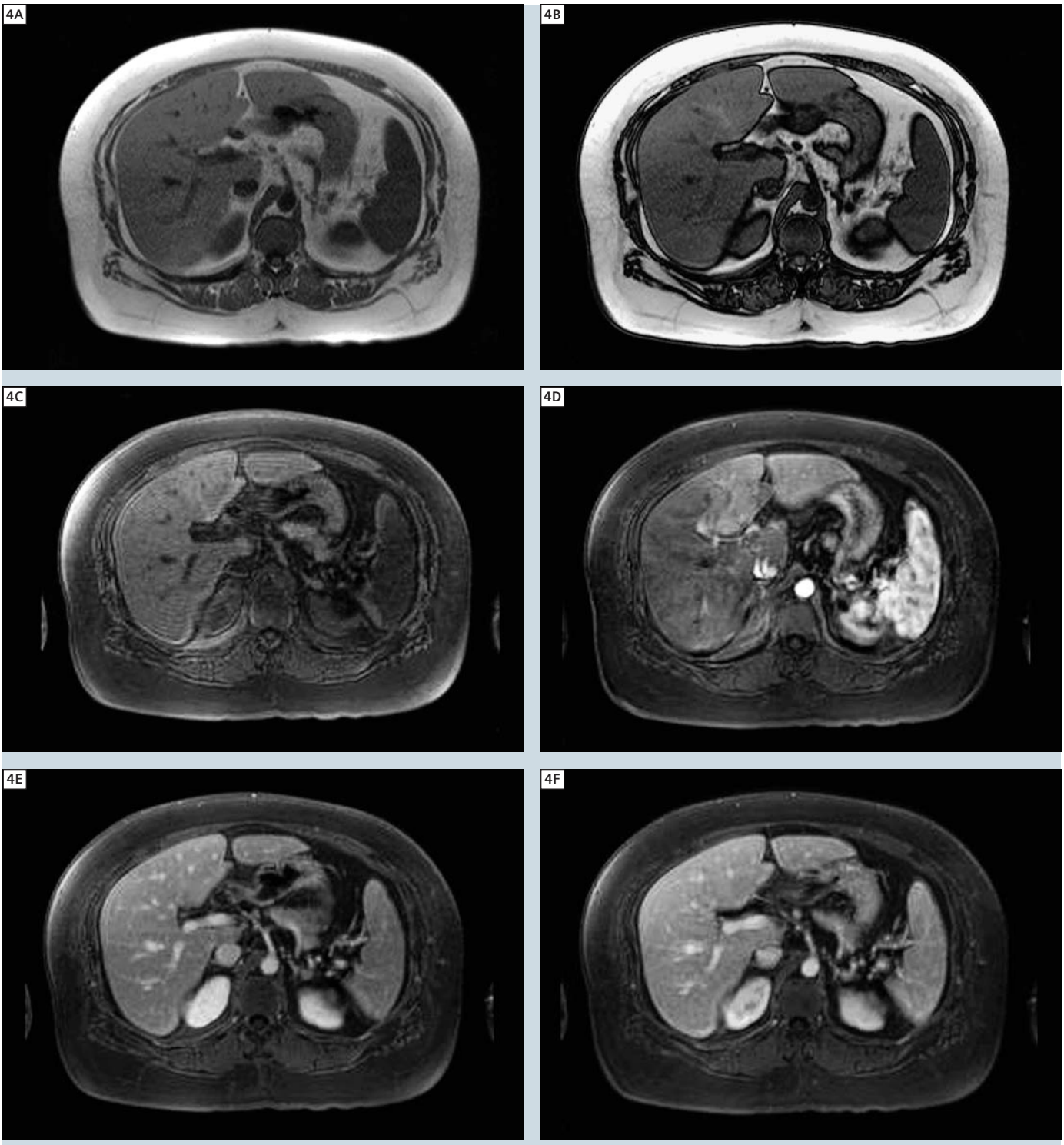


**4 Case non-alcoholic steatohepatitis (NASH)**
Patient with biopsy-proven NASH: **(A)** FLASH in-phase; and **(B)** opposed-phase; **(C)** pre-contrast; **(D)** arterial; **(E)** venous; and **(F)** delayed phase DCE 3D VIBE. Images show diffuse steatosis (note liver signal drop on opposed phase images with mild focal sparing in segment 4). While the pre, venous, and delayed phase images show uniform liver signal and enhancement, the arterial phase images show transient marked non-uniform enhancement. This finding has been previously shown to correlate in magnitude to the degree of active hepatitis and requires optimal arterial phase timed image capture for diagnosis. Venous phase images are used to assess portal system and abdominal vasculature and the delayed images may be used to assess chronic changes of hepatitis (for example, **Fig. 3C**). In this case, no evidence of hepatic fibrosis or sequelae of portal hypertension is identified, correlating with only minimal stage bridging fibrosis on the pathology specimen.

liver MRI timing methods. Based on the clinical need to improve DCE liver exams, we developed and implemented a bolus tracking technique which we call Automated Breath-hold Liver Exam (ABLE) for our clinical routine protocols. Through the combination of our observations and techniques, and in close cooperation with Siemens Healthcare, a fully automatic procedure was developed that provides a clear simplification of timing methodology and MR image acquisition for the average user. This new workflow optimizing approach (Abdomen Dot Engine*) offers patient-specific DCE liver MRI for routine clinical application. This software helps to define or even provide full automation of

1) defining vascular reference points;
2) optimizing timing delays between the arrival of contrast bolus, providing the breath hold commands, and initiation of sequence acquisition; and
3) adapting imaging sequence programming to bolus-timing specifications.

The images presented in this article were all generated with the ABLE bolus tracking technology. The real-time bolus track imaging was implemented in this approach using a fast 2D FLASH sequence, with acquisitions every 0.5–1.0 second and on-the-fly image reconstruction (450 mm FOV, 256 matrix, TR/TE = 4.1/1.23 ms, flipangle 10°, 50 mm slice thickness, 100 dynamics, scan time = 100 seconds). The sequence was oriented along the abdominal aorta, and initiated at the same time as contrast administration. The real-time images were then displayed using an Inline viewer on the console and the software triggered the DCE scan upon reaching a certain threshold within a manually placed region of interest (ROI). For the shown DCE liver images in this article, a 3D VIBE imaging sequence with a segmented k-space acquisition was used with the following parameters: 360 mm FOV (75–90% phase FOV), 256 matrix (70% phase resolution), TR/TE = 4.1/1.7 ms, flipangle 10°, 400 Hz/pixel bandwidth, 94 slices, 3 mm slice thickness, acceleration factor = 2 (*syngo* GRAPPA) and SPAIR fat saturation. Following acquisition of the arterial phase image set, venous and delayed interstitial phase image sets were obtained. Based on our clinical experience with the ABLE technique, this approach leads to a clear improvement in reproducible DCE liver scan arterial timing with improved diagnostic yield. This approach provides optimized images for tumor detection and characterization and for therapy monitoring DCE protocols. Uniformity of arterial phase timing between patients with liver tumors, and for an individual patient who is studied by multiple MRI scans over time, is critically improved using the bolus-timing strategy described here.

**Contact**
D. R. Martin, M.D., Ph.D.
Professor of Radiology
Director of MRI
Director of the Clinically Applied
Research Body MRI Program
Emory University
Atlanta, GA
USA
dmartin@emory.edu

*The information about this product is being provided for planning purposes. The product is pending 510(k) review, and is not yet commercially available in the U.S.

References

1 Schlund JF, Semelka RC, Kettritz U, Eisenberg LB, Lee JK. Transient increased segmental hepatic enhancement distal to portal vein obstruction on dynamic gadolinium-enhanced gradient echo MR images. J Magn Reson Imaging 1995; 5:375-377.
2 Mitchell DG. Liver I: Currently available gadolinium chelates. Magn Reson Imaging Clin N Am 1996;4:37-51.
3 Earls JP, Rofsky NM, DeCorato DR, Krinsky GA, Weinreb JC. Hepatic arterial-phase dynamic gadolinium-enhanced MR imaging: optimization with a test examination and a power injector. Radiology 1997;202:268-273.
4 Kanematsu M, Semelka RC, Matsuo M, et al. Gadolinium-enhanced MR imaging of the liver: optimizing imaging delay for hepatic arterial and portal venous phases--a prospective randomized study in patients with chronic liver damage. Radiology 2002;225:407-415.
5 Martin DR, Seibert D, Yang M, Salman K, Frick MP. Reversible heterogeneous arterial phase liver perfusion associated with transient acute hepatitis: findings on gadolinium-enhanced MRI. J Magn Reson Imaging 2004;20:838-842.
6 Martin DR, Semelka RC. Magnetic resonance imaging of the liver: review of techniques and approach to common diseases. Semin Ultrasound CT MR 2005;26:116-131.
7 Rofsky NM, Lee VS, Laub G, et al. Abdominal MR imaging with a volumetric interpolated breath-hold examination. Radiology 1999; 212:876-884.
8 Martin DR, Yang M. First Pass Perfusion Kinetics of Liver: High temporal imaging for demonstration of the true arterial capillary phase of enhancement. In: ISMRM Symposium on Molecular MR Imaging of Malignancy, 2002:A7.
9 Brown ED, Semelka RC. Contrast-enhanced magnetic resonance imaging of the abdomen. Magn Reson Q 1994;10:97-124.
10 Semelka RC, Chung JJ, Hussain SM, Marcos HB, Woosley JT. Chronic hepatitis: correlation of early patchy and late linear enhancement patterns on gadolinium-enhanced MR images with histopathology initial experience. J Magn Reson Imaging 2001;13:385-391.
11 Materne R, Horsmans Y, Jamart J, Smith AM, Gigot JF, Van Beers BE. Gadolinium-enhanced arterial-phase MR imaging of hypervascular liver tumors: comparison between tailored and fixed scanning delays in the same patients. J Magn Reson Imaging. 2000 Mar;11(3):244-9.
12 Hussain HK, Londy FJ, Francis IR, Nghiem HV, Weadock WJ, Gebremariam A, Chenevert TL. Hepatic arterial phase MR imaging with automated bolus-detection three-dimensional fast gradient-recalled-echo sequence: comparison with test-bolus method. Radiology. 2003 Feb;226(2):558-66.
13 Vade A, Olson MC, Vittore CP, Subbaiah P. Hepatic enhancement analysis in children using smart prep monitoring for 2 : 1 pitch helical scanning. Pediatr Radiol 1999;29:689-693.
14 Tatli S, Lipton MJ, Davison BD, Skorstad RB, Yucel EK. From the RSNA refresher courses: MR imaging of aortic and peripheral vascular disease. Radiographics 2003;23 Spec No:S59-78.

# Don’t miss the talks of experienced and renowned experts covering a broad range of MRI imaging

**Jörg Barkhausen, M.D.**
*University Hospital Essen*

**Dynamic 3D MRA – Clinical Concepts**
(*syngo* TWIST)

**John A. Detre, M.D.**
*University of Pennsylvania*

**Clinical Applications of Arterial Spin Labeling**
(*syngo* ASL)

**Tammie L. S. Benzinger, M.D., Ph.D.**
*Washington University School of Medicine*

**Clinical Applications of Diffusion-Tensor Imaging**
(*syngo* DTI)

**John F. Nelson, M.D.**
*Battlefield Imaging*

**Breast Cancer Management –**
**Cross Modality Approach**

**John A. Carrino, M.D., M.P.H.**
*Johns Hopkins University, School of Medicine*

**MRI in Sports Medicine**

Visit us at
**www.siemens.com/magnetom-world**
Go to
**Education > e-trainings & Presentations**

# Case Reports:
# Tumor Detection by Diffusion-Weighted MRI and ADC-Mapping with Correlation to PET/CT Results

**Matthias Philipp Lichy, M.D.; Philip Aschoff, M.D.; Christina Pfannenberg, M.D.; Schlemmer Heinz-Peter, M.D., Ph.D.**

*Department of Diagnostic and Interventional Radiology, University of Tuebingen, Germany*

The early and correct estimation of metastatic spread is essential for a patient-specific and efficient therapy regime. Therefore knowledge of total tumor load, extent of lymph nodes and distant metastases as well as potential threats e.g. infiltration of vertebral body with high risk of fracture, is required. During recent years significant efforts have been undertaken to improve the detection of metastases – either by spiral multi-slice computed tomography (CT) or magnetic resonance imaging (MRI). By providing best soft tissue contrast compared to CT, high-resolution whole-body (wb) MRI proved itself as a powerful tool in oncology [1, 2, 3]. However, detection of metastases and therapy monitoring with wbMRI is mainly based on morphological changes. Integration of metabolic data (acquired e.g. by MR spectroscopic imaging) and functional information (e.g. dynamic contrast enhanced scans) is potentially possible with MRI, but due to time constraints these methods could prove its clinical impact only in dedicated applications e.g. detection of prostate cancer within the prostatic gland and cannot easily be implemented in wbMRI so far.
The amount and complexity of wbMRI data also hampers the widespread use of this technique in clinical routine. Positron emission tomography (PET) with an integrated CT scanner (PET-CT) provides combined morphological and metabolic information. Compared to wbMRI, however, PET-CT is associated to x-ray exposure and the tracer production, transport and its application are more labor- and cost intensive. Sensitivity and specificity of PET-CT and examinations depends also on tumor type, applied tracer and tissue of interest. Therefore, the selection of the appropriate staging modality is highly dependent on histology and the pattern of metastastic spread [4].
However, cancer is not only characterized by pathologic metabolism e.g. high glucose uptake; also higher cellularity and therefore restriction of water diffusion have also been found to be common features of tumors. Diffusion-weighted imaging (DWI) with high b-values has therefore been applied for imaging metastasis. However, comparisons of DWI with other imaging modalities and with special focus on wbPET/CT are not widely available. In the following two case reports, results of MRI and wbDWI are compared to 18F-FDG PET/CT findings.

## Imaging techniques

CT was conducted with application of intravenous contrast agent (Ultravist 370, Schering AG, Germany) and oral administration of negative contrast dispersion as multi-phase protocols [7]. All PET-CT scans were performed on a single dual modality scanner (Biograph 16, Siemens Medical, Knoxville, USA) consisting of a 16-row multi-slice CT system (minimal rotation time of 0.5 sec) and a full ring lutetium oxortho-silicate (LSO) PET. WbMRI and DWI were performed on a 1.5 Tesla MR tomography with 32 receiver channels (MAGNETOM Avanto, Siemens Medical, Germany). For (wb) DWI application, a single-shot echo-planar-imaging (EPI) sequence with diffusion-module and fat-suppression-pulse was used (*syngo* REVEAL). This sequence has the ability for navigator-based respiratory triggering (PACE). For respiratory-triggered DWI sequence, data was acquired in expiration. In case of non-triggering, the patient was breathing freely. Water diffusion was measured with a 3-scan-trace technique and b-values of 0, 400 and 1000 s/mm$^2$; apparent diffusion coefficient maps were generated automatically (*syngo* Inline Diffusion). Sequence parameters of the single-shot echo-planar-imaging (EPI) sequence with diffusion-module and fat-suppression-pulse used in these two cases were: TR / TE 3900 (1500 for non-triggered DWI) / 76 ms, slice thickness 4 mm, FOV 380 x 380, 192 Matrix, EPI factor of 192, 4 averages, PAT factor of 2 (*syngo* GRAPPA), resulting voxel size 2 x 2 x 4 mm$^3$, TA 1:52 (non-triggered, 30 slices; for triggered DWI depending on respiration cycle TA approximate 5 min).

## Case 1: Malignant Melanoma

This case shows the results of wbPET/CT and wbMRI including DWI of a female patient with an advanced malignant melanoma (stage IV). The DWI sequences were able to visualize even the extensive tumor spread within the bowel wall as well as lymph node metastasis in detail. All suspicious lymph nodes as well as the diffuse tumor infiltration of the bowel wall are characterized by a high restriction of water diffusion (compare with ADC map). However, the extension of this advanced melanoma and therefore the irresectability is already proven with the standard contrast-enhanced single-phase CT scan. However, comparing the thick-slice MIP of the inverted original b=1000 s/mm² DWI images, providing a "PET-like" image, with the corresponding PET image it is clearly shown that the resolution of the DWI here is clearly superior to the PET image and lymph node metastases and bowel infiltration are well delineated. However, fat-suppressed, contrast enhanced T1w and fat-suppressed T2w MRI are also able to display all metastases. While the ADC-map is essential to differentiate real restriction of diffusibility from T2-shine-through artifacts, this image cannot be used for a fast assessment of tumor spread. However, original b-value images especially at b=1000 s/mm² are characterized by suppression of all healthy tissue with exception of the spleen and clearly elevated signal intensity of the metastases.

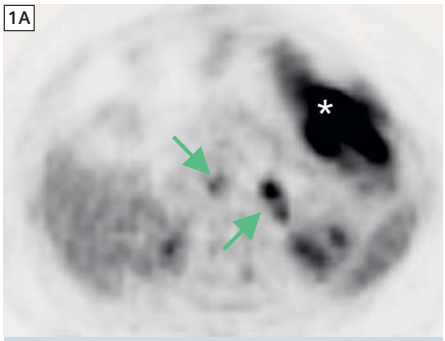


**1** **A:** Corresponding original attenuation-corrected PET image (*bowel infiltration, arrows lymph node metastases).

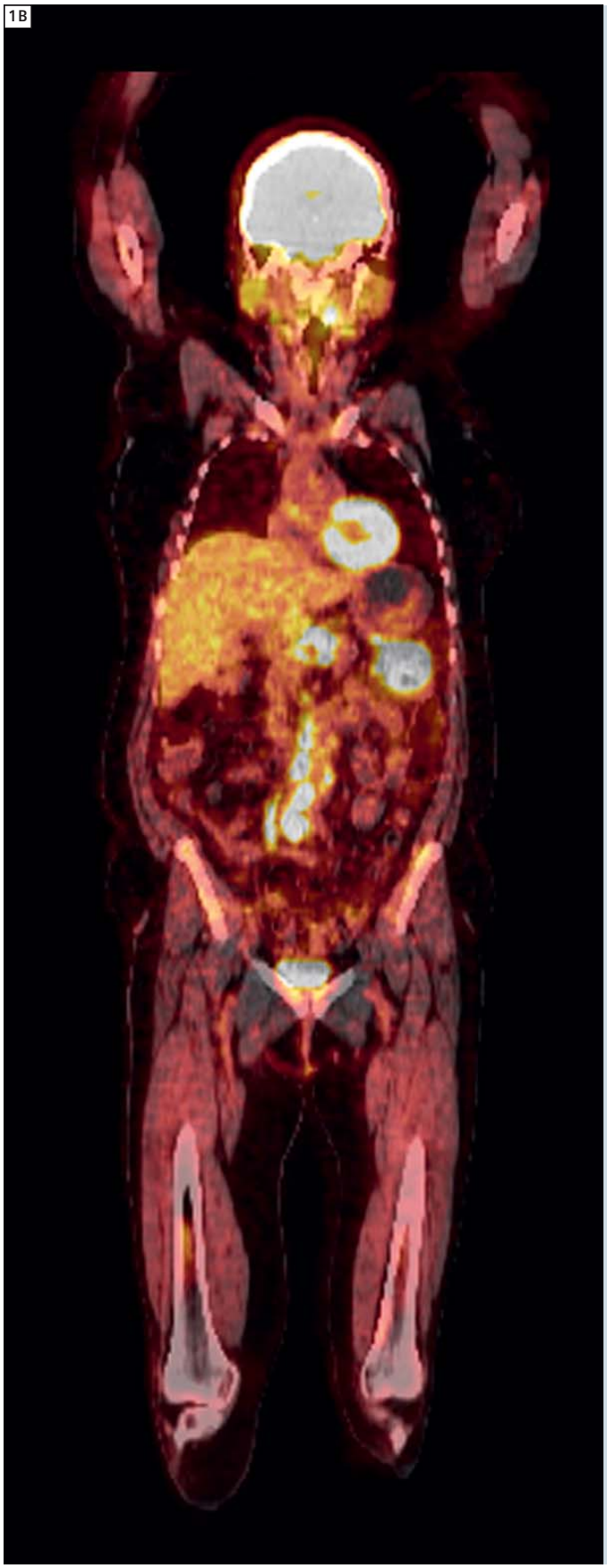


**1** **B:** Fused 18F-FDG PET/CT demonstrating multiple paraortic metastases and diffuse bowel infiltration of a malignant melanoma (stage IV).

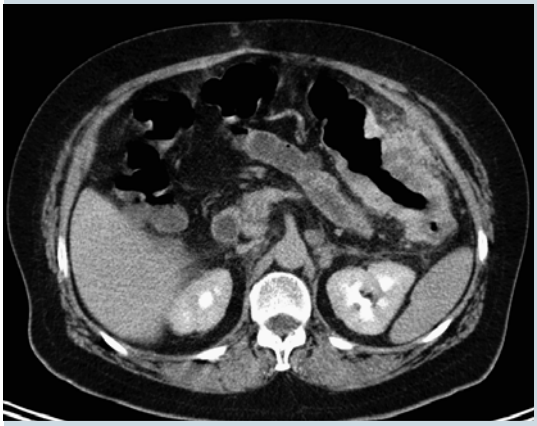

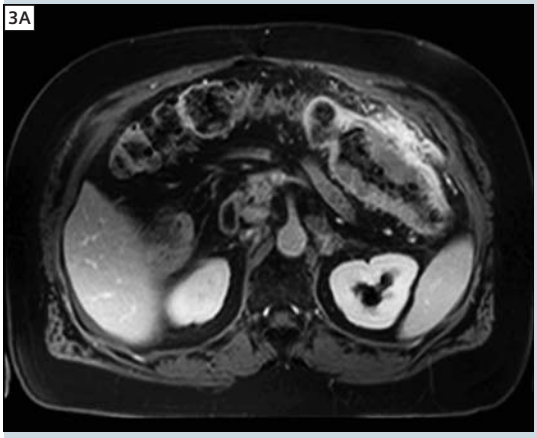


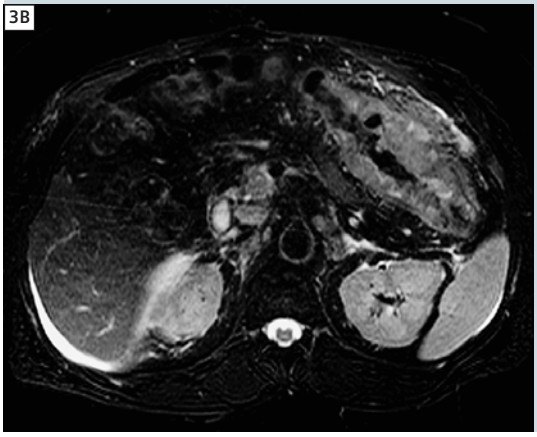


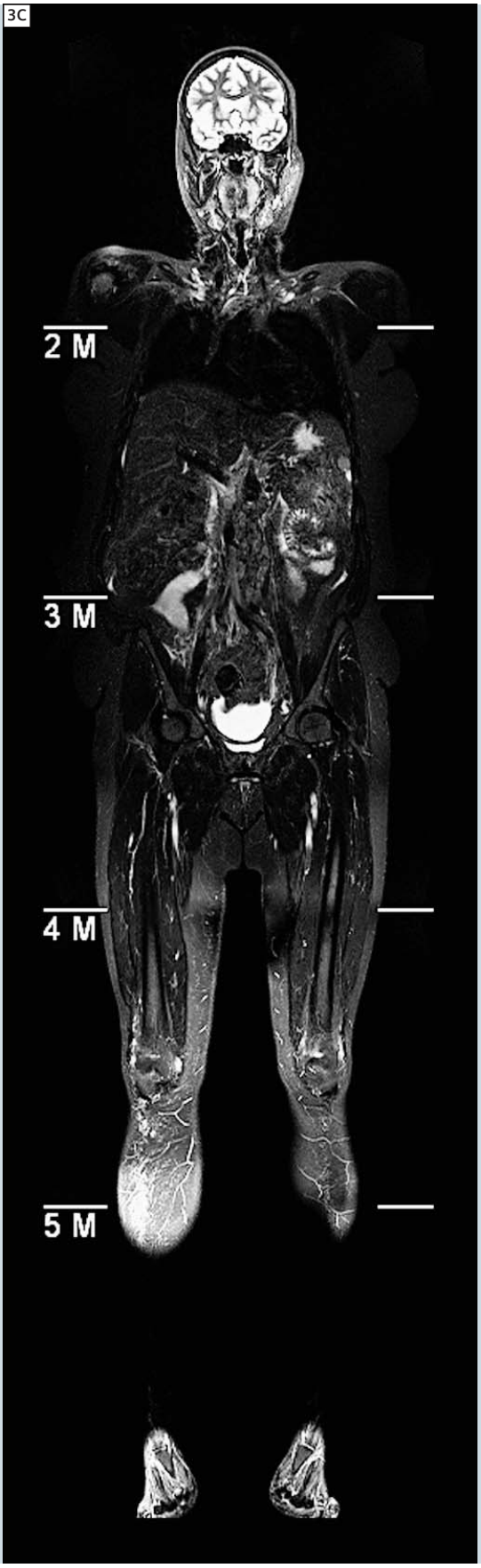


**2** Corresponding single-phase CT scan (acquired during PET/CT scan).

**3** **A:** Contrast-enhanced T1w 2D Flash MRI (breathhold).
**B:** T2w TSE with spectral fat-suppression (free breathing, triggered with PACE).
**C:** Composed whole-body T2 TIRM.

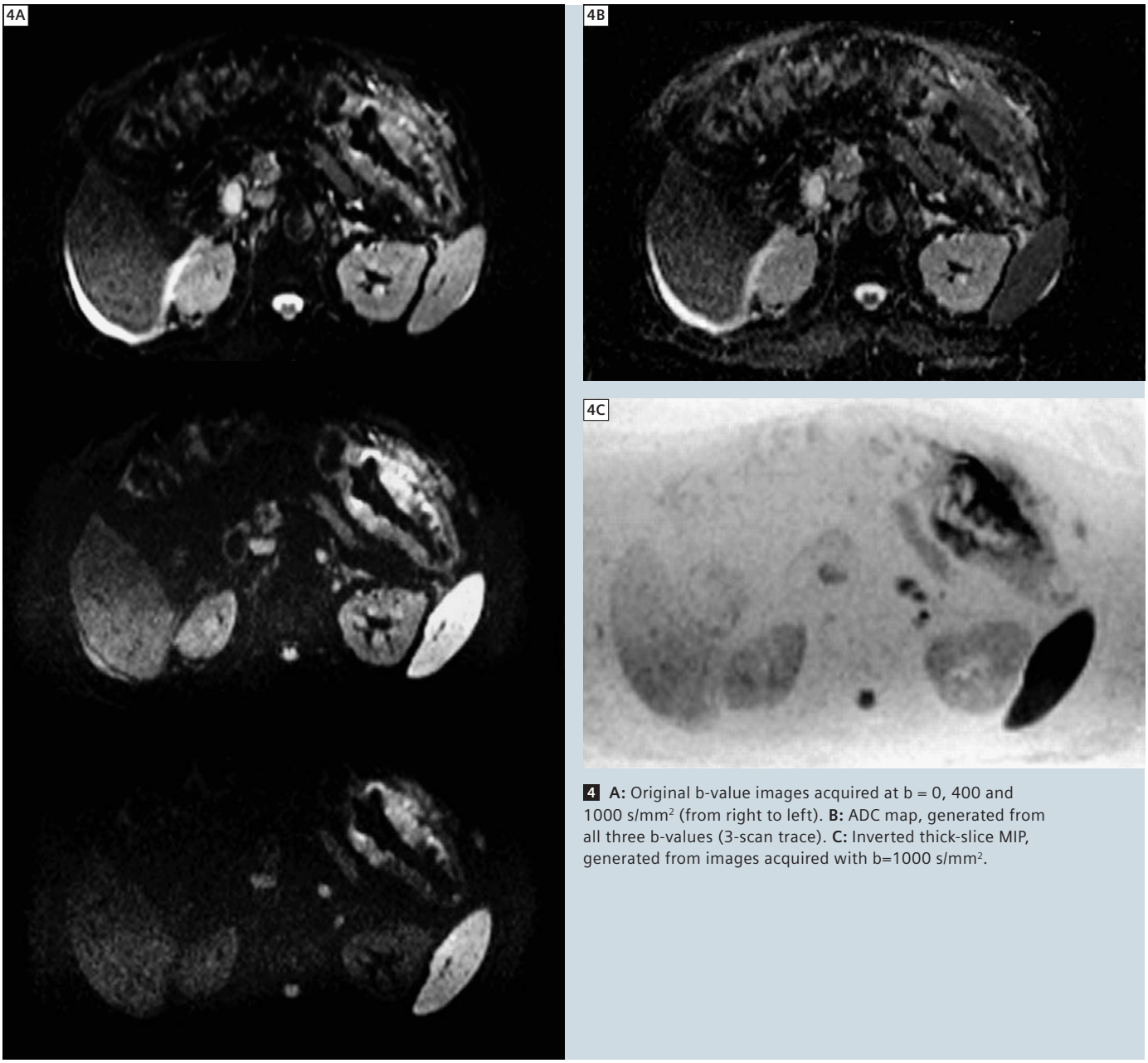


**4** **A:** Original b-value images acquired at b = 0, 400 and 1000 s/mm² (from right to left). **B:** ADC map, generated from all three b-values (3-scan trace). **C:** Inverted thick-slice MIP, generated from images acquired with b=1000 s/mm².

## Case 2: Non-Hodgkin Lymphoma

In this case, the results of PET-CT and DWI examination of a male patient with a non-Hodgkin lymphoma are shown. PET-CT with $^{18}$FDG revealed a diffuse tumor infiltration of the muscles and also of the right ventral skin of the right thigh. High b-value imaging was able to visualize diffuse tumor infiltration in detail even of the cutis. However, if one had to rely only on a single b-value image, in this case a clear differentiation of restriction of diffusibility from potential insufficient spectral fat suppression would be problematic and therefore hamper the correct diagnoses. Muscle atrophy of the right gluteal muscle results in restriction of water mobility, too, and also a pathologic signal of the femoral bone marrow is obvious at b = 0 and 400 s/mm² values. $^{18}$FDG uptake was not suspicious, either in the bone marrow or in the atrophic muscles, but based on MRI tumor could not be ruled out. The ADC-map also shows unexpectedly high ADC-values in the muscles with high tracer uptake compared to the atrophic gluteal one. Atrophy of the right gluteal muscles is also obvious on fat-suppressed T2w and contrast-enhanced, fat-suppressed T1w MRI.

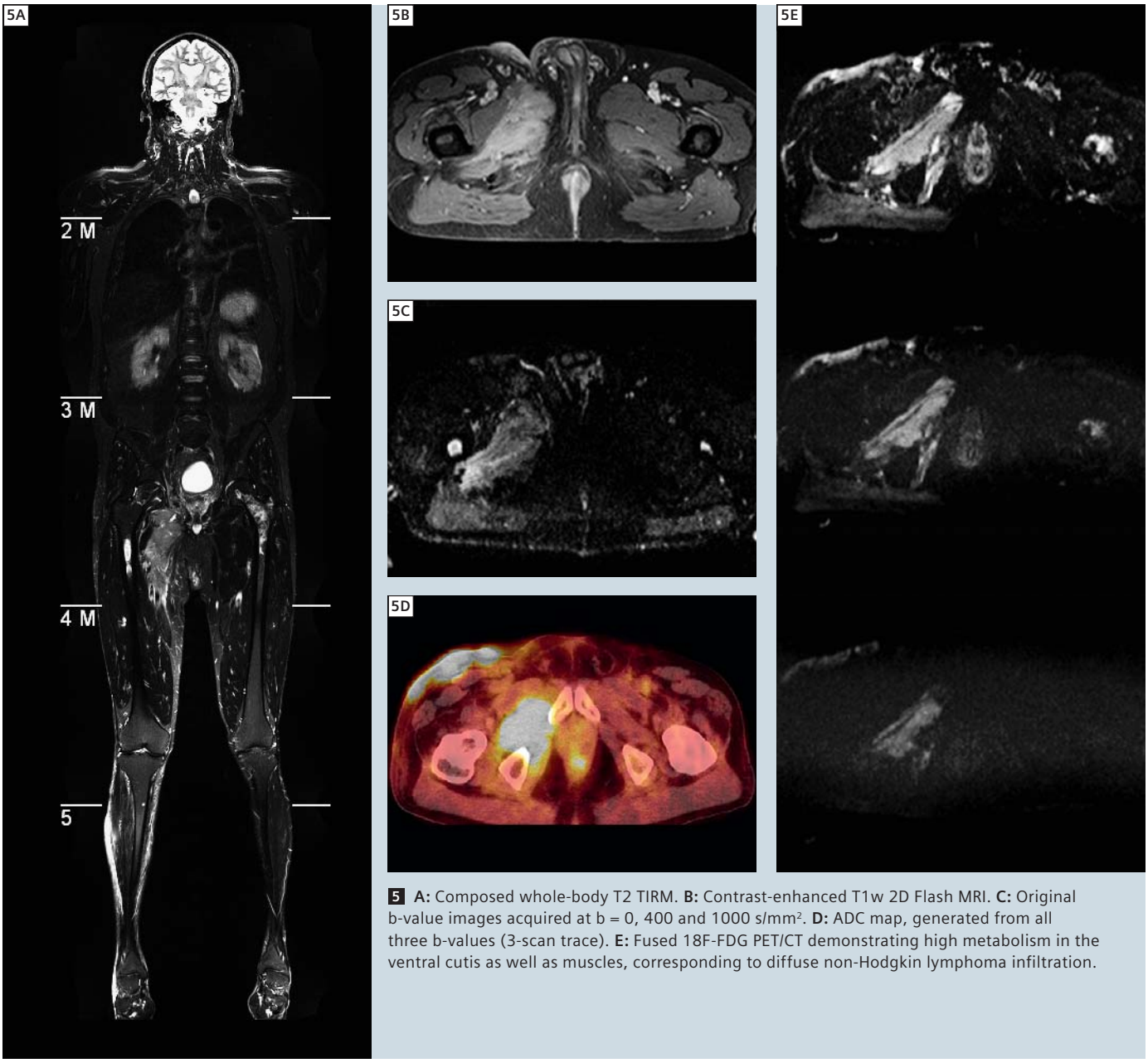


**5** **A:** Composed whole-body T2 TIRM. **B:** Contrast-enhanced T1w 2D Flash MRI. **C:** Original b-value images acquired at b = 0, 400 and 1000 s/mm². **D:** ADC map, generated from all three b-values (3-scan trace). **E:** Fused 18F-FDG PET/CT demonstrating high metabolism in the ventral cutis as well as muscles, corresponding to diffuse non-Hodgkin lymphoma infiltration.


**References**

1 Walker R, Kessar P, Blanchard R, Dimasi M, Harper K, DeCarvalho V, Yucel EK, Patriquin L, Eustace S. Turbo STIR magnetic resonance imaging as a whole-body screening tool for metastases in patients with breast carcinoma: preliminary clinical experience. J Magn Reson Imaging 2000; 11(4):343-50.

2 Lauenstein TC, Goehde SC, Herborn CU, Goyen M, Oberhoff C, Debatin JF, Ruehm SG, Barkhausen J. Whole-body MR imaging: evaluation of patients for metastases. Radiology 2004; 233(1):139-48

3 Schlemmer HP, Schafer J, Pfannenberg C, Radny P, Korchidi S, Muller-Horvat C, Nagele T, Tomaschko K, Fenchel M, Claussen CD. Fast whole-body assessment of metastatic disease using a novel magnetic resonance imaging system: initial experiences. Invest Radiol 2005; 40(2):64-71.

4 Schmidt GP, Baur-Melnyk A, Herzog P, Schmid R, Tiling R, Schmidt M, Reiser MF, Schoenberg SO. High-resolution whole-body magnetic resonance image tumor staging with the use of parallel imaging versus dual-modality positron emission tomography-computed tomography: experience on a 32-channel system. Invest Radiol. 2005; 40(12):743-53.



**Contact**
Matthias Lichy, M.D.
Siemens AG, Healthcare Sector,
Marketing Magnetic Resonance
P.O. Box 32 60
91050 Erlangen
Germany
matthias.lichy@siemens.com

# Whole-Body MRI for Accurate Assessment of Tumor Load of Bone Metastases Originate from Mamma Carcinoma

**Philip Aschoff; Christina Pfannenberg; Claus Claussen; Heinz-Peter Schlemmer**

*Department of Diagnostic and Therapeutic Radiology, University Hospital of Tuebingen, Tuebingen, Germany*

## Background

While large efforts in the early and precise detection of mamma carcinoma and therefore detection in a potentially curative stage have been undertaken, mamma carcinoma remains the main leading cause of cancer-related deaths in women. It is also known from a variety of tumor entities that the accurate and precise detection of metastases and estimation of tumor load is of high relevance for patient-adopted individualized therapy regimes. While mammography and ultrasound do play an important role for local assessment of tumor extend / recurrence, ultrasound of, for example, the liver and to some extent also the conventional x-ray of, for example, the chest do play a role in detection of extended diseases; the indications and clinical benefit of these imaging modalities for staging of metastatic breast cancer is the subject of debate. Another routinely-used technique for detection of distant metastases is bone scintigraphy. However, it is not an uncommon finding of mamma carcinoma bone filiae that they are characterized as lytic lesions without surrounding reaction of the bone matrix. In combination with the limited spatial resolution, this fact reduces the sensitivity of bone scintigraphy and can result therefore in an inaccurate or even false negative estimation of metastatic spread [1]. Additionally the pressure to optimize the diagnostic pathways in regards to staging accuracy, time consumption (including multiple referrals), costs and finally patient comfort have lead to an increased usage of computed tomography for fast and precise coverage of soft tissue and bones in patients with extended tumor disease. But relying mainly on morphologic changes, small bone metastases, as well as diffuse bone marrow infiltration and small lymph node filiae, are missed easily [2]. Within recent years, the application of PET/CT has increased especially the specificity in the detection of malignant lymph nodes. In combination with contrast-enhanced CT scans, a clear advantage of an 18F FDG PET/CT exam compared to the M-staging with x-rays, ultrasound and CT alone can be claimed. In contrast to other tumor entities, like lung cancer or malignant melanoma, however, the larger variation of degree of increased glucose metabolism of mamma carcinoma cells can result in more false negative PET findings [3, 4]. It has already been shown by several working groups, and for different tumor entities including breast cancer, that MRI with T2w fat saturated imaging sequences is superior to bone scinitgraphy and CT [5]. In the following two cases we show the advantages of MRI for imaging bone metastases originating from breast cancer. In both cases, there was the high clinical suspicion of a tumor recurrence with metastastic spread. The patient underwent therefore a combined whole-body 18F FDG PET/CT and a whole-body MRI (32-channel MAGNETOM Avanto) to complete tumor staging with special focus on the brain, liver and bone marrow. The whole-body MRI protocols were performed according to [6, 7]. For detection of bone metastases mainly three sequences were used:

**a)** coronal TIRM
**b)** transversal T2w TIRM covering the body trunk from pelvis to skull base and
**c)** contrast-enhanced transversal 2D (pelvis and abdomen; FLASH) or 3D (chest, VIBE) GRE sequences with fat saturation.

In the presented cases, our imaging protocol did not include a whole-body DWI with ADC mapping for improved tumor detection and for providing additional functional parameter for follow-up of therapy responses. Nevertheless, in all three cases, MRI had to be considered the most sensitive methodology for detection of bone metastases; however, the influence of the whole-body imaging modalities on the clinical outcome with the given therapy options for such advanced breast cancer patients has still to be answered. Nevertheless, whole-body (bone) MRI presents itself as the imaging modality of choice when an accurate assessment of bone metastases is required. To increase further the diagnostic confidence and to provide additional information about tumor biology and biological activity, future developments will combine PET with MRI within one examination and also different PET tracers such as 18Fluoride will be used.

## Case 1

In this case a 66-year-old patient underwent a breast-preserving mastectomy 12 years ago (R0 resection). Two years later a local tumor recurrence was observed and therefore a breast ablation and later augmentation was performed. Within a time-period of approximately 1 ½ years a slow but constant increase of the CA 15–3 tumor marker has been observed. In contrast to PET/CT, MRI showed multiple small lesions with T2w hyperintense signal and corresponding contrast-media uptake. Most of these lesions measured less than one centimeter in their maximum diameter (Figs. 1D, E). In retrospect, a discrete irregular bone configuration /sclerosis with implied focal FDG uptake can be found, corresponding to a larger metastases. Neither a further pathologic focal FDG uptake nor lytic / sclerotic CT lesions could be detected. Based on MRI and in concordance to the clinical follow-up, a diffuse metastatic spread had to be diagnosed in this case.

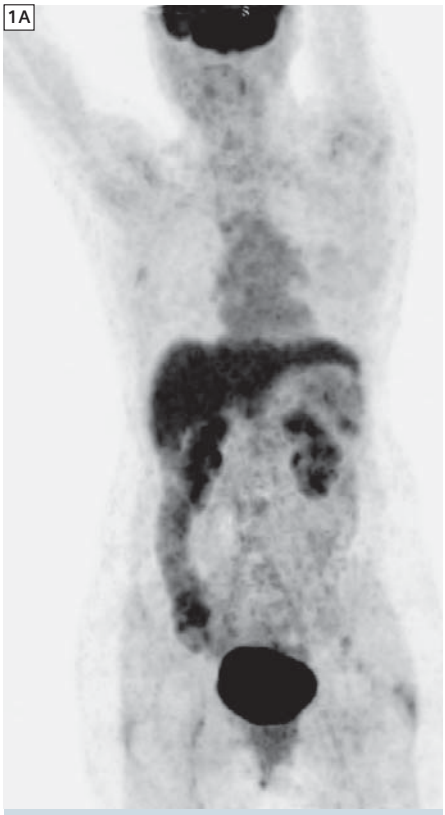

**1A** MIP of the FDG-PET examination.

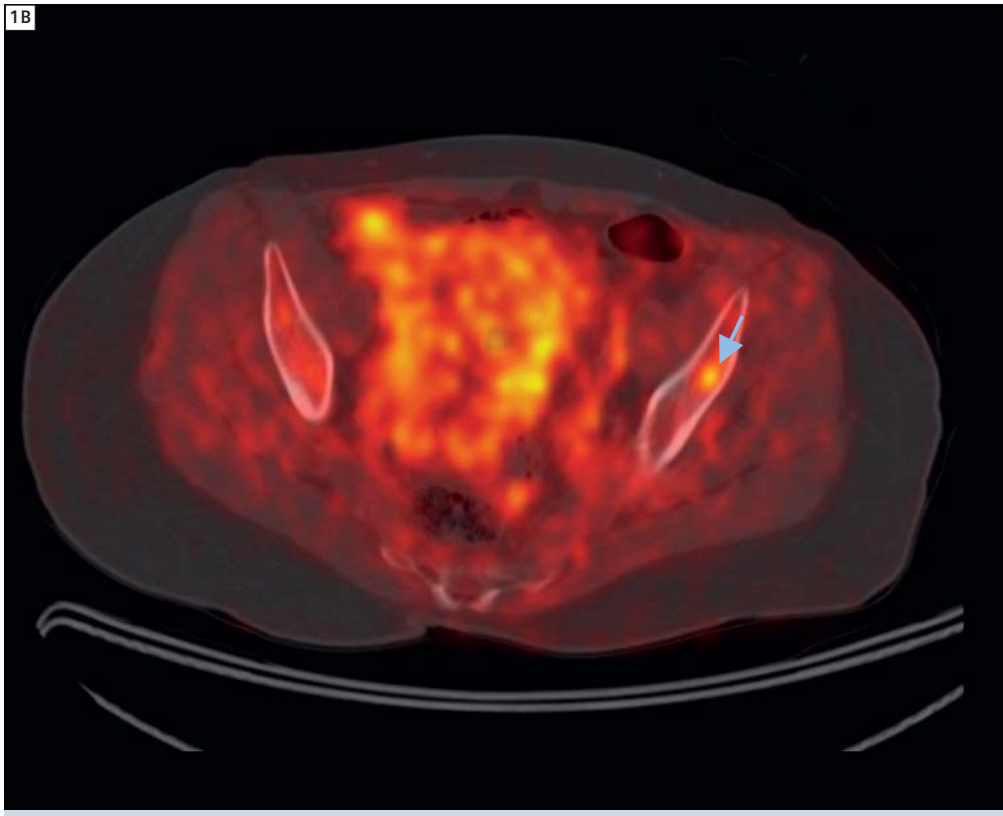

**1B** Focal uptake within the left iliac bone.

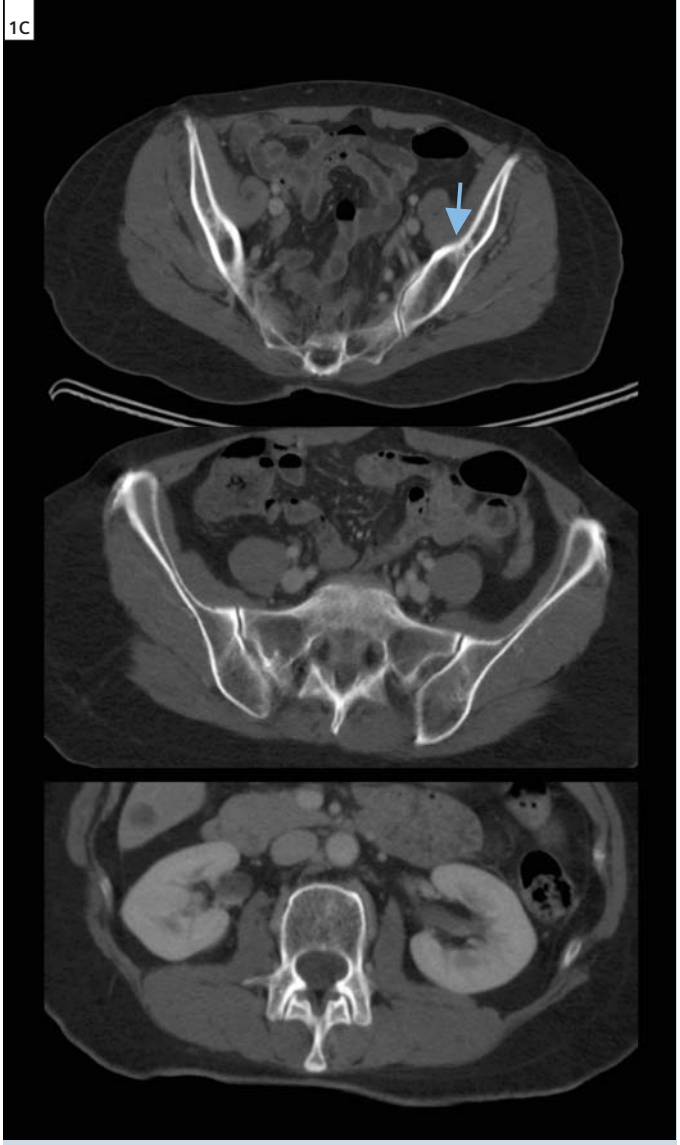

**1C** Corresponding to the PET scan, CT was able to visualize a small irregular sclerosis; further bone lesions could not be detected by FDG PET/CT.

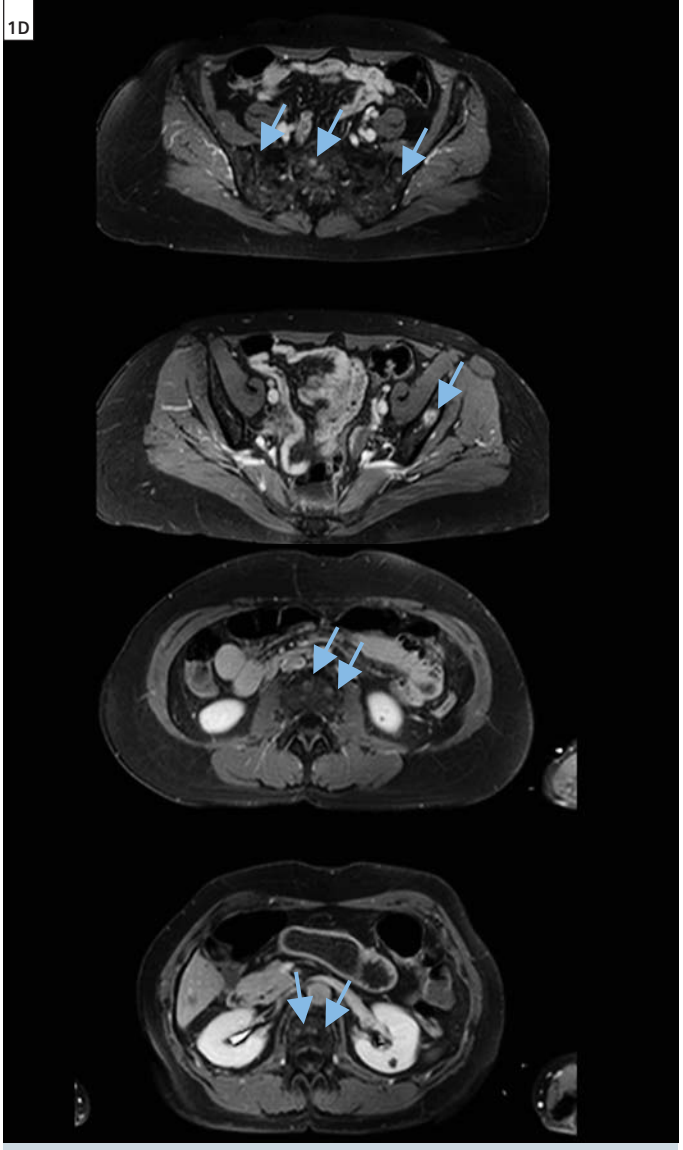

**1D** Contrast-enhanced T1w 2D FLASH, demonstrating multiple smallest bone metastases.

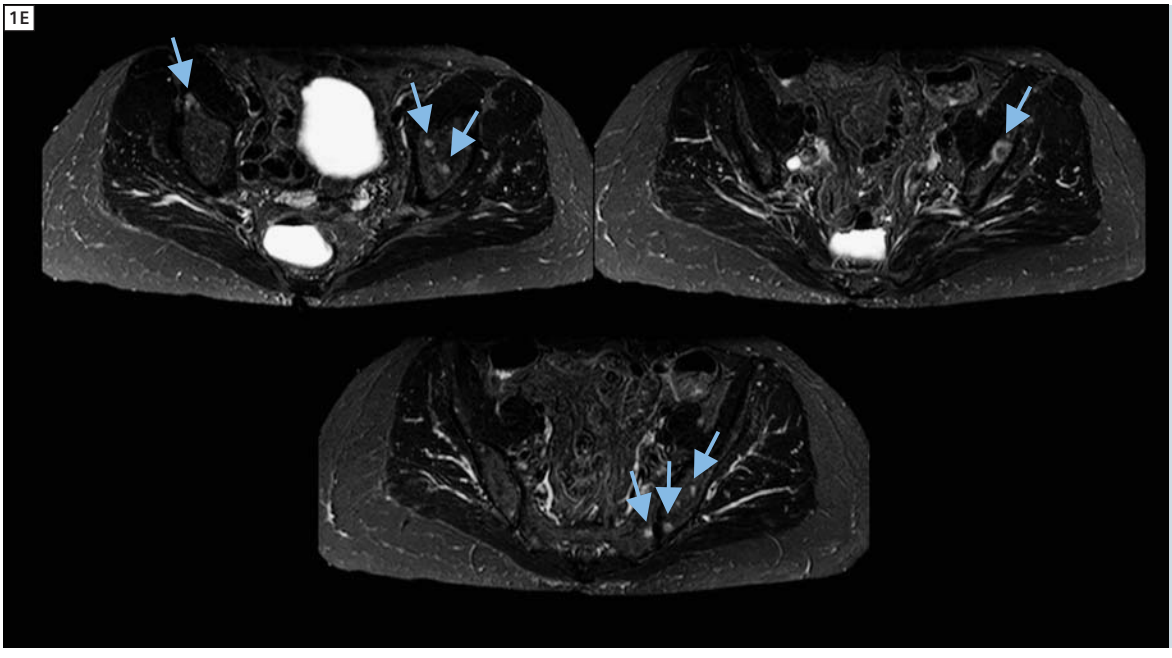

**1E** T2w TIRM; diffuse metastatic spread is obvious.

## Case 2

A 46-year-old patient underwent whole-body imaging because the routinely-acquired bone scintigraphy was inconclusive for bone metastases (Fig. 2A). A CT scan was performed directly after the bone scan but did not lead to a clear rule out or confirmation of a tumor recurrence. It should be mentioned that there were no other signs of tumor recurrence reported than the unclear bone scan, and the tumor markers were within normal range. The patient was initially diagnosed

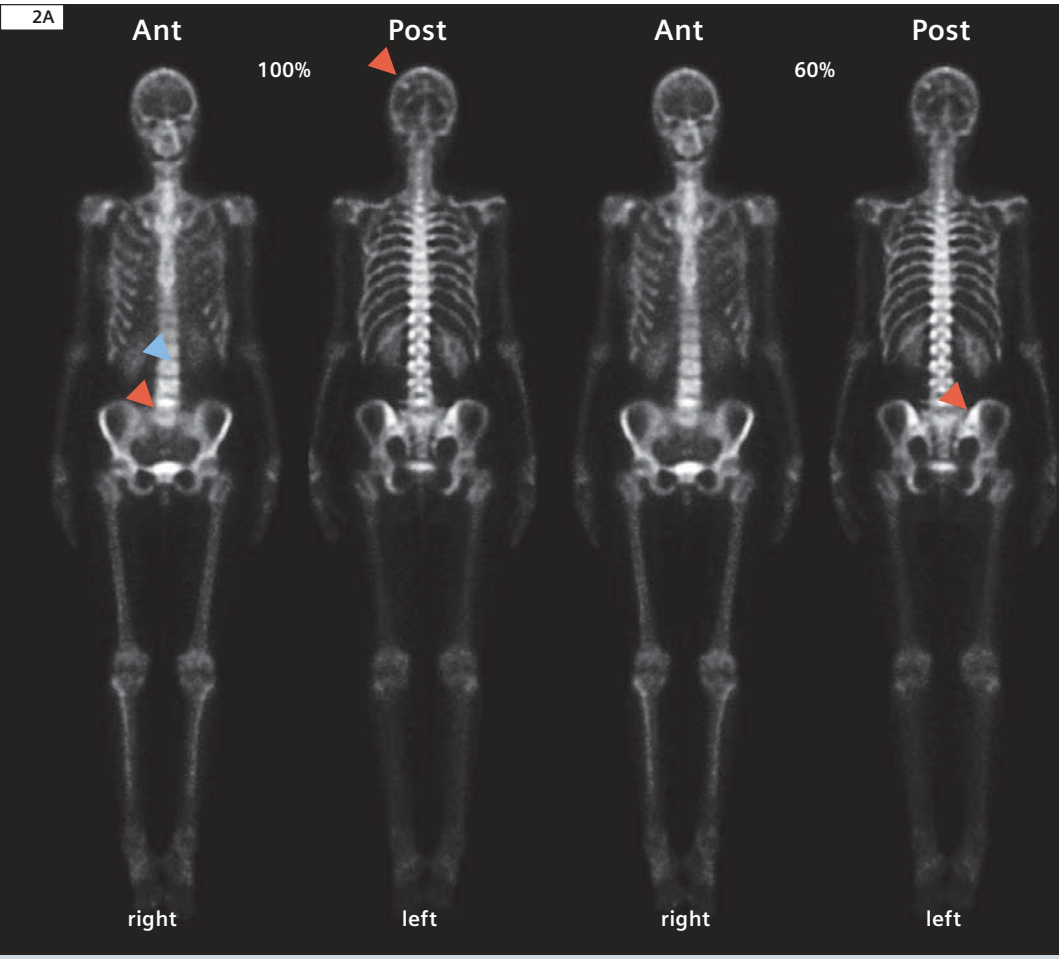


**2A** Bone scan suspicious for metastases (arrows).

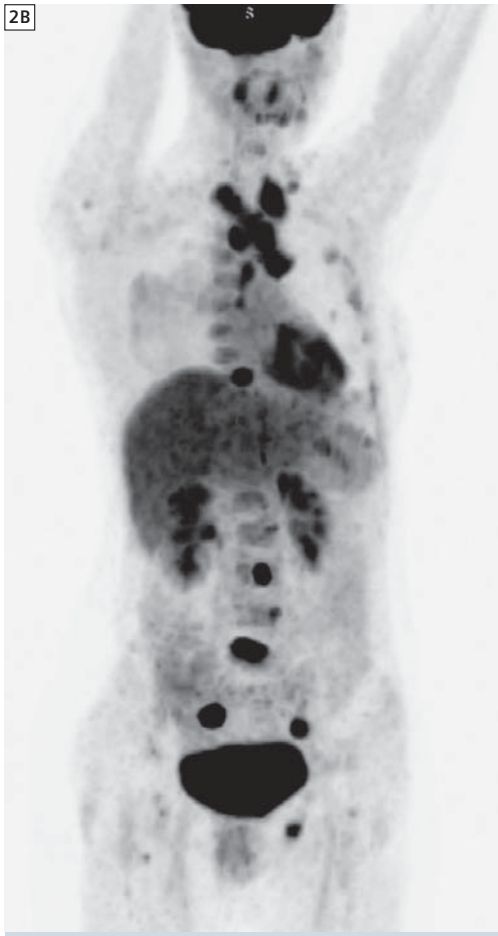


**2B** MIP of the FDG PET: multiple bone and lymph node metastases with clearly increased glucose metabolism are shown.

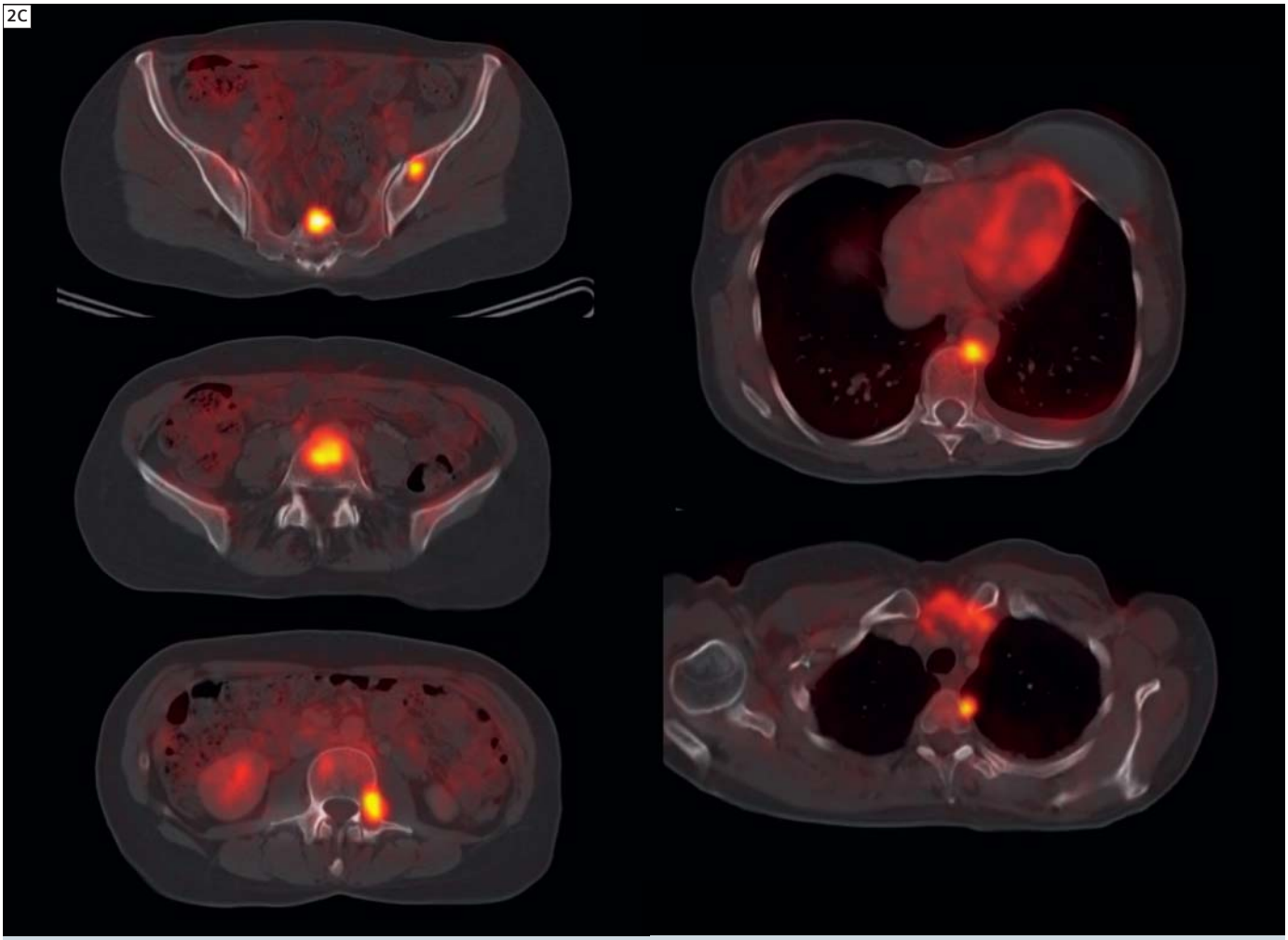


**2C** Corresponding PET/CT images demonstrating the extend of the multiple lytic bone metastases.

ten years ago with a breast cancer (pT1c pN1a (1/21) G2-3 M0) und underwent R0 breast ablation and LNE. Two years later a local tumor recurrence was diagnosed which resulted in a re-surgery, radiotherapy and chemotherapy. To definitively answer the question of a tumor recurrence, the patient was than sent to our department for a whole-body PET/CT and MRI. Based on PET/CT and MRI findings, an advanced tumor recurrence was diagnosed. Multiple osseous as well as mediastinal and cervical lymph node metastases are detected by high glucose metabolism on PET/CT (Figs. 2B, C) and MRI (Figs. 2D, E). MRI could visualize bone infiltration in more detail and its relationship to the spinal canal; however no differences in the total tumor load are obvious between the two imaging modalities. A hormone therapy was started and a partial remission could be achieved for this patient to date (18 months follow-up period; not shown).

References

1 Hamaoka T, Madewell JE, Podoloff DA, Hortobagyi GN, Ueno NT. Bone imaging in metastatic breast cancer. J Clin Oncol. 2004 Jul 15;22(14):2942-53.

2 Groves AM, Beadsmoore CJ, Cheow HK, Balan KK, Courtney HM, Kaptoge S, Win T, Harish S, Bearcroft PW, Dixon AK. Can 16-detector multislice CT exclude skeletal lesions during tumour staging? Implications for the cancer patient. Eur Radiol. 2006 May;16(5):1066-73.

3 Du Y, Cullum I, Illidge TM, Ell PJ. Fusion of metabolic function and morphology: sequential [18F] fluorodeoxyglucose positron-emission tomography/computed tomography studies yield new in-

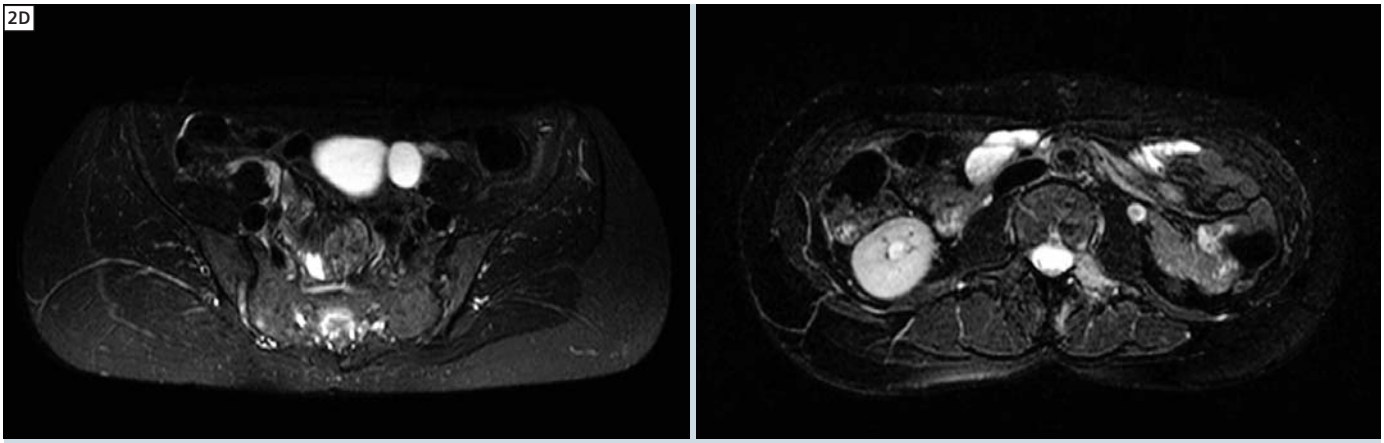

**2D** T2w TIRM MRI provides best delineation of bone metastases and the relationship to the spinal canal.

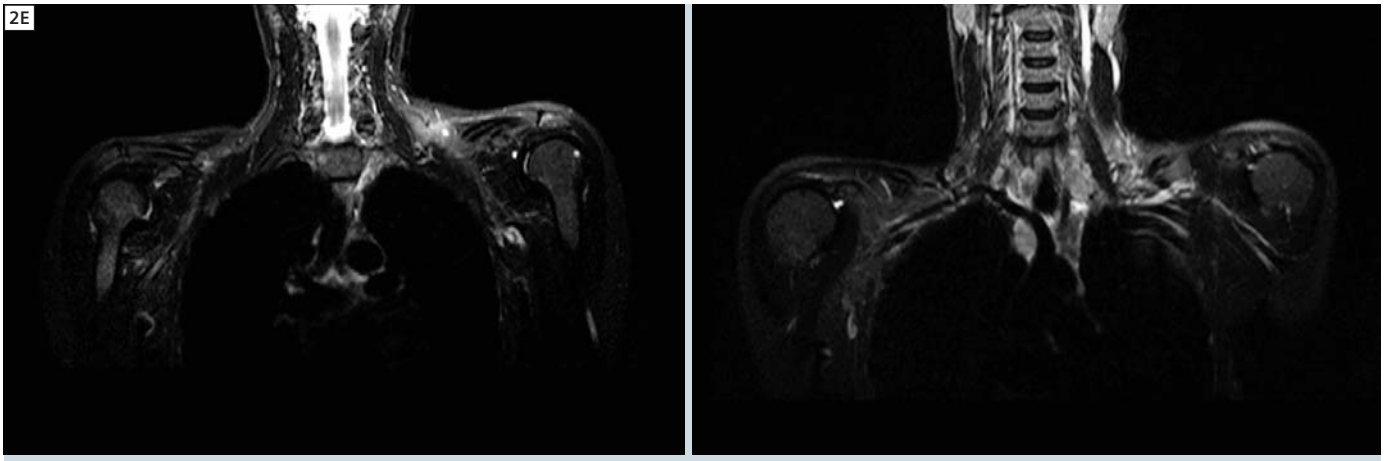

**2E** While PET/CT shows a higher diagnostic accuracy for small lymph nodes, in the presented case, MRI (coronal TIRM) could also stage the extension of the lymph node involvement correctly.

sights into the natural history of bone metastases in breast cancer. J Clin Oncol. 2007 Aug 10;25(23):3440-7.

4 Gil-Rendo A, Martínez-Regueira F, Zornoza G, García-Velloso MJ, Beorlegui C, Rodriguez-Spiteri N. Association between [18F]fluorodeoxyglucose uptake and prognostic parameters in breast cancer. Br J Surg. 2009 Feb;96(2):166-70.

5 Costelloe CM, Rohren EM, Madewell JE, Hamaoka T, Theriault RL, Yu TK, Lewis VO, Ma J, Stafford RJ, Tari AM, Hortobagyi GN, Ueno NT. Imaging bone metastases in breast cancer: techniques and recommendations for diagnosis. Lancet Oncol. 2009 Jun;10(6):606-14.

6 Walker R, Kessar P, Blanchard R, Dimasi M, Harper K, DeCarvalho V, Yucel EK, Patriquin L, Eustace S. Turbo STIR magnetic resonance imaging as a whole-body screening tool for metastases in patients with breast carcinoma: preliminary clinical experience. J Magn Reson Imaging. 2000 Apr;11(4):343-50.

7 Schlemmer HP, Schäfer J, Pfannenberg C, Radny P, Korchidi S, Müller-Horvat C, Nägele T, Tomaschko K, Fenchel M, Claussen CD. Fast whole-body assessment of metastatic disease using a novel magnetic resonance imaging system: initial experiences. Invest Radiol. 2005 Feb;40(2):64-71.

**Contact**
Philip Aschoff, M.D.
Department of Diagnostic and Therapeutic Radiology
University Hospital of Tuebingen
Hoppe-Seyler-Strasse 3
72076 Tuebingen
Germany
philip.aschoff@med.uni-tuebingen.de

# Case Report: Klippel-Trénaunay-Weber Syndrome

Chawla Tanya, M.D.[1]; Scott Enns[1]; Melissa Charette[1]; Nancy Talbot[1]; Karen Bodolai[1]; Sunil Kumar S. L., M.D.[2]

[1]*Princess Margaret Hospital, University Health Network, Toronto, Canada*
[2]*Siemens Healthcare, Toronto, Canada*

## Patient history

We report on a 31-year-old female patient with known Klippel-Trénaunay-Weber syndrome. The patient was gravid and at 27 weeks gestation*. Referral to our institution was to confirm the presence of a venous malformation and aid obstetrical planning to determine if a Caesarean section was technically feasible.

The Klippel-Trénaunay-Weber syndrome is a rare congenital disease characterised

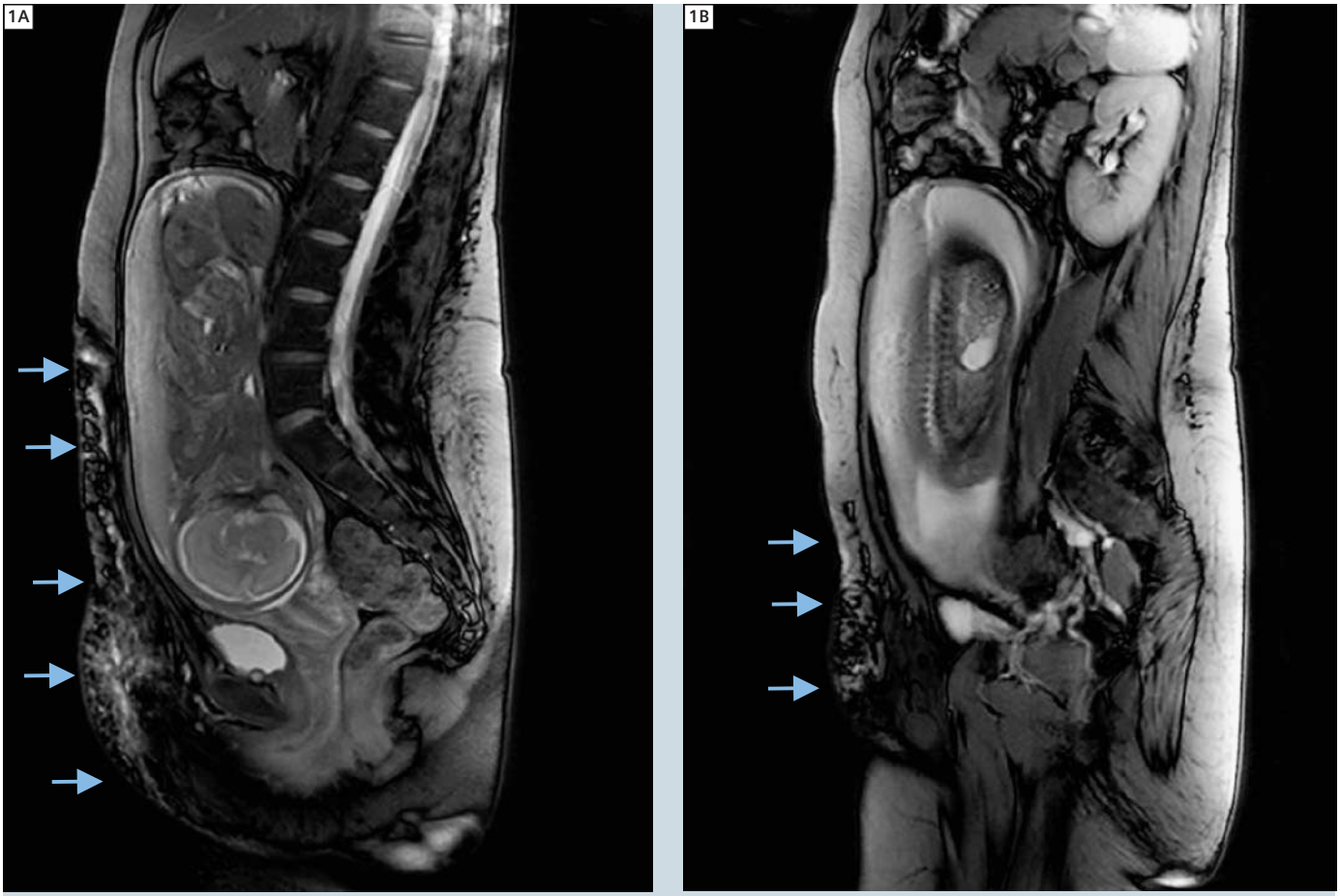


**1** Composed sagittal TrueFISP images, consisting of two measurements. The extensive venous malformation is well delineated (arrows).

by a triad of capillary hemangioma (port-wine stain), large venous malformations as well as lymphangiomas. The haemangioma is of variable depth and can involve the deep sub-cutaneous tissues as well as involving adjacent visceral organs or bowel. It is also associated with focally limited gigantism (in very rare cases also dwarfism). The Klippel-Trénaunay-Weber syndrome is therefore also described as angiodysplasia with dominantly venous-cavernous type and hypertrophy of the affected extremity. Most cases are sporadic, although a few cases in the literature report an autosomal dominant pattern of inheritance. If arteriovenous malformations are present within the affected extremities, this special form is often described as Parkes Weber syndrome.

## Sequence details

All images were acquired at 1.5T (MAGNETOM Avanto, 32-channel, SQ-Engine) with the usage of two Body Matrix coils and the integrated spine coil. The anatomical area covered with this MR exam reached from the upper lower extremities towards the upper abdomen. The examination was performed as a multistep MR exam. The scanner is equipped with the Tim Planning Suite. Because of the limited breath-hold capabilities of the patient, short and robust imaging sequence were mainly used (HASTE, TrueFISP). The protocol comprised: transversal (TR / TE 1380 / 76 ms, FOV 317 x 315 mm, matrix 220 x 256 Px, SL 7 mm), coronal (TR / TE 1375 / 76 ms, FOV 350 mm, matrix 243 x 256 Px, SL 7 mm) and sagittal (TR / TE 1380 / 76 ms, FOV 350 x 350 mm, matrix 243 x 256 Px, SL 7 mm) HASTE and TrueFISP (TR / TE 3.69 / 1.85 ms, FOV 350 x 350 mm, matrix 486 x 512 Px, SL 7 mm, respectively). For evaluation of potential large arterial feeder of the large vascular malformation, a dynamic MR sequence was used (3D FLASH in coronal orientation, 41 measurements, temporal resolution 6 seconds, TR / TE 2.13 / 0.76 ms, FOV 450 x

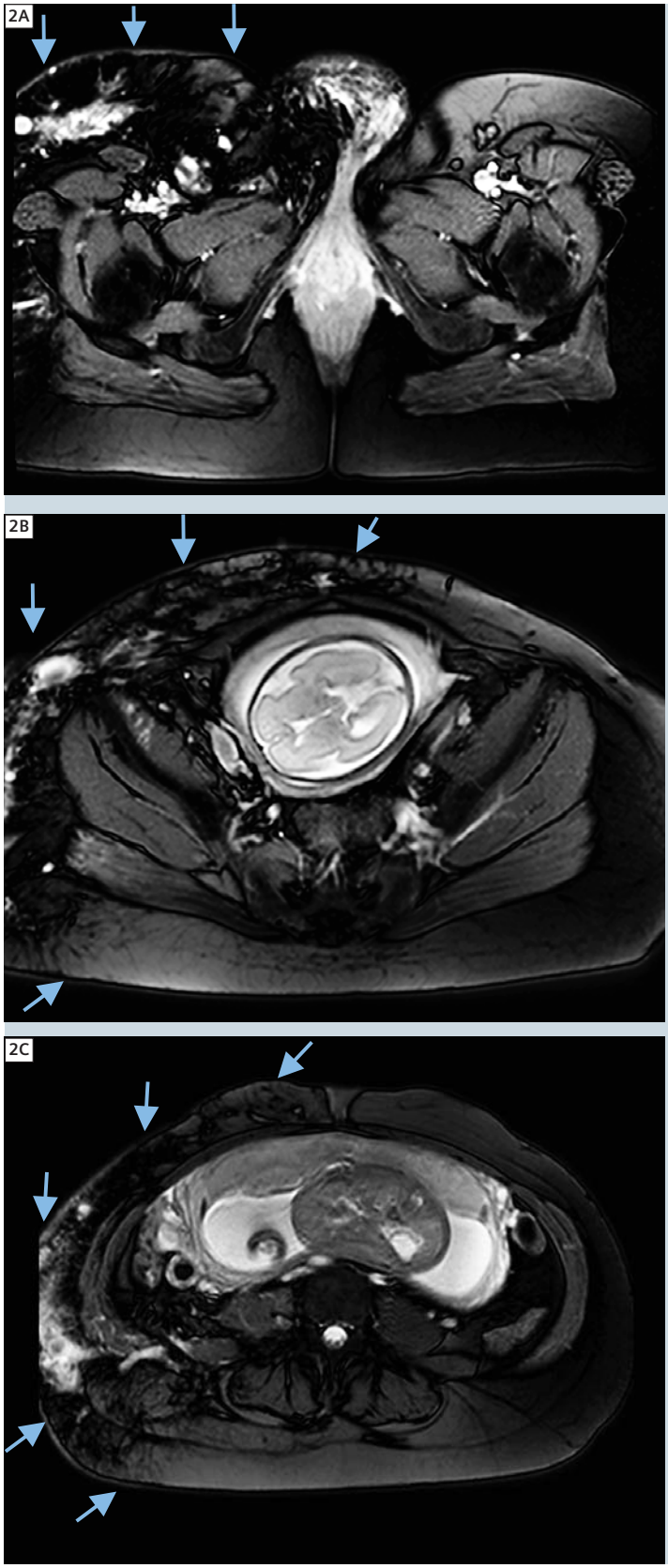


**2** Transverse TrueFISP images. The involvement of the right thigh, pubis and abdominal wall by the vascular malformation is well visualised.

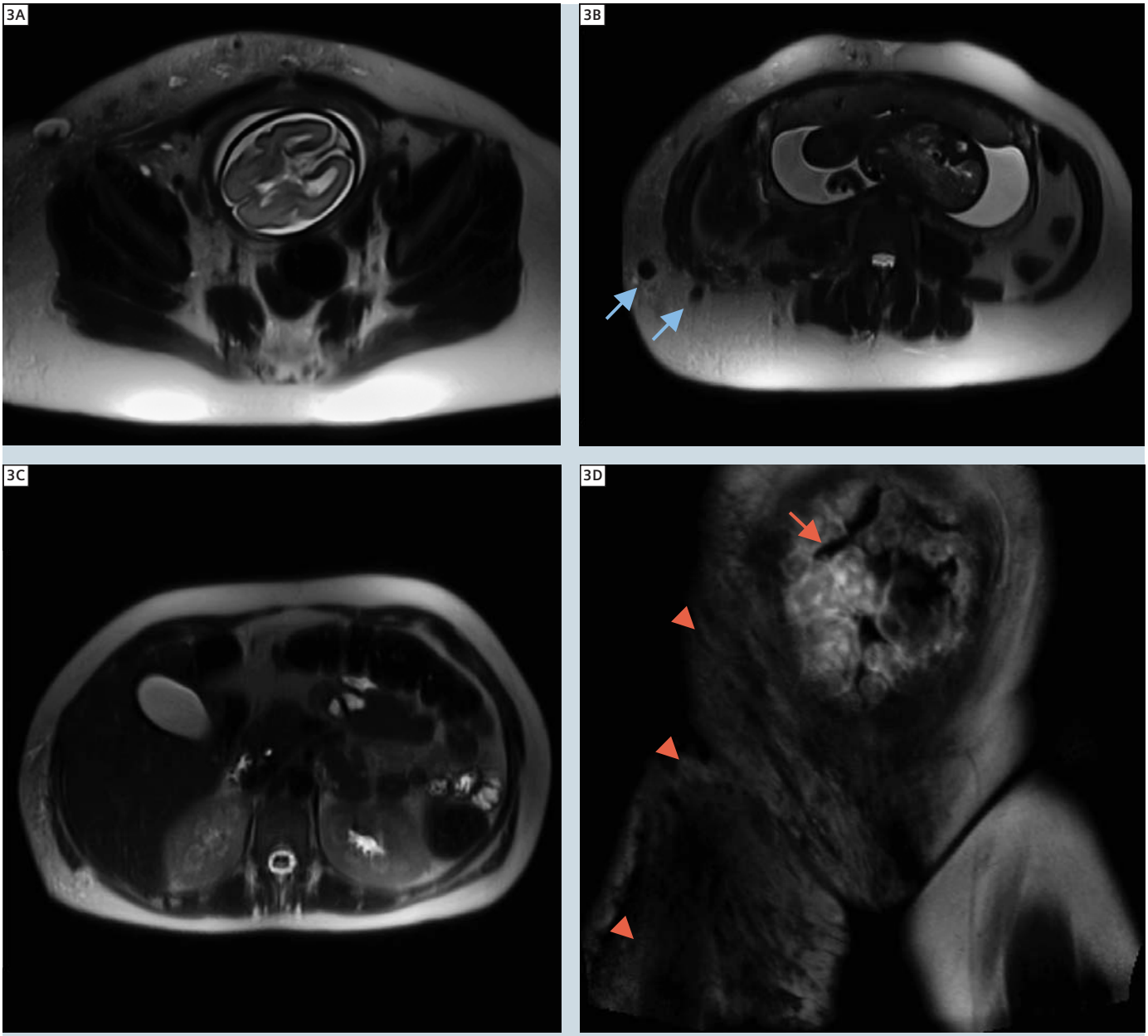


**3** Corresponding transverse HASTE images **(3A–C)** show bright signal of the vascular malformation, indicating a low flow. However, two large vessels are shown with a clear flow-void (arrows, **3B**). Based on dynamic MRI, no arteriovenous malformation can be detected within the large vascular malformation (red arrowheads). Enhancement of the placenta is noted (red arrow).

450 mm, matrix 240 x 320 Px, SL 7 mm). Venous drainage was visualized by applying a 3D VIBE in sagittal orientation after contrast-media injection (TR / TE 5.41 / 1.72 ms, FOV 400 x 400 mm, matrix 240 x 320 Px, SL 5 mm).

## Imaging findings

An extensive subcutaneous slow flow vascular malformation extending from the right thigh involving the right vulva, pubis, right lower abdomen and right flank was found. A large subcutaneous vein drained the malformation and entered the right retroperitoneum posteriorly at the level of L5/S1. An additional large subcutaneous vessel was identified in the right lower abdominal wall, which was favoured to comprise part of the venous drainage of the large malformation. No pelvic vascular malformations were seen. Also based on the dynamic MR scan, no evidence of an arterio-

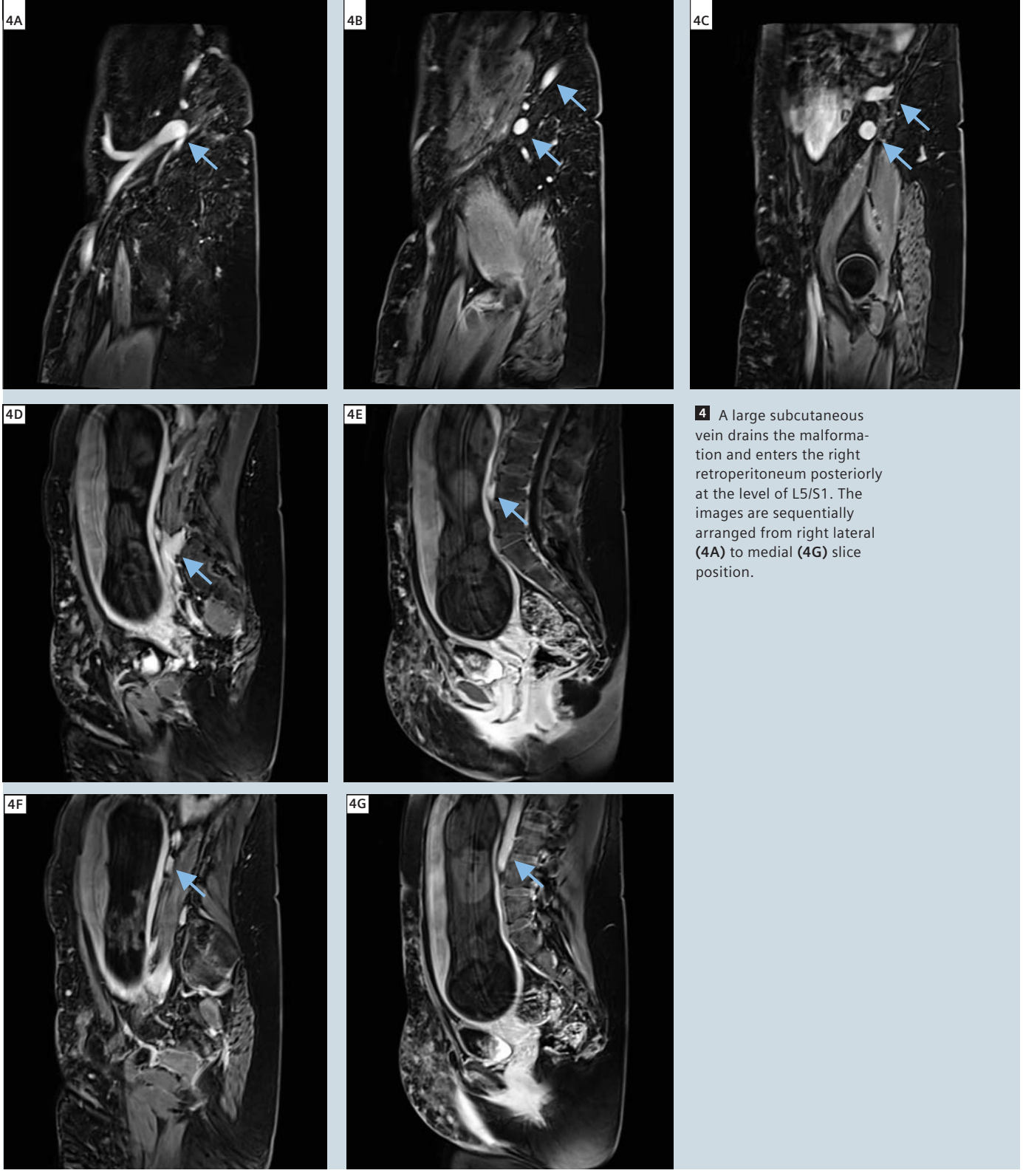


**4** A large subcutaneous vein drains the malformation and enters the right retroperitoneum posteriorly at the level of L5/S1. The images are sequentially arranged from right lateral **(4A)** to medial **(4G)** slice position.

venous shunt was found. The venous malformation crossed the midline to the contralateral abdominal wall; however, there were no venous malformations visible on the left side of the abdomen.

*The safety of imaging fetuses has not been established.

**Contact**
Dr. Chawla Tanya
Assistant Professor and Staff Radiologist
MRCP FRCR FRCPC
Princess Margaret Hospital, University Health Network
610 University Avenue
Toronto, ON M5G 2M9
Canada
nancy.talbot@uhn.on.ca

# Cerebral Blood Flow Imaging with 3D GRASE ASL Sequence Increases SNR and Shortens Acquisition Time

**David A. Feinberg**[1,2,3]**; Matthias Günther**[1,4,5]

[1]*Advanced MRI Technologies, LLC, Sebastopol, CA, USA*
[2]*University of California, Berkeley and San Francisco, CA, USA*
[3]*Redwood Regional Medical Group, Santa Rosa, CA, USA*
[4]*mediri GmbH, Heidelberg, Germany*
[5]*University Hospital Mannheim, Neurology, Heidelberg, Germany*

## Abstract

Arterial Spin Labeling (ASL) is a technique capable of measuring cerebral blood flow (CBF) in humans. However, ASL is limited by low sensitivity given blood is ~3% by volume in brain parenchyma. Single-shot 3D GRASE ASL technique has made possible whole brain coverage with over twice the signal-to-noise ratio (SNR) of 2D EPI ASL. To achieve even higher spatial resolution in fast acquisitions, a segmented version of the 3D GRASE ASL sequence is combined with a 32-channel coil at 3 Tesla to achieve 128 and 256 matrix images in 1 to 2 minutes.

## Introduction

In the early 1980s when the very first MRI blood flow images were shown at conferences, Nobel Prize laureate Prof. Paul Lauterbur commented, "As MR imaging techniques develop, blood flow imaging will advance with them." This is fortelling of the recent developments describing the uniquely powerful Arterial Spin Labeling (ASL) method of blood flow imaging [1–6], since it is very flexible and can be adapted to several different MR imaging sequences. Each imaging technique is differs in speed, image quality and ability to quantify blood flow. To be discussed below are the advantages of 3D sequences [1, 2, 26, 27] compared to 2D MRI in overcoming physiologic limitations in obtaining whole brain coverage. The 3D gradient and spin echo (GRASE) [1, 2, 18] readout scheme has advantages of refocusing many more signals than RARE / TSE / FSE or EPI sequences for higher SNR which translates into greatly reduced imaging time and much higher spatial resolution (Fig. 1). It has additional advantages of reduced susceptibility artifacts compared to Spiral and EPI techniques for improved image quality. Several examples of 3D GRASE ASL are presented here along with a fuller discussion of these differences.

## What is ASL imaging?

To measure blood perfusion in brain tissue, it is necessary to quantify signal

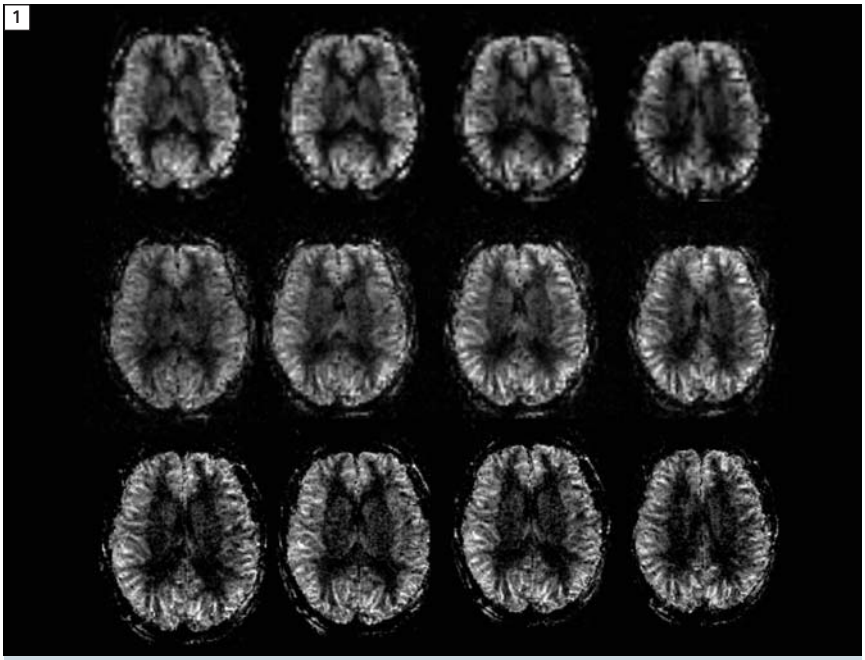

**1** 3D GRASE ASL with 32-channel coil **row 1)** 64 matrix, resolution 4 x 4 x 4 mm³ voxel, 26 images, 16 s, **row 2)** 128 matrix, resolution 2.5 x 2.5 x 2.0 mm³ in 1 min **row 3)** 256 matrix, resolution 1.5 x 1.5 x 3.0 mm³, 26 images, 2:04 min.

2A

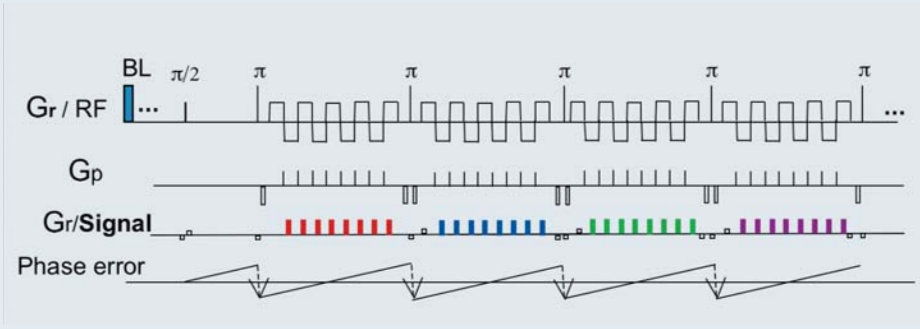


2B

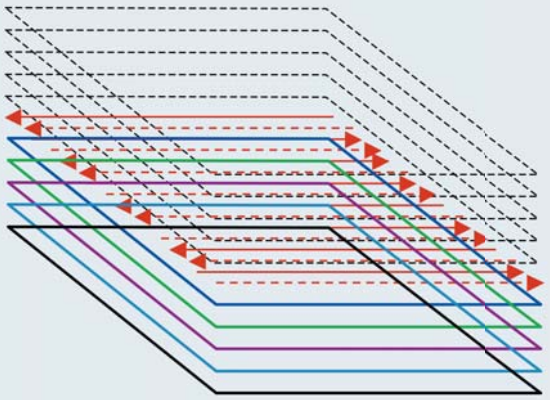

3D GRASE ASL

**2** 3D GRASE ASL. The 180° RF refocusing pulses (π) prevent large phase error. EPI type gradient refocusing (Gr) gives maximum number of signals, (BL) blood labeling and background suppression pulses.

changes independent of the signal from the partial volumed static brain tissue. ASL obtains two images, each with identical signals from brain tissue but different blood signal as affected by the presence / absence of blood labeling RF pulses (typically inversion RF pulses). Ideally, subtraction of the two images removes static brain tissue signal leaving only blood signal which intensity reflects hemodynamic parameters of cerebral blood flow (CBF) and the blood bolus arrival time (BAT) to the tissue. Critical to the success of ASL, the blood spin labeling is achieved by manipulating the longitudinal magnetization, which stores the "labeled" (tagged) spin magnetization with T1 decay (~1200–1500 ms) rather than with shorter T2 decay (~150 ms). The longer T1 decay enables enough time for the spins in blood to reach the brain tissue upstream from the arterial location of labeling. The tagging of the inflowing blood spins can either occur in a small localized region but over a long period of time of several seconds (continuous ASL [2, 3, 7, 9, 14, 24]) or at a larger region at a defined point in time (pulsed ASL [28–31]. After labeling preparation the tagged blood spins are given an inflow time TI to allow them to move into the microvasculature of the imaging region. A typical inflow time is 1500 ms. The beginning of the image readout sequence typically occurs with a 90° excitation pulse followed by either a gradient echo train sequence such as EPI or spiral, where the signal decays with T2* or by a spin echo based sequence like RARE or GRASE, where the signal decays with a combination of T2 and a component of stimulated echoes with longer T1 decay. As mentioned above, the measured signal will be dominated by brain tissue signal with blood signal being in the range of a few percent. Therefore, additional application of background suppression pulse schemes are incorporated to reduce the amplitude of static signal so errors in net subtracted signal is reduced for more reliable measurement of blood signal [32]. For quantification of cerebral blood flow several models exist [6, 12, 13] with the one-compartment model [12] being used most often. One of the most critical aspects of quantification is the variation of arrival times of the labeled blood bolus at different regions of the brain. Several techniques have been developed to reduce the sensitivity to this bolus arrival time (BAT) [4, 6]. Time-consuming sampling the inflow of the labeled blood into the tissue allows the measurement of BAT as an additional hemodynamical parameter. For whole brain application, this technique requires an efficient ASL technique, which provides sufficient SNR to reduce overall scan time and supports large region coverage.

## 2D and 3D ASL slice coverage limitations of hemodynamic timing

One of the major drawbacks of 2D EPI based ASL is a limitation on the number of images, preventing whole brain coverage. The EPI images are readout sequentially. With the acquisition of each EPI image ~50 msec, the blood inflow time of each slice increases with this time increment until the net range of inflow time is too large to ensure that the labeled blood is in the same vascular compartment in all slices. The 3D MRI sequences entirely overcome this problem because all images are readout

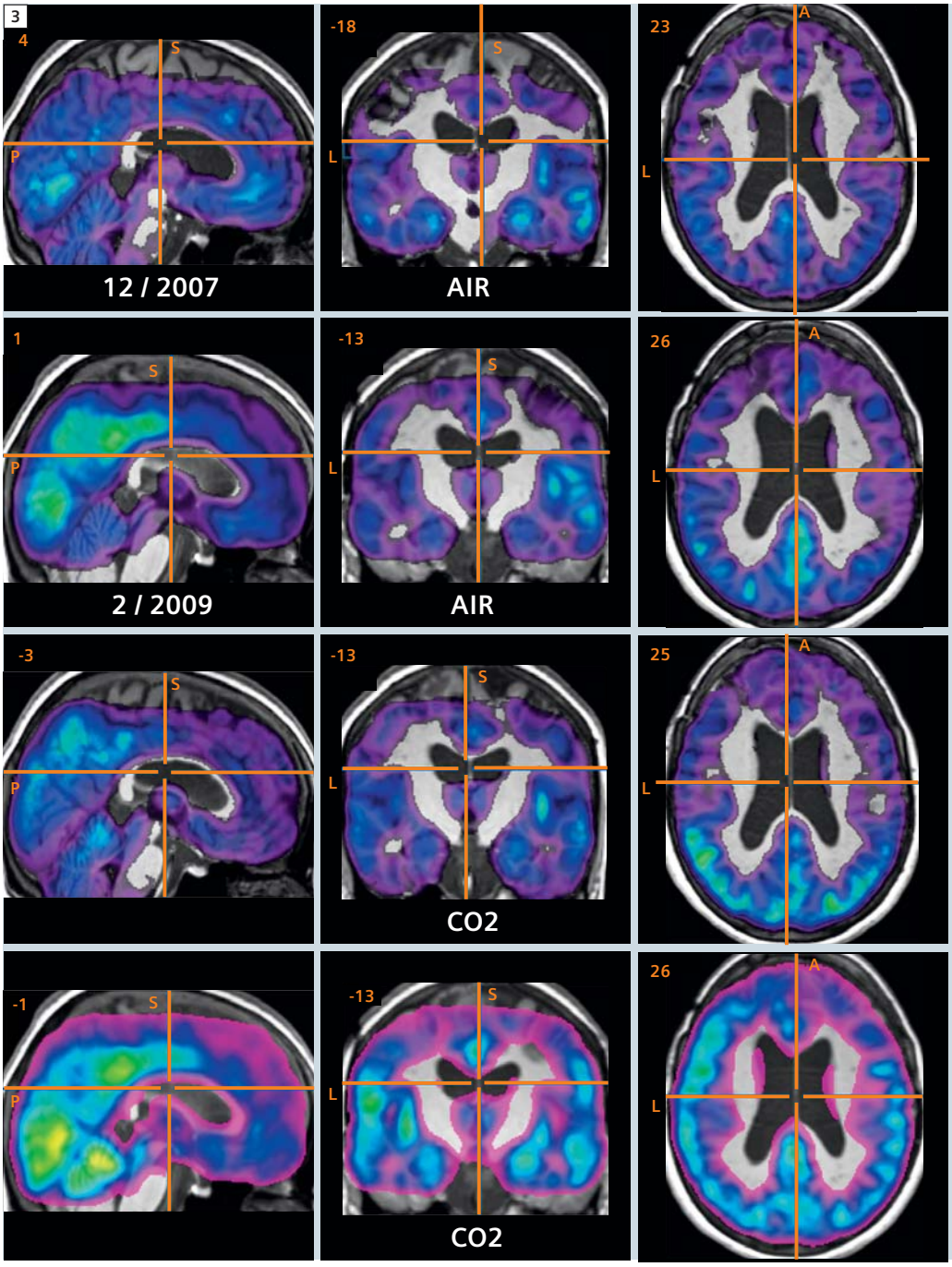


**3** CBF maps of MoyaMoya patient.
**Rows 1 and 2:** control image while breathing air.
**Rows 3 and 4:** hypercapnia, $CO_2$ challenge.
**Rows 1 and 3:** 12/2007 pre-surgery.
**Rows 2 and 4:** 2/2009 post-surgery show greater vascular reactivity post-surgery. The CBF maps from 3D GRASE ASL overlaid on anatomic images. *(Courtesy of Rik Achten, GIfMI, UGent, Belgium.)*

simultaneously rather than in temporal sequential order. The spins move into the brain tissue and at a specified time, all slices are encoded simultaneously beginning with a single 90 degree pulse covering a thick slab 3D volume [1, 27], not a single slice [11]. The echo train reads out all slices together which are then separated by a 3D Fourier Transform, which has additional sqrt(N) advantage of higher SNR compared to 2D EPI. Similarly, in a 3D readout the inversion pulse timing for background suppression is optimal for all slices, while in sequential 2D imaging there is variation between slices in the effectiveness of background suppression [32].

## Artifacts in 3D GRASE compared to RARE, Spiral, EPI

Basically any echo train sequence can be used for 3D ASL readout but each differs in their number of echoes, accumulative phase errors causing susceptibility artifacts, and SNR efficiency [25, 17]. Echo volume imaging (EVI) is the 3D variant of EPI which has an echo train time lim-

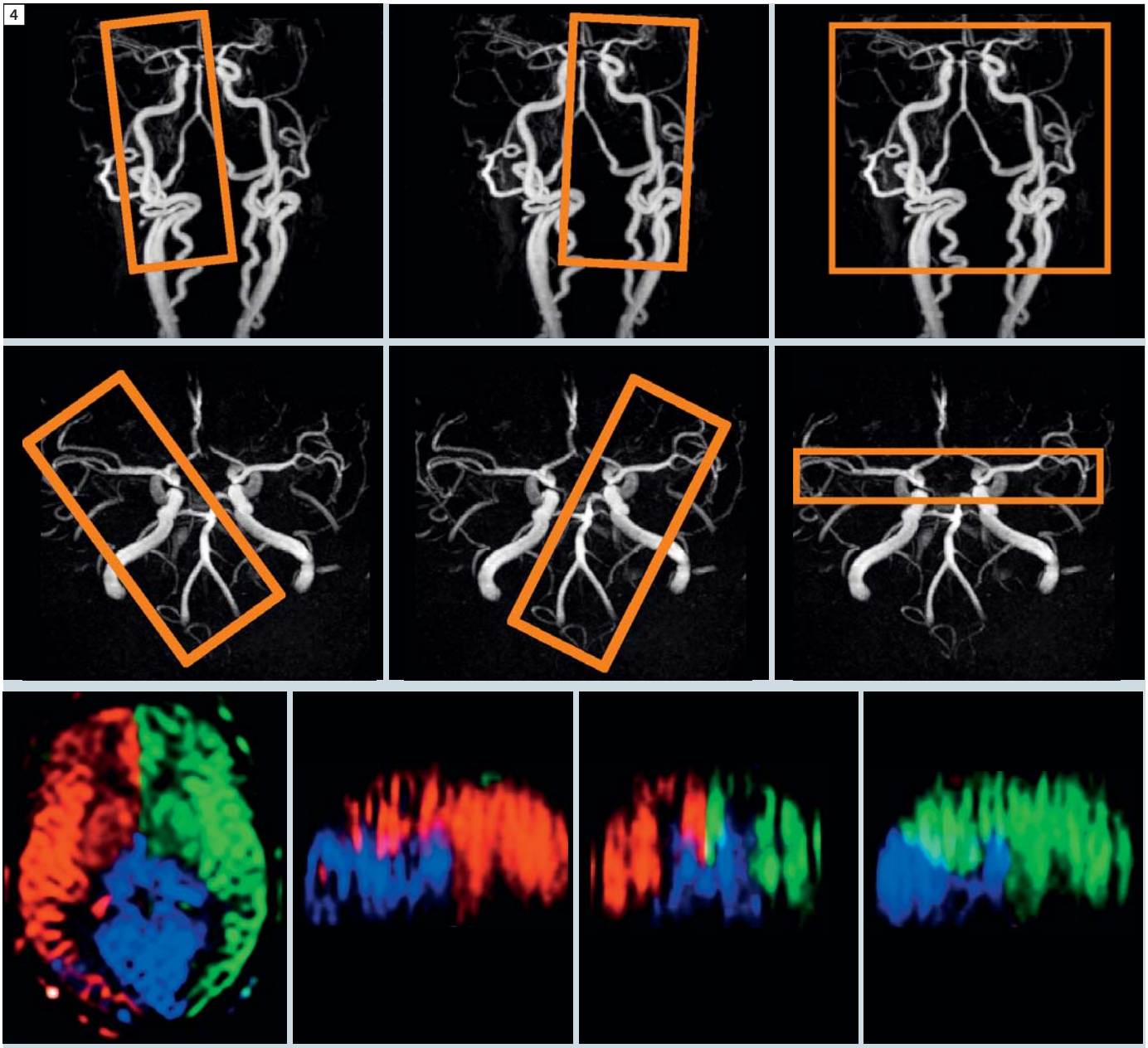

**4** Color-coded visualization of vascular territories in transverse, sagittal and coronal orientation. Three excitation regions shown in MRA (yellow box) A–P (top) and C–C (middle).

ited to under ~80 ms due to rapid T2* decay and it has large phase errors leading to susceptibility artifacts with regions of signal loss (similar to spiral and rectilinear EPI). 3D GRASE sequences has many RF refocusing pulses which maintains a low level of phase error and permits a sustainable echo train for up to 300 ms. RARE / TSE has similar net sequence time, however, there is a large fraction of time spent on RF refocusing pulses, 1 per signal. GRASE uses switched gradient rephrasing of signals to produce several times as many signals as TSE, which translates into faster imaging time and higher SNR per imaging time. A similar and useful variant, Spiral RARE (or Spiral GRASE) also has efficiency advantages, however, it places the beginning of the spiral, the center of k-space, on a gradient echo position at the beginning of each time interval between RF pulses, increasing susceptibility weighting. Furthermore, non-Cartesian image reconstruction methods are required. The key to success of 3D GRASE has been its high SNR, low arti-

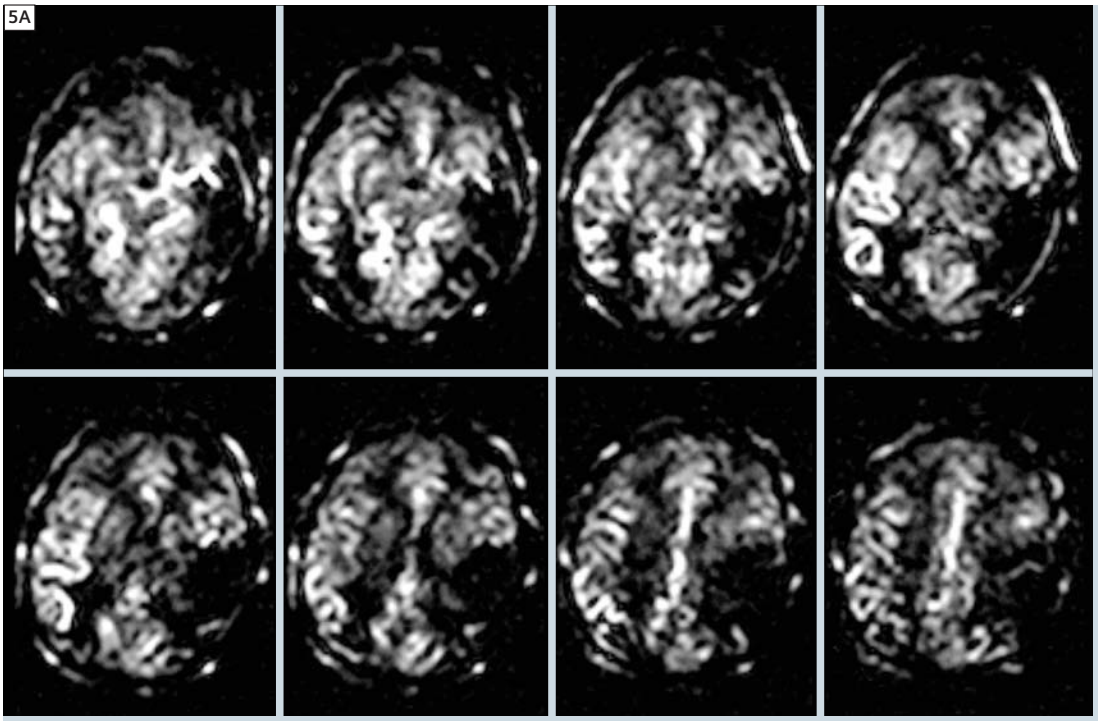


**5** Single-shot 3D ASL of two patients with acute stroke. **A:** in left MCA territory,

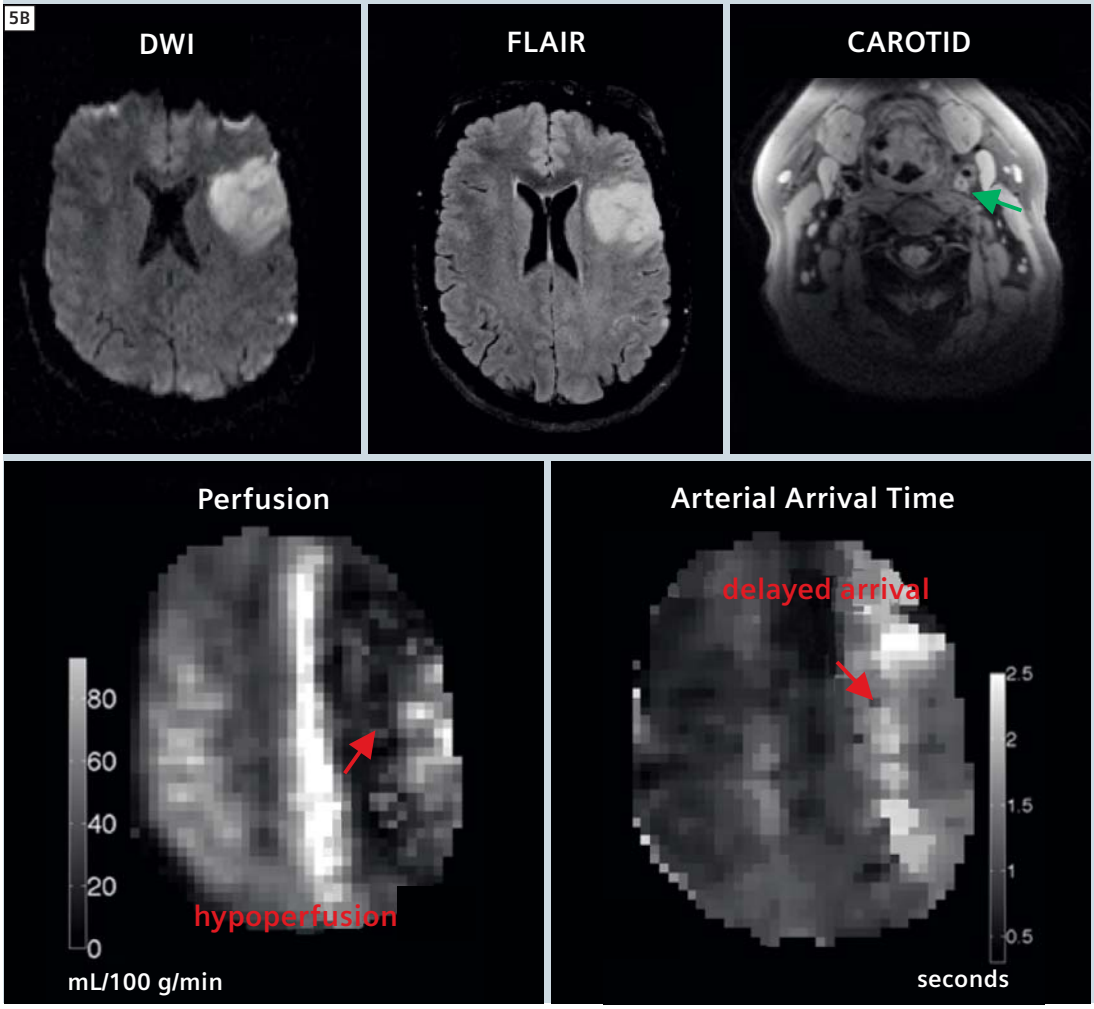


**5B** In second patient (48 hour) with hypoperfusion and delayed bolus arrival time (BAT) (red arrows) in ischaemic hemisphere, MRA reveals a near 100% occlusion in the left ICA (yellow arrow). *(Reproduced with permission of: BJ MacIntosh, P Jezzard et al., ISMRM 2009).*

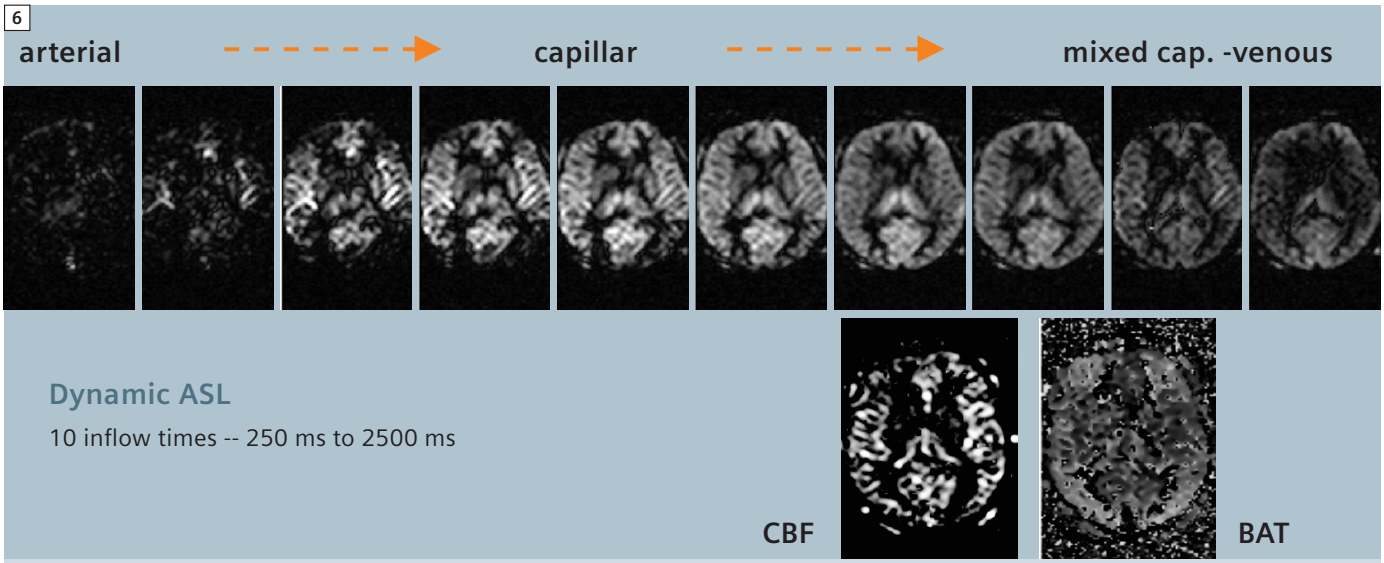


6 Dynamic ASL data acquisition with calculated CBF and BAT maps, 1 of 26 slices shown in a 3D whole brain coverage, inflow time (TI).

fact load due to the CPMG (Carr-Purrcell-Meiboom-Gill echos) timing, and whole brain coverage made possible with the simplified physiological timing in 3D acquisitions.

## The source of high SNR and fast data acquisition of 3D GRASE

The number of echoes produced in a single echo train of EPI, TSE and GRASE is dependent on the rate of echo refocusing which is relatively slow in RF refocusing (~4 ms) versus fast with switched gradient refocusing (~0.2 ms). It is no less dependent upon the signal decay times of T2 and T1 stimulated echo compared to shorter T2* of EPI. In relative terms the number of refocused echoes is in EPI (2 signal / ms x 30 ms) 60 echoes, TSE (1 signal / 3 ms x 300 ms) 100 echoes, and 3D GRASE (1.5 signal / ms x 300 ms) 450 echoes. Therefore, EPI has the fastest rate of echo generation by means of gradient switching but the shortest 'echo train time', ETT, due to T2* decay. TSE has the slowest rate using RF refocusing but a long ETT, whereas 3D GRASE has the benefit of both a fast refocusing rate and a long ETT which are multiplicative for much higher net signal (Fig. 2). In addition to increasing spatial resolution and image speed, the image SNR is dependent on square root of N signals in the Fourier transform. Therefore, the relative SNR of EPI, TSE and 3D GRASE is sqrt(60), sqrt(100) and sqrt(450), 7.7, 10.0 and 21.2 respectively. The possible earlier TE of EPI to a lesser extent mitigates some of this large SNR disadvantage to 3D GRASE, which nets to nearly a factor of 2.5 higher SNR and, thus, 3D GRASE has a factor of 6–8 in scan time reduction (fewer signal averages) at constant SNR.

## 32-channel RF head coil effects speed and resolution

Utilizing a 32-channel coil yields another ~2 higher SNR in cortical brain regions for all imaging techniques, and these SNR gains are multiplied in 3D GRASE. This allows either extremely fast ASL acquisitions or higher resolution than previously achieved in ASL images at 3 Tesla [25] (Fig. 1).
The 32-channel coil has therefore been used to acquire larger matrix images with higher resolutions, with up to 256 matrix in reasonable scan times of 2 minutes. Instead of going to higher resolution, the reduced acquisition time can be used to sample variable inflow times to separately quantify CBF from bolus arrival time BAT using parametric curve fitting (Fig. 6). It should be noted that 3D GRASE can be combined with several different ASL encoding schemes [22, 24].

## Resolving vascular territories in the brain

The images can be performed with separation of vascular territories by labeling different downstream vessels separately, (Fig. 4). Hadamard encoding has permitted to incorporate vascular territory sensitivity into an ASL protocol without loss of SNR compared to non-selective (standard) ASL to keep scan times in an acceptable range for clinical applications [21]. Stroke patients may be studied with 3D vascular territory ASL to evaluate changes occurring during recovery or to assess therapies (23). Patients with arterio-venous malformations (AVM) or aneurysms can have altered flow circuitry in the circle of Willis and downstream cerebral arteries identifiable as changes in vascular territory perfusion [20].

## High spatial resolution ASL

The segmented sequence version of 3D GRASE ASL provides shorter RF pulse intervals in the CPMG spin echo sequence [27]. This reduces susceptibility artifact and concurrently shortens the time of

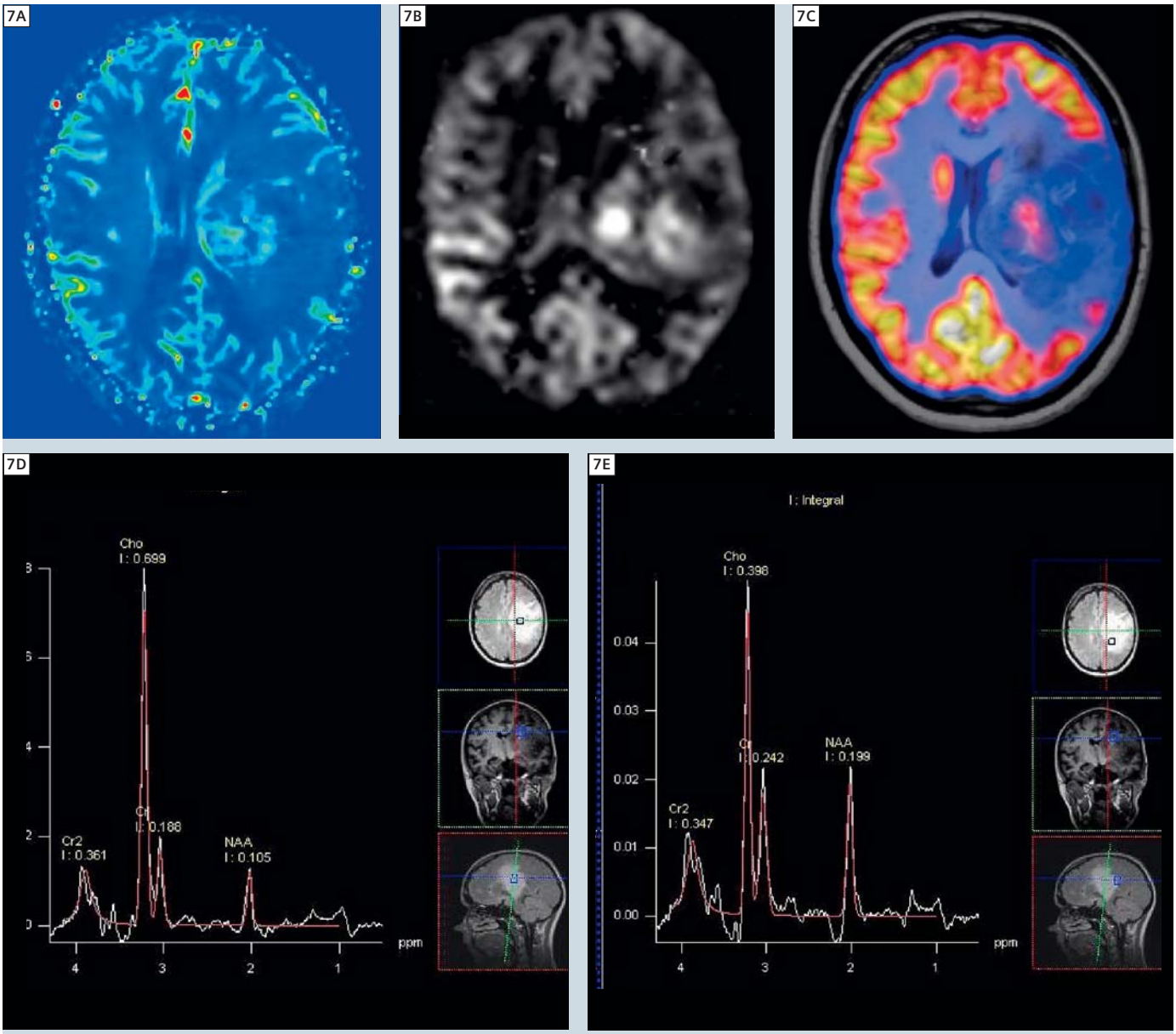


**7** ASL perfusion of Glioma. **A:** Dynamic susceptibility contrast, increased perfusion in center of a recurrent Glioma, originally grade II, **B:** ASL CBF map from dynamic ASL, showing increased perfusion **C:** PET image fused to MRI. A biopsy was performed in the location of highest perfusion in ASL CBF and a grade III was diagnosed. **D, E:** At time of biopsy, MRS showed the Cho/Cr was highest in biopsy location. *(Courtesy of Rik Achten, GIfMI, UGent, Belgium.)*

each of several echo trains for reduced through-plane blurring compared to the single-shot sequences. Image distortions were also reduced using the 128 matrix instead of 64 matrix as the larger FOV allowed swapping the phase and read axes, placing the highly switched read axis onto the head's lateral axis with less physiologic stimulation to allow higher bandwidth and closer echo spacing for less distortions. One unexpected fortuitous finding is that the segmented 3D GRASE sequence does not have artifacts from CSF or brain motion and the labeling pulses normalizes blood inflow and the larger 3D volume further removes slice inflow artifacts.

The SNR gains from the 32-channel coil/receiver system enabled higher resolution ASL images. The ASL encoding used pulsed ASL (PASL) sequence with QUIPSS II (QUantitiativ Imaging of Perfusion using a Single Subtraction) variants and background suppression pulses, previously described [1].

One can incorporate the 3D ASL sequence into a clinical protocol, requiring only 8–16 second scan time for whole brain coverage at 4 mm isotropic resolution or 2–4 minutes to

obtain highly quantitative BAT and CBF maps (Fig. 6), useful for evaluation of therapeutic responses to drugs and surgical interventions (Fig. 3), following brain recovery after stroke (Fig. 5), or evaluation of tumors (Fig. 7).
In conclusion, with ASL scan times now reduced from ~15 minutes 6 years ago, to ~16 seconds for a whole brain slice coverage, perfusion images should become just another image contrast mechanism, utilized in all routine clinical screening brain studies. With such fast scans and no need for contrast agents, ASL based perfusion imaging is an important new contrast mechanism that may be used by the radiologist in all routine clinical brain screening studies. Already with these refinements, ASL is faster than CT perfusion contrast imaging, and avoids x-ray dosage and risks of iodinated contrast agent to the patient. The rapid automated image processing of ASL perfusion maps enables their practical use in emergency medical studies. The ability of MRI to rapidly show several different contrast mechanisms in images (T1-weighted, FLAIR, diffusion-weighted imaging (*syngo* DWI)) and now CBF from 3D ASL without contrast injections, further establishes MRI as an invaluable diagnostic examination of brain disease.

Acknowledgment: N.I.H. National Inst. Neurological Disease and Stroke: grant no. 5R44NS059223

References


1 Gunther, M., K. Oshio, and D.A. Feinberg, Single-shot 3D imaging techniques improve arterial spin labeling perfusion measurements. Magn Reson Med, 2005. 54(2): p. 491–8.
2 M. A. Fernandez-Seara, Z.W., J. Wang, M. Korczykowski, M. Guenther, D. Feinberg, J. A. Detre. 3T Pseudo-continuous ASL Perfusion fMRI with Background-Suppressed Single Shot 3D GRASE During Memory Encoding. in International Society for Magnetic Resonance in Medicine. 2006. Seattle.
3 Detre, J.A., et al., Perfusion imaging. Magn. Reson. Med., 1992. 23: p. 37–45.
4 Alsop, D.C. and J.A. Detre, Reduced transit-time sensitivity in noninvasive magnetic resonance imaging of human cerebral blood flow. J. Cereb. Blood Flow Metab., 1996. 16: p. 1236–1249.
5 Gonzalez-At, J.B., D.C. Alsop, and J.A. Detre, Perfusion and transit time changes during task activation determined with steady-state arterial spin labeling. Magn. Reson. Med., 2000. 43: p. 739–46.
6 Wong, E.C., R.B. Buxton, and L.R. Frank, Quantitative imaging of perfusion using a single subtraction (QUIPSS and QUIPSS II). Magn Reson Med, 1998. 39: p. 702–8.
7 Yang, Y., et al., Transit time, trailing time, and cerebral blood flow during brain activation: measurement using multislice, pulsed spin-labeling perfusion imaging. Magn Reson Med, 2000. 44(5): p. 680–5.
8 Ye, F.Q., et al., Correction for vascular artifacts in cerebral blood flow values measured using arterial spin tagging techniques. Magn. Reson. Med, 1997. 37: p. 226–35.
9 Alsop, D.C. and J.A. Detre, Multisection cerebral blood flow MR imaging with continuous arterial spin labeling. Radiology, 1998. 208: p. 410–16.
10 McLaughlin, A.C., et al., Effect of magnetization transfer on the measurement of cerebral blood flow using steady-state arterial spin tagging approaches: a theoretical investigation. Magn Reson Med, 1997. 37(4): p. 501–10.
11 Wang, J., et al., Comparison of quantitative perfusion imaging using arterial spin labeling at 1.5 and 4.0 Tesla. Magn Reson Med, 2002. 48(2): p. 242–54.
12 Wong, E.C., R.B. Buxton, and L.R. Frank, A theoretical and experimental comparison of continuous and pulsed arterial spin labeling techniques for quantitative perfusion imaging. Magn. Rason. Med., 1998. 40: p. 348–55.
13 Buxton, R.B., et al., A general kinetic model for quantitative perfusion imaging with arterial spin labeling. Magn Reson Med, 1998. 40(3): p. 383–96.
14 Williams, D.S., et al., Magnetic resonance imaging of perfusion in the isolated rat heart using spin inversion of arterial water. Magn Reson Med, 1993. 30(3): p. 361–5.
15 Wang, J., et al., Empirical analyses of null-hypothesis perfusion FMRI data at 1.5 and 4 T. Neuroimage, 2003. 19(4): p. 1449–62.
16 Feinberg, D.A. and K. Oshio, GRASE (gradient- and spin-echo) MR imaging: a new fast clinical imaging technique. Radiology, 1991. 181(2): p. 597–602.
17 Feinberg, D.A., B. Kiefer, and G. Johnson, GRASE improves spatial resolution in single shot imaging. Magn Reson Med, 1995. 33(4): p. 529–33.
18 Feinberg DA, Kiefer B, Litt AW. High resolution GRASE MRI of the brain and spine: 512 and 1024 matrix imaging. J Comput Assist Tomogr. 1995 Jan-Feb;19(1):1–7.
19 Luh, W.M., et al., QUIPSS II with thin-slice TI1 periodic saturation: a method for improving accuracy of quantitative perfusion imaging using pulsed arterial spin labeling. Magn Reson Med, 1999. 41(6): p. 1246–54.
20 Sallustio F, Kern R, Günther M, Szabo K, Griebe M, Meairs S, Hennerici M, Gass A. Assessment of intracranial collateral flow by using dynamic arterial spin labeling MRA and transcranial color-coded duplex ultrasound.Stroke. 2008 Jun;39(6):1894–7. Epub 2008 Apr 10.
21 Günther M. Efficient visualization of vascular territories in the human brain by cycled arterial spin labeling MRI. Magn Reson Med. 2006 Sep;56(3):671–5.
22 Fernández-Seara MA, Edlow BL, Hoang A, Wang J, Feinberg DA, Detre JA. Minimizing acquisition time of arterial spin labeling at 3T. Magn Reson Med. 2008 Jun;59(6):1467–71.
23 MacIntosh BJ, Pattinson KT, Gallichan D, Ahmad I, Miller KL, Feinberg DA, Wise RG, Jezzard P. Measuring the effects of remifentanil on cerebral blood flow and arterial arrival time using 3D GRASE MRI with pulsed arterial spin labelling.J Cereb Blood Flow Metab. 2008 Aug;28(8):1514–22. Epub 2008 May 28.
24 Fernández-Seara MA, Wang Z, Wang J, Rao HY, Guenther M, Feinberg DA, Detre JA. Continuous arterial spin labeling perfusion measurements using single shot 3D GRASE at 3 T.Magn Reson Med. 2005 Nov;54(5):1241–7.
25 McKinstry RC, Feinberg DA. Ultrafast magnetic resonance imaging. A new window on brain research. Science. 1998 Mar 20;279(5358):1965-6. No abstract available.
26 Feinberg DA, Ramanna S, Gunther M, Evaluation of new ASL 3D GRASE sequences using Parallel Imaging, Segmented and Interleaved k-space at 3T with 12- and 32-Channel coils. ISMRM, Honolulu, 2009
27 Talagala SL, Ye FQ, Ledden PJ, Chesnick S. Whole-Brain 3D Perfusion MRI at 3.0 T using CASL with a separate labeling Coil, Mag Res Med, 52: 131–140 (2004)
28 Edelman, R. R., B. Siewert, et al. (1994). "Signal targeting with alternating radiofrequency (STAR) sequences: application to MR angiography." Magn Reson Med 31(2): 233–8
29 Kwong, K. K., D. A. Chesler, et al. (1995). "MR perfusion studies with T1-weighted echo planar imaging." Magn Reson Med 34(6): 878–87.
30 Luh, W. M., E. C. Wong, et al. (1999). "QUIPSS II with thin-slice TI1 periodic saturation: a method for improving accuracy of quantitative perfusion imaging using pulsed arterial spin labeling." Magn Reson Med 41(6): 1246–54.
31 Wong, E. C., R. B. Buxton, et al. (1998). "Quantitative imaging of perfusion using a single subtraction (QUIPSS and QUIPSS II)." Magn Reson Med 39(5): 702–8.
32 Ye, F. Q., J. A. Frank, et al. (2000). "Noise reduction in 3D perfusion imaging by attenuating the static signal in arterial spin tagging (ASSIST)." Magn Reson Med 44(1): 92–100.


**Contact**
David Feinberg, M.D., Ph.D.
Advanced MRI Technologies
652 Petaluma Ave.,
J Sebastopol, CA, 95472
USA
david.feinberg@advancedmri.com

# Case Report: Cervical Spine MRI. *syngo* SPACE in a Claustrophobic Patient with Congenital Scoliosis

**Marietta Garmer, M.D.; Serban Mateiescu; Martin Busch, Ph.D.; Dietrich Grönemeyer, M.D.**

*Grönemeyer Institute of Microtherapy, Bochum, Germany*

## Patient history

38-year-old female patient presented with chronic pain of the neck and shoulder for imaging of intervertebral disk disease. Previous imaging of the lumbar spine has revealed congenital scoliosis with hemivertebrae and fusion of vertebral bodies. The patient suffers from severe claustrophobia, MRI was accepted after proposing sedation and a "quick" examination. Moreover the known scoliosis was expected to impair a detailed study.

## Sequence details

All images have been acquired with an open bore 1.5T MAGNETOM Espree scanner (Siemens Healthcare, Erlangen) with software version *syngo* MR B15. The lower part of the Head Matrix coil, the Neck Matrix coil and the first elements of

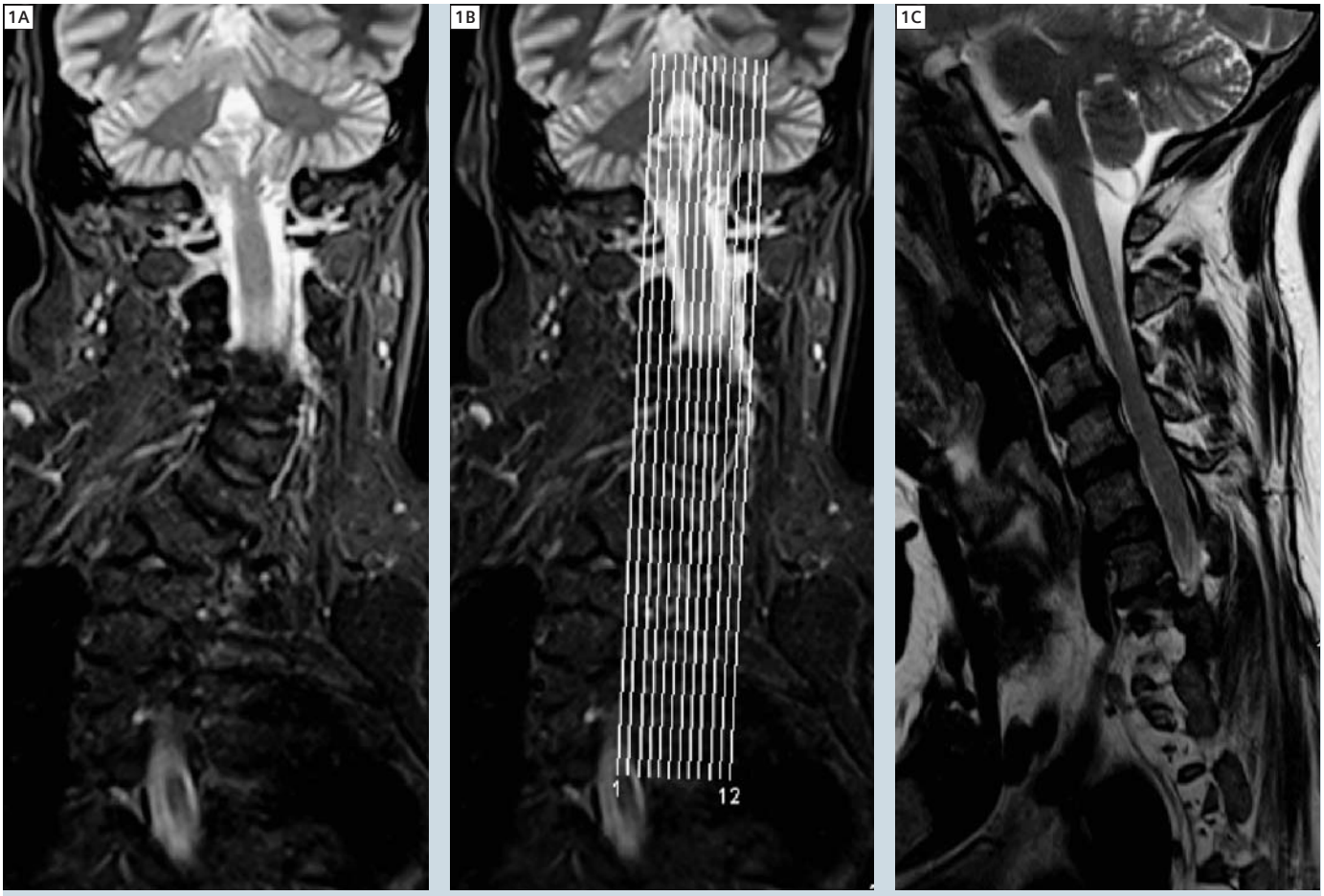


**1** **1A**: STIR cor, **1B:** Locator T2-TSE, **1C:** T2-TSE-sag

the Spine Matrix coil were used.
A coronal STIR overview (Fig. 1A) revealed a pronounced curvature of the cervical and upper thoracic spine, thus the standard T2-TSE sagittal sequences (Figs.1B, C) with 12 slices of 3 mm were obviously not able to cover the spine with standardized orientation to both sides with adequate coverage of anatomical structures. The 3D SPACE (localizer Fig. 2A and Figs. 2B, C), measured with 64 slices of 1.5 mm in a sagittal orientation with good overall image quality and similar contrast, enables the full coverage of the spine segments without the need for additional sequences.

Axial images were also acquired with 3D SPACE. Coronal images were based on MPR reconstration based on the sagittal oriented *syngo* SPACE sequence (Figs. 3A, B).

**Overall, the following sequences were applied in this case:**

- STIR-cor (Fig. 1A): TR = 4240 ms, TE = 49 ms, Slices = 15, Thickness = 4 mm,
- Matrix = 224 x 256i, iPAT *syngo* GRAPPA, Ref. Lines = 24, TA = 1:14 min.
- T2-TSE sagittal (Fig. 1C): TR = 4141 ms, TE = 125 ms, Slices = 12, Thickness = 3 mm,
- Matrix = 282 x 512, iPAT *syngo* GRAPPA, Ref. Lines = 32, TA = 3:33 min.
- 3D SPACE sagittal (Fig. 2B, C): TR = 1500 ms, TE = 124 ms, Slices = 64,
- Thickness = 1.5 mm, Matrix = 310 x 320, iPAT *syngo* GRAPPA, Ref. Lines = 24, TA = 3:33 min.
- 3D SPACE axial (Fig. 3): TR = 1500 ms, TE = 123 ms, Slices = 40,
- Thickness = 1.6 mm, Matrix = 318 x 320i, iPAT *syngo* GRAPPA, Ref. Lines = 24, TA = 2:30 min.

## Imaging findings

Coronal reconstruction clearly showed the hemivertebra Th1 on the right, the sagittal cleft at the level of Th2 (Fig. 3A) and Th4 resulting in the shape of a butterfly and a unilateral bar at the level of Th4 and 5 on the left (Fig. 3B).

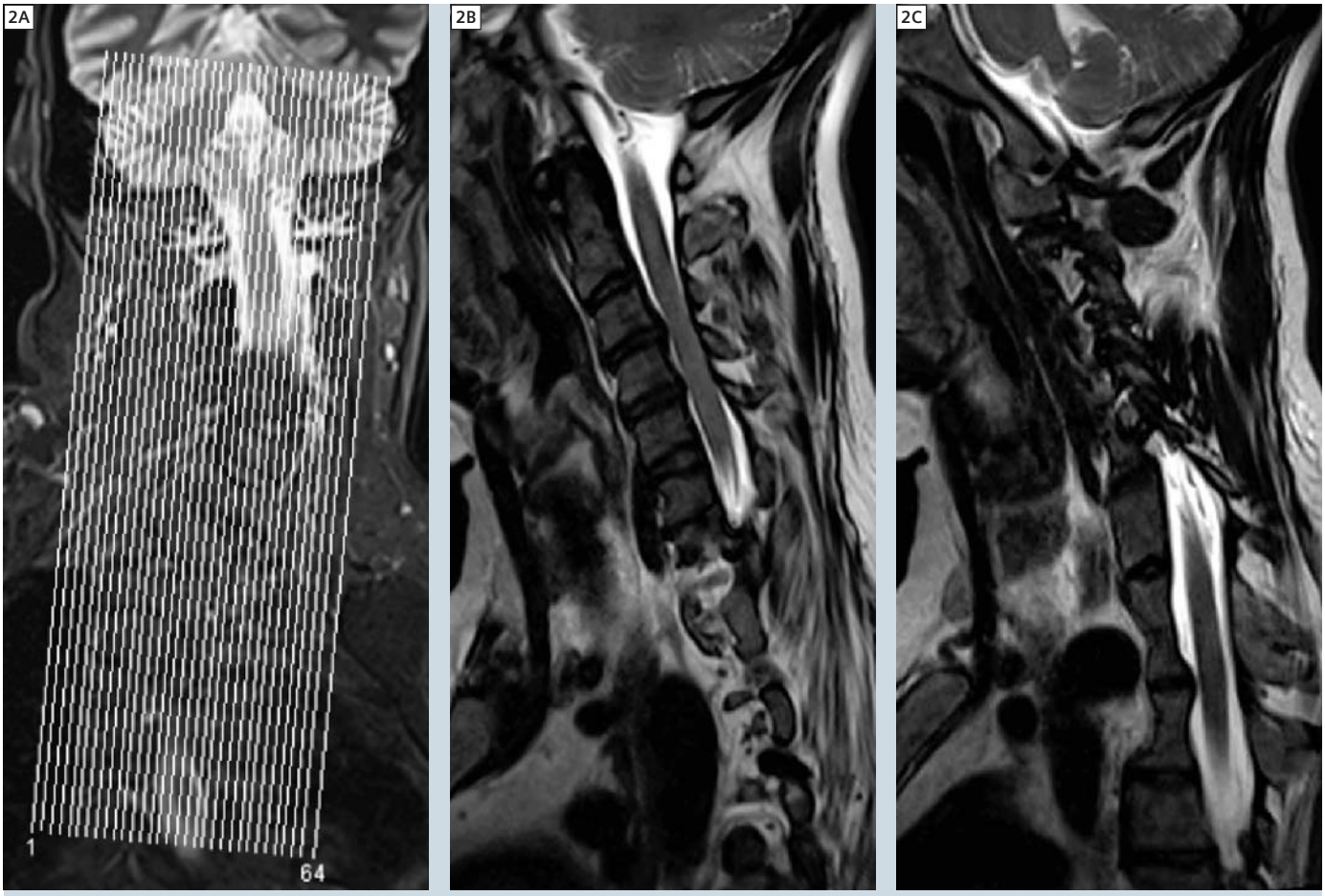


**2** **2A:** Localizer SPACE , **2B:** 3D SPACE sagittal, **2C:** 3D SPACE sagittal

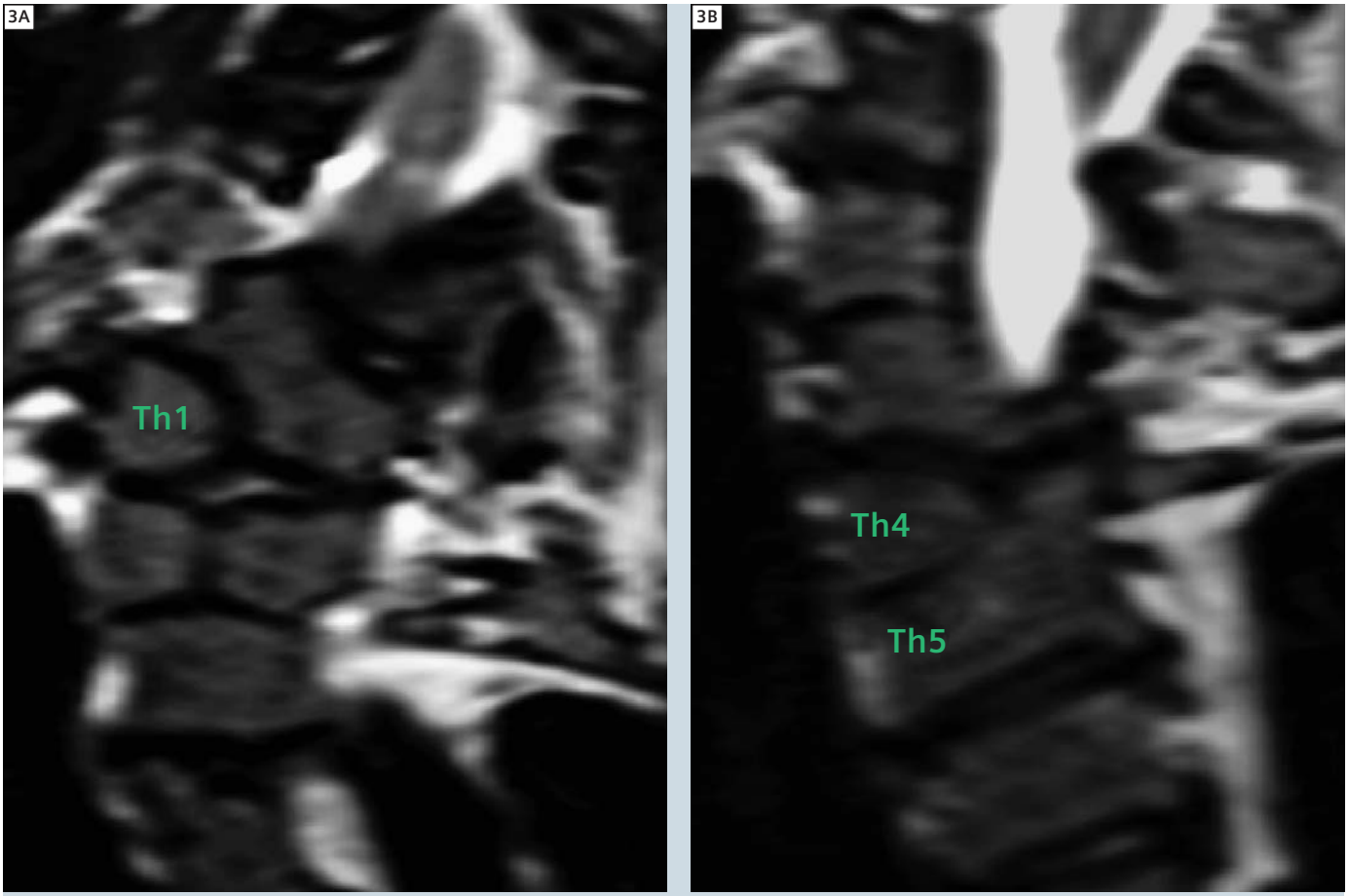


**3** **3A:** Coronal reconstruction, **3B:** Coronal oblique reconstruction

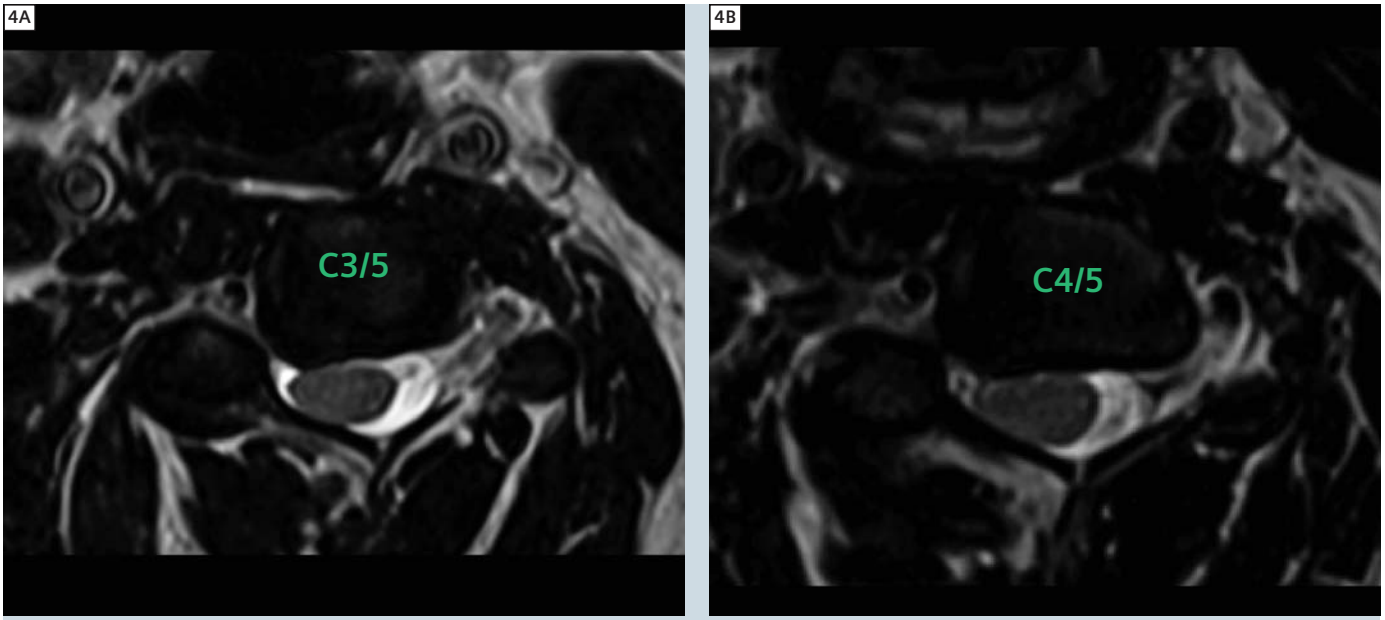


**4** **4A, 4B:** 3D SPACE axial

Disk herniation could be clearly demonstrated in axial SPACE at the level of C3/4 (Fig. 4A) and C 4/5 with a slight impression of the myelon (Fig. 4B). Associated foraminal stenosis was depicted in sagittal oblique reconstruction on the right (Fig. 5A) whereas at the level of the hemivertebra the spinal nerves on both sides were clearly seen (Figs. 5B, C).

## Discussion

MRI of the cervical spine is a well-known routine procedure commonly performed with standard T1 and T2-weighted sagittal and axial 2D sequences, which rarely require adaptions. However, this case demonstrates clearly the value of 3D imaging with *syngo* SPACE in a patient with congenital scoliosis. The patient was claustrophobic, which limited the scan time. The normal 2D T2w TSE sequence would require more than 8 min scan time for a sufficient, but smaller, coverage than the *syngo* SPACE sequence. Additionally, with 2D-slices, no oblique reconstruction is possible. With *syngo* SPACE a complete coverage of the bend cervical spine was obtained and the possibility of multiplanar reconstruction allowed the correct interpretation of the complex malformation of the vertebral elements and the damage of the intervertebral disks.
It should be noted that patients with congenital scoliosis also have a high incidence of abnormalities in other organs (heart problems, kidney or bladder problems) and should be screened for spinal cord malformations.

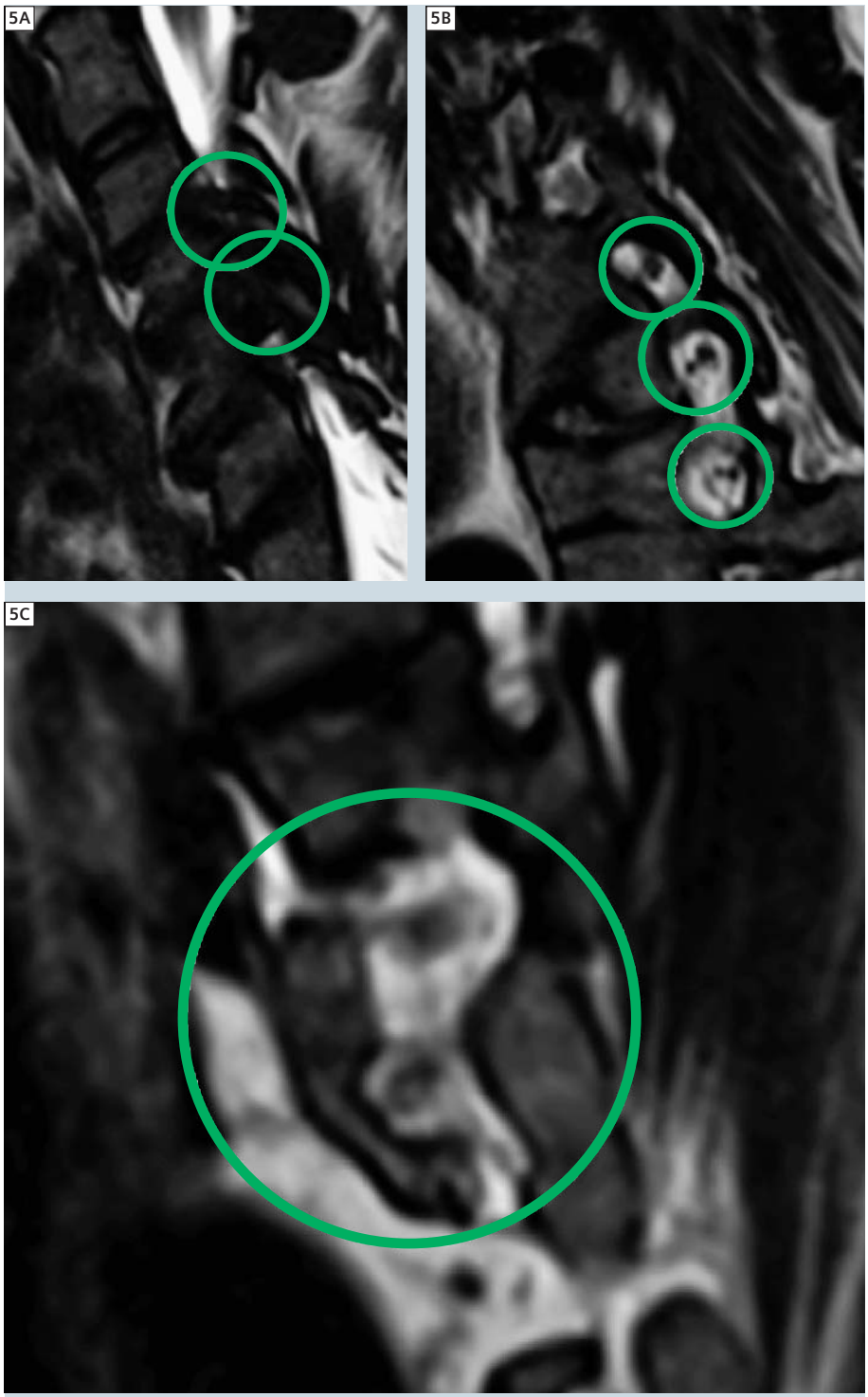


**5** **5A, B, C:** Sagittal oblique reconstruction of 3D SPACE.

**Contact**
Dr. Martin Busch
Grönemeyer Institute of Microtherapy
Universitätsstr. 142
D-44799 Bochum
Phone: +49 (0) 234 9780-139
busch@microtherapy.de

# IMRIS*neuro* 70 cm Bore 3T in Intra-Operative Neurosurgery

**Jeanne Elliott**

*IMRIS, Winnipeg, Manitoba, Canada*

1

**1** IMRIS*neuro* 3T system. *(Image courtesy of: the Seaman Family MR Research Centre, Foothills Medical Centre, Calgary, Alberta, Canada.)*

The first IMRIS*neuro* system using a MAGNETOM Verio 3T magnet was installed at the Foothills Medical Centre in Calgary, Canada in early 2009.

## Physicians appreciate High Field MR

The Seaman Family MR Research Centre at Foothills Medical Centre, under the leadership of Dr. Garnette Sutherland recently upgraded their 10-year old prototype 1.5T magnet to the latest IMRIS*neuro* with 3T MAGNETOM Verio technology. After successfully treating more than 1,000 neurosurgical patients using the 1.5T technology, the centre was ready to upgrade its capabilities. It became clear that the 3T Verio system including Diffusion Tensor Imaging (*syngo* DTI) and functional MRI would add significant value to surgical planning and intra-operative imaging.

The benefits of applying MR imaging during surgery has been recognized for many years. However, more recently the field has seen major growth in awareness and usage of MR guided imaging for neurosurgery. Many peer reviewed articles report the benefits of MR imaging including one, which concluded that in 41% of cases, the use of intra-operative MRI resulted in extended tumor resection. A different study concluded that in 27.5% of cases the original surgical plan was altered based on the intra-operative MR findings.

Many of the original observations were often based on past generation high field intra-operative MR technologies. They provided good image quality, but lacked the ability to deliver efficient workflow as the patient had to be moved to the MRI. Seeking the best in intra-operative MR technology, leading institutes like Barnes-Jewish Hospital (St. Louis, MO, USA), Johns Hopkins Hospital (Baltimore, ML, USA), Mayo Clinic (Jacksonville, FL, USA), Cleveland Clinic (Cleveland, OH, USA), Seaman Family MR Research Centre (Calgary, Canada), and PLA 301 Army Hospital (Beijing, China) have selected IMRIS*neuro*. These systems include the 1.5T MAGNETOM Espree or the 3T MAGNETOM Verio magnets and provide superior imaging capabilities with a technology workflow that brings MR to the patient. When the MR scanner is not in the operating room, the surgical team has full 360-degree access to the patient, and relocation of the magnetic field enhances operating room safety.

IMRIS*neuro* with the Siemens Verio or Espree magnets provide industry-leading capability and may also be used for diag-

2

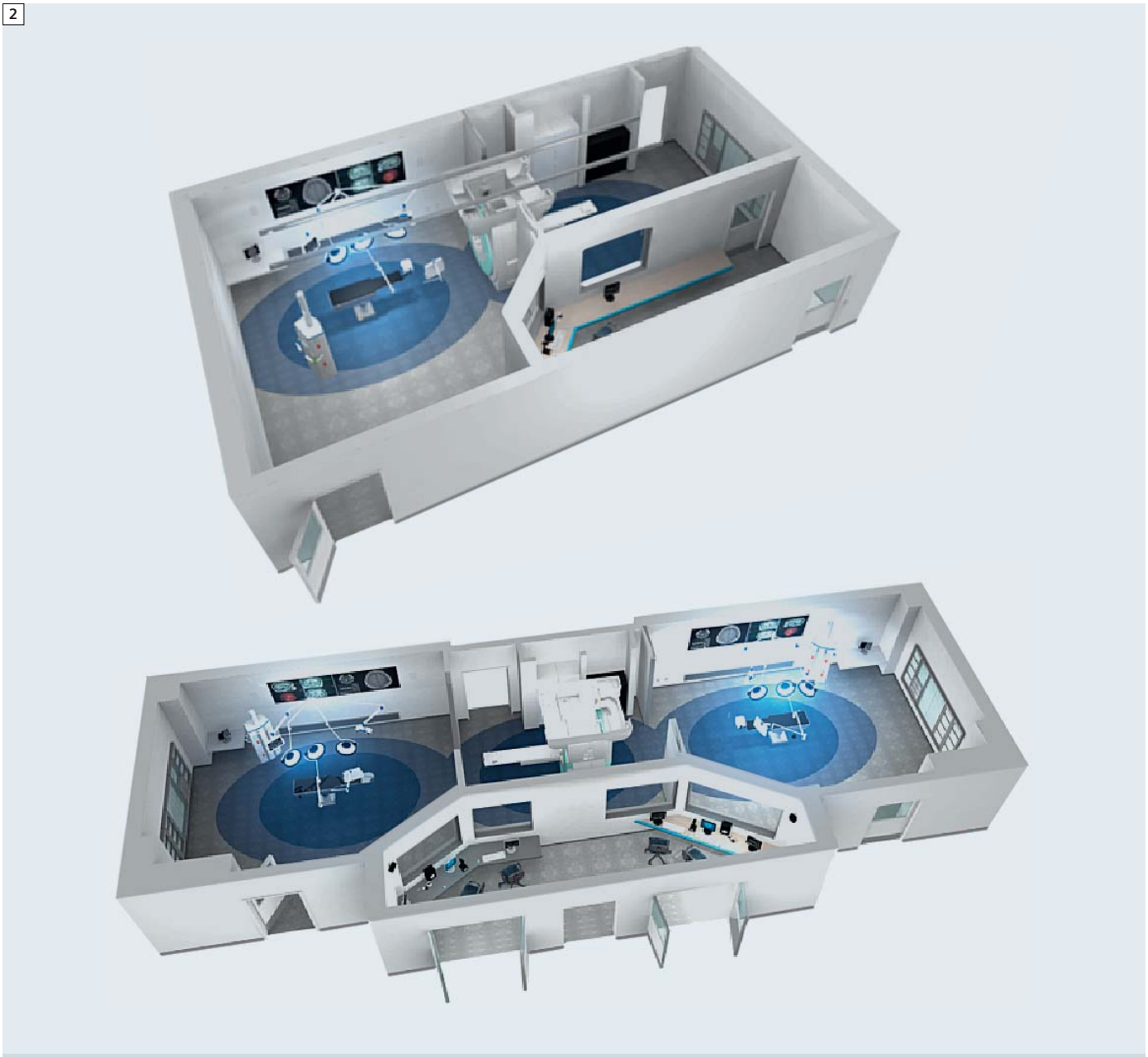

**2** IMRIS*neuro* 2-room and 3-room configurations.

nostic examination of non-surgical patients who require the service of anesthesia or critical support. The IMRIS*neuro* solution is available in five configurations that allow the use of the 3T or 1.5T magnets for routine diagnostic imaging procedures while the system is not in use intra-operatively. For centers with significant surgical volumes, the magnet can move between two separate operating rooms further enhancing efficiency and the ability to offer better patient care.

## Clinical cases with IMRIS*neuro* 3T MAGNETOM Verio

The moving magnet concept began with Dr. Garnette Sutherland's desire to bring the imaging benefits of an MRI to the neurosurgical operating room environment. His motivation was to preserve the current surgical workflow and to avoid moving the positioned surgical patient. IMRIS translated Dr. Sutherland's concept to pioneer the original 1.5T moving magnet design. More than 10-years later, Dr. Sutherland is also the first in the world to use the advanced IMRIS*neuro* with 3T MAGNETOM Verio: "The images obtained using the upgraded 3T intra-operative MRI system are of remarkable quality. The new system has been used for over 75 surgeries, in surgical planning, assessment during surgical dissection and for quality assurance. We have taken advantage of complex imaging techniques including fibre tracking, MR angiography and the rapid image pro-

cessing software. I am pleased that this innovation has turned into a commercial product that has gone on to benefit close to 3000 patients throughout the world."
It is well understood in normal MR diagnostic scans that 3T image quality offers superior resolution and definition of soft tissue structures in the brain versus 1.5T. Initial intra-operative experience with the 3T MAGNETOM Verio shows the same advantages existing in image quality before, during and after surgery. The state-of-the-art imaging techniques and rapid processing times characteristic of the 1.5T are enhanced through the inherent higher signal-to-noise ratio (SNR) of the 3T. Surgical planning intra-operative MR images were obtained from a 61-year-old woman with a left subtentorial meningioma. Diffusion tensor imaging (*syngo* DTI) sequences show well the relationship of fibers to the tumor. Interdissection images (not shown) demonstrated deformation for the fiber tracks as a result of tumor removal. Knowledge of these relationships increased the safety of tumor resection.

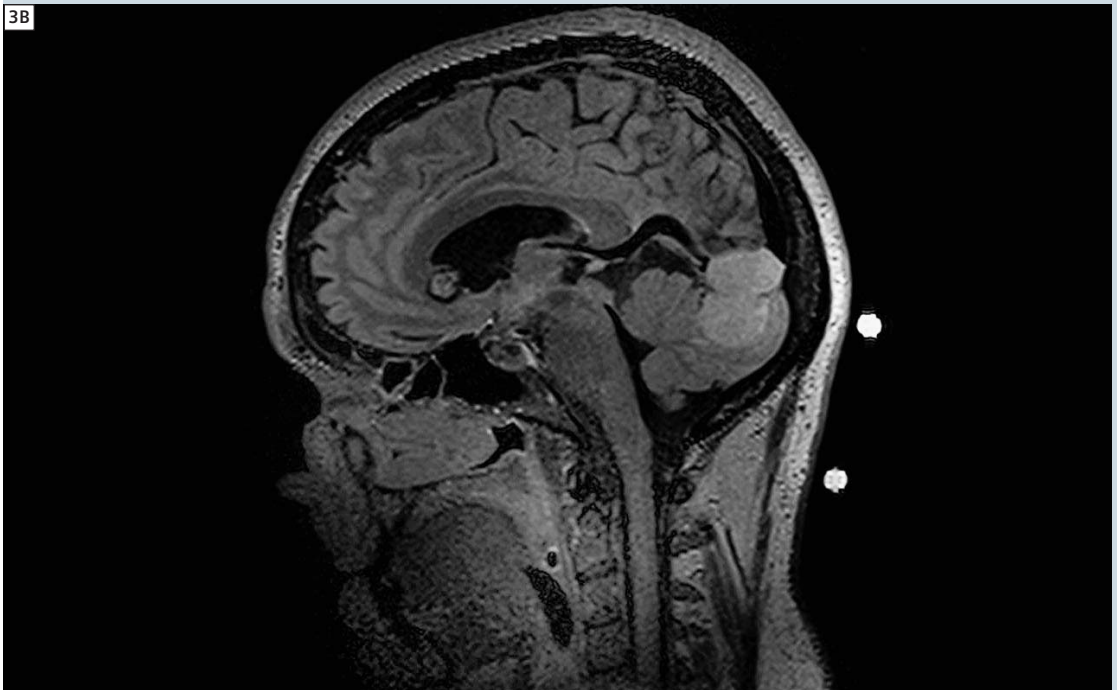


**3** 3T intra-operative. (*Images courtesy of the Seaman Family MR Research Centre, Foothills Medical Centre, Calgary, Alberta Canada 2009).*

## New and additional clinical applications

The unique wide bore 70 cm 3T MAGNETOM Verio system is extremely valuable for intra-operative and interventional procedures. More often than not, interventional procedures require specialized patient positioning that can only be fully achieved with the 70 cm bore MAGNETOM Verio and Espree magnets. Positioning patients in lateral or prone positions is easily achievable with the use of wide bore, moving MR technology from IMRIS.

Excellent patient positioning and imaging capability is further supported by the enhancements made to the IMRIS*neuro* surgical bed. This newly developed surgical table is MR-compatible and X-Ray translucent for spine imaging and applications. The bed allows use of a single plane X-ray system in combination with MR imaging in the operating room (OR).

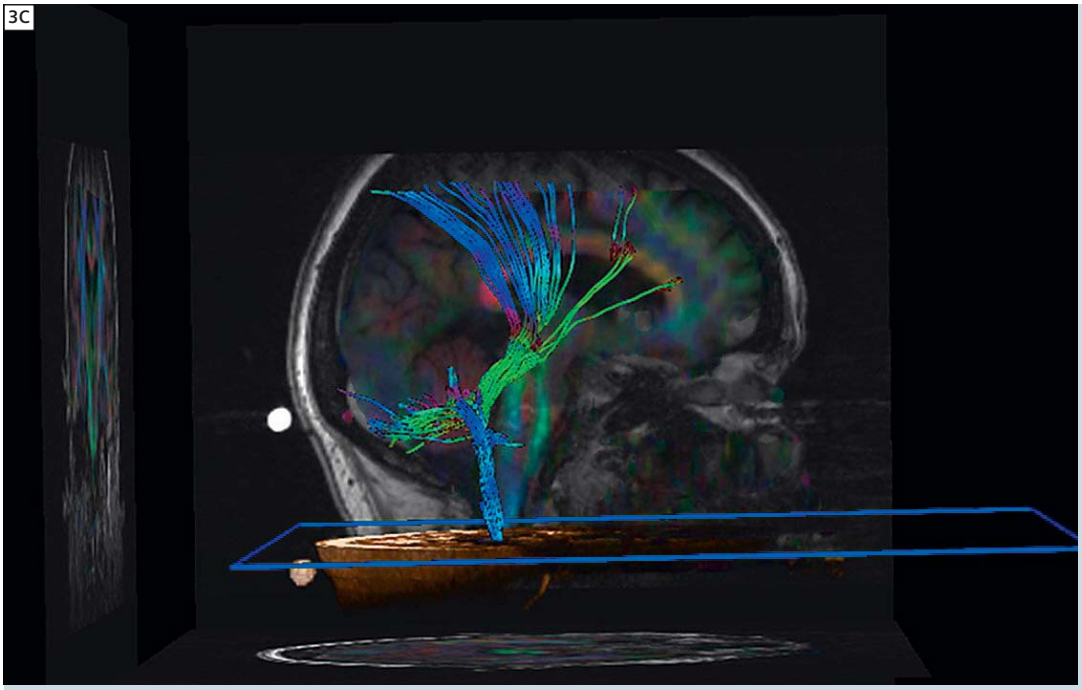


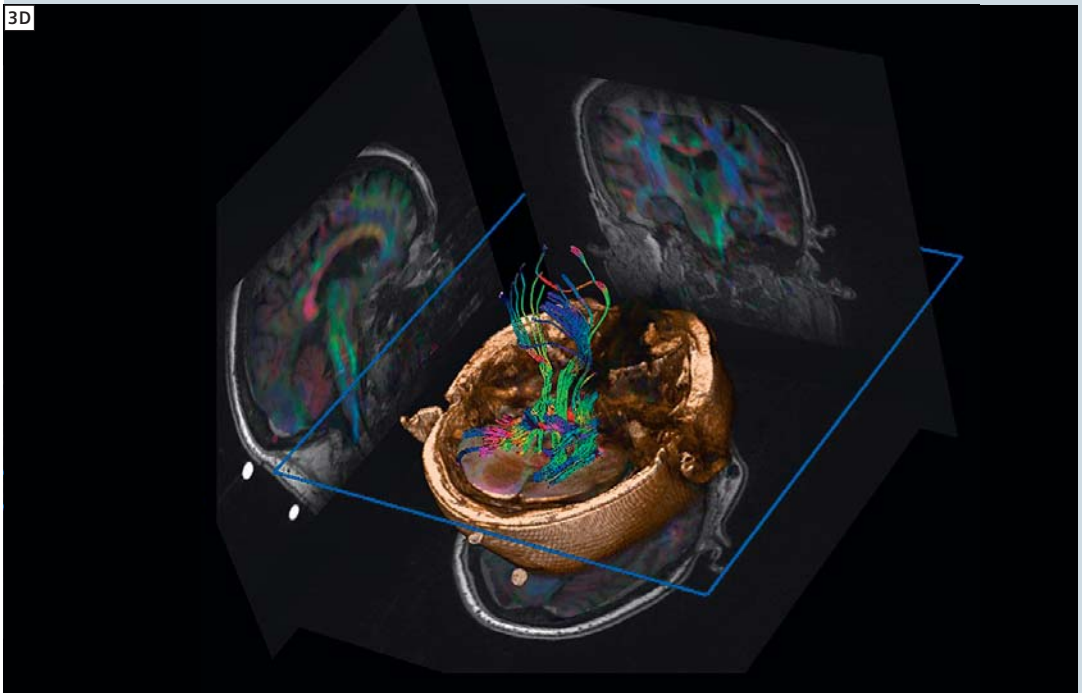


**3** 3T intra-operative. (*Images courtesy of the Seaman Family MR Research Centre, Foothills Medical Centre, Calgary, Alberta Canada 2009).*

**4** IMRIS*neuro* surgical bed and collage images of prone/lateral/supine positioning. *(Images courtesy of IMRIS, Inc., Canada, 2009.)*

**5** IMRIS$_{NV}$ and IMRIS$_{cardio}$

## Future applications and technologies

IMRIS is widening the use of its image guided therapy solutions by expanding into new applications, combining 3T or 1.5T MR with single and bi-plane X-ray systems. IMRIS$_{NV}$ and IMRIS$_{cardio}$ are unique and advanced interventional suites providing an imaging environment that physicians may apply in providing stroke management and neurovascular care and in performing structural cardiac and minimally invasive procedures.

References

1 Intraoperative Visualization for Resection of Gliomas Nimsky C, Ganslandt O, Buchfelder M, Fahlbusch R. "Intraoperative visualization for resection of gliomas: the role of functional neuronavigation and intraoperative 1.5T MRI". Neurological Research 28(5): 482–7, July 2006.

2 Intraoperative High-Field-Strength MR Imaging: Implementation and Experience in 200 Patients. Nimsky C, Ganslandt O, von Keller B, Romstöck J, Fahlbusch R. 'Intraoperative High-Field Strength MR Imaging: Implementation and Experience in 200 Patients." Radiology 2004; 233:67–78.

**Contact**
Jeanne Elliott
IMRIS
100 – 1370 Sony Place
Winnipeg, Manitoba
Canada, R3T 1N5
jelliott@imris.com

# Whole-body DCE MR Imaging for Evaluation of Bone Marrow Enhancement in Multiple Myeloma

**Alexandre Vignaud, Ph.D.[1]; Chieh Lin, M.D.[2]; Alain Luciani, M.D, Ph.D.[2]; Alain Rahmouni, M.D.[2]**

[1] *Siemens Healthcare, Saint Denis, France*
[2] *Service de Radiologie, Centre hospitalo-universitaire Henri Mondor, Assistance Publique-Hopitaux de Paris, Université Paris XII Créteil, France*

## Patient history

A 55-year-old patient with newly diagnosed multiple myeloma (MM) underwent high-dose therapy followed by autologous stem cell transplantation (ASCT). After completion of ASCT, serum immunoglobulin G level decreased from 50 g/L at baseline to 3 g/L. However, despite a good clinical response, whole-body dynamic contrast-enhanced (DCE) MR imaging depicted persistent early-enhancing focal lesions over the rib and the pelvic bone (outside the usually imaged spine MR examination in MM). The patient had confirmed disease progression two months later.

1

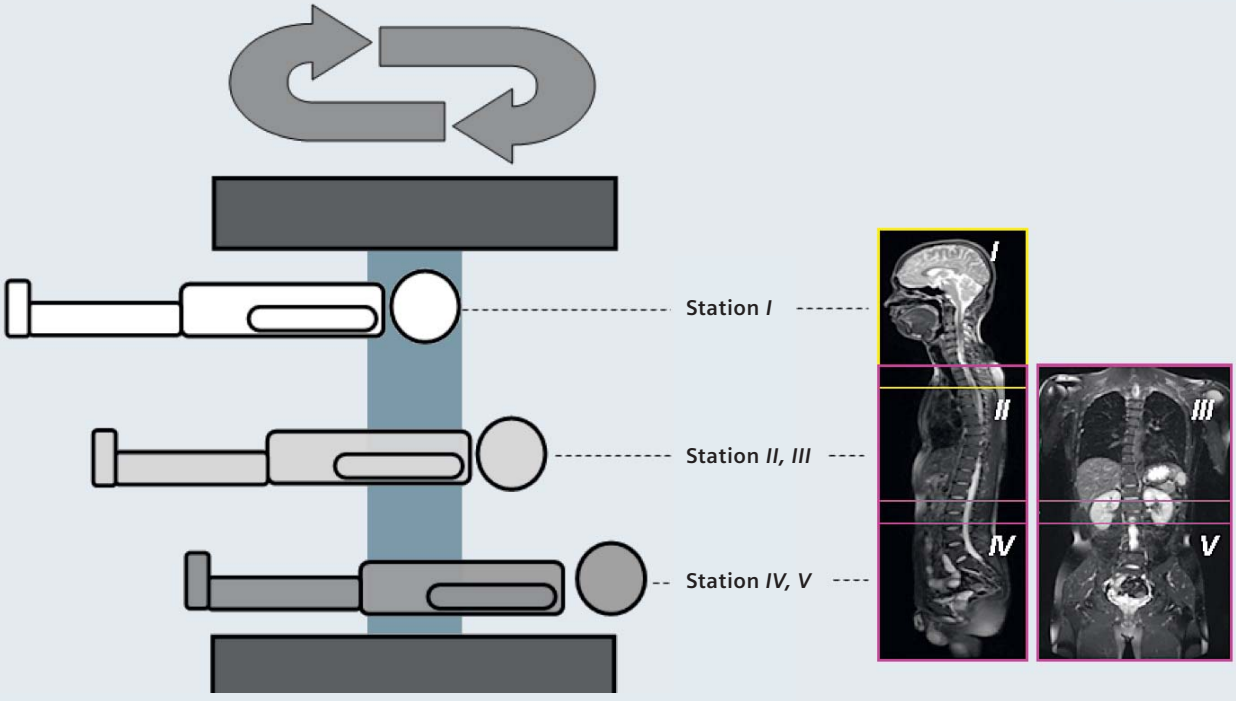


**1** Overview of the applied MR Protocol: T1 SE and T2 FS TSE sequences in sagittal (I, II, and IV) and coronal (III and V) planes. DCE studies were performed using a 3D VIBE sequence, which was acquired sequentially at five stations (I-II-III-IV-V) and repeated seven times.

## Sequence details

After institutional approval, in Henri Mondor University Hospital (Creteil, France) patients suspected with MM or during their MM chemotherapy follow-up, undergo a newly published dynamic whole-body MR examination [1, 2].
It has been demonstrated that micro-circulation parameters of dynamic MR examination, such as the maximal enhancement (Emax), correlate well with histologic infiltration grade, micro-vessel density (MVD) and serum markers of disease activity [3–7]. A reduction in these parameters has been observed in patients who respond to treatment [3, 4, 5]. These parameters could potentially serve as non-invasive surrogate biomarkers for response assessment. However, in the past, these parameters could only be obtained on acquisition protocols in which the maximal field-of-view (FOV) was limited to 400 mm, whereas myeloma can involve bone marrow throughout the body and even tissue outside the bone marrow space [8].
A rolling table platform with combined multichannel phased array-surface coils which cover the head, neck, trunk and proximal extremities along with parallel imaging has made it feasible to perform whole-body dynamic MR imaging without compromising spatial and temporal resolutions.
The protocol is articulated as described in figure 1. All sequence parameters are detailed in tables 1 and 2. Acquisition was done on a 1.5T Siemens MAGNETOM Avanto 76x18 SQ. Standard T1-weighted Spin Echo (SE) and T2-weighted Fat Saturated (FS) Turbo Spin Echo (TSE) sequences were acquired both in sagittal and coronal planes before contrast agent injection over the whole FOV to assess fat and bone marrow repartition [9].
A cyclic contrast media was administrated during an ultra-fast dynamic T1-weighted FS 3D VIBE (Volume Interpolated Breath-hold Examination), Gradient

**Table 1: Parameters for whole-body T1- and T2-weighted sequences.**

| Parameters | T1 SE | T2 FS TSE |
|---|---|---|
| Stations imaged | *I, II, IV, V* | *I–V* |
| TR/TE (msec) | 400/10 | 4200/70 |
| Turbo Factor | 1 | 21 |
| FOV (mm²) | 500 x 500 | 500 x 500 |
| Matrix | 448 x 358 | 448 x 358 |
| Averaging | 1 | 2 for stations *I, II, IV*<br>1 for stations *III* and *V* |
| Slice thickness/Gap (mm) | 4/0 sagittal<br>4/1.2 coronal | |
| Number of slices | 20 for stations *I, II, IV*<br>50 for station *V* | 20 for stations *I, II, IV*<br>50 for stations *III* and *V* |
| *syngo* GRAPPA acceleration factor | 2 for stations *I, II, IV*<br>3 for station *V* | 2 for stations *I, II, IV*<br>3 for stations *III* and *V* |
| TA (sec) | 112 for stations *I, II,* and *IV*; 186 for station V | 93 for stations *I, II,* and *IV*; 84 for stations *III* and *V* |

Stations' FOV and orientations are described in figure 1. Coronal T2-weighted fat-saturated (FS) turbo spin echo (TSE) imaging was performed by using a respiratory-triggering belt.

**Table 2: Parameters for whole-body 3D VIBE five-station DCE MR imaging.**

| Parameter | Stations *I, II,* and *IV* (sagittal) | Stations *III* and *V* (coronal) |
|---|---|---|
| TR/TE (msec) | 3.6/1.3 | 3.3/1.3 |
| Flip angle (°) | 20 | 20 |
| Bandwidth (Hz/pixel) | 490 | 490 |
| FOV (mm³) | 500 x 500x 72 | 500 x 500 x 200 |
| Matrix | 256 x 192 x 24 | 256 x 192 x 40 |
| Acquired voxel size (mm³) | 2.0 x 2.6 x 3.0 | 2.0 x 2.6 x 5.0 |
| *syngo* GRAPPA acceleration factor | 2 | 2 |
| TA (sec) | 7 | 9 |

Stations' FOV and orientations are described in figure 1.

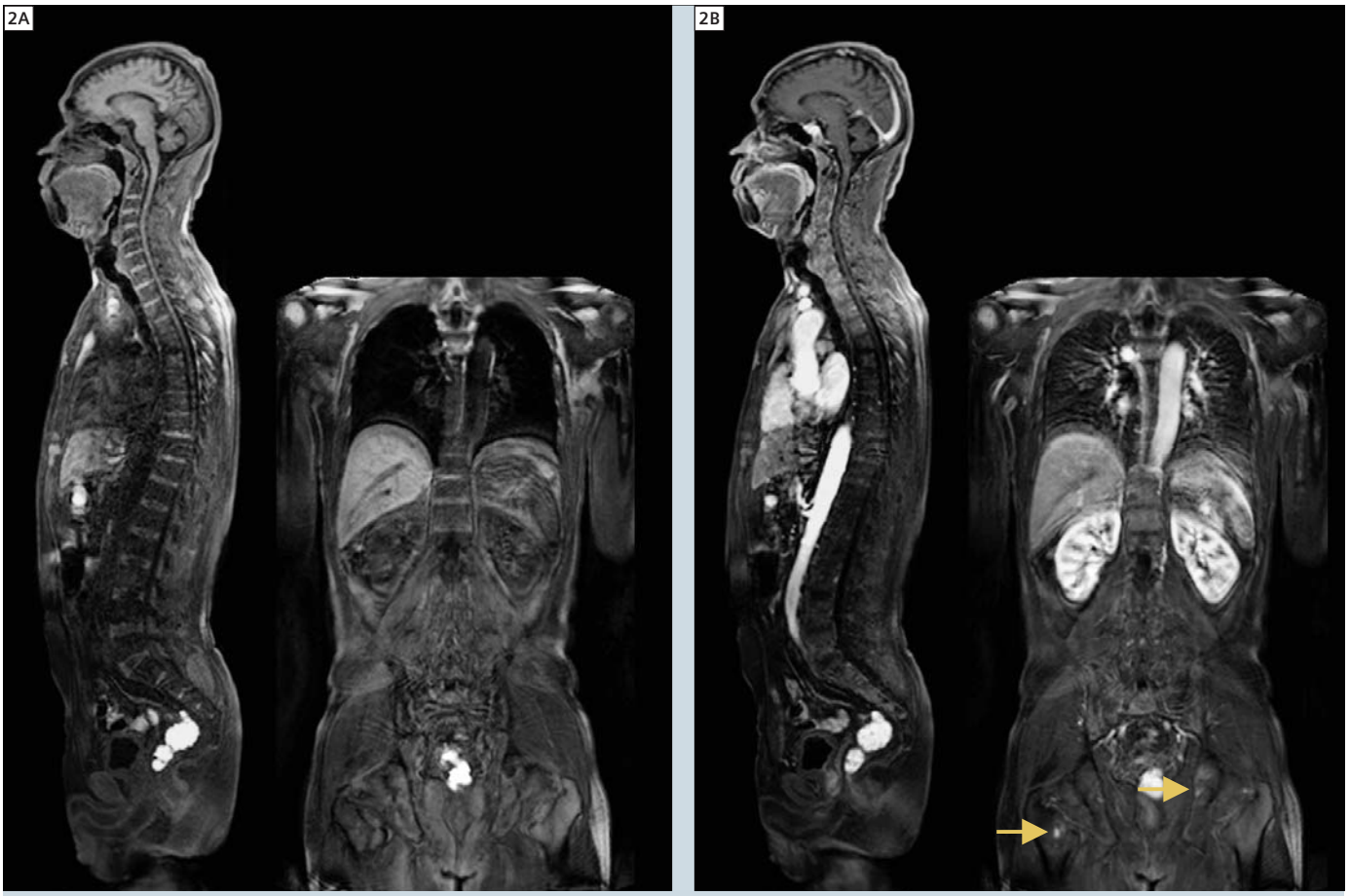


**2** Composing of the 3 sagittal stations (left) and the 2 coronal stations (right) with ultra fast 3D VIBE sequence both before **(A)** gadolinium injection and right after **(B)** the injection. This patient had a good clinical response after treatment. Nevertheless persistent enhancing focal lesions over pelvic bone and right femur are visible on selected images after gadolinium injection (white arrows).

Recalled Echo (GRE)-like, sequence applied over the whole FOV in 3 sagittal and 2 coronal stations. The acquisition time of each station was set under 10 seconds. The time to complete acquisition of the 5 stations was 60 s including three table movements. The total duration of whole-body DCE study was set at 7 minutes.

## Imaging findings

This patient has been monitored using our MR protocol right after completion of therapy. He had a good clinical response. Fig. 2 shows whole-body five-station dynamic MR images obtained before and immediately after contrast agent administration in this patient. The bone marrow enhancement is within normal range but tiny early-enhancing focal lesions are depicted. Another 8 cm left rib mass was also noted (image not shown). Two months later the patient complained of back pain and underwent the same MR examination (Fig. 3). Numerous early-enhancing focal lesions were seen, confirming previous MR findings and the relapse of the disease.

## Discussion

Preliminary findings using this method gave time-signal intensity curves for both bone marrow indicating the degree of diffuse infiltration and focal lesions on a whole-body scale. They allowed the differentiation between normal and infiltrated bone marrow and to assess the disease activity of each imaged focal lesion. Whole-body DCE MR imaging might be proven useful in treatment response assessment in MM patients. Further investigations have been conducted successfully to evaluate this potential and will be soon published [2].

References

1 C. Lin, A. Luciani, K. Belhadj, et al. Patients with Plasma Cell Disorders Examined at whole-body dynamic contrast-enhanced MR imaging: initial experience. Radiology 2009;250:905-915.
2 C. Lin, A. Luciani, K. Belhadj, et al. Multiple Myeloma Treatment Response Assessment by Whole-Body Dynamic Contrast-enhanced MR Imaging. Radiology in Press.
3 T.M. Moehler, H. Hawighorst, K. Neben, et al,. Bone Marrow microcirculation analysis in multiple myeloma by contrast-enhanced dynamic

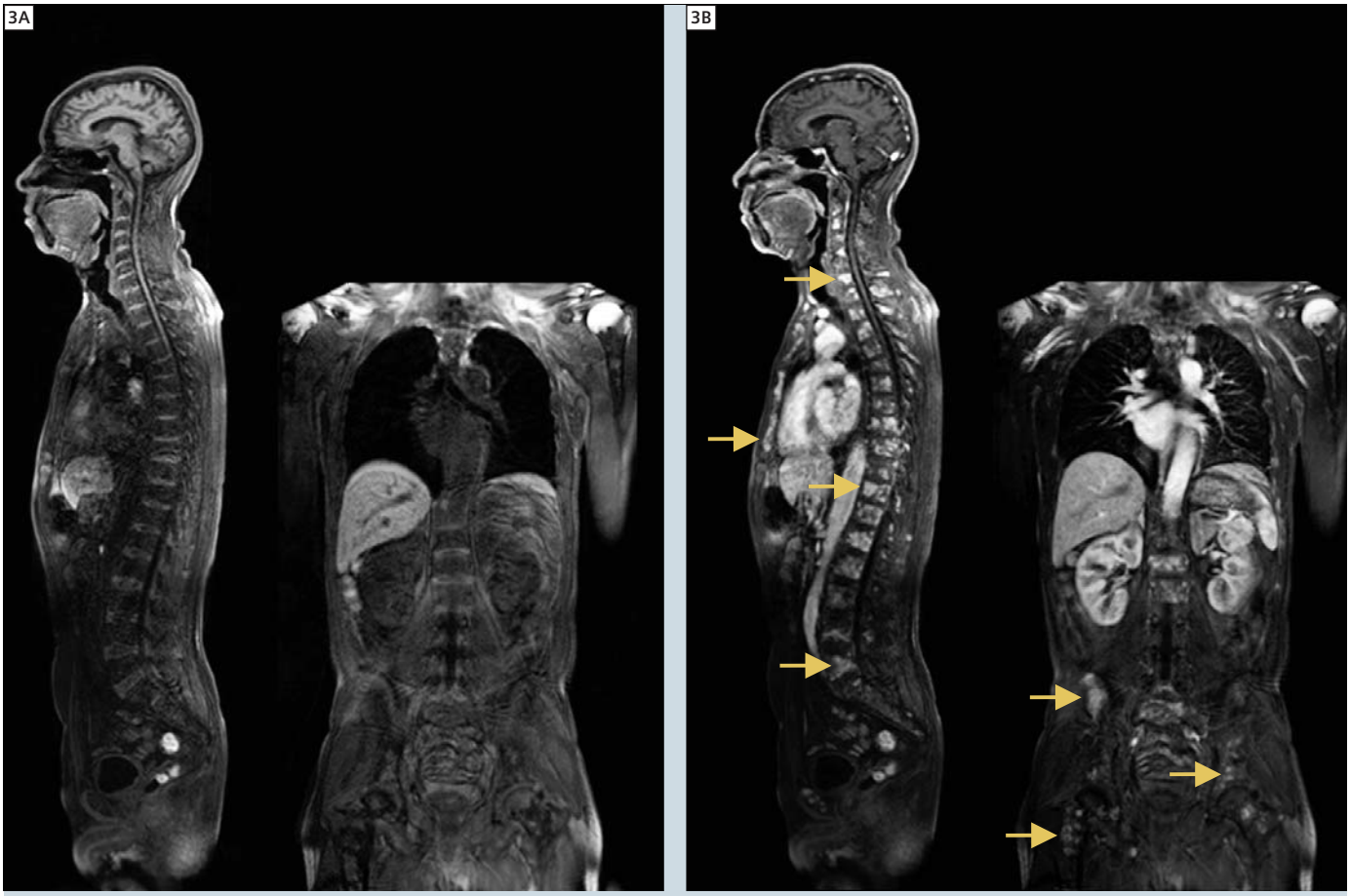


**3** Whole-body DCE MR examination of the same patient as in Fig. 2 two months later, before **(A)** and right after **(B)** gadolinium injection. Numerous new focal lesions had appeared and were visible (white arrows) on the post-contrast images.

magnetic resonance imaging. Int J. Cancer 1001; 93: 862-868.

4 A. Rahmouni, J.L. Montazel, M. Divine, et al. Bone marrow with diffuse tumor infiltration in patients with lympoproliferative diseases: dynamic gadolinium-enhancement MR imaging. Radiology 2003; 229:710-717.

5 A. Scherer, C. Strupp, H.J. Wittsack, et al. Dynamic contrast-enhanced MRI for evaluating bone marrow microcirculation in malignant hematological diseases before and after thalidomide therapy. Radiologe 2002; 42:222-230.

6 A. Baur, R. Bartl, C. Pellengahr, V. Baltin. M. Reiser. Neovascularization of bone marrow in patients with diffuse multiple myeloma: a correlative study of magnetic resonance imaging and histopathology findings. Cancer 2004; 101: 2599-2604.

7 S. Nosas-Garcia, T. Moehler, K. Wasser, et al. Dynamic contrast-enhanced MRI for assessing the disease activity of multiple myeloma: comparative study with histopathology and clinical markers. J. Magn. Reson. Imaging 2005; 22: 154-162.

8 S.Y. Huang, M. Yao, J.L. Tang, et al. Epidemiology of multiple myeloma in Taiwan: increasing incidence for the past 25 years and higher prevalence of extramedullary myeloma in patients younger than 55 years. Cancer 2007; 110:896–905.

9 B.C. Vande Berg, F.E. Lecouvet, L. Michaux , A. Ferrant , B. Maldague, J. Malghem. Magnetic resonance imaging of the bone marrow in hematological malignancies. Eur Radiol 1998; 8:1335-44.

**Contact**
Alexandre Vignaud
Siemens Healthcare
9, boulevard Finot
93527 Saint-Denis
France
Phone: 00-33-6-07-33-40-87
alexandre.vignaud@siemens.com

# 3D High Resolution MRI of the Knee at 3T Using a Moderately T2-weighted 3D-TSE-fs (*syngo* SPACE) sequence – Useful or Not?

A. Horng[1], M. Notohamiprodjo[1], J. Raya[1], J. Park[1], W. Horger[2], A. Crispin[1], M. F. Reiser[1], C. Glaser[1]

[1]*Department of Clinical Radiology, University of Munich – Grosshadern Campus, Munich, Germany*
[2]*Siemens Healthcare, Erlangen, Germany*

## Background

Magnetic resonance imaging (MRI) of the knee is justifiably one of the most commonly performed MRI examinations, as it offers excellent direct depiction of cartilage, ligaments, menisci and periarticular soft tissue. This can be achieved by standard application of fat-saturated moderately T2-weighted 2D Turbo Spin Echo (TSE)-sequences in three orientations [1, 2]. However, conventional TSE-sequences are not isotropic, hence structures and signal alterations / lesions with a size less than the usual slice thickness of 3 to 6 mm, i.e. meniscal roots, may not be completely detected. A slice thickness below 3 mm is rarely acquired because of its reduced signal-to-noise ratio (SNR) and contrast-to-noise ratio (CNR) and because of the prolonged acquisition time for complete joint coverage. Furthermore post-processing options for 2D-sequences for the assessment of structures, which are captured in an oblique course through several slices, like the anterior cruciate ligament or the femoral trochlear cartilage [3] are limited.
In this setting the introduction of a highly resolved 3D moderately T2-weighted (3D-T2w-TSE) sequence may be useful. In the literature time efficient 3D-T2w-TSE sequences have already been evaluated for the central nervous system [4] and recently for the body trunk [5, 6]. They enable data acquisition with high isotropic spatial resolution and allow for an interactive 3-dimensional visualization. Such post-processing after an initial isotropic data acquisition has been proven successful in many other MR and CT-based applications.

## Technical considerations for *syngo* SPACE

Recently a 3D-TSE-sequence with moderate T2-weighting called "Sampling Perfection with Application optimized Contrasts using different flip angle Evolutions" (*syngo* SPACE), was developed for 3T systems. A restore pulse and variable flip angle distribution enable extremely large turbo factors. The variable flip angles provide a particular evolution of the signal during the echo train resulting in a "pseudo steady-state" with constant signal level neglecting relaxation [7]. Additionally, SAR is reduced by this acquisition scheme. The usage of this technique on a high field 3T system allows integration of parallel imaging with excellent SNR and CNR at reasonable acquisition times [8, 9].
The application of *syngo* SPACE at 3T might establish a new approach to MRI of the knee. Parallel imaging facilitates blockwise 3D-data acquisition with isotropic spatial resolution for evaluation of the whole knee in a reasonable time window. The acquisition time should be either less or at least comparable to acquisition times of conventional 2D TSE datasets in three planes. The advantage of an isotropic 3D-dataset is the possibility of 3-dimensional multiplanar reformatting (MPR), which may enhance the evaluation of small delicate or oblique structures like meniscal roots or the fascicles of the anterior cruciate ligament. Disadvantages might be slightly decreased in-plane resolution as compared to conventional 2D-TSE-fs-sequences and some additionally required time for the 3D reconstructions.
Recently our research group evaluated *syngo* SPACE for isotropic highly resolved MRI of the knee at 3T (MAGNETOM Trio, Siemens Healthcare, Erlangen, Germany) with consecutive 3-dimensional-MPR in comparison to conventional 2D-TSE-fs-sequences in three planes (coronal, sagittal, axial) [10].
Sequence parameters for *syngo* SPACE and for the moderately T2w-2D-TSE-fs-sequence are given in table 1. Fat saturation in *syngo* SPACE was performed with the SPectral selection Attenuated Inver-

sion Recovery (SPAIR) technique. Parallel imaging was performed with the k-space based technique *syngo* GRAPPA with an acceleration factor R = 2. For signal reception, a dedicated multichannel knee coil with 8 independent RF-channels was used. Reformation of the datasets was performed on a *syngo* MultiModality Workstation (Leonardo, software version VB15A, Siemens Healthcare, Erlangen, Germany).

Analysis of axial, sagittal and coronal reformations (MPR) of 0.5 mm, 1 mm and 2 mm slice thickness suggest a slice thickness for MPR of 1 mm ($SPACE_{1mm}$) to be optimal for the visualization of anatomical structures (Fig. 1). This slice thickness provides significantly higher SNR for ligaments, subchondral bone and menisci and at least equal SNR for cartilage, bone marrow, muscle and fat of *syngo* SPACE as compared to conventional 2D-TSE-fs. Though identification of anatomical structures was comparable for *syngo* SPACE and 2D-TSE-fs, the $SPACE_{1mm}$ showed significantly better visualization of menisci in axial sections and meniscal roots in coronal sections despite slightly inferior CNR (joint fluid/cartilage, joint fluid/menisci, fat/ligaments and bone marrow/subchondral bone) as compared to 2D-TSE-fs.

## Clinical application

The reconstruction time for one *syngo* SPACE dataset was below 30 s, the data acquisition time was 10 min 35 sec with *syngo* SPACE versus 12 min 48 sec with 2D TSE in three planes (table 1). Thus the overall acquisition time for *syngo* SPACE was comparable to the acquisition of the 2D-TSE-fs datasets in three

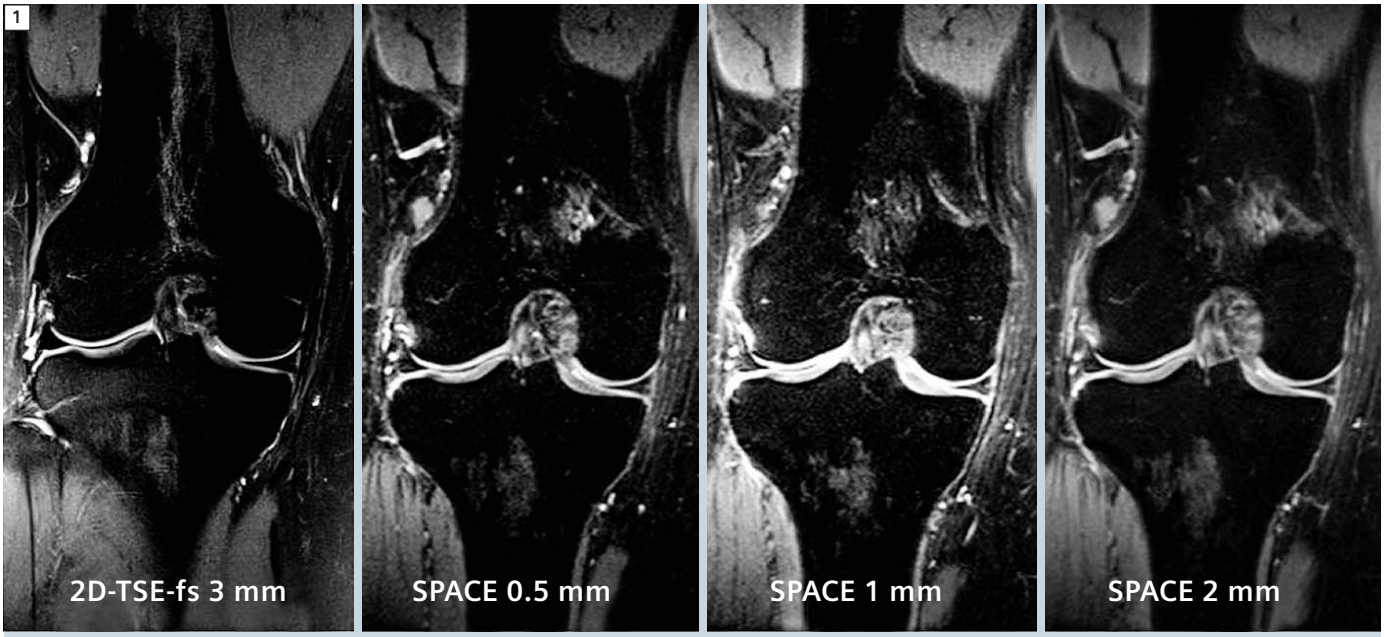


**1** Coronal *syngo* SPACE reconstructions in 0.5 mm, 1 mm and 2 mm show a good homogeneity throughout the image as compared to the T2w-2D-TSE-fs.

**Table 1: Sequence parameters for the *syngo* SPACE and the T2w-2D-TSE-fs-sequences.**

| | TR [ms] | TE [ms] | FA [°] | Resolution [mm³] | FOV [cm] | Matrix | Parallel Imaging | $T_{akqis}$ |
|---|---|---|---|---|---|---|---|---|
| ***syngo* SPACE** | 1200 | 30 | 120 | 0.5 | 16 | 320 x 320 | GRAPPA r=2 | 10'35" |
| **T2w-2D-TSE-fs** | 3200 | 30 | 180 | 0.36 x 0.36 x 3 | 16 | 448 x 448 | GRAPPA r=2 | 12'34" |

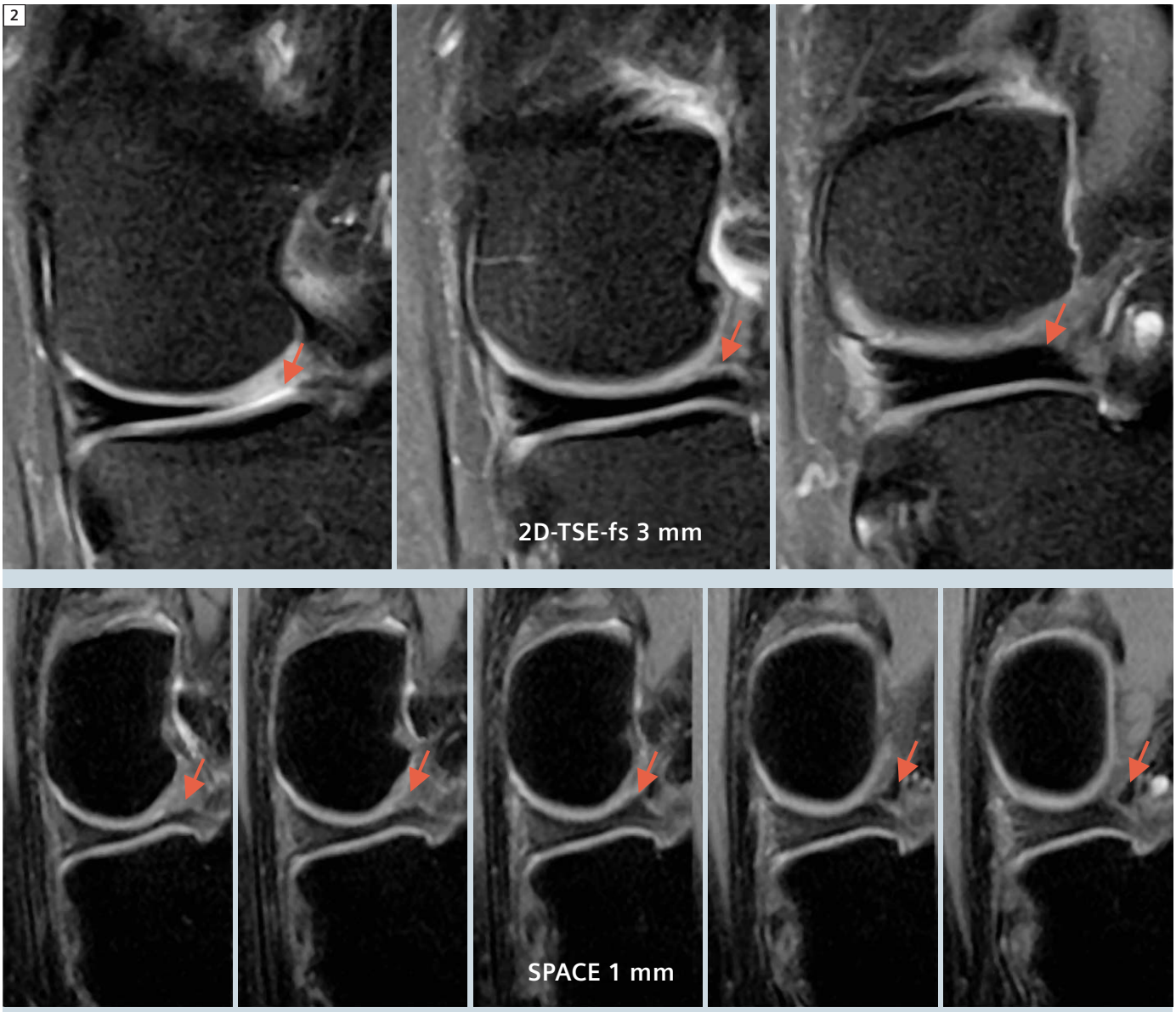


**2** Coronal reconstructed *syngo* $SPACE_{1mm}$ and 2D-TSE-fs of a healthy volunteer. SPACE provides better visualization of the posterior medial meniscal root as compared to T2w-2D-TSE-fs, where the insertion of the root is blurred because of larger partial volume effects.

planes suggesting that the technique is feasible for daily clinical use.
The advantage of *syngo* SPACE over 2D-TSE-fs is the possibility of free multiplanar isotropic reconstructions at comparable SNR resulting in a slightly improved detection and differentiation of relevant small ligamenteous (Fig. 2) and meniscal structures (Figs. 3, 4). Clinical relevance thus might be better visualization of small avulsive ligamenteous lesions, e.g. of meniscal roots and of radial or complex meniscal tears whose configuration is challenging to interpret on conventional angulated thick sagittal or coronal sections (Fig. 5). The signal / image characteristics of *syngo* SPACE appear more similar to TSE image characteristics than to GRE and therefore are unlikely to require a big adjustment of the radiologist's reading and interpretation habits to the new sequence.
Usage of the free 3D-reformation according to the course of oblique anatomical structures as seen for femoral trochlear cartilage (Fig. 6) and the anterior cruciate ligament (Fig. 7) may aid in the evaluation of primarily difficult anatomical sites or a complicated situation after injury.

## Conclusion

Blockwise acquired *syngo* SPACE is a new approach to MRI of the knee at 3T. It allows highly-resolved isotropic true 3-dimensional acquisition and subsequent reconstruction. Overall acquisition time is shorter than that of three separate 2-dimensional datasets and SNR for 1 mm reconstructions is similar to con-

Continued on page 90

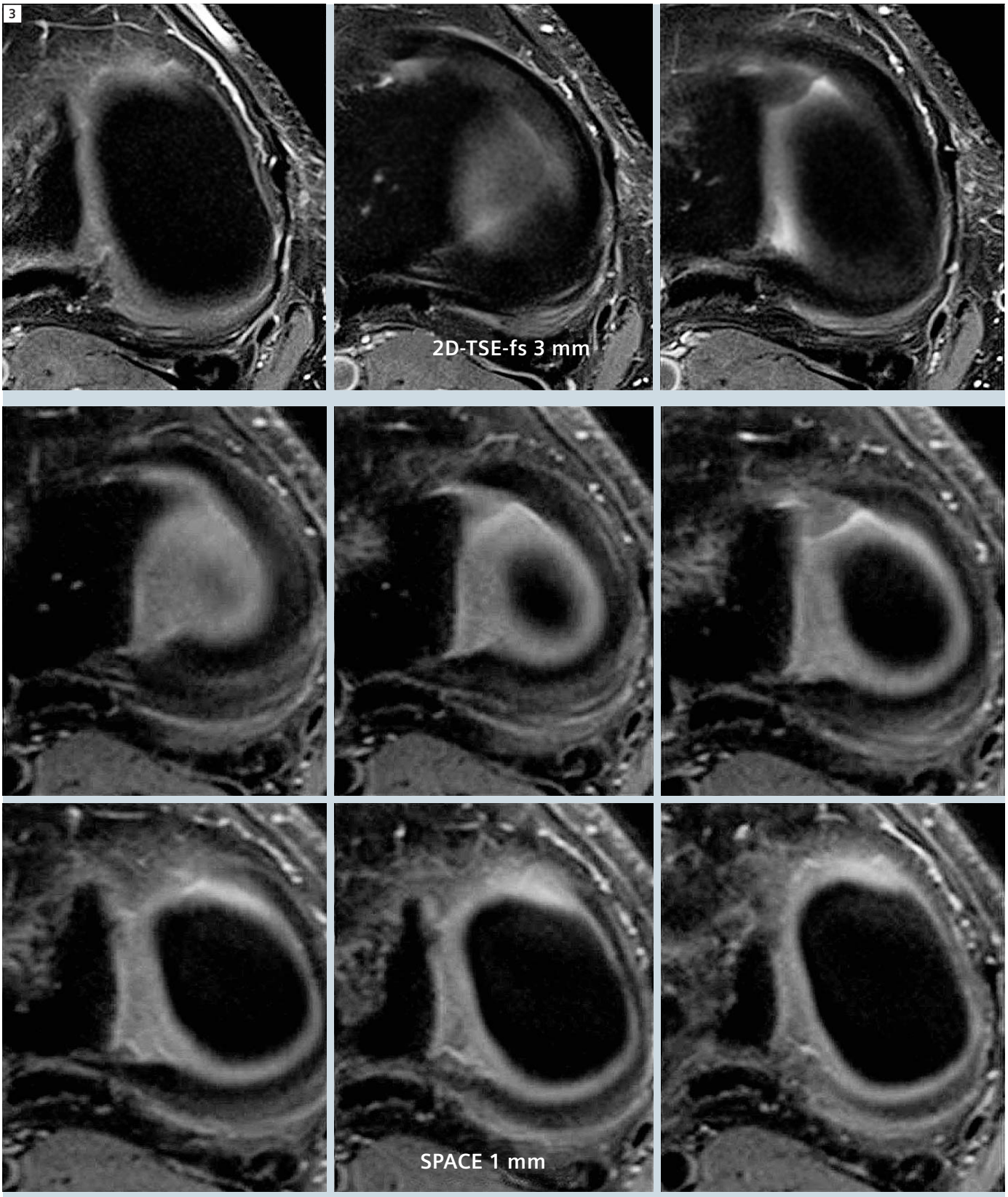


**3** Axial sections of the medial meniscus of a healthy individual. *syngo* SPACE provides more detailed depiction of the meniscus throughout a higher number of slices as compared to 2D-TSE-fs. Both the meniscal body and its attachments (meniscal roots) are clearly visualized in SPACE while in 2D-TSE-fs parts of those are masked by partial volume effects.

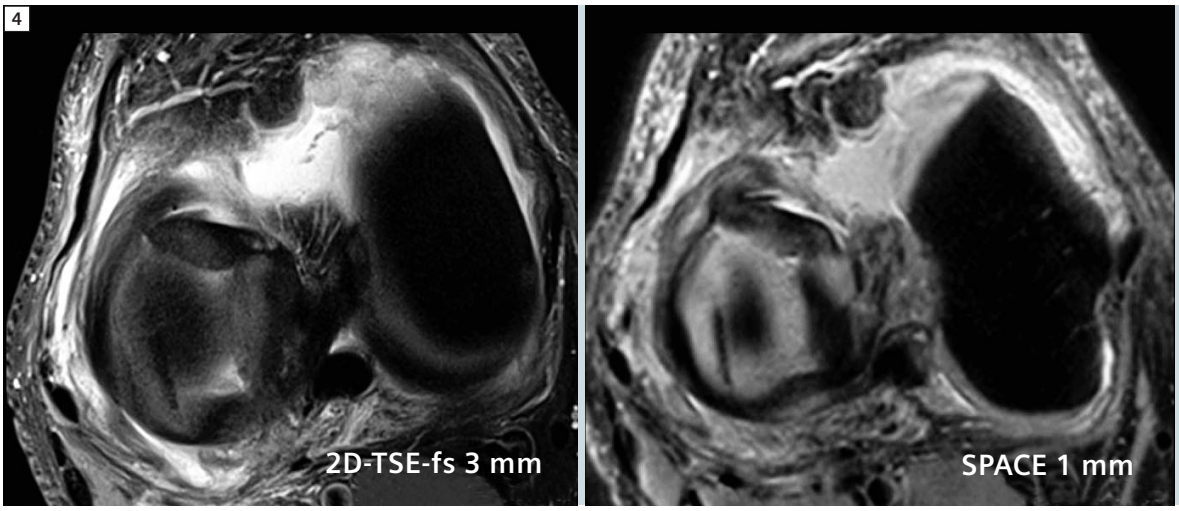


**4** Axial reconstructed *syngo* $SPACE_{1mm}$ and 2D-TSE-fs of a patient with a bucket handle tear. SPACE provides better visualization of the configuration of the bucket handle tear as compared to T2w-2D-TSE-fs, in which delineation is impaired due to partial volume effects.

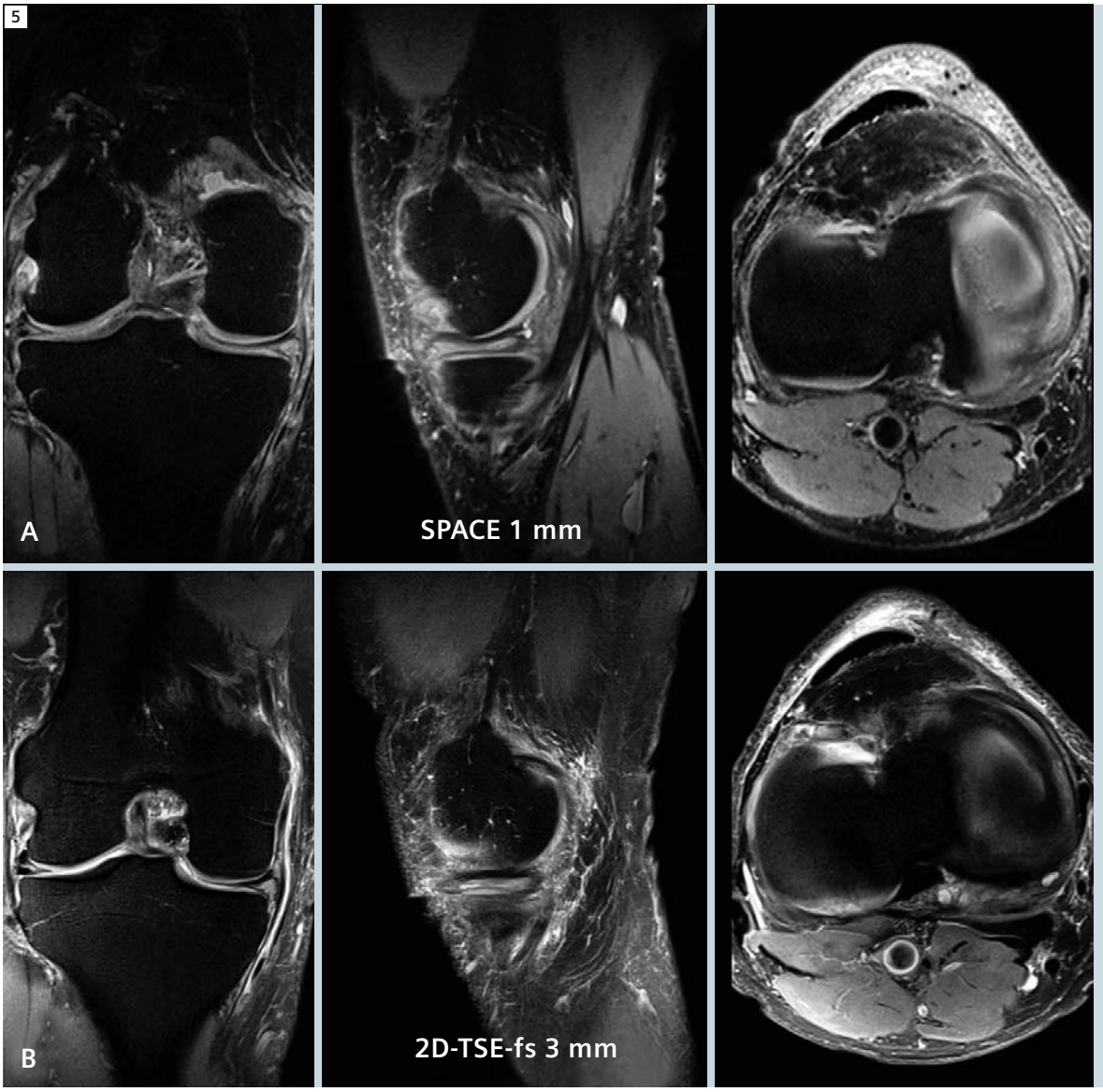


**5** Coronal, sagittal and axial reconstructed *syngo* $SPACE_{1mm}$ images (row A) show a good delineation of a horizontal tear within the medial meniscus which approach the quality of the T2w-2D-TSE-fs sequence (row B) and provide an even clearer depiction of the lesion's borders and its extent.

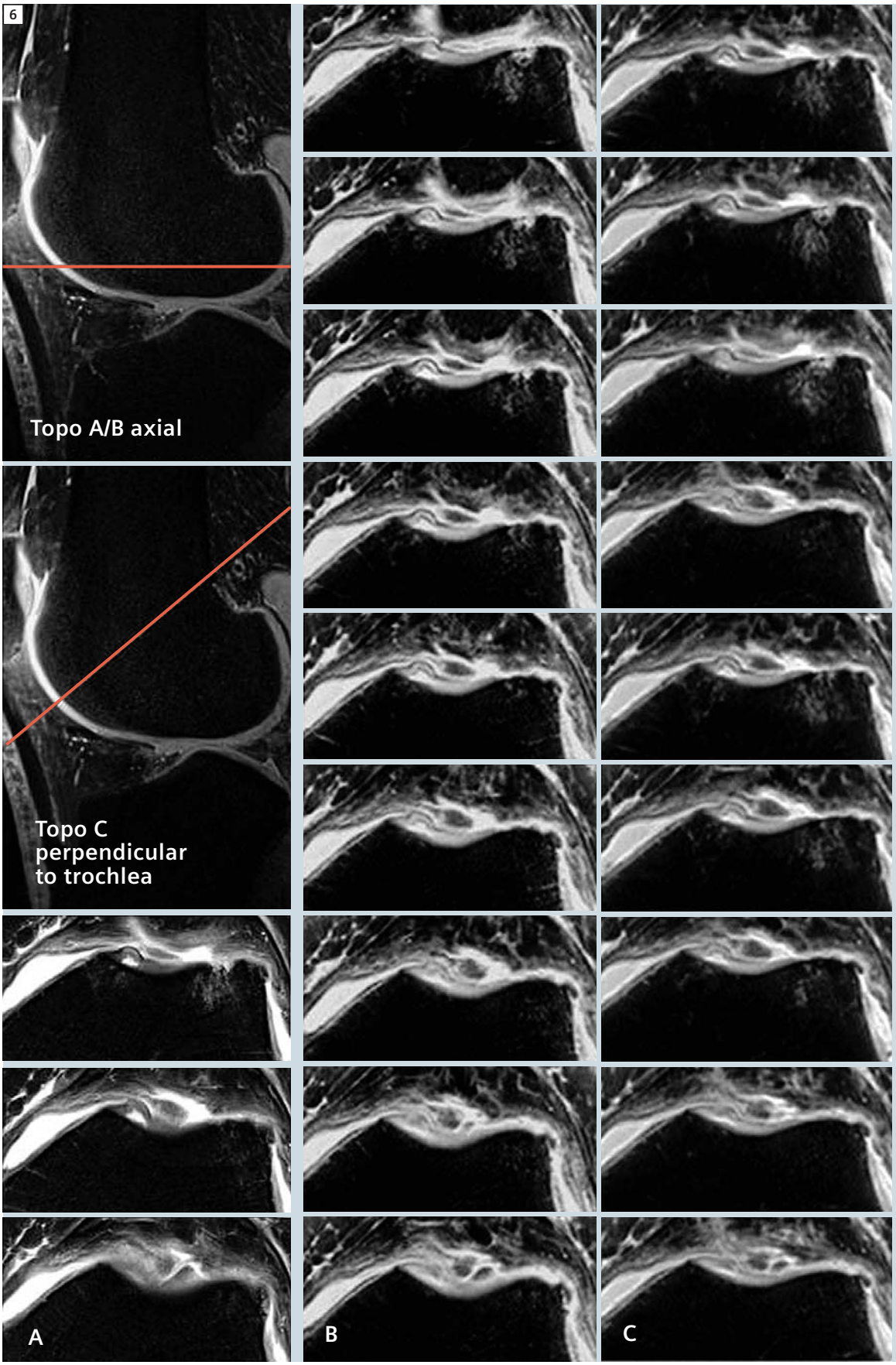


**6** Axial reconstructed *syngo* $SPACE_{1mm}$ and 2D-TSE-fs of a patient with a trochlear cartilage delamination. In strictly axially acquired 2D-TSE-fs (Topo A/B and series A) the femoral trochlear cartilage is partially blurred because of partial volume effects, whereas depiction in $SPACE_{1mm}$ (B/C) is sharper. Axially reconstructed $SPACE_{1mm}$ (Topo A/B and series B) is able to cover the trochlear cartilage on more slices than 2D-TSE-fs enabling a more detailed depiction. MPR perpendicular to the trochlear cartilage (Topo C and series C) even allows a clearer depiction of cartilage height and the lesion.

Continued from page 86

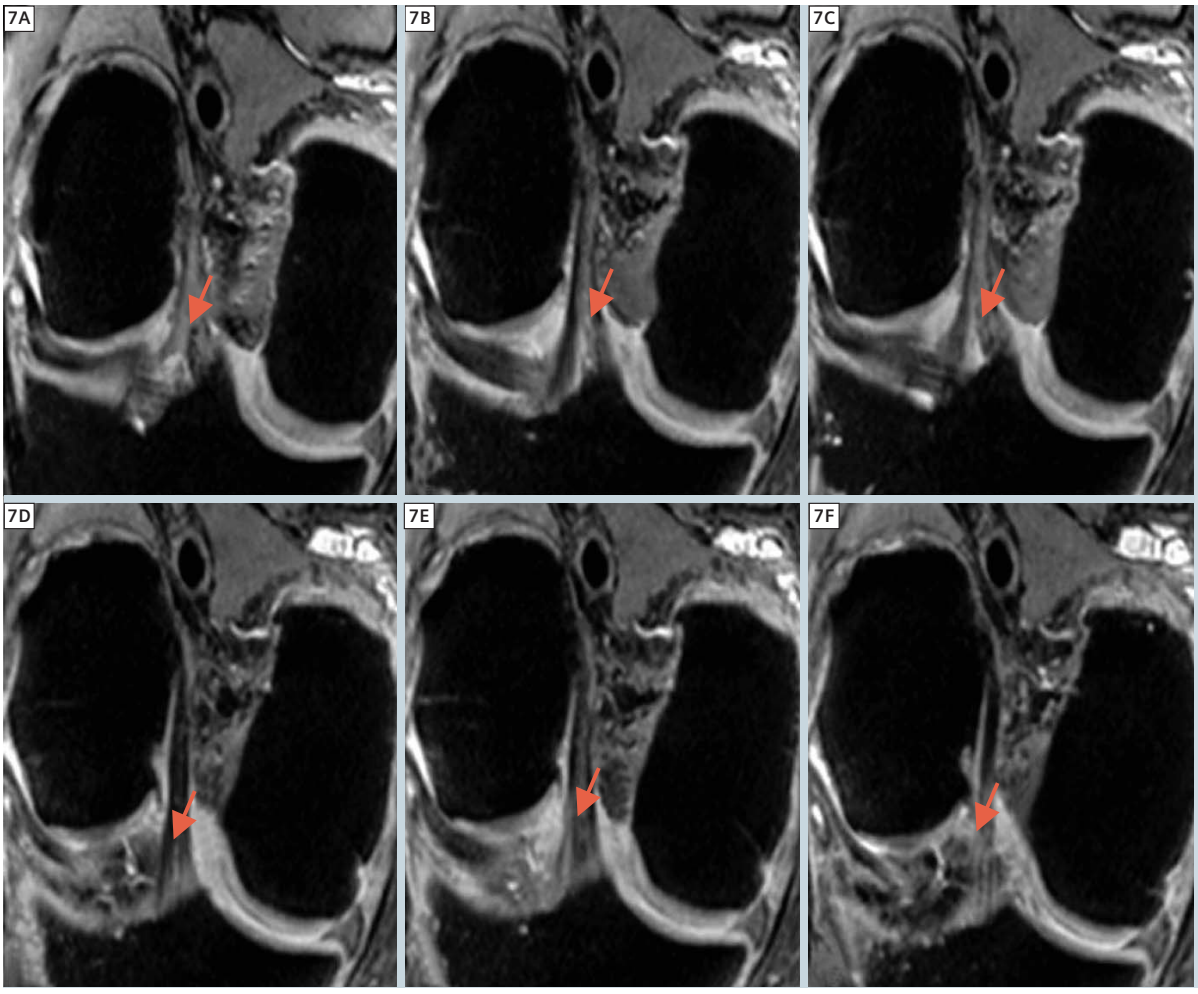


**7** Anterior cruciate ligament of a healthy volunteer (sequence A–F). *syngo* $SPACE_{1mm}$ tilted to the course of the anterior cruciate ligament allows excellent traceability of the two bundles.

ventional 2D-TSE-fs. The identification of anatomical structures at least equals the conventional sequence and allows superior discrimination of relevant small ligamentous structures.

These data suggest that a protocol comprising 1 mm *syngo* SPACE reconstructions in three orientations would be useful for clinical evaluation. The additional possibility of free 3-dimensional reconstruction depending on the specific clinical need may become useful for the diagnosis of difficult anatomical situations and presurgical planning, i.e. for traumatic ligamenteous lesions or complex meniscal tears.

References

1 Glaser, C., et al., [Meniscus and ligament injuries]. Radiologe, 2006. 46(1): p. 26-35.
2 Protocols for MRI examinations of joints and the spine as recommended by the AG MSK of the Deutsche Röntgengesellschaft. Rofo, 2006. 178(12): p. 128-130.
3 Mosher, T.J., Musculoskeletal imaging at 3T: current techniques and future applications. Magn Reson Imaging Clin N Am, 2006. 14(1): p. 63-76.
4 Mugler, J.P., 3rd, et al., Optimized single-slab three-dimensional spin-echo MR imaging of the brain. Radiology, 2000. 216(3): p. 891-9.
5 Lichy, M.P., et al., Magnetic resonance imaging of the body trunk using a single-slab, 3-dimensional, T2-weighted turbo-spin-echo sequence with high sampling efficiency (SPACE) for high spatial resolution imaging: initial clinical experiences. Invest Radiol, 2005. 40(12): p. 754-60.
6 Isoda, H., et al., MRCP imaging at 3.0 T vs. 1.5 T: preliminary experience in healthy volunteers. J Magn Reson Imaging, 2007. 25(5): p. 1000-6.
7 Alsop, D.C., The sensitivity of low flip angle RARE imaging. Magn Reson Med, 1997. 37(2): p. 176–84.
8 Masi, J.N., et al., Cartilage MR imaging at 3.0 versus that at 1.5 T: preliminary results in a porcine model. Radiology, 2005. 236(1): p. 140-50.
9 Link, T.M., et al., 3.0 vs 1.5 T MRI in the detection of focal cartilage pathology--ROC analysis in an experimental model. Osteoarthritis Cartilage, 2006. 14(1): p. 63-70.
10 Notohamiprodjo, M., et al., A New Approach for High Resolution MRI of the Knee at 3T – Evaluation of a Moderately T2-Weighted 3D-TSE-Fs (SPACE) Sequence, Investigative Radiology, 2009 44(9): p.585-597.

**Contact**
Annie Horng, M.D.
Department of Clinical Radiology
University Hospitals Munich –
Campus Grosshadern
Marchioninistrasse 15
81377 Munich
Germany
Phone: +49 89 7095 3620
annie.horng@med.uni-muenchen.de

# Musculoskeletal Advisory Board Provides Protocols for 1.5 and 3T MAGNETOM systems

We have launched the MSK Advisory Board website, providing proven MSK protocols (.edx files) for download. To support Technologists there are also coil positioning videos and tips & tricks.

**Board members are:**

- Christian Glaser, LMU Grosshadern, Germany
- Jürg Hodler, Balgrist University Hospital, Switzerland
- Young-Jo Kim, Harvard Medical School, Children's Hospital Boston, USA
- Tallal Charles Mamisch, Bern University, Switzerland
- Michael Recht, New York University, USA
- Siegfried Trattnig, AKH Wien, Austria
- Lawrence M. White, University of Toronto, Canada

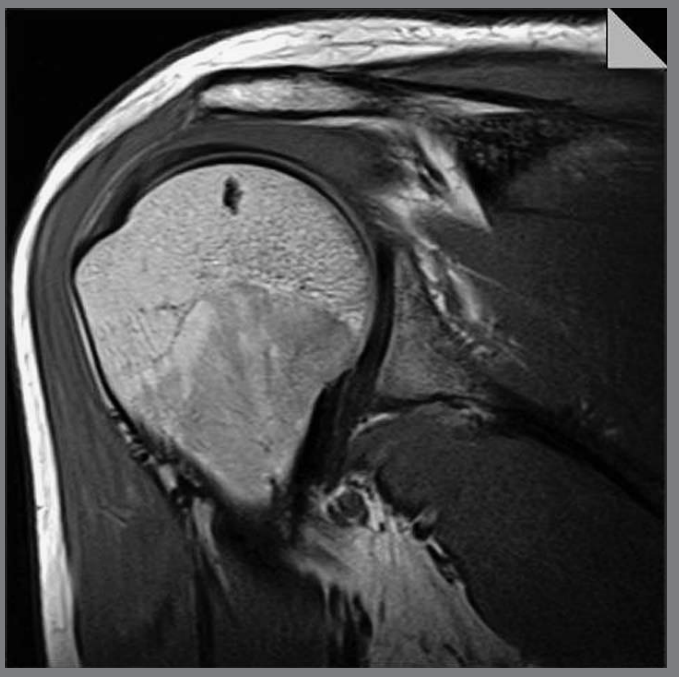

Visit us at

**www.siemens.com/magnetom-world**

# FABS View of the Elbow for Visualization of Distal Biceps Tendon

Peter Cazares, RT (R) (CT) (MR)

*MR Clinical Education Specialist, Siemens Healthcare, Iselin, NJ, USA*

## Introduction

Imaging of distal bicep tendon in MR can be somewhat difficult at times given the position of the elbow in relation to the general scanning environment. Common axial / coronal sequences demonstrate the tendon in an oblique projection that make it difficult to appreciate it in its entirety. By using the FABS (**f**lexed elbow, **ab**ducted shoulder, forearm **s**upinated) technique, imaging of the distal biceps tendon can be acquired "in plane" with excellent visualization and comfortable patient positioning.

## Conclusion

Distal biceps tendon pathology will be greatly appreciated using this technique and can be incorporated with standard elbow imaging when this clinical referral is presented. Also greater success can be achieved with greater patient comfort using this technique and position.

**Contact**
Peter Cazares
Siemens Healthcare USA, Inc.
HQ Application Specialist – MR
170 Wood Avenue South
Iselin, NJ 08830
USA
peter.cazares@siemens.com

## Procedure

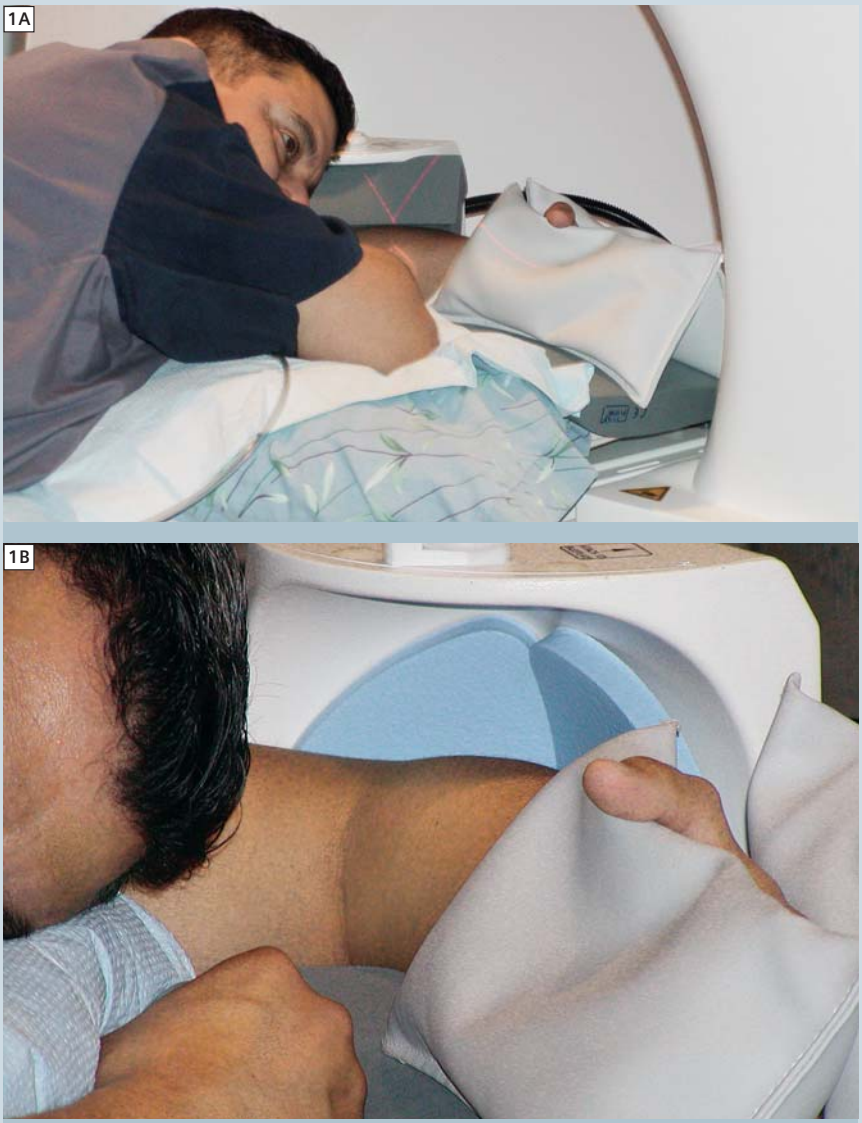


**1 Step 1:** We position the patient using our standard shoulder coil configuration. Have the patient lay on their stomach as comfortable as possible. Flex the elbow 90 degrees and place the elbow in the shoulder coil with the forearm and wrist supinated. Secure the forearm and wrist with either sandbags or a channeled positioning sponge to insure immobilization.

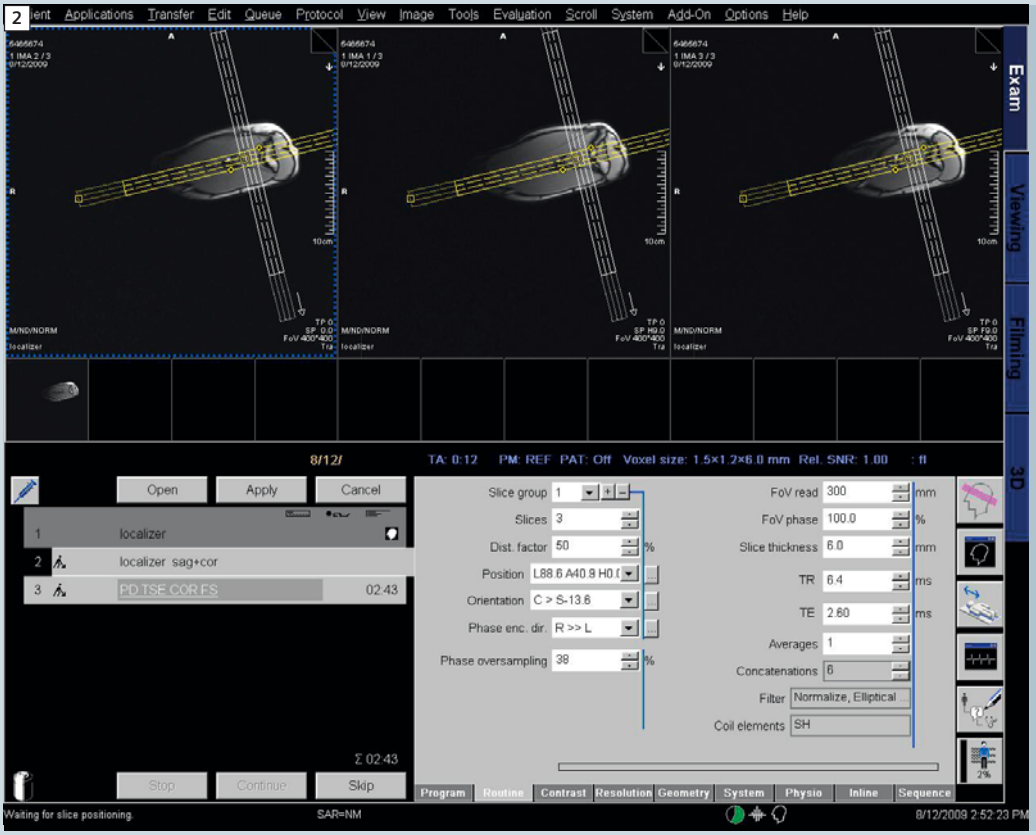


**2 Step 2:** Landmark at the center of the coil and localize. Perform two additional localizers in long and short axis in relation to the elbow.

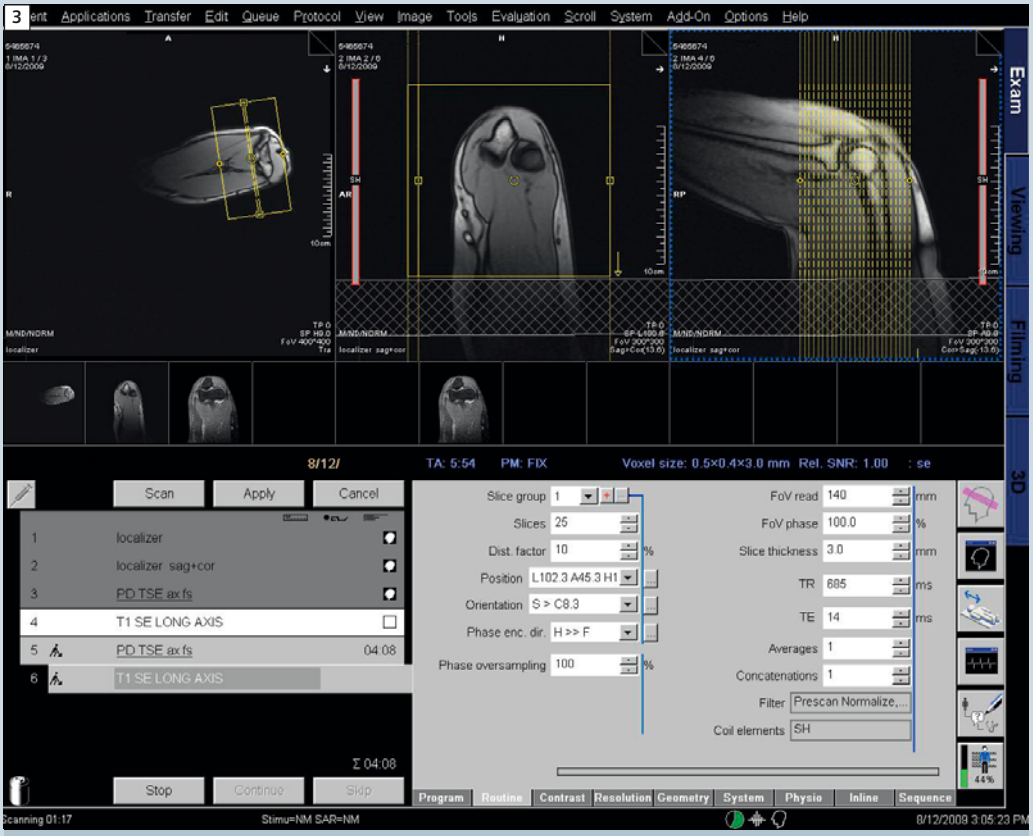


**3 Step 3:** Select sequences so as to image the biceps tendon "in plane". T1-weighted Spin Echo (SE) no fatsat, PD TSE fatsat are one recommendation.

**4** As seen, the distal biceps tendon is presented "in plane" along with the insertion at the radial tuberosity.

1

The Mater Misericordiae University Hospital (MMUH) in Dublin, Ireland

# MAGNETOM Symphony Tim Upgrade: The Mater Misericordiae University Hospital Experience

**Bolster F, Moynagh M, Dolan A, Cradock A, Murray J G**

*Dept of Radiology, The Mater Misericordiae University Hospital, Dublin, Ireland*

The Mater Misericordiae University Hospital (MMUH) is a public, acute voluntary teaching hospital and a tertiary referral center which was established in 1861. Located in Dublin's north inner city it provides a 24 hour on call service to the local and county area and contains approximately 600 beds. The MMUH not only treats patients from its local catchment area but due to its regional and national status, sees patients from all over Ireland. The MMUH houses the national center for cardiothoracic surgery, the national spinal injuries unit and is a designated national cancer centre. The Radiology Department at the MMUH performed 160,000 radiology studies including over 5000 MRIs in 2008.

## Problems

- **Old scanner:** The MMUH had a single 1.5T Siemens MAGNETOM Symphony scanner in operation since its installation in October 2000.
- **New applications, teaching and research:** As a university teaching hospital and national referral center there was a need to maintain state of the art MR imaging facilities not only for patient care, but also to train radiology and radiography staff as part of national programs, and to facilitate meaningful research programs.

- **Demand for services:** In the first full year of operation 3,200 MR scans were performed. This had risen by 38% to 5,208 MR scans in 2008. However the number of requests for MR had been steadily rising by 5–10% per annum since scanner installation. The waiting list for MR had become unacceptably long necessitating outsourcing of low risk MR studies.
- **Funding:** Any proposal to address the above issues had to be budget neutral. In addition new staff could not be hired due to a government imposed hiring embargo. This precluded purchase of a second scanner.
- **MR in 'Listed Building':** The MR was located in an architecturally preserved 'listed building'. When the scanner was initially installed in 2000, access was gained through an inner back wall via a central courtyard. Since that time further structural building work had taken place in this courtyard which made this route inaccessible. Thus a full upgrade with removal of the magnet bore would have produced serious logistical and secondary cost issues.
- **Downtime:** The MMUH has only a single MR scanner. A short installation time was thus important to ensure continuity of service.

## Why the Tim upgrade in the MMUH?

- **Software applications:** Gave access to the same full range of sequences available as if a new magnet purchased. This addressed the clinical, teaching and research issues.
- **Productivity:** We estimated that with the new technology we could increase the throughput in our MR department by about 15% or 3 extra scans per day. With the increase in throughput, we believed that the upgrade would be "cost neutral" over a three-year period of time.
- **Staffing:** No new staff would be required.
- **Architecturally preserved building:** Because the Tim upgrade involved keeping the original magnet bore, the upgrade did not involve buiiding works.
- **Short installation time:** The Tim upgrade process was estimated to take 10 days to complete. This involved two weekends and as such a loss of just six working days.

## Our experience

**Installation:**

- The old scanner was stripped to its bare magnet and new hardware in the form of new external casing and table top, a new RF system, new standard (and optional coils), a new computer system with new software were installed. A mobile MR provided coverage during installation.
- The entire upgrade process took 5 days longer than anticipated. We continued an inpatient and urgent outpatient service from the mobile unit. Engineers worked around the clock to sort out teething difficulties but it was worth the wait!

**Technology:**

Several tailored upgrade packages were also purchased to the specific services of the adult population with congenital heart defects. We have now applied it to venous and tumor imaging. The *syngo* BLADE sequence has become invaluable to us and is generally used in patients with movement disorders or patients who are slightly confused. It has greatly reduced the need to sedate these patient groups. The cardiac package included the PMU wireless physio control and vector ECG tracing which has greatly increased the efficiency of our cardiac clinic. The old ECG device was cumbersome and frequently needed replacing and a good trace proved difficult to attain in certain patients. We invested in the 8-channel knee coil and are impressed with the image quality attainable for MR arthrography, foot, ankle and wrist imaging with this device. Parallel imaging technology has greatly reduced scan times for many of our sequences. A new, sturdier head and neck coil replaced the old. Compared to the former flexible neck coil, a clear gain in signal-to-noise ratio (SNR) is obvious and also clinical advantages by application of parallel imaging e.g. for MR angiography of the supraaortic vessel are obvious. However, the old flexible neck coil is sometimes greatly missed, especially for our spinal trauma patients. Our

2

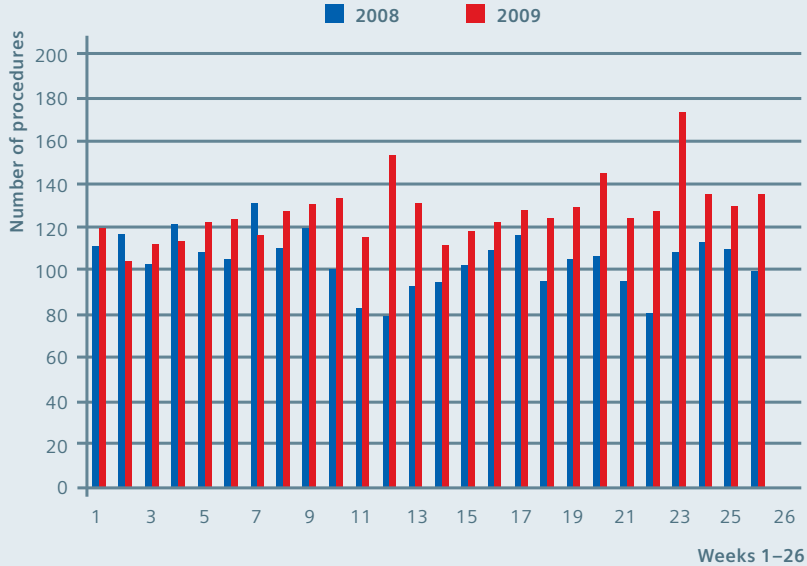


**2** Comparison of exam numbers performed per week at the MMHU before and after the Tim upgrade. Red columns: with Tim upgrade, blue columns: corresponding data before upgrade. Note that the graph includes the start-up period.

**3** Example of a whole-spine exam. **3A–C** composed sagittal T2w TSE images, consisting of three stages (TR / TE = 4000 / 100 ms; slice thickness 3 mm). Note the slight scoliosis (best shown in **3C**). Magnified images do demonstrate multiple degenerative changes of the cervical spine with narrowing of the spinal canal **(3D)** and the compression fracture of the first lumbar spine without relevant stenoses of the canal **(3E)**.

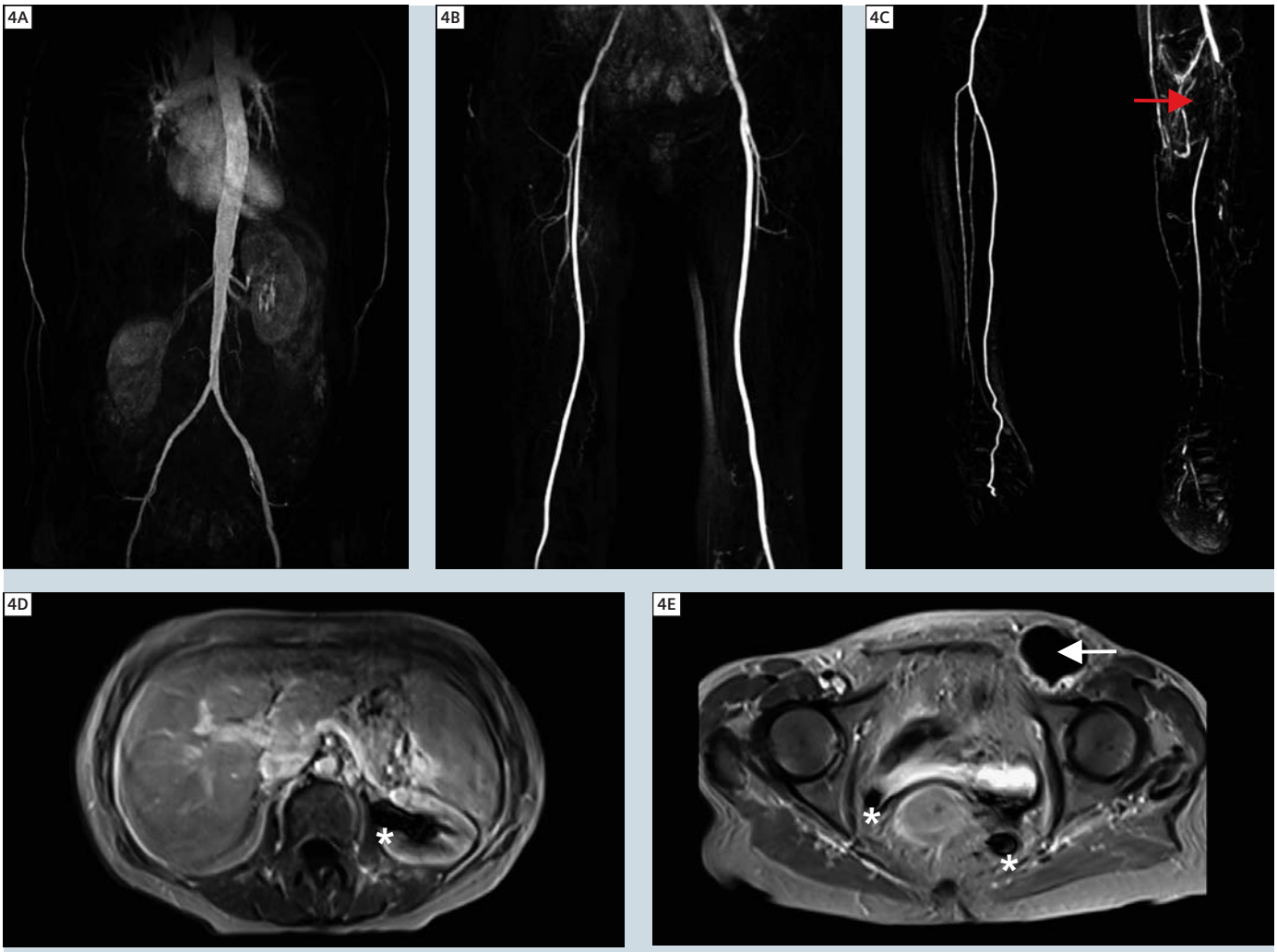


**4** Multi-step MR angiography of a 55-year-old female patient with limited breath-hold capabilities. **4A–C** MIP based on the large-FOV MR angiography (TR / TE = 3.10 / 1.08 ms, FOV 328 x 500 mm, matrix 214 x 383, slice thickness 1.4 mm). Complete occlusion of the left poplitean artery is found (red arrow). Note also a seroma on the left inguinal side (white arrow) and susceptibility artifacts at the area of the ureters on both sides (marked by stars). **4D, E:** ce 2D FLASH.

image quality is compromised in these patients as the new neck coil will not fit over spinal immobilization devices and tracheostomy tubes.

**Productivity:**
Since the upgrade there has been a notable increase in throughput and productivity due to faster scanning and examination times. Over the same 6 month period one year prior to and after installation of the Tim upgrade there has been a 20%* increase in the number of procedures performed. Faster scan times amount to a significant increase of at least 4 procedures per day or an average of at least 20 MR studies per working week.

**Cost:**
The approximate cost for our institution of outsourcing an MR scan in 2008 was € 220.00. Based on achieved additional throughput of 20 scans per week (Fig. 2) for an operational 50 weeks of the year the total savings will pay for the upgrade including VAT (value added tax) at 21% and our interest costs in 3 years.
In summary the Tim upgrade has allowed us to achieve state of the art imaging on site on a cost neutral basis. This was achieved by a commitment on the part of all staff to increase patient numbers without additional staff.

*Results may vary. Data on file.

**Contact**
Dr. John Murray, M.D.
Dept of Radiology
The Mater Misericordiae
University Hospital
Eccles Street
Dublin 7
Ireland
jmurray@mater.ie

# Siemens Healthcare – Customer Magazines

Our customer magazine family offers the latest information and background for every healthcare field. From the hospital director to the radiological assistant – here, you can quickly find information relevant to your needs.

**Medical Solutions**
Innovation and trends in healthcare. The magazine, published three times a year, is designed especially for members of the hospital management, administration personnel, and heads of medical departments.

**News**
Our latest topics such as product news, reference stories, reports, and general interest topics are always available at www.siemens.com/healthcare-news

**AXIOM Innovations**
Everything from the worlds of interventional radiology, cardiology, fluoroscopy, and radiography. This semi-annual magazine is primarily designed for physicians, physicists, researchers, and medical technical personnel.

**MAGNETOM Flash**
Everything from the world of magnetic resonance imaging. The magazine presents case reports, technology, product news, and how-to's. It is primarily designed for physicians, physicists, and medical technical personnel.

**SOMATOM Sessions**
Everything from the world of computed tomography. With its innovations, clinical applications, and visions, this semiannual magazine is primarily designed for physicians, physicists, researchers, and medical technical personnel.

**Perspectives**
Everything from the world of clinical diagnostics. This semi-annual publication provides clinical labs with diagnostic trends, technical innovations, and case studies. It is primarily designed for laboratorians, clinicians and medical technical personnel.

For current and older issues and to order the magazines, please visit **www.siemens.com/healthcare-magazine**

# Listen – Discuss – Share
# 7th MAGNETOM World Summit

## May 27–30, 2010, Shenzhen, China

The MAGNETOM World Summit is an excellent platform to establish personal contacts, exchange valuable information, learn from the experience of other users and to share your own expertise.

Lectures and presentations from experts in the field will allow you to be exposed to new ideas and alternative clinical approaches that might help you to improve your clinical and financial outcomes.

For details on the agenda and registration, please visit **www.siemens.com/magnetom-world**

MAGNETOM Flash – Imprint
© 2009 by Siemens AG, Berlin and Munich,
All Rights Reserved

Publisher:
**Siemens AG**
Medical Solutions
Business Unit Magnetic Resonance,
Karl-Schall-Straße 6, D-91052 Erlangen,
Germany

Editor-in-Chief: Dr. Matthias Lichy, M.D.
(matthias.lichy@siemens.com)

Associate Editor: Antje Hellwich
(antje.hellwich@siemens.com)

Editorial Board: Dagmar Thomsik-Schröpfer, Ph.D.; Okan Ekinci, M.D.; Ignacio Vallines, Ph.D.; Wellesley Were; Milind Dhamankar, M.D.; Michelle Kessler; Gary McNeal; Sunil Kumar, M.D.

Production: Norbert Moser, Siemens AG, Medical Solutions

Layout: independent Medien-Design
Widenmayerstrasse 16, D-80538 Munich

Printers: Farbendruck Hofmann, Gewerbestraße 5, D-90579 Langenzenn, Printed in Germany

**MAGNETOM Flash is also available on the internet:**
www.siemens.com/magnetom-world

Note in accordance with § 33 Para.1 of the German Federal Data Protection Law: Despatch is made using an address file which is maintained with the aid of an automated data processing system.
MAGNETOM Flash with a total circulation of 20,000 copies is sent free of charge to Siemens MR customers, qualified physicians, technologists, physicists and radiology departments throughout the world. It includes reports in the English language on magnetic resonance: diagnostic and therapeutic methods and their application as well as results and experience gained with corresponding systems and solutions. It introduces from case to case new principles and procedures and discusses their clinical potential.
The statements and views of the authors in the individual contributions do not necessarily reflect the opinion of the publisher.
The information presented in these articles and case reports is for illustration only and is not intended to be relied upon by the reader for instruction as to the practice of medicine. Any health care practitioner reading this information is reminded that they must use their own learning, training and expertise in dealing with their individual patients. This material does not substitute for that duty and is not intended by Siemens Medical Solutions to be used for any purpose in that regard. The drugs and doses mentioned herein are consistent with the approval labeling for uses and/or indications of the drug. The treating physician bears the sole responsibility for the diagnosis and treatment of patients, including drugs and doses prescribed in connection with such use. The Operating Instructions must always be strictly followed when operating the MR system. The sources for the technical data are the corresponding data sheets. Results may vary.
Partial reproduction in printed form of individual contributions is permitted, provided the customary bibliographical data such as author's name and title of the contribution as well as year, issue number and pages of MAGNETOM Flash are named, but the editors request that two copies be sent to them. The written consent of the authors and publisher is required for the complete reprinting of an article.
We welcome your questions and comments about the editorial content of MAGNETOM Flash. Please contact us at magnetomworld.med@siemens.com. Manuscripts as well as suggestions, proposals and information are always welcome; they are carefully examined and submitted to the editorial board for attention. MAGNETOM Flash is not responsible for loss, damage, or any other injury to unsolicited manuscripts or other materials. We reserve the right to edit for clarity, accuracy, and space. Include your name, address, and phone number and send to the editors, address above.

# Subscription

**Please enter your business address**

Institution

Department

Function

Title

Name

Street

Postal Code

City

State

Country

MR system used

**Please include me in your mailing list for the following Siemens Healthcare customer magazine(s):**

- ☐ Medical Solutions
- ☐ MAGNETOM Flash
- ☐ SOMATOM Sessions
- ☐ AXIOM Innovations

**Stay up to date with the latest information Register for:**

- ☐ the monthly e-Newsletter

E-mail

- ☐ Yes, I consent to the above information being used for future contact regarding product updates and other important news from Siemens.
- ☐ unsubscribe from info service

Please print clearly!

# MAGNETOM Flash

Siemens AG
Medical Solutions
Magnetic Resonance
Antje Hellwich - Marketing
P.O. Box 32 60
D-91050 Erlangen
Germany

→ Visit www.siemens.com/magnetom-world for case reports, clinical methods, application tips, talks and much more clinical information.

**SUBSCRIBE NOW!**

– and get your free copy of future MAGNETOM Flash! Interesting information from the world of magnetic resonance – gratis to your desk. Send us this postcard, or subscribe online at www.siemens.com/MAGNETOM-World

**Global Siemens Headquarters**

Siemens AG
Wittelsbacherplatz 2
80333 Muenchen
Germany

**Global Siemens Healthcare Headquarters**

Siemens AG
Healthcare Sector
Henkestr. 127
91052 Erlangen
Germany
Phone: +49 9131 84-0
www.siemens.com/healthcare

**www.siemens.com/healthcare-magazine**

Order No. A91MR-1000-66C-7600 | Printed in Germany | CC MR 01000 ZS 110920. | © 11.09, Siemens AG

On account of certain regional limitations of sales rights and service availability, we cannot guarantee that all products included in this brochure are available through the Siemens sales organization worldwide. Availability and packaging may vary by country and is subject to change without prior notice. Some/All of the features and products described herein may not be available in the United States.

The information in this document contains general technical descriptions of specifications and options as well as standard and optional features which do not always have to be present in individual cases.

Siemens reserves the right to modify the design, packaging, specifications and options described herein without prior notice.
Please contact your local Siemens sales representative for the most current information.

Note: Any technical data contained in this document may vary within defined tolerances. Original images always lose a certain amount of detail when reproduced.

**Global Business Unit**

Siemens AG
Medical Solutions
Magnetic Resonance
Henkestr. 127
DE-91052 Erlangen
Germany
Phone: +49 9131 84-0
www.siemens.com/healthcare

**Local Contact Information**

**In Asia**
Siemens Pte Ltd
The Siemens Center
60 MacPherson Road
Singapore 348615
Phone: +65 6490-8096

**In Canada**
Siemens Canada Limited
Medical Solutions
2185 Derry Road West
Mississauga ON L5N 7A6
Canada
Phone: +1 905 819-5800

**Europe/Africa/Middle East**
Siemens AG
Medical Solutions
Henkestr. 127
91052 Erlangen
Germany
Phone: +49 9131 84-0

**Latin America**
Siemens S.A.
Medical Solutions
Avenida de Pte. Julio A. Roca No 516,
Piso 7
C1067ABN Buenos Aires
Argentina
Phone: +54 11 4340-8400

**USA:**
Siemens Medical Solutions U.S.A., Inc.
51 Valley Stream Parkway
Malvern, PA 19355-1406
USA
Phone: +1-888-826-9702